Boundary Layer Variations and Convective Regimes during UNSTABLE, 2008

by

Robyn Rae Dyck

A Thesis submitted to the Faculty of Graduate Studies of

The University of Manitoba

in partial fulfilment of the requirements of the degree of

MASTER OF SCIENCE

Department of Environment and Geography

University of Manitoba

Winnipeg

Abstract

UNSTABLE was a field project in the summer of 2008 to better understand the large-scale and mesoscale forcings of summer storms. This thesis objective is to better understand boundary layer characteristics and convective environments in the Alberta foothills. Three sub-objectives are designed to address the overall thesis goal: (1) Characterize the daily evolution of the boundary layer during different convective regimes, (2) distinguish conditions between days with deep, shallow and no convection, and (3) to illustrate how targeted soundings can be useful for severe storm prediction. Non-convective days exhibited a warmer atmospheric column. Days with shallow convection exhibited a mid-level inversion. Deep convective days commonly displayed unstable low-levels and cooler upper levels, deep low-level moisture and the mountain-plains circulation. When compared to the pre-existing operational upper air network, mobile UNSTABLE soundings better captured the near storm environment of two tornadic events in terms of available instability and shear profiles.

Acknowledgements

I would like to first thank my advisor, Dr. John Hanesiak, who after completing a four year degree, a two month Arctic field campaign, and now a three and a half year masters with, has always been fantastic to work with and has been a huge influence on my meteorological career.

I would like to recognize my committee; Dr. Ron Stewart (University of Manitoba) and Dan Fulton (Environment Canada) for being a part of this work and guiding me through this process.

Gratitude is extended to all of the UNSTABLE PI's and field personnel who gathered data used in this thesis, especially Neil Taylor (Environment Canada), who personally took the time for providing data, analysis maps, editing and helpful discussions along the way. Special thanks also to Dr. Dave Sills (Environment Canada) for valuable feedback and Craig Smith (Environment Canada) who lead the upper air program for UNSTABLE. UNSTABLE funding pertinent to this thesis was provided by Environment Canada and an NSERC Discovery Grant (to Hanesiak allowing U. Manitoba contributions to UNSTABLE).

I would like to thank all of my coworkers at Environment Canada for always keeping me on my toes and for making me the meteorologist I am and will become. Specifically, thank you to my managers, Pat McCarthy, Brian Bukoski and Mike McDonald for making my masters degree possible. Thank you to Jason Knight for coding guidance, Natalie Hasell for defense preparation, James Cummine for editing and who was always willing to share much needed and welcome discussion or insight, and Dale Marciski for starting me on this Meteorological adventure.

Thank you to Shannon Fargey and Michelle Curry for ongoing advice, data manipulation guidance, addressing stupid questions and camaraderie.

Dedication

To my mom who always supported my meteorological education and career path. To my Auntie Karen who inspired my love of weather.

To Louis, for everything.

Table of Contents

List of Tables

List of Figures

List of Symbols, Abbreviations and Nomenclature

Symbol	Definition
B	buoyancy
U, V	Velocity at mid and low-levels
ω_H	Horizontal component of vorticity
ρ	Density
f	Coriolis force
σ	Standard Deviation
μ	Mean
w	Wind component in z direction
g	Gravity
q	Specific humidity
r	Mixing ratio
T	Temperature
Td	Dew point
PW	Precipitable Water
kt	Knot
UTC	Coordinated Universal Time Zone
θ	Potential temperature

θ_e	Equivalent potential temperature
°	Degrees
C	Celsius
K	Kelvin
hPa	Hectopascal
g kg^{-1}	Grams of dry air per kilograms of moist air
J kg^{-1}	Joules of energy per kilogram
m s^{-1}	Meters per second
XSM	Strathmore Radar
WMI	Weather Modification Inc. Radar
MB1	Mobile sounding site #1
MB2	Mobile sounding site #2
EA3	Sounding site located at Olds, AB
WVX	Sounding site located at Water Valley, AB
DC	Deep Convective Day Type
SC	Shallow Convective Day Type
NC	Nil Convective Day Type
CAPE	Convective Available Potential Energy

CIN	Convective Inhibition
SRH	Storm Relative Helicity
LI	Lifted Index
BRN	Bulk Richardson Number
SI	Showalter Index
SWEAT	Severe Weather Threat Index
BL	Boundary Layer
CI	Convective Initiation
LFC	Level of Free Convection
LCL	Lifted Condensation Level
CCL	Cloud Condensation Level
IOD	Intensive Observation Day
IOP	Intensive Observation Period
SUP	Supercell producing large hail
TOR	Tornadic supercell
Svr	Severe thunderstorms
Non Svr	Non severe thunderstorms
AGL	Above Ground Level

MUCAPE	Most Unstabe CAPE
MULCL	Most Unstable LCL
CAPPI	Constant Altitude Plan Position Indicator
PPI	Plan Position Indicator

CHAPTER 1

1. INTRODUCTION

1.1. Motivation

Forcing mechanisms leading to Convective Initiation (CI) are neither well understood nor adequately reproduced in weather forecast models (Wulfmeyer et al, 2008). Thunderstorms and deep convection in general are an important ingredient in many high impact events, but the present capability for forecasting convection is poor (Browning, 2007). Thunderstorms, especially on the Canadian Prairie provinces in the summer, are a large part of everyday weather. To better understand the forcing mechanisms that initiate them, high-resolution, detailed four-dimensional observations of the atmosphere are necessary. This makes thunderstorm initiation and development more predictable, contributing to more accurate and timely warnings, watches and forecasts. Weather has a direct impact on our recreational and economical activities. It affects the growth of crops and availability of water. It dictates what areas of the world are habitable or uninhabitable. However, it can pose a serious threat to our health and safety (Environment Canada, 2014). Severe weather, specifically summer severe weather, including thunderstorms, can be exceptionally dangerous. There is an average of 224 severe weather reports received by Environment Canada each summer, with an average of 81 in Alberta (McDonald, 2010). Lightning kills 9 to 10 people in Canada every year. It is also responsible for about 42% of all forest fires. Forest fires caused by lightning alone costs an estimated $14 billion annually between 1979 and 1993 (McDonald, 2010). With the increasing population of Canada and our changing climate, it is expected that weather will become increasingly important in the future.

1.2. Thesis Objectives

The Understanding Severe Thunderstorms and Alberta Boundary Layers Experiment (UNSTABLE) was conducted in central Alberta in July 2008 with the overall goal of better understanding convective initiation processes and severe storm environments. UNSTABLE had several specific research questions (see Taylor et al., 2008 for more information) and this thesis will contribute to the overall UNSTABLE goals.

This research will contribute to the existing thunderstorm initiation and development science, focusing on a better understanding of deep convective processes and mechanisms in Alberta so as to contribute to improved prediction. Upper air soundings have been used in previous research over a smaller geographical area to study the Alberta boundary layer (Strong, 1989; Strong and Smith, 2001). What makes this research unique is the geographical location and spatial coverage of the soundings.

Specifically, the thesis objective is to better understand boundary layer characteristics and convective environments in the Alberta foothills. Three sub-objectives are designed to address the main objective:

1. Characterize the daily evolution of the boundary layer during different convective regimes throughout the intensive observation period (IOP) of the UNSTABLE field campaign,
2. Distinguish conditions between days with deep, shallow and no convection,
3. Illustrate how targeted soundings can be useful for severe storm prediction.

The datasets used are those collected during UNSTABLE 2008, and hence, the research objectives pertain to the utilization of these data. The sub-objectives will be accomplished with three main tasks:

1. Compare average (composite) soundings for the four different sounding locations and times of day.
2. Differentiating between meteorological parameters from different radiosonde sites and day types using various standard statistical metrics.
3. Use other meteorological data, such as satellite, radar, upper air and surface maps to augment the above tasks as required.

There will be an emphasis on meteorological parameters used in an operational setting; such as Lifted Index (LI), Convective Available Potential Energy (CAPE), Convective Inhibition (CIN), wind shear and synoptic scale analyses. Definitions of these parameters will be provided in the forthcoming chapter.

1.3. Structure of Thesis

In Chapter 2, a detailed background will be given on the topic of boundary layer evolution followed by convective initiation including triggering mechanisms and the necessary ingredients for convection. Chapter 2 will also provide a summary of Alberta thunderstorm research and forecasting issues. In Chapter 3, data and methods of analysis will be detailed. Chapter 4 through 6 will address the results. Chapter 4 will cover the first objective by focusing on four meteorological parameters to characterize boundary layer evolution. Chapter 4 will also determine statistical differences between sounding sites to examine the meteorological value of having four sites and to test whether eco-climate zones play a role in differences. Chapter 5 will give a detailed analysis comparing deep, shallow and nil convective composites within the IOP. Chapter 5 will also cover determining statistical differences between severe weather parameters on DC, SC and NC day types. Chapter 6 will contribute to the third sub-objective by presenting

an analysis of two tornadic events that occurred within the IOP. Specifically, it will identify sounding representativeness of the near and pre-storm environment. The thesis concludes in Chapter 7 with a review of the findings of this research, its limitations and its contribution to science.

CHAPTER 2

2. BACKGROUND

2.1. Boundary Layer Evolution

The boundary layer (BL) is the layer near the ground that is influenced by the diurnal cycle of radiative heating between the Earth and the air. The upper limit, or depth of the BL, is identified by a sharp increase in temperature, or capping inversion (Stull, 2000). Understanding BL evolution including diurnal changes in mesoscale processes is critical to anticipating the initiation and development of summer severe weather. The evolution of moisture and instability, including depth and magnitude of the BL, can dictate whether thunderstorm activity will initiate, and if so, the potential severity of the thunderstorms. Banta (1984) illustrated the observed θ profiles of the convective boundary layer in mountainous terrain, as shown in Figure 2.1. The evolution of the BL over mountainous terrain is similar to the evolution over a homogeneous surface. The main difference is cold air pooling in surface depressions or valleys. Cold air pooling greatly affects the timing of the erosion of the nocturnal inversion. The nocturnal inversion is seen in the lowest 300 m of the column with downslope directed winds. This occurs due to surface cooling overnight. After sunrise, the layer of air closest to the surface warms, inducing a pressure gradient which produces a weak upslope flow. The depth and magnitude of this upslope flow increases as surface warming increases throughout the day. The vertical wind structure is strongly correlated to the vertical thermal structure. Therefore, when the inversion is eroded, stronger winds from aloft are realized at the surface as gusts as well as a change in wind direction. Above the inversion exists a constant θ. As the surface layer warms with diurnal heating, the surface layer becomes well mixed and dry adiabatic, indicating a neutrally stable layer with respect to dry air parcels that exist within the BL.

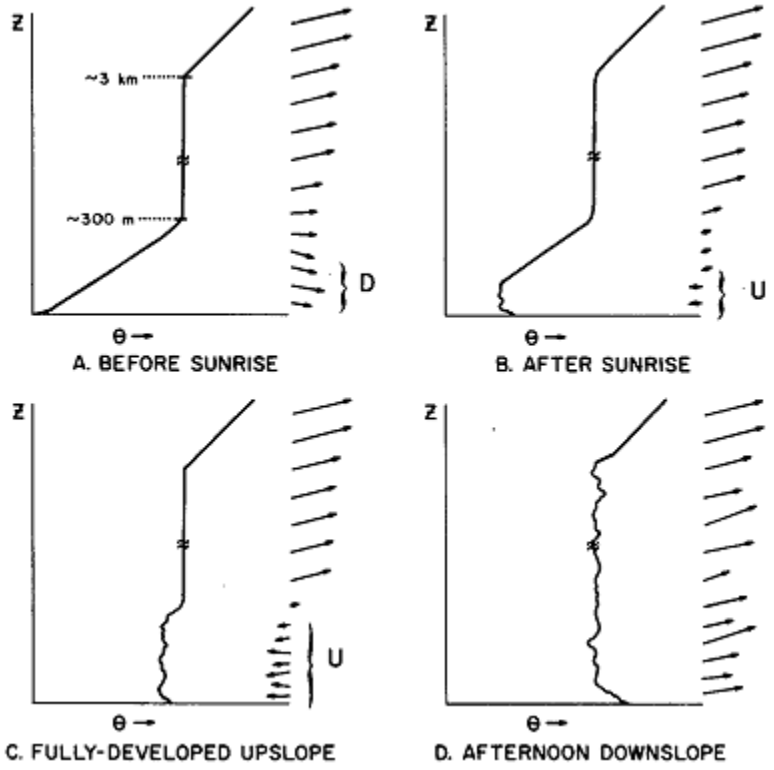

Figure 2.1: *From Banta (1984). Illustrating the θ profiles throughout the day of the convective boundary layer in mountainous terrain. The evolution of downslope winds (D) and upslope (U) winds are shown on the right of the profiles. ©American Meteorological Society. Used with permission*

In Figure 2.2a, a stable low layer is identified with stratified, cold θ closer to the surface, indicative of the nocturnal inversion. In Figure 2.2b, θ increases first near the terrain ridge top, inducing upslope flow. In b, the surface layer warms and is shown as a higher θ value. In c the mixed layer is becoming deeper and more well mixed when in d, it is at its maximum depth and is fully mixed with downslope winds throughout the column.

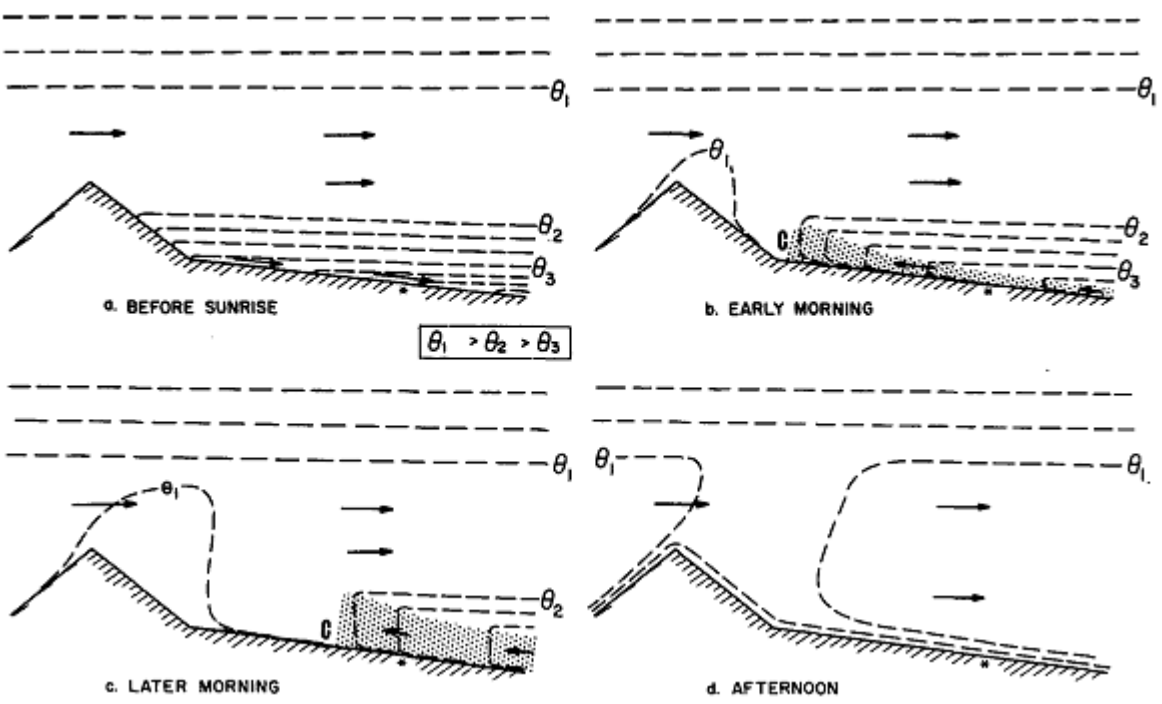

Figure 2.2: *From Banta (1984) illustrating the idealized cross sections of the daily evolution of wind and potential temperature. Dashed lines are isentropes at arbitrary intervals. Each correspond to the soundings in figure 2.12. The "C" indicates the location of the lee side convergence zone. ©American Meteorological Society. Used with permission*

An important observation, as indicated in Figure 2.3, is the change in wind direction from the morning to afternoon. The shift does not occur simultaneously at all of the site locations, resulting in convergence. It is responsible for convective initiation earlier on the higher terrain and later at lower elevations. If this low-level mesoscale convergence is accompanied by favorable synoptic scale conditions, deep convection can be generated.

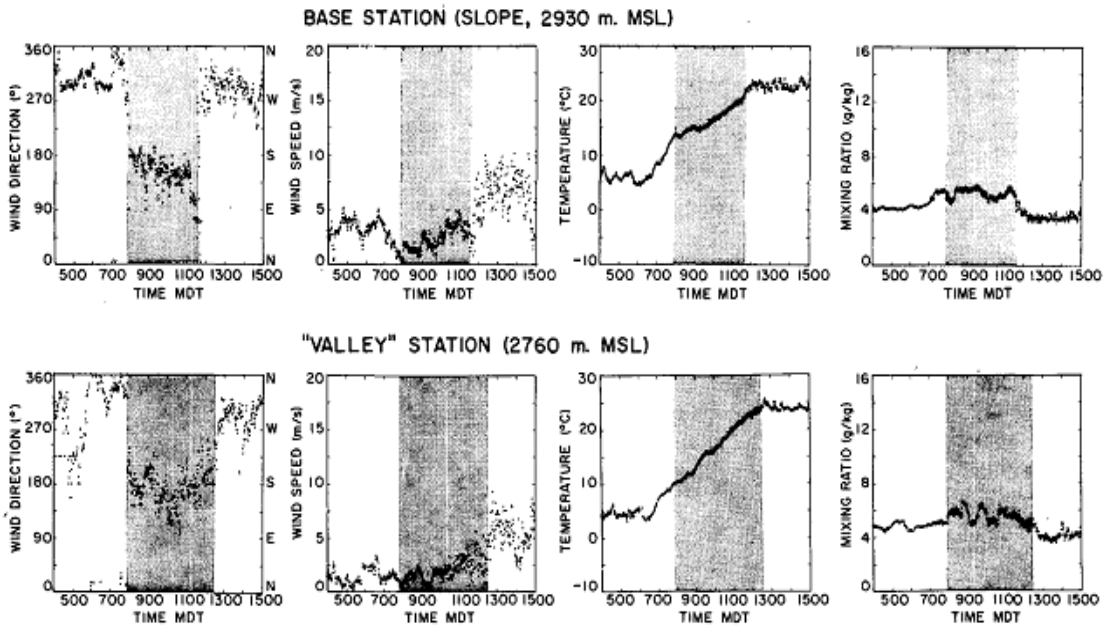

Figure 2.3: *From Banta (1984) illustrating the change in four meteorological parameters, wind speed, wind direction, temperature and mixing ratio throughout the day at two sites, one situated at a higher elevation (top) and the other situated at a lower elevation (bottom).Grey shading highlights the timing of the easterly wind direction. ©American Meteorological Society. Used with permission*

Strong (1989) studied the near mountain BL in detail during LIMEX. LIMEX focused on the pre-storm evolution of the capping inversion in the Limestone Mountain region of the Alberta foothills and its role in thunderstorm initiation. The existence of the morning nocturnal inversion was observed. It lifted to 750 hPa throughout the late morning to early afternoon, almost disappearing by 2000 UTC. This lifting occurs via surface convergence and warming near the foothills, creating a mid-level capping inversion. This is shown below in Figure 2.4 a through d.

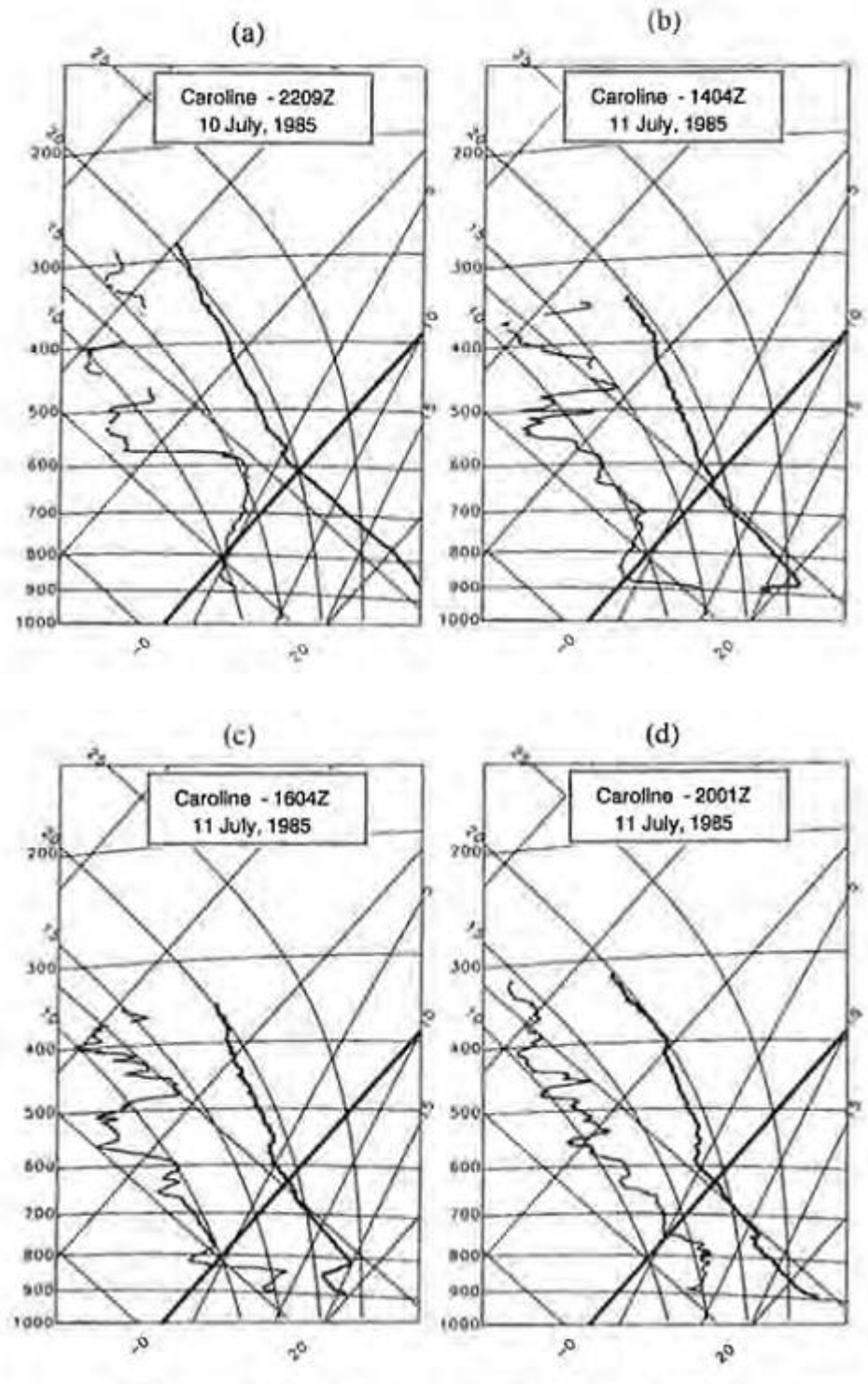

Figure 2.4: *From Strong (1989) illustrating the temporal variation at Caroline illustrating the development (due to subsidence) and breakdown (due to ascent) of the capping lid. Reproduced with permission of the Canadian Meteorological and Oceanographic Society.*

Strong (1989) also displayed the spatial extent of the capping inversion through the high resolution upper air soundings launched during LIMEX-85. Nine sites were employed with launches every 2 hours. In contrast to the UNSTABLE data sets, the sites were 50 km apart, closely spaced to be able to resolve the pre-storm mesoscale capping inversion. The UNSTABLE upper air network covered a larger geographical area to capture the BL over contrasting surface characteristics and initiation features. Comparing soundings from different sites at the same time, it was observed that the capping inversion was not evident further west, over the foothills (Limestone Mountain West), but was evident at Caroline and Red Deer. Caroline, located in between Limestone Mountain West and Red Deer, had a stronger inversion at 800 hPa while Red Deer, further east, had an inversion of weaker magnitude and lower in altitude, at about 850 hPa. This is illustrated in Figure 2.5.

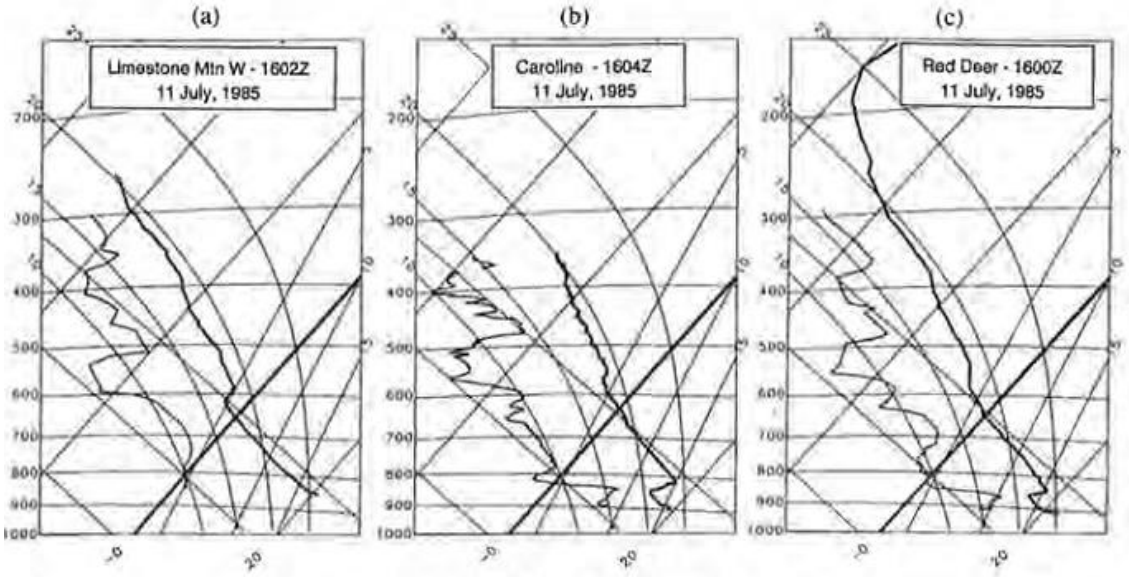

Figure 2.5: *From Strong (1989). Series of soundings illustrating the spatial variability of the capping lid across the LIMEX upper air network from southwest of Limestone Mountain peak to Red Deer. Reproduced with permission of the Canadian Meteorological and Oceanographic Society.*

2.2. Convective Initiation Processes

The Alberta foothills are a favorable area to conduct thunderstorm research since it is an area of frequent convective (lightning) activity as shown in Figure 2.6. Burrows and Kochtubajda (2010) demonstrated the diurnal cycle of lightning which indicates a small fraction (less than about 0.2) of cloud to ground (CG) lightning in the Alberta foothills occurs overnight, from 22:30 to 10:30 local solar time (not shown). This further emphasizes the need for research in the topic of day time heating and surface based convective initiation.

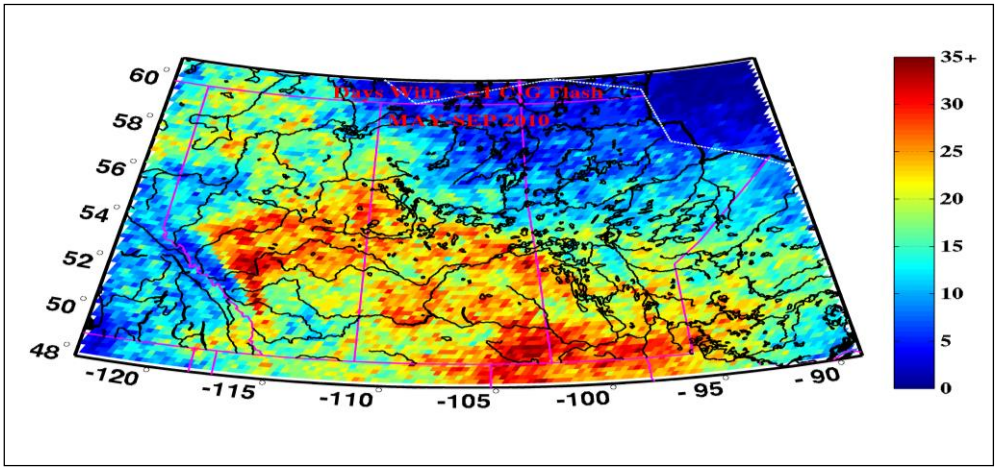

Figure 2.6: *1999 to 2009 Flash Density map (Taylor et al., 2008) ©American Meteorological Society. Used with permission.*

The following ingredients are necessary for surface based convective initiation as well as determining the mode and/or severity of thunderstorms (e.g.; Fawbush, 1951; Newton 1963; Miller 1972; Lawford, 1970; Smith and Yau, 1993a).

1. Low-level moisture: A large amount of latent energy (low-level, boundary layer moisture),

2. Convective instability: A rising air parcel is significantly warmer than the environmental temperature throughout much of the troposphere,
3. A trigger: A mechanism (e.g. convergence line or front) that forces surface and/or boundary layer parcels to a height where they become positively buoyant to release the latent energy available for deep convection, and
4. Vertical wind shear (speed and direction) of the horizontal wind.

The first two ingredients; latent energy and instability, identify if there is the potential for convection to occur. The third, a trigger, if necessary, provides the mechanism to realize the potential energy. Lastly, wind shear, can determine the convective mode; that is, how organized and long-lived the storm(s) will be. The first three ingredients will be discussed in the current section, whereas wind shear will be discussed in Section 2.4 Deep Convective Processes.

Low-level moisture, or latent energy, is the storms' fuel by contributing to the buoyancy of the parcel, as well as lowering the lifted condensation level (LCL), the level of free convection (LFC) and the cloud condensation level (CCL). The LCL is the level at which the parcel becomes saturated (with respect to water) once lifted by a trigger. This is the point at which cloud forms. The CCL is the height of the cloud base, once air has become freely buoyant and the convective temperature has been reached. The LFC is the level at which the parcel temperature first becomes warmer than the environmental temperature. The lower the LFC, the sooner an air parcel becomes freely buoyant and therefore a dynamic trigger is either not necessary or does not have to be strong. Moisture available within a column, referred to as precipitable water (PW) translates into the potential amount of precipitation a storm can produce. The low-level BL moisture contributes to a lower LFC and LCL producing more convective

potential energy and therefore, greater likelihood of convective initiation and development. More moisture can also contribute to more severe thunderstorms in regards to higher rainfall rates due to higher moisture content and less evaporation, especially of smaller particles. It may also contribute to stronger wind gusts due to precipitation drag and loading. However, in contrast, higher low-level moisture content and less evaporation can lessen the magnitude of the wind gusts.

Warmer low-level temperatures and cooler upper levels produce higher lapse rates, while creating a more unstable environmental profile and therefore, stronger up and down drafts. Stronger accelerations of buoyant air parcels, either by addition of moisture (reducing the density of the air parcel) or instability, contribute to: updrafts potentially reaching higher in the atmosphere and therefore, colder temperatures, longer growth time for particles resulting in larger hail, stronger downdrafts contributing to stronger cold pools, stretching of the column contributing to increased vertical vorticity, reduced entrainment, enhanced convergence at the updraft base and divergence at the updraft top. Each of these contribute to a further developed thunderstorm, and potentially more severe associated weather.

2.3. Convective Indices

The parameters used to measure convective potential are numerous. In this section, some of the main parameters (CAPE, CIN, SWEAT, BRN) used in this thesis and of relevance to Alberta and Canadian operational forecasting are defined.

2.3.1. CAPE

The amount of energy of a lifted conditionally unstable or absolutely unstable parcel can be measured as Convective Available Potential Energy (CAPE). It is the positive area between the

parcel temperature and the environmental temperature profiles from the LFC to the Equilibrium Level (EL), the level at which the parcel temperature becomes colder than the environmental temperature on a tephigram (Figure 2.7 and Equation 1).

Equation 1 describes the amount of potential energy that will be available to the storm if it is released (Tsonis, 2007). T_p is the temperature of the parcel (K), T_a is the ambient environment temperature (K) and R =287.04 J kg^{-1} K^{-1}, which is the Specific Gas constant for dry air. A large amount of instability is characterized by steep lapse rates produced in the higher terrain and high equivalent potential temperature (θ_e) air advected northward from the Gulf of Mexico (Markowski and Richardson, 2010) or locally produced moisture via evapotranspiration (ET). Equation 2 from Weisman and Klemp (1986) relates CAPE to the maximum speed of the updraft $(W_{ad})_{max}$. It ignores perturbation effects, water loading and mixing.

Equation 1: *Convective Available Potential Energy*

$$CAPE = -R \int_{LFC}^{EL} (Tp - Ta) d\ ln\ p$$

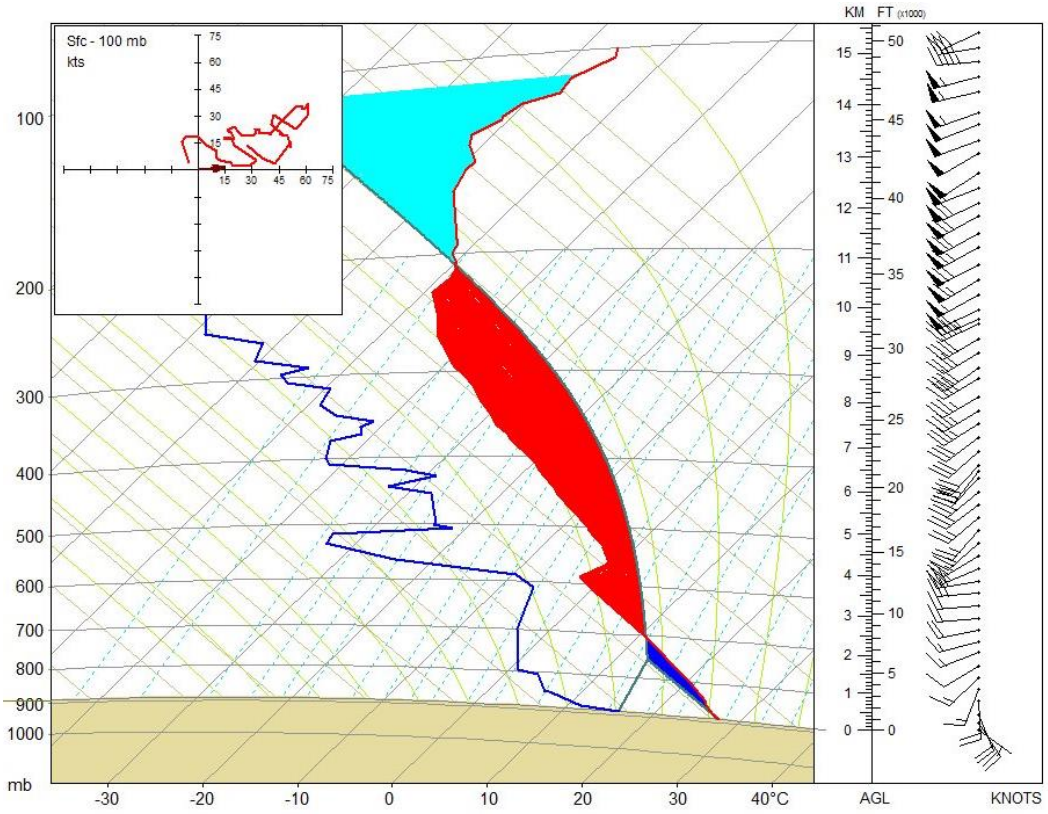

Figure 2.7: *Soundings from EA3 July 21 0000 UTC. CAPE is shaded in red and CIN in dark blue.*

Equation 2*: Maximum updraft speed (W)*

$$\frac{1}{2}(W_{ad})^2_{max}=\text{CAPE}$$

2.3.2. CIN

If there is any negative buoyancy, or Convective Inhibition (CIN) present, this prevents the CAPE from being realized (Colby, 1984). It is a measure of the strength of the cap, inhibiting parcels below the level of the CIN from freely ascending (Equation 3). The cap is important to allow temperatures and moisture in the low-levels to increase over time, creating the "loaded gun" sounding, which could produce an outbreak of deep convection, once the CIN has been

eliminated (Browning et al, 2007). CIN can be eliminated in a few ways. For example, a trigger could lift the parcels above the CIN and/or daytime temperatures and dew points may also increase enough to erode the cap on their own. Colby (1984) found during Severe Environmental Storms and Mesoscale Experiment (AVE/SESAME2), lower CIN values were a good predictor of thunderstorm initiation. CIN is the negative shaded area on a tephigram, also in Figure 2.7, shaded in blue, between the surface and the LFC.

Equation 3: *Convective Inhibition (CIN)*

$$CIN = -R \int_{Lfc}^{Sfc} (Tp - Ta) d \ln P$$

The most common triggers in Alberta are drylines and land surface effects. In fact, over the 17 day UNSTABLE field campaign drylines were present on up to possibly nine of these days (Taylor 2015, personal communication). Drylines can have horizontal moisture variations of several grams per kilogram and can be concentrated in a few kilometers. Differences in land surface character (besides terrain) will affect the surface sensible and latent heat fluxes, influencing thunderstorm initiation. For example, a crop surface compared to a forested area has a potentially higher surface moisture flux, resulting in potentially higher CAPE and lower LFC. However, the convective boundary layer depth would also potentially be reduced via a lower sensible heat flux (e.g. Hanesiak et al., 2004). As well, Hanesiak et al. (2004) showed these types of surfaces on the Canadian Prairies, with varying moisture fluxes, can induce their own mesoscale circulations, increasing convergence potentially leading to convective initiation.

Close to the Rocky Mountains, the terrain serves as a trigger. The Thunderstorm Project, conducted by Byers and Braham (1949) noted three reasons why terrain can act to initiate convection. First, the temperature of the air is warmer closer to the terrain due to more

absorption of solar radiation as compared to the absorption of solar radiation of air at the same altitude adjacent to the terrain. This would then contribute to upward vertical motion over the sloped terrain that would draw air from the flatter terrain regions into the sloped terrain. The air being drawn towards the higher terrain is then forcibly lifted to potentially form clouds that rise to their LFC, and realize the instability in a conditionally unstable air mass. In addition, the roughness of the terrain creates perturbations in the flow, mechanical turbulence or eddies, which may cause convective processes in a conditionally unstable air mass.

2.3.3. SI

The Showalter Index (SI) is one of many measures of instability that is used in operational meteorology as illustrated in Equation 4. (Showalter,1953).

Equation 4: *Showalter Index*

$$SI = T_{500} - T_{850}$$

The 850 hPa parcel is lifted dry adiabatically to saturation and then lifted pseudo-adiabatically to the 500 hPa level. The lifted 500 hPa temperature (T_{850}) is then subtracted algebraically from the observed 500 hPa temperature (T_{500}). A negative number indicates instability and a positive number indicates stability (Showalter, 1953). This index assumes:

1. There is enough convergence, frontal activity or orographic lifting to cause convection exchange of potentially unstable air between the 850 hPa and 500 hPa levels.
2. Condensation takes place at temperatures above freezing in convective clouds that extend to levels with temperature below freezing.
3. The rising moist air reaches the Level of Free Convection below the 500 mb level.

4. There is cooling aloft or warming with increasing moisture at low-levels.

2.3.4. LI

The lifted index (LI), a similar parameter as SI for measuring instability, is defined as the temperature difference between the observed 500 hPa temperature (T_{500}) and the assumed 500 hPa temperature of a mean parcel lifted from the modified lower 3000 foot layer next to the ground (T_{p500}), as in Equation 5. Indices are negative for parcel temperatures that are warmer than the environment. Since it was derived from the SI, it has the same assumptions. It is similar to the SI, except for the determination of the level from which a parcel is lifted and the fact that the Lifted Index is a forecast index whereas the SI is an observed static index (Brown, 1992; Galway, 1956).

Equation 5: *Lifted Index (LI)*

$$LI = T_{500} - T_{p500}$$

2.3.5. SWEAT

The Severe Weather Threat index (SWEAT) (Equation 6), uses a combination of instability and shear to measure potential severity of a thunderstorm where 150-300 is a slight possibility of severe, 300-400 severe is possible and greater than 400 tornadic thunderstorms are possible (Miller,1972).

Equation 6: *Severe Weather Threat Index* ***(****SWEAT)*

$$SWEAT = 12(850Td) + 20(TT - 49) + 2(V850) + (V500) + 125Sin((dd500 - dd850) + 0.2)$$

Where:$TT = (T850 - T500) + (Td850 - T500)$.

V = wind speed

dd = directional veering

2.3.6. BRN

The Bulk Richardson Number (BRN) is a non-dimensional convective parameter that is defined as the ratio of available kinetic energy, to available potential energy and attempts to quantify the CAPE versus shear proportion as seen in Equation 7 (Moncrieff and Green, 1972).

Equation 7: *Bulk Richardson Number (BRN)*

$$R = \frac{CAPE}{\frac{1}{2}(\overline{U}^2 + \overline{V}^2)}$$

U and V are vector components of the difference between the environmental wind speeds at low and mid -levels. It is a measure of the low-level wind shear (Weisman and Klemp, 1986). Any value less than 45 indicates a favorable ratio of SBCAPE to shear for supercell development (Thompson et al, 2003; Moncrieff and Green, 1972).

In summary, severe storms take place in high CAPE and high shear environments, falling in the favorable BRN range. High CAPE, if distributed in the lower levels of the column, would indicate high updraft speeds. CIN may be necessary in the early afternoon to retain BL moisture, however, the CIN must diminish later in the day to allow air parcels to be freely buoyant, otherwise a trigger would be required for convective initiation. LI and SI would be below 0, possibly quite negative, in the -5 to -10 range for strong thunderstorms. SI could also be utilized overnight to indicate the potential for elevated thunderstorms. SWEAT, incorporating both shear and instability, would be greater than 300, in a high CAPE and high shear environment. All of

these indices are used in combination in an attempt to characterize the thunderstorm potential and severity on any given summer day.

2.4. Deep Convective & Severe Storm Processes

An important contributor to severe storms is wind shear, the last important thunderstorm ingredient, which can determine the convective mode or type of storm. Chisholm and Renick (1971) presented hodographs displaying the shear from each of the three types of thunderstorms and described the resultant weather. Speed shear gives rise to asymmetry in the storm. It exerts a force on the up-shear side of the updraft, creating high pressure on the up-shear side and low pressure on the down-shear side. This tilts the updraft, as seen in Figure 2.8, offsetting the updraft from the downdraft, and therefore, prevents the precipitation from falling into the updraft, increasing the duration of the storm and therefore, the potential for severe weather such as large hail and tornadogenesis.

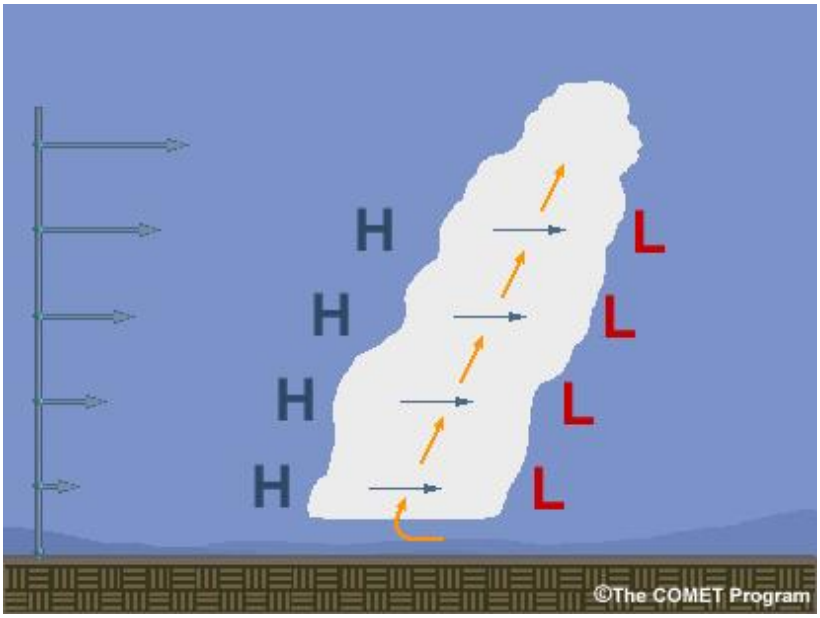

Figure 2.8: *Persistent updraft with vertical evnvironmental speed shear inducing high (H) and low (L) pressure indicated on the upshear and downshear respective sides. The source of this material is the COMET® Website at http://meted.ucar.edu/ of the University Corporation for Atmospheric Research (UCAR), sponsored in part through cooperative agreement(s) with the National Oceanic and Atmospheric Administration (NOAA), U.S. Department of Commerce (DOC). ©1997-2014 University Corporation for Atmospheric Research. All Rights Reserved.*

The downdraft produces a gust front, which continues lifting parcels to enhance the updraft, as shown in Figure 2.9. If the cold pool is moving at the same speed as the storm, the storm can be long lived due to the continuous lift of parcels on the cold pool edge into the updraft (Marwitz, 1972; Chen, 1980).

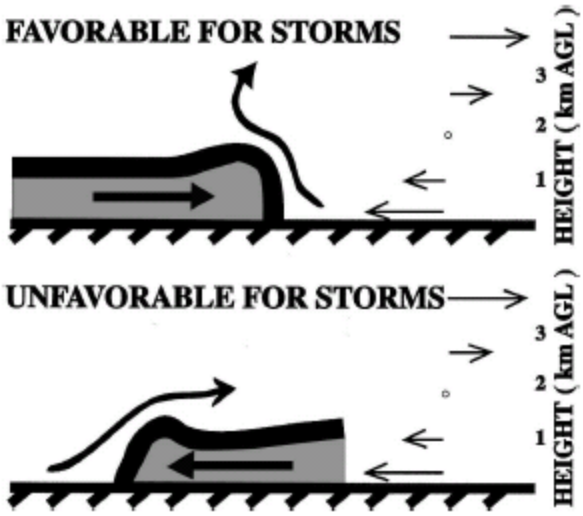

Figure 2.9: *From Weckworth and Parsons, 2006, illustrating the cold pool motion shown in the upper frame favorable for continuous redevelopment. ©American Meteorological Society. Used with permission.*

Horizontal vorticity is generated by environmental speed shear, creating horizontal vorticity rolls. The updraft tilts these horizontal vorticity rolls in the vertical (to create vertical vorticity) which generates rotation in the storm, (Weiseman, 1986), as illustrated in Figure 2.10. If the directional shear is weak or non-existent, the precipitation falls into the middle of updraft, causing the storm to split into two, with each storm propagating to the right (cyclonic rotating storm) and left (anti-cyclonic rotating storm) of the original direction (Klemp and Wilhelmson,1978) as in Figure 2.10.

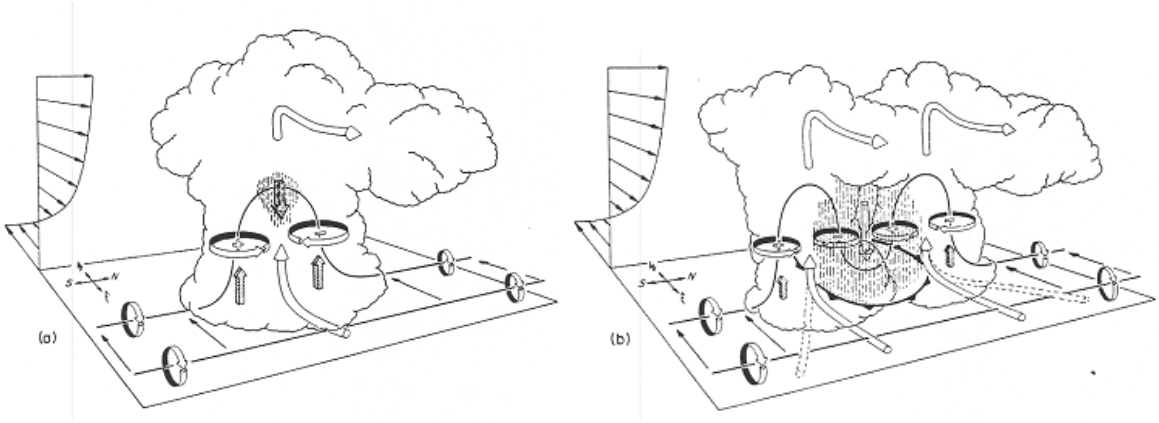

Figure 2.10: *From Klemp, 1987. It illustrates the unidirectional environmental shear with the precipitation into the updraft, creating two sets of vorticity couplets. The cylindrical arrows show the direction of the cloud-relative flow and heavy solid lines represent the vortex lines. Shaded arrows represent the up and down drafts. (a) Initial stage and (b) the splitting stage with the downdraft forming between the two to create two vortex pairs.*

If there is directional shear with height, the high-low couplets are rotated horizontally and are displaced, enhancing the updraft as air rushes from high to low, as shown in Figure 2.11. By enhancing the up and down drafts, the vertical vorticity is increased due to stretching, and is concentrated at the surface (Weisman and Klemp, 1982). At this mature stage, characteristics such as a deep persistent mesocyclone, radar based structures such as the presence of a bounded weak echo region (BWER) and a hook-shaped echo are evident, and the storm is defined as a supercell storm (Chisholm and Rennick, 1972; Moller et al., 1994). For supercell storms, it is important to have the most turning (directional shear) in the lower layers of the troposphere (Maddox, 1976 Davis-Jones, 1984). This directional shear produces a long-lived low-level rotating mesocyclone, which is the main characteristic of supercell storms. These storms can produce large hail and tornadoes.

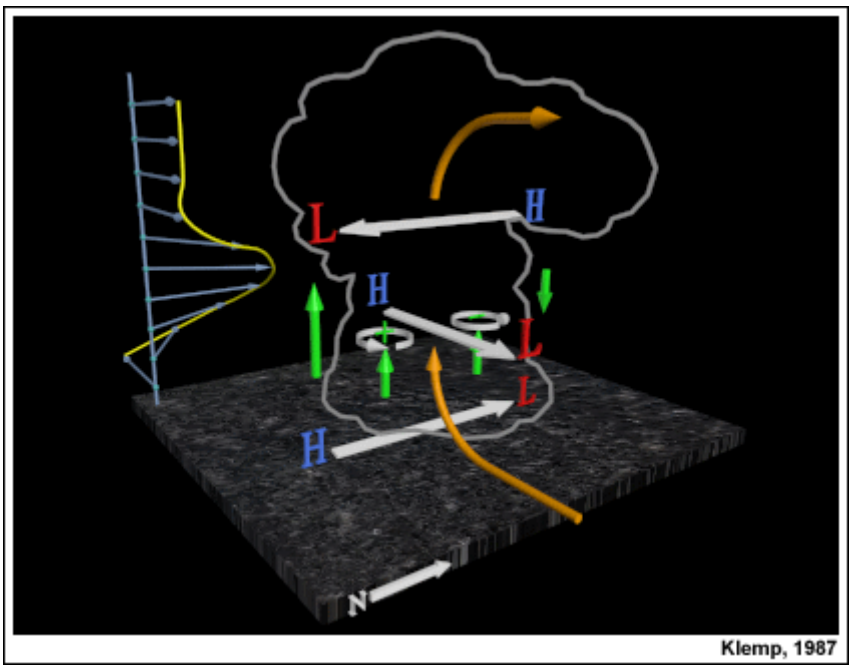

Figure 2.11: *Environmental directional shear displaces the high (H) and low (L) pressure. The source of this material is the COMET® Website at http://meted.ucar.edu/ of the University Corporation for Atmospheric Research (UCAR), sponsored in part through cooperative agreement(s) with the National Oceanic and Atmospheric Administration (NOAA), U.S. Department of Commerce (DOC). ©1997-2014 University Corporation for Atmospheric Research. All Rights Reserved.*

Tornadic storms require one last characteristic, Storm Relative Helicity (SRH). It is a measure of the direction of the inflow (velocity vector) relative to the horizontal vorticity (Davis-Jones, 1984). If the inflow is parallel to the horizontal vorticity tubes (velocity vector aligned with the vorticity vector) and is collocated with the cyclonic rotating updraft, the storm ingests rotating air making it easier to create a mesocyclone and tornado. This is called streamwise vorticity (Davis-Jones, 1984; Markowski et al., 1998). If the inflow is perpendicular to the horizontal vorticity rolls (vorticity vector), it is crosswise vorticity. A high value of SRH indicates more streamwise vorticity as seen in Figure 2.12. The effective storm relative helicity (ESRH) has a varying depth of which the SRH is calculated. It is calculated for the layer in the

sounding that is buoyant, however, not strongly capped. These parameters are all important in predicting whether thunderstorms have the potential to produce rotating updrafts, increasing the potential to become severe, including potential tornadogenesis (Thompson, Mead and Edwards 2007).

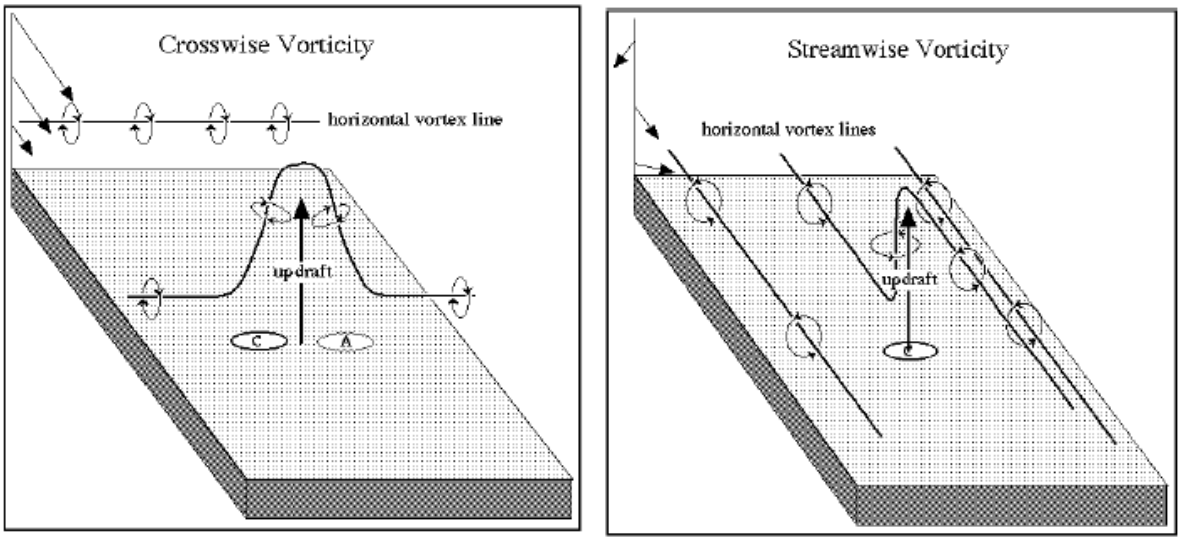

Figure 2.12: *From Doswell, 2000 illustrating crosswise vorticity above and streamwise vorticity below. Copyright © C. Doswell, used with permission.*
http://www.cimms.ou.edu/~doswell/vorticity/vorticity_primer.html

2.5. Alberta Thunderstorm Research

Smith and Yau (1992) describe very specific synoptic patterns leading to three different convective types in Alberta. This research was during the Limestone Mountain Experiment (LIMEX) which was conducted in the lee of the Rocky Mountains to study subsident effects on storm environments (Strong, 1986). Severe convective outbreaks consist of two stages. Stage one is characterized by warm air aloft associated with an upper ridge streaming over the foothills capping convection. Moderate to weak shear is present due to weak flow in the upper ridge and

weak, if any, induced surface upslope flow from a weak mountain-plain circulation. Stage two begins on day two by 1200 local time when the ridge has progressed eastward with most of the foothills ahead of the upper trough as shown in Figure 2.13. Convection initiates off of the foothills with cooling aloft and surface heating contributing to steep lapse rates, large CAPE and deep surface convection. The mountain-plain circulation develops quickly, as shown in Figure 2.14. This results in moisture transport upslope under the cap, enhancing the present convection. With the easterly surface flow and southwest upper flow, this provides ample shear to produce long-lived severe thunderstorms.

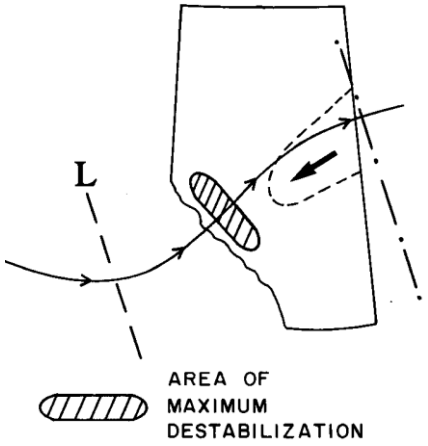

Figure 2.13: *Synoptic pattern leading to a severe weather outbreak in Alberta, from Smith and Yau (1992). ©American Meteorological Society. Used with permission.*

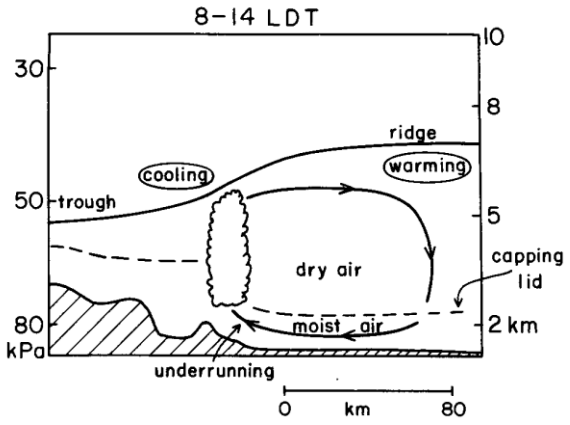

Figure 2.14: *Vertical cross section of the mountain-plain circulation with underrunning of the capping lid from Smith and Yau (1992). ©American Meteorological Society. Used with permission.*

For weak, isolated convection, the upper ridge is positioned over the Alberta-B.C. border with subsidence producing mostly clear skies. Weak easterly winds do develop; however, the main flow is a downslope flow, not only drying through subsidence, but also by advecting higher dew points from the prairie evapotranspiration further east. A slight upslope flow closest to the terrain remains with strong surface heating weakening the cap, and in many cases does manage to initiate isolated, weak thunderstorms along the foothills.

For widespread, moderate convection, an upper shortwave typically tracks over central Alberta in the early morning. In contrast to the severe convection case, the cap as well as the upper flow is weaker. If cloudy skies occur, there would be a lack of strong surface heating, reducing the upslope component of the wind, diminishing the advection of higher dew points into the foothills. However, with an upper trough moving through the area, moderate widespread, convection can be initiated due to steep lapse rates and upper level forcing (e.g. divergence/diffluence aloft) inducing low-level convergence.

An example of 500 hPa and surface synoptic charts from a DC day type are shown in Figure 2.15. The synoptic set up described is an example of what was described by Strong and Smith (2001), in Figure 2.16, as a classical set up for severe thunderstorm development.

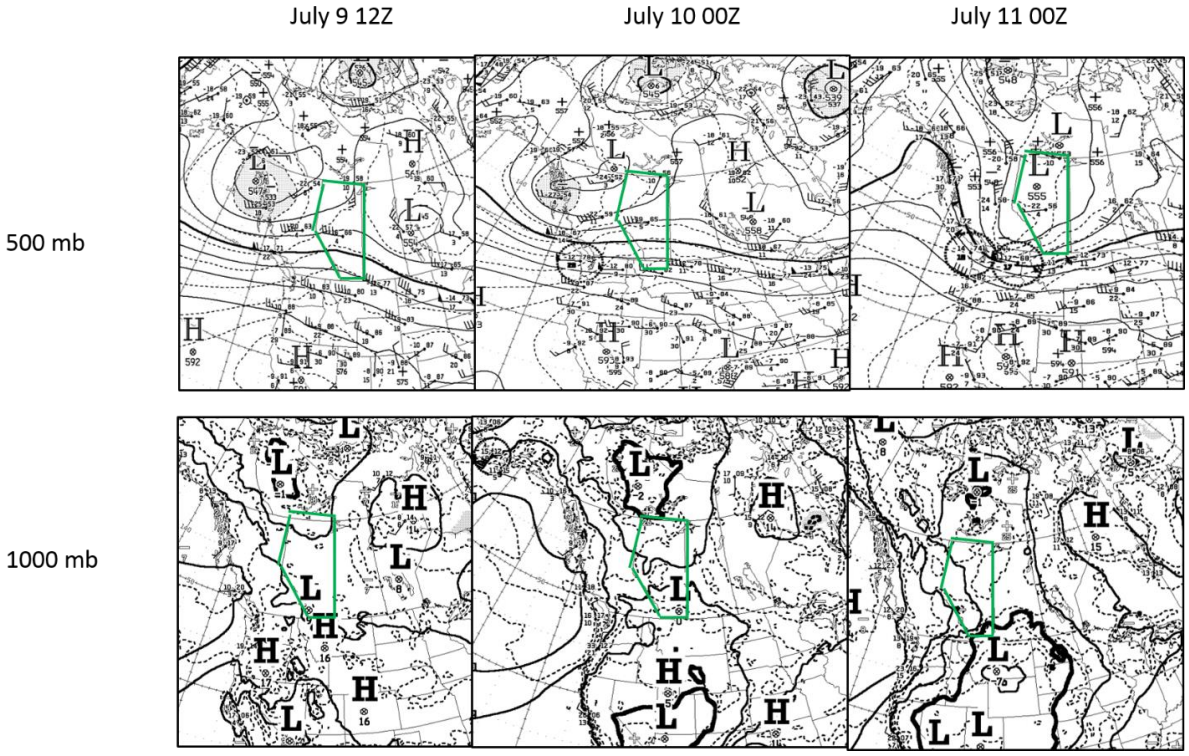

Figure 2.15: *Upper air and surface charts from July 9th and 10th, 2008.*

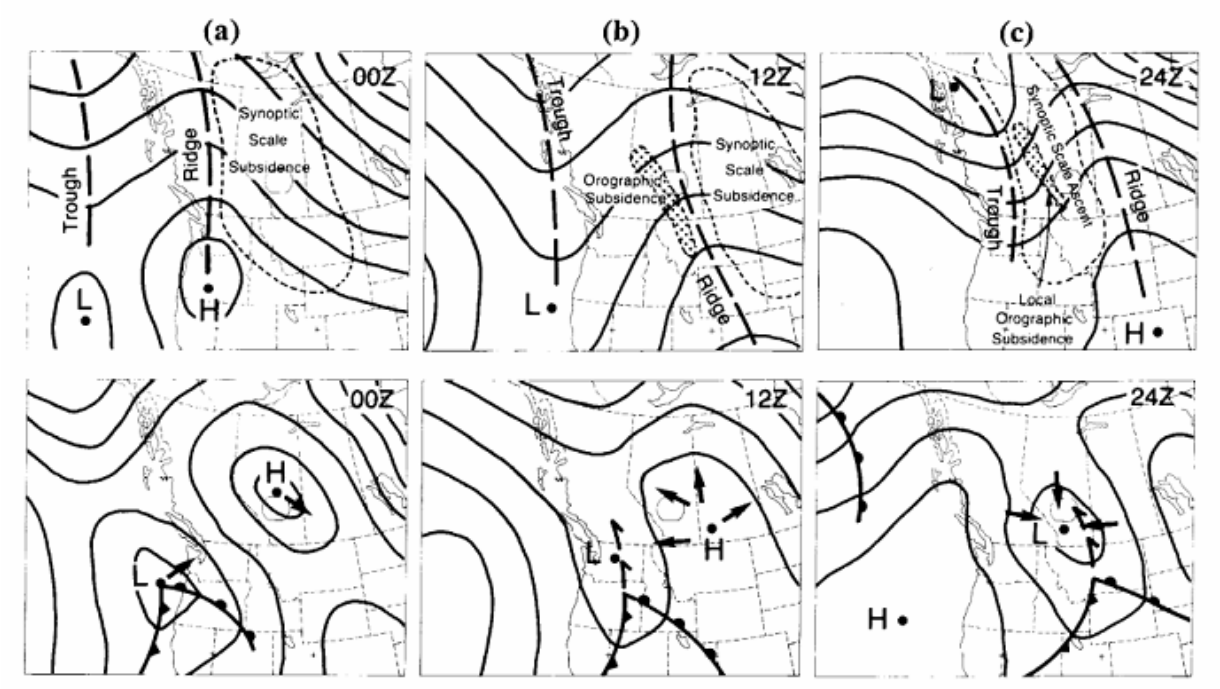

Figure 2.16: *From Strong and Smith (2001) illustrating the synoptic pattern leading to deep convection at 0000 UTC the day before (left), 1200 UTC the morning of (middle) and 0000 UTC (right) at 500 hPa (top) and at the surface (bottom). Reproduced with permission of the Canadian Meteorological and Oceanographic Society.*

Underrunning caused by the mountain-plain circulation, shown in Figure 2.17, was also described by Strong and Smith (2001) as leading to deep convection. It is similar to what was presented in Banta (1984), as an idealized cross sections of the daily evolution of horizontal wind and potential temperature as shown in Figure 2.3. The direction also affected the strength of lift by the terrain. A southeast wind direction is parallel to the terrain, creating little or weak lift, whereas northeast, perpendicular to the terrain would provide stronger lift.

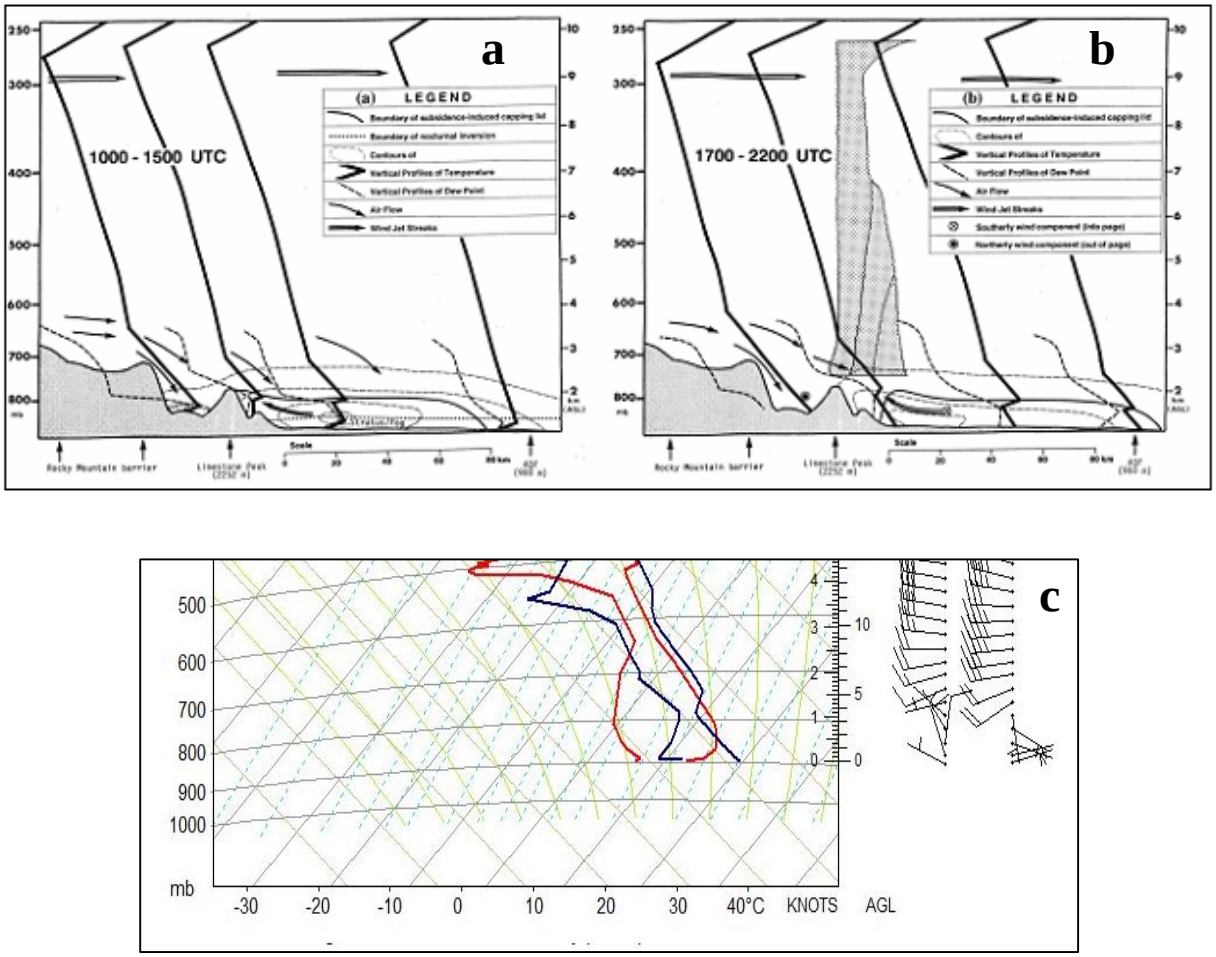

Figure 2.17: *From Strong (2000) (top), illustrating the temporal and special variation of the capping lid in the A.M. (a) and P.M. (b). For comparison, an example from UNSTABLE (bottom); EA3 A.M. (red) and P.M. (blue) composite soundings on July 13th, 2008, a DC day type (c). This sounding is most similar to the sounding example furthest to the east in (a) and (b). Reproduced with permission of the Canadian Meteorological and Oceanographic Society.*

Little (1990) discussed a specific case (Aug 09/90) as described by Smith and Yau (1992) for thunderstorm initiation under weak supporting dynamics in Alberta. She described a low-level southerly flow combined with differential cooling in a weak westerly upper level flow producing weak support for severe weather. Convection initiated over the terrain was enhanced by daytime heating and low-level convergence. These thunderstorms produced severe rainfall.

Chisholm and Rennick (1972) reviewed the initiation environment in the Alberta foothills during the Alberta Hail Project (AHP). It was observed that moderate to strong instability with adequate low-level moisture is necessary for the development of hailstorms.

Marwitz (1972) described initial environmental conditions associated with multi-cell storms during the AHP. Most of the values of convective parameters were similar for multi-cell and supercell thunderstorms. The main characteristic that distinguished between them was the light winds in the sub cloud layer observed in the multi-cell storms.

2.6. Alberta Geography and Land Use Issues

Alberta was once completely covered by glaciers, creating the rugged terrain as seen in Figure 2.18. The southern plains that once was covered with tall grass, is now farmland. In the southeast, badlands of the cypress hills are dry and can sustain little vegetation.

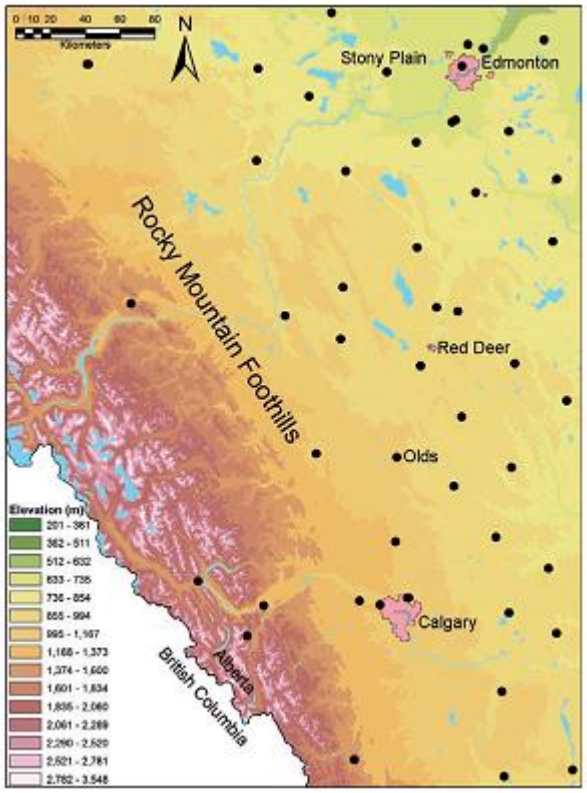

Figure 2.18: *Relief map showing the Edmonton– Calgary corridor, the Stony Plain upper-air station, and existing real-time surface observation locations available to forecasters (black circles). The foothills region is characterized by the transition from lower- lying agricultural areas (east) to the Rocky Mountains (west). Very few real-time surface observations are available over the Alberta foothills. From Taylor et al., (2011) © American Meteorological Society. Used with permission.*

An increase of population has demanded an increase of land use for farming purposes. This has replaced the natural tall grass, with cereals, oilseeds, vegetables and pastures. Each different type of crop has a different effect on the land-atmosphere interaction. Each crop has a different root zone, which alters the potential amount of evapotranspiration (e.g. Hanesiak et al., 2004). Evapotranspiration provides low-level moisture to the dry Alberta BL. This can be the difference between convection occurring or not. Once August and September arrives, grain crops

"head out" and evapotranspiration virtually ceases. In years of low soil moisture, this is reflected in lower hail and thunderstorm frequencies (Strong, 1997; Raddatz, 1998).

The domain of UNSTABLE is located on a sharp transition zone from mixed grass and crop land to the mountains and subalpine (Figure 2.19). This surface variation has a large control on evapotranspiration and as a result the surface energy budget and BL moisture (Hanesiak et al., 2004; Pielke, 2001; Raddatz, 2004).

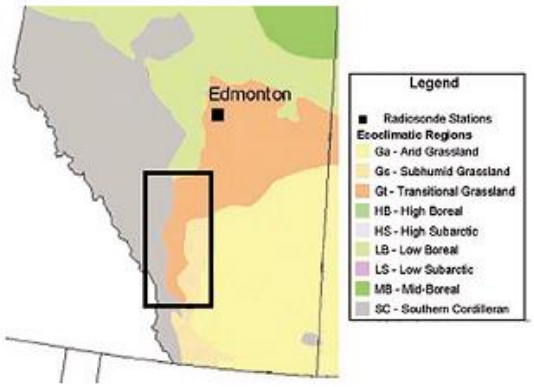

Figure 2.19: *Eco-climate zones or surface types of southern Alberta (Taylor et al., 2008). The black rectangle indicates the eco-climate transition zone. ©American Meteorological Society. Used with permission*

The crop report issued by Alberta Agriculture (2008) (not shown) indicated that the UNSTABLE field domain received at least near normal precipitation accumulation from April 1 to July 19, 2008, as compared to the 1961-2008 normal, with much above normal in many southern areas. This would indicate that moisture, including soil moisture, was not a limiting factor in the potential evapotranspiration from the vegetation in the area of study. This is important as it contributes to the moisture gradients that form due to surface type variations. These gradients are responsible for mesoscale circulations that create low-level convergence and

moisture availability contributing to thunderstorm initiation and development or severity (Segel et al., 1989). Surface moisture was 86% in the good to excellent category.

Spring wheat and canola, make up a large percentage of the crop in the central region, and were 68% and 61% in the good to excellent condition respectively. Evapotranspiration can be inferred from the NESDIS Center for Satellite Applications and Research images as seen in Figure 2.20 to Figure 2.23**.** These images are derived from satellite observations, biophysical theory of vegetation, response to the environment, data processing and interpretation. The moisture and thermal stress images confirm the crop report indication that moisture was not a limiting factor in growth of crops in the Alberta foothills region in 2008. For reference, 2007 and 2009 have been included. In 2009, moisture may have been a factor limiting plant growth. The VHI, or vegetation health index, is a combined measure of thermal and moisture stress to estimate vegetation health. VHI is in the 60-100 category, indicating plentiful production was expected. The Normalized Difference Vegetation Index (NDVI) showed all three years in the 0.65 category, indicating at this time of year, the crops were in prime phenological stage, implying maximum evapotranspiration was possible.

The typical large gradient in soil moisture from central to southern Alberta was not obviously apparent due to above normal precipitation in the spring and summer of UNSTABLE 2008. This could have led to weaker than normal soil moisture-enhanced/induced mesoscale effects on convection initiation in 2008 (Taylor et al., 2008).

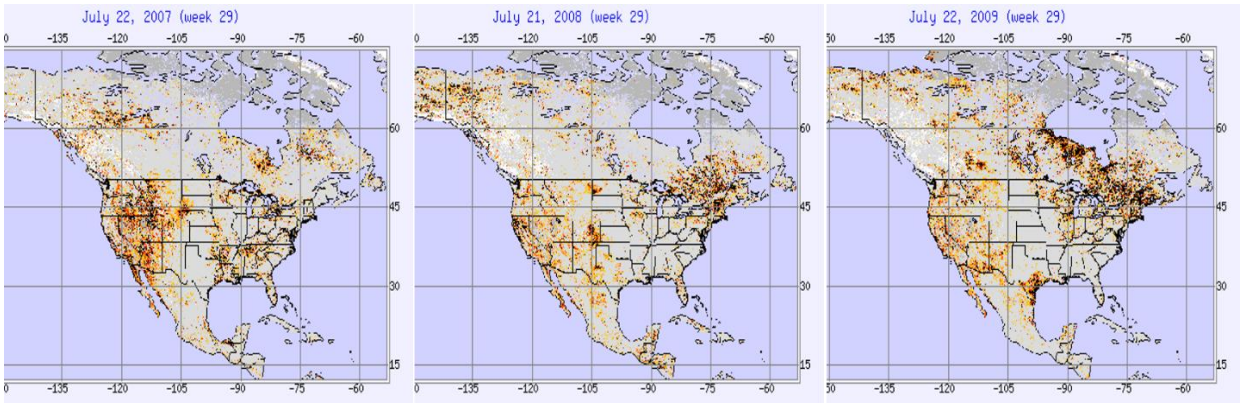

Figure 2.20: *Moisture stress for week 29 2007 (left), 2008 (middle) and 2009 (right). © NOAA/NESDIS Center for Satellite Applications and Research.*

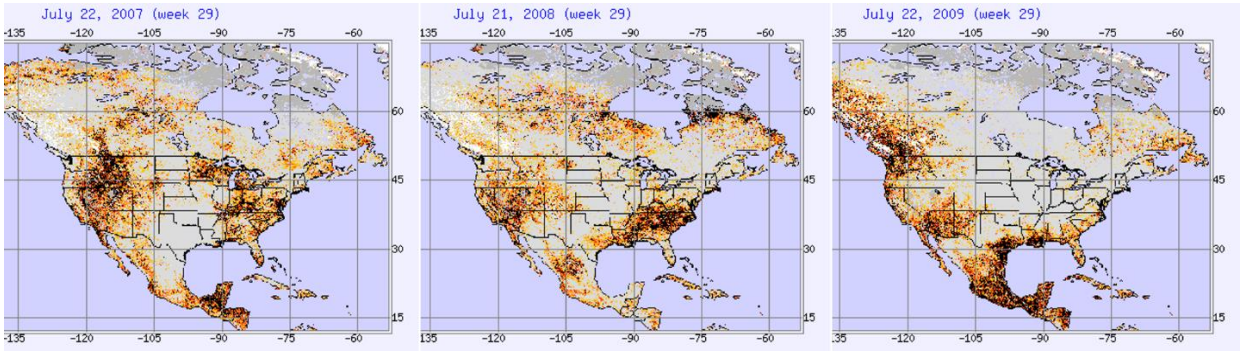

Figure 2.21: *Thermal stress for week 29 2007 (left), 2008 (middle) and 2009 (right). © NOAA/NESDIS Center for Satellite Applications and Research*

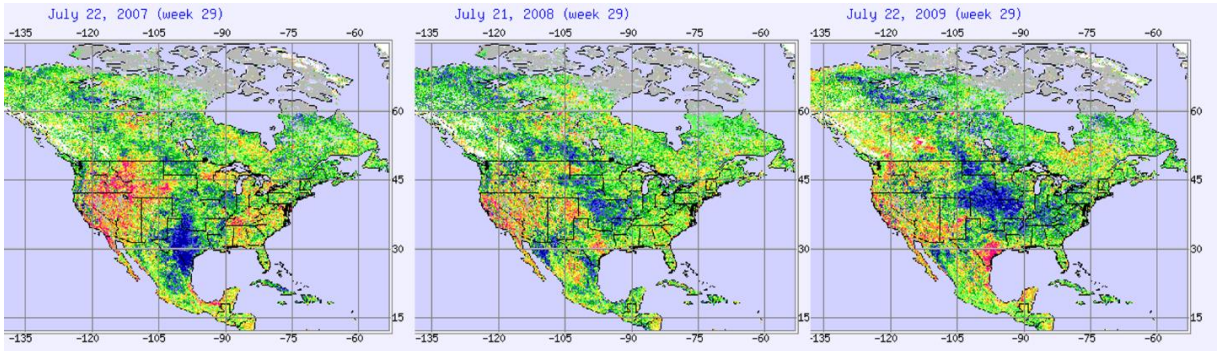

Figure 2.22: *Vegetation Health Index for week 29 2007 (left), 2008 (middle) and 2009 (right). © NOAA/NESDIS Center for Satellite Applications and Research*

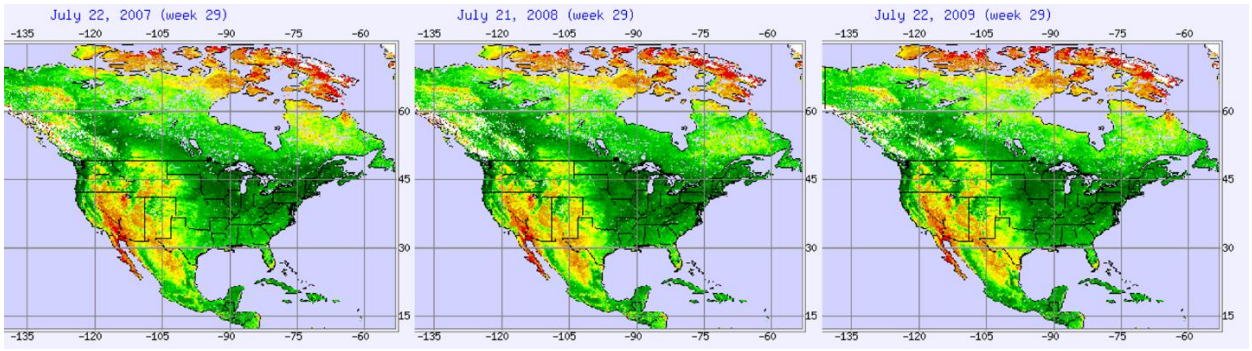

Figure 2.23: *NDVI Greenness for week 29 2007 (left), 2008 (middle) and 2009 (right). © NOAA/NESDIS Center for Satellite Applications and Research*

CHAPTER 3

3. DATA AND METHODOLOGY

3.1. UNSTABLE Field Campaign Location Description

This chapter will describe the locations of radiosonde launches, data sources and analysis methods used to characterize convection and the Alberta boundary layer. Four sounding sites were used in this analysis. Two sounding were released from Olds-Didsbury, AB (EA3); 51.78°N and 114.1°W and Water Valley AB (WVX); 51.8°N and 113.58°W. Two additional soundings were mobile and were therefore launched according to the dominant weather feature of the day. For example, on either side of a dry line. The four UNSTABLE sounding launch sites were anywhere from 30 to 150 km apart. WVX was located in a forested surface type, which would be characteristic of a lower albedo, higher sensible energy and therefore, lower evapotranspiration. The second stationary site, EA3, was within an agricultural land cover type which would display a higher albedo and larger evapotranspiration. MB2 was usually placed in a cropped or grassland area, while MB1 was typically placed in a foothill Boreal Forest area; occasionally this was not the case (see APPENDIX A for site locations for each Intensive Observation Day (IOD)).

Each site had a different number of launches each day, again depending on how many were required by the Principal Investigators (PIs) to best resolve the weather phenomena of the day. IODs consisted of 2 hourly soundings from 1200 to 0000 UTC. On days that were not deemed as IODs, soundings were done less frequent; one or two in the morning to gauge the state of the atmosphere from one or two sites. There were eight IODs in total. Each IOD was

associated with a specific weather feature or phenomenon that was expected to be the main weather focus for the day, as seen in Table 3.1.

Table 3.1: *Summary of Missions including date, focus and IOD number. WVG refers to a Water Vapor Gradient mission and CI refers to a Convective Initiation mission (Taylor et al., 2008).*

IOD	DATE	FOCUS
1	July 9, 2008	Dryline
2	July 12, 2008	BL moisture gradient due to soil moisture differences (WVG1)
3	July 13, 2008	Dryline
4	July 14, 2008	Dryline
4a	July 15, 2008	CI1 *Partial operations
5	July 17, 2008	CI2
6	July 20, 2008	BL moisture gradient due to vegetation differences between cropped and forested surfaces (WVG2)
7	July 21, 2008	CI3
8	July 22, 2008	CI4

The location of instrumentation used during the field campaign is shown in Figure 3.1 below.

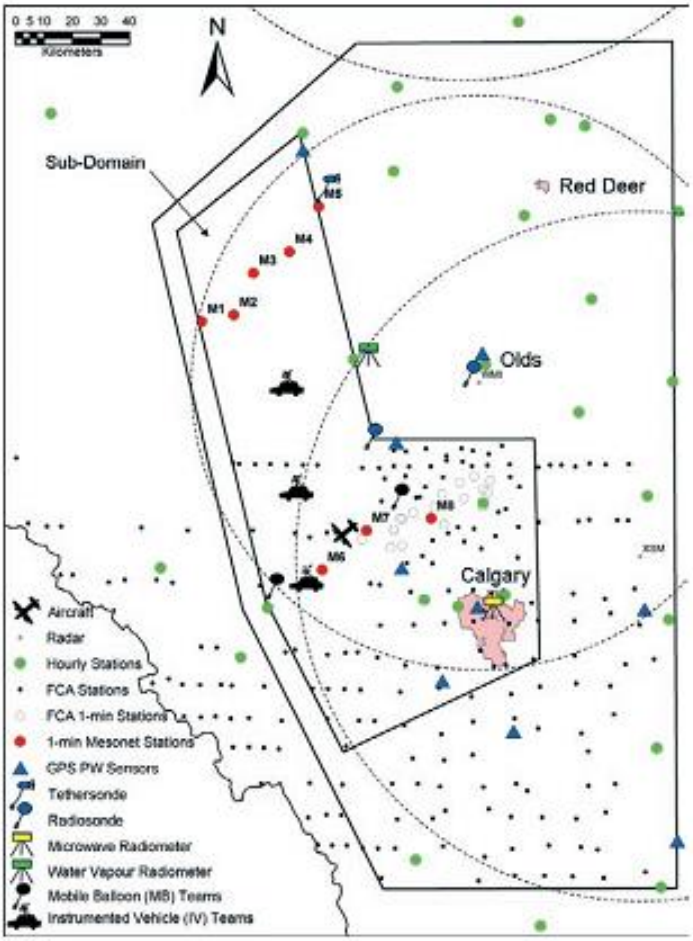

Figure 3.1: *UNSTABLE Instrumentation map from (Taylor et al., 2008). ©American Meteorological Society. Used with permission*

3.2. Data Sources

The Environment Canada and NavCanada operational observation network was supplemented by networks unique to UNSTABLE. Of relevance to this thesis, they include fixed and mobile radiosondes, mentioned previously, and the UNSTABLE surface network made up of Automated Transportable Meteorological Observing Systems (ATMOS). Surface data from the

UNSTABLE surface network were only available during IODs. For non IODs, surface data were augmented by surface maps from the National Weather Service (NWS) Storm Prediction Center (SPC). These data were not as high resolution as data obtained from the UNSTABLE network. Satellite data were provided by Environment Canada. Radar data were provided by Weather Modification Incorporated (WMI) and Environment Canada. Upper air isobaric analysis charts were obtained from the Environment Canada and NWS SPC.

The radiosonde data used in this analysis are from Vaisala model RS92-SGP sondes. The sonde is attached to a helium filled weather balloon which ascends to an estimated 25 km above the surface. They record in-situ measures of temperature, moisture and pressure. The GPS instrumentation triangulates the balloon's position to record wind speed and direction. The measurements are relayed to the surface instrumentation by radio waves. Radiosonde limitations are provided in Table 3.2 (McAuley-Weber, 2013).

Table 3.2: *Limitations of Vaisala radiosonde*

Sensor limitations	Response time	Resolution	Accuracy
Temperature	<1s (up to 100 hPa)	0.1 °C	0.5 °C
Humidity	<0.5s (+20 °C) < 20s (-40 °C)	1% RH	5%
Pressure	N/A	0.1 hPa	1 hPa

Soundings were corrected for moisture biases from the instrumentation as recommended by Miloshevich et al. (2009). Soundings identified as requiring moisture correction was based on cloud observed at each location; if 5/10 of cloud or less was observed, then dew point correction

was required. This model of the Vaisala radiosonde produces a moisture bias as a function of height and time of day. Miloshevich et al (2009) created an empirical relationship to correct for this bias. Soundings were identified by McAulay-Weber (2013) as requiring the moisture correction or not.

3.3. Data Analyses

Days were categorized into three convective day types; nil convection (NC), shallow convection (SC) and deep convection (DC) days. This was done initially using satellite. If there was no convective cloud, this was deemed an NC day, if there was scattered cumulus or towering cumulus with no severe reports, this was deemed a shallow convective day. Lastly, if there was widespread towering cumulus and thunderstorm signatures such as overshooting tops or shadows indicating tall updrafts, this was deemed a deep convective day. Radar and lighting data were then used to discern between shallow and deep convective days. Standard synoptic charts were also used to confirm day type. For example, a synoptic surface ridge further confirmed a non-convective day. The threshold from A.M. to P.M of 1800 UTC, or 12 P.M. MDT was used. Alberta observes daylight savings time and therefore their conversion from UTC to local is UTC-6 hours.

3.3.1. Remote Sensing Analysis

3.3.1.1. Satellite

Satellite images were obtained from Environment Canada. The satellite used was the Geostationary Operational Environmental Satellite (GOES). Imagery was available a maximum of every 15-minutes. Water vapor imagery was used to get an overall top down view of the upper atmosphere. It can be used to infer large synoptic scale flow such as low pressure, high pressure,

jet streaks, troughs and ridges. Visible satellite imagery was analyzed to infer smaller mesoscale phenomenon such as boundaries and convective initiation and development.

3.3.1.2. Radar

Radar analysis was completed using Environment Canada's Strathmore (XSM) and Weather Modification Inc. (WMI) radars for the entire two week period, July 7-23 2008. XSM included more detailed radar information including Doppler velocity data and Environment Canada operational algorithms. Data were gathered on convective initiation location, storm tracks, convective development and severity.

3.3.2. Synoptic analysis

Upper air and surface analyses of each day was completed using archived analyzed upper air maps at standard meteorological levels (250, 500, 700 and 850 hPa) and times (0000 and 1200 UTC) using Environment Canada's CMC's standard suite of synoptic maps and the NWS SPC archive map page. The NWS SPC archive reaches as far north as about 54°N. The SPC maps use the NAM 0600 and 1800 UTC as a first guess for the analysis of temperature, dew point and pressure. Observations of baroclinic zones, wind maximums (jets), low and high pressure centers and troughs and ridges helped to better characterize each case in this thesis.

3.3.3. Sounding analysis

All sounding analysis was done using the RAwinsonde OBservation Program (RAOB) software. Convective sounding parameters were calculated for all soundings. They were all chosen due to their availability in RAOB and relevance to operational meteorology. They were analyzed using two methods; by day type (nil, shallow and deep convective days) and by time of day (A.M. and P.M.).

Composite or average soundings were created using the merge function available in RAOB. Composite soundings were created for each day type (nil, shallow or deep convective day) and time of day (A.M. and P.M.), for each site and for individual days. The P.M. composite soundings were used when describing convective potential. The number of soundings used to create composites for each day type is provided in Table 3.3 and by site in Table 3.4. The populations of NC day type and some sites by A.M. and P.M are smaller than 30. However, all data were statistically tested and was found to be normally distributed.

***Table 3.3**: Number of soundings in each day type composite and used for statistical comparisons.*

Day Type	Daily	A.M.	P.M.
DC	71	39	32
SC	64	31	33
NC	44	24	20

***Table 3.4:** Number of soundings at each site used in statistical comparisons.*

Site	Daily	A.M.	P.M.
EA3	50	28	22
WVX	58	38	20
MB1	41	16	25
MB2	30	12	18

Soundingrams or profiles of individual sounding measurements were created for temperature (°C), equivalent potential and potential temperature (K), mixing ratio (g kg^{-1}), dew point (°C), wind speed (kt) and direction (°). Temperature, dew point, wind speed and direction were chosen due to their relevancy in operational meteorology and ease of access. Equivalent potential temperature was chosen due to its conserved nature and its incorporation of moisture and temperature (instability) within one parameter. Mixing ratio and potential temperature were chosen due to their use in other academic papers of relevance. These plots were created in RAOB's soundingram display.

3.3.4. Statistical Analysis

All data were tested using a K-S one-sample test to determine normality. It was determined that all of the data were normal, however, at different significance levels; 0.05, 0.1 and 0.2. Hypothesis tests, F tests and Student's T tests were performed to quantitatively compare the P.M. severe weather parameters by day type; deep convective (DC) versus shallow convective (SC) versus nil convective days (NC). The F Test returns the two-tail probability, or p-value, that the variances between two arrays are not significantly different. Once it was determined whether the variances were different or not, the two-tail, two-sample student's T Test; either assuming equal or unequal variances, was used to determine whether the two arrays had different means. It also returns a p-value. The hypotheses used were:

$\mu = m$ - The null hypothesis; no statistical difference in the variances/means

$\mu \neq m$ - The alternative hypothesis; a statistical difference in the variances/means

Hypothesis testing does have inherent weaknesses (Potvin, 2010). For example, rejecting the null hypothesis only occurs when sufficient evidence to reject it has been found. A statistical difference may exist, however, it may not be a meaningful difference.

The significant levels chosen were 0.1 and 0.2. They were identified by Hanesiak and Wang (2005) as being acceptable for climate studies. In addition, 0.05 was also used due to its prevalence in other research. A resultant p-value less than the significance level results in the rejection of the null hypothesis and a statistical difference exists between the two samples' means or variances. A p-value greater than the significance level, results in not rejecting the null hypothesis and no difference exists between the two samples' means or variances. Throughout the thesis, these significance levels will apply to specific data due to their normality at that level.

Box and whisker plots were created to better illustrate the spread of the data between the convective regimes. Comparing the results from the statistical tests to the box and whisker plots made for better interpretation of the differences between day types and time of day. This was also a method utilized in other research that will be incorporated into this analysis to further describe UNSTABLE results.

F Tests and T Tests were also used to determine the statistical difference in variances and means between sounding data at different sounding locations, or eco-climate zones. It was accomplished by comparing the measurements of temperature, specific humidity, wind speed and direction using two methods. The first method was comparing p-values from the entire sounding profiles between days and sites. The second method was comparing p-values at individual pressure levels between the sounding data measured at individual sites. Pressure level data were tested for normality at all standard pressure levels (850, 700, 500 and 250 hPa). By

completing two different methods, the differences between sites can first be identified, using the entire profile. Then by focusing on pressure levels, specific levels of the atmospheric profile that are different or similar can be identified. This analysis is similar to the analysis completed in McAulay-Weber (2012). Refer to McAulay-Weber (2012) for full number of samples for each pressure level. Soundings used in this analysis are displayed in Table 3.5.

Table 3.5: *Soundings used in statistical calculations. Summary of radiosonde launch date and times by location. Times (hours) are in UTC. Only the first two digits are shown for ease of visualization. 6 soundings not listed for MB2 due to unknown dates and times. ()=meets requirements to be used for corrected Vs Uncorrected. Bold times=used corrected. * not included in analysis, missing raw data. WVX was always located in the forest and EA3 was always located in crop. For each IOD the table below indicates if the mobile sites were located in either forest (F), crop (C) or on the transition zone (T). CO represents soundings corrected and UC uncorrected for moisture bias as described in section 3.2.*

DATE	MB1		MB2		EA3	WVX
	Hour (UTC)	Crop/Forest Surface Type	Hour (UTC)	Crop/Forest Surface type	Hour (UTC)	Hour (UTC)
July 7	22*					15*, 17*
July 8	19*				22*	16*
July 9 (IOD1)	16,17,19,21,**23**	F			11*, 13*	11*, 13*, **(15), (17), 19,** 21, 23
July 10					11*	11*
July 11			18*			11*
July 12 (IOD2)	**13,** 15, 17, **(19), 21, 23**	C	13*, 15, 17, 19, **21, 23**	C	13*, 15, 17, 19, **(21), (23)**	
July 13 (IOD3)	16*, 17*, **(19), 21,** 23	F	**(16),** 17, 19, **(21), (23)**	T	11*, 14*, 15, **20**, 21, 23	11*, 13*, 15, 17, 19, 21, 23

Table 3.6: *Soundings used in statistical calculations. Summary of radiosonde launch date and times by location. Times (hours) are in UTC. Only the first two digits are shown for ease of visualization. 6 soundings not listed for MB2 due to unknown dates and times. ()=meets requirements to be used for corrected Vs Uncorrected. Bold times=used corrected. * not included in analysis, missing raw data. WVX was always located in the forest and EA3 was always located in crop. For each IOD the table below indicates if the mobile sites were located in either forest (F), crop (C) or on the transition zone (T). CO represents soundings corrected and UC uncorrected for moisture bias as described in section 3.2.*

DATE	MB1		MB2		EA3	WVX
	Hour (UTC)	Crop/Forest Surface Type	Hour (UTC)	Crop/Forest Surface type	Hour (UTC)	Hour (UTC)
July 14 (IOD4)	16, **17**, 19, **(21), (23)**	F	12*, 14*, 16	F	11*, 13*, **15**, 18*, **19**, 21, **(23)**	11*, 13*, **15, 17, 19**, 21, 23
July 15						11*
July 16					12*	11*
July 17 (IOD5)	16, 17, **19, 21, 23**	F	17, 19, **21, 23**	F	12*, 13, 15, 19, 21, **(23)**	11*, 13*, 15, 17, 19, **21**, 23
July 18					11*	11*
July 19						11*, 14*
July 20 (IOD6)	15, 17, 19, 21	F	15, 17, 19, 21	C	11*, 13*, 15, 17, 19, 21	12*, 14*, 15, 17, 19, 21
July 22 (IOD8)	16, 17, **19, 21, 23**	C	**16,** 17*, **19, 21, 23**	F	11*, 13*, 15, 18, 19, 21, **23**	11*, 13*, **15, 17, 19, 21, 23**
July 21 (IOD7)	17, 19, 21, 23	T	17, 19, 21, 23	C	11*, 13*, 15, 17, 19, 21, 23	11*, 13*, 15, 17, 19, 21, 23
Total used for CO vs UC	6		3		3	2

Table 3.7: *Soundings used in statistical calculations. Summary of radiosonde launch date and times by location. Times (hours) are in UTC. Only the first two digits are shown for ease of visualization. 6 soundings not listed for MB2 due to unknown dates and times. ()=meets requirements to be used for corrected Vs Uncorrected. Bold times=used corrected. * not included in analysis, missing raw data. WVX was always located in the forest and EA3 was always located in crop. For each IOD the table below indicates if the mobile sites were located in either forest (F), crop (C) or on the transition zone (T). CO represents soundings corrected and UC uncorrected for moisture bias as described in section 3.2.*

DATE	MB1		MB2		EA3	WVX
	Hour (UTC)	Crop/Forest Surface Type	Hour (UTC)	Crop/Forest Surface type	Hour (UTC)	Hour (UTC)
Total CO Used	16		11		8	12
Total used in Analysis	37		27		32	34
Total soundings	41		36		51	58

CHAPTER 4: RESULTS

4. BOUNDARY LAYER EVOLUTION

4.1. Overview

This chapter focuses on the first thesis sub-objective "Characterizing the daily evolution of the boundary layer during different convective regimes throughout the intensive observation period of the UNSTABLE field campaign". The distance between the sites and the surface characteristics in which they were placed will cause differences in the soundings' evolution of the boundary layer. First, BL composite tephigrams of the entire IOP is presented for the two stationary sites; EA3 and WVX. This is followed by an analysis by day type; Non-Convective Days in Section 4.2, Shallow Convective Days in Section 4.3 and Deep Convective Days in Section 4.4. In Section 4.5, two statistical methods are used in an attempt to distinguish between eco-climate zones and their effect on the BL. A synoptic overview for each day type of the UNSTABLE region using supplemental metrological data will be presented first to give context to the potential differences between day type. Boundary layer comparisons between composites of meteorological parameters will be presented by time of day and site, using individual days as examples. The non IOD's launched fewer soundings usually from fewer sites. They will be used as supplemental data to add to the IOD BL evolution analysis. Lastly, forecasting applications of boundary layer evolution analysis are described.

The overall boundary layer evolution for the entire IOP is illustrated in Figure 4.1 and Figure 4.2. These figures display evolution in the boundary layer over the course of the day. The most prominent feature to note is the nocturnal inversion in the first two soundings at both EA3

and WVX which eroded between 1500 to 1600 UTC. This indicates that this was a feature that was present throughout the entire field project. The soundings displayed are in 2 hourly intervals, demonstrating how rapidly conditions change, indicating the need for higher resolution observations to not just resolve changes in horizontal space, but also in time. In the afternoon, the low-levels at both sites become dry adiabatic with a switch in wind direction from southwest to south at WVX and to southeast at EA3. Another difference between the sites was an increase in low-level wind speed in the afternoon EA3 sounding, not observed at WVX. The moisture at EA3 became deeper in the afternoon whereas at WVX it seemed to remain contained to the surface layer. This may be reflective of the surface type difference between the sites and/or due to EA3 being located slightly further east than WVX. At WVX, with a boreal forest surface type, evapotranspiration is less than what occurs over a crop surface. With less moisture, sensible heating is larger, creating a deeper afternoon mixed layer, diluting this already limited moisture, but displaying a persistent layer of surface moisture. In contrast, EA3, in the crop and grassland surface type, has higher evapotranspiration. Higher latent heating reduces the sensible heating and therefore the depth of the boundary layer, preventing the dilution of the moisture. A higher magnitude of moisture may then extend deeper into the column.

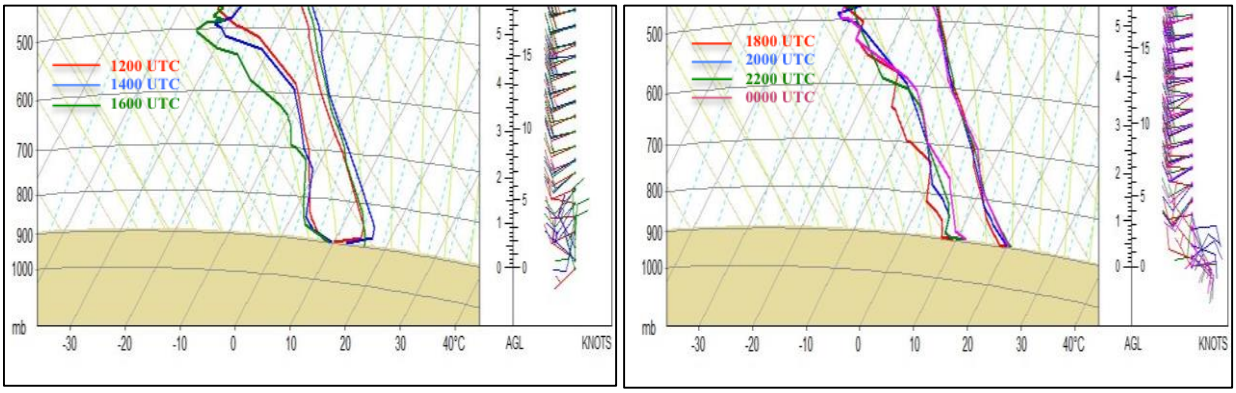

Figure 4.1: *Tephigrams of composite soundings by hour from July 7-23, 2008 at EA3 with soundings before 1800 UTC (left) and soundings after 1800 UTC (right). Times are 1200 (red), 1400 (blue), 1600 UTC (green) on the left and 1800 (red), 2000 (blue), 2200 (green) and 0000 UTC (pink) on the right.*

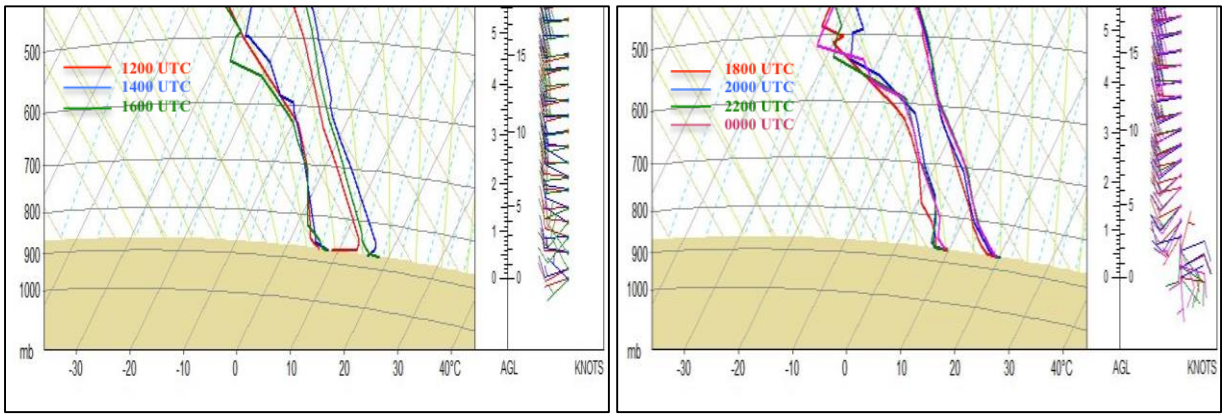

Figure 4.2: *Tephigrams of composite soundings by hour from July 7-23, 2008 at WVX with soundings before 1800 UTC (left) and soundings after 1800 UTC (right). Times are 1200 (red), 1400 (blue), 1600 UTC (green) on the left and 1800 (red), 2000 (blue), 2200 (green) and 0000 UTC (pink) on the right.*

To give an overall illustration of the BL evolution of the three day types at each site, the composites of θ over the IOP are presented in Figure 4.3. Surface θ increases significantly with the layer just above the surface, decreasing with height in the afternoon, indicating increasing instability. This unstable layer is more unstable in the DC day type case as compared to the SC

day type case. The SC day type case has a stable layer at 2 km (or 700 hPa) that is more evident at WVX and MB2. NC day types have higher θ throughout the column with a much shallower layer of decreasing θ just above the surface. Within the following sections, examples from individual days representing typical scenarios will aid in further characterizing BL evolution.

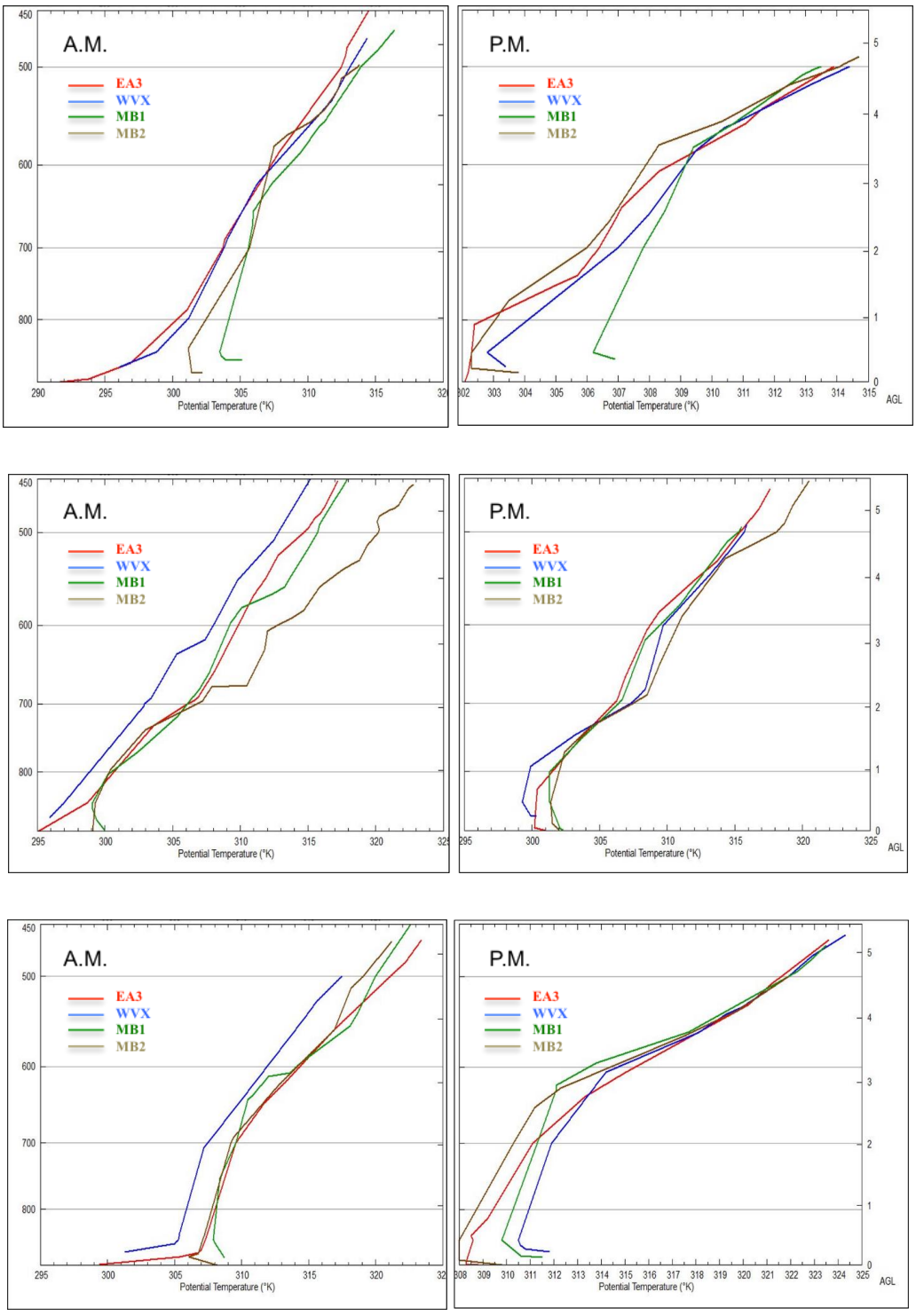

Figure 4.3: *θ Profiles of day type composites for DC days (top), SC days (middle) and NC days (bottom) by A.M. (left) and P.M. (right). Individual sites are displayed with EA3 in red, WVX in blue, MB1 in green and MB2 in brown.*

4.2. Non-Convective Day Type (NC)

Upper levels were usually characterized by a ridge of high geopotential heights at 250 and 500 hPa with associated increasing 1000-500 hPa thicknesses. Ridging was also present in the middle and lower-levels at 700 and 850 hPa over the Rocky Mountains following a departing low. These features are not conducive for convective initiation. The 850 hPa geopotential heights displayed a weak north to south trough of low heights through central Alberta. A thermal ridge straddled the Rocky Mountains. A weak surface low pressure system usually tracked from the southern foothills to the southeast, with ridging over the northern Rocky Mountains. In some cases radar indicated anomalous propagation (AP) indicating a stable boundary layer.

In Figure 4.4 the overall evolution of the boundary layer throughout the field project of NC day types is shown. It is evident that the EA3 and WVX sites have stronger nocturnal inversions than MB1 and MB2. This is simply due to the time of the A.M. soundings; EA3 and WVX had 1200 UTC soundings whereas MB1 and MB2 usually did not launch their first soundings until 15-1600 UTC and therefore, did not capture the nocturnal inversion. As seen in EA3 and WVX, the nocturnal inversion was eroded before 1800 UTC. In the P.M. composites of the different sites, it is evident that low-level lapse rates (below 1 km) are steeper and more similar between MB2 and WVX. Since WVX was near the forest -crop transition zone, its boundary layer characteristics would be strongly influenced by low-level wind direction. In the composite tephigrams in Figure 4.4, the WVX wind direction is south to southeast. This may indicate that the boundary layer may be exhibiting characteristics found in the crop surface type, which would make them similar to MB2, which was more frequently located in the crop surface type. Low-level lapse rates at EA3 and MB1 are similar, however, weaker than MB2 and WVX. EA3 and MB1 seemed to have a higher magnitude of moisture confined to the low-level than

MB2 and WVX. EA3 being located in the crops was expected to exhibit a higher magnitude of low-level moisture due to higher evapotranspiration. MB1, usually located in the forest, would have less evapotranspiration and would be expected to show a lower magnitude of low-level moisture. However, since MB1 was located in the crop region two out of the eight IODs, the cause for their higher magnitude of low-level moisture may be difficult to interpret.

Low-level winds in the afternoon only slightly backed from southerly to south-southeasterly for NC days. This could indicate that NC day types had a weaker mountain-plain circulation resulting in possibly less moisture advection and upslope lift.

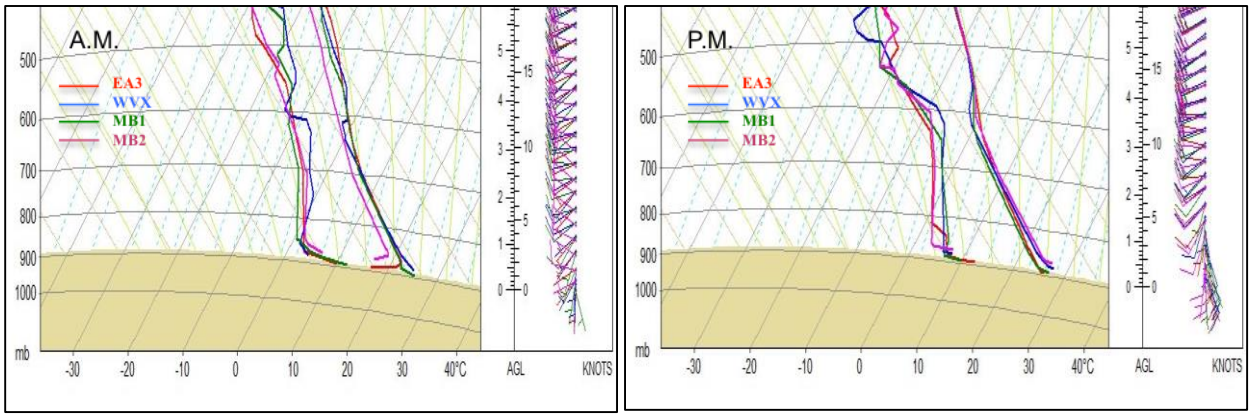

Figure 4.4: *Tephigrams of composite soundings by A.M. (left) and P.M. (right) by site EA3 (red), MB1 (green), MB2 (blue) and WVX (pink) for the NC day type.*

There was a large diurnal boundary layer temperature change of about 15°C at WXV and EA3 but only a diurnal variation of 4°C at MB1 and MB2. This could be due to the lack of early morning soundings before 1500 UTC at MB1 and MB2. MB1 and MB2 had inversions present at about 600 hPa or 3.7 km. EA3 and WVX displayed these inversions on some but not all NC days and when they were observed, they were not as strong as those observed at MB1 and MB2. This

could be due to the fact that MB1 and MB2 were usually located closer to the terrain, and therefore, would experience stronger subsidence, creating a stronger mid-level subsident inversion. The mid–level inversions combined with upper level warming act inhibit convection. Below the inversion, in the boundary layer, most soundings exhibited dry adiabatic lapse rates in the afternoon. Examples are of these are illustrated in Figure 4.5, with circles highlighting the nocturnal and subsident inversions. Mixing depths ranged between sites from MB1 having the deepest on June 21st up to 550 hPa or 4 km and shallowest mixing depth at MB2 on the 20th up to 785 hPa or 1.1 km.

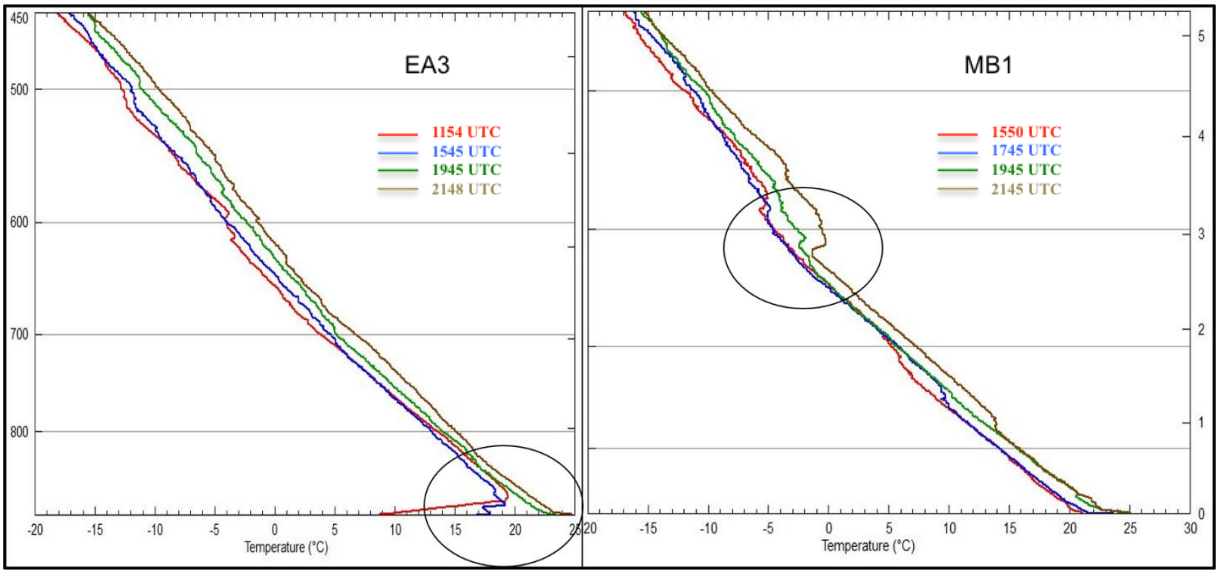

Figure 4.5: *Temperature profiles of EA3 (left) and MB1 (right) on July 20th, 2008 at 2-3 hourly intervals with pressure in hPa and height in m AGL on the y-axes and temperature in °C on the x-axis. The profile colors for EA3 are 1154 (red), 1545 (blue), 1945 (green), 2148 UTC (brown) and for MB1 1550 (red), 1745 (blue), 1945 (green) and 2145 UTC (brown). Winds at MB1 at 3 km associated with the subsident inversion were westerly and the dew point depression increased throughout the day.*

EA3 on July 20 in Figure 4.6, is shown as an example of an NC day type. It displayed a large surface increase in θ_e, of almost 25-30 K. MB1 is shown in Figure 4.7 for comparison. Just off

the surface all sites exhibited an increase of about 10 K. Above the boundary layer there was an increase between the sites of only 2-4 K. θ indicated decreasing values (increasing instability) in the near surface layer, however, it was very shallow with neutral stability for a large portion of the layer below 700 hPa with increasing values (increasing stability) above this level. The surface wind direction indicated an early shift from west to east at EA3 and a consistent easterly surface wind at MB1.

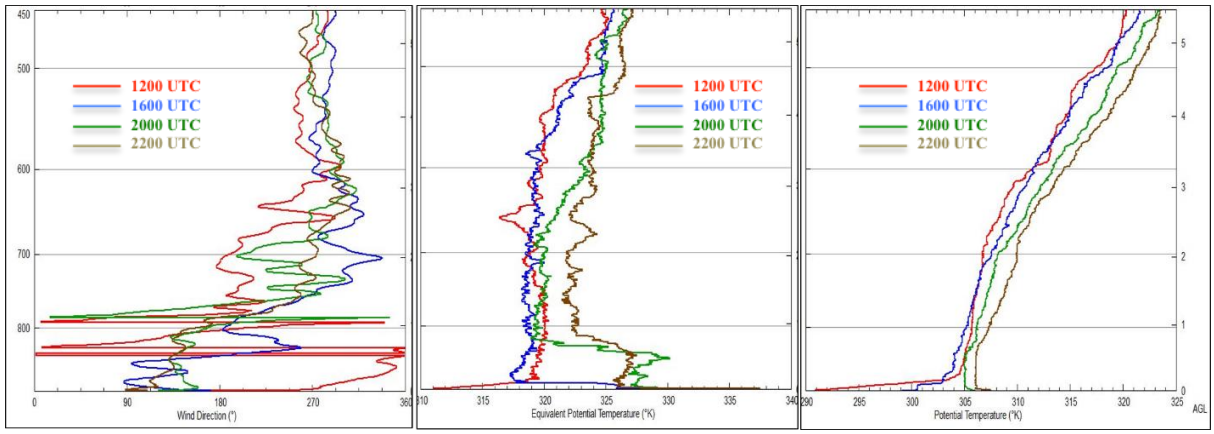

Figure 4.6: *Profiles of wind direction in ° (left), θ_e in K (middle) and θ in K (right) from 4 hourly soundings at EA3 on July 20, 2008. Y-axes are pressure in hPa and height in m AGL. Times are 1200 (red), 1600 (blue), 2000 (green) and 2200 UTC (brown).*

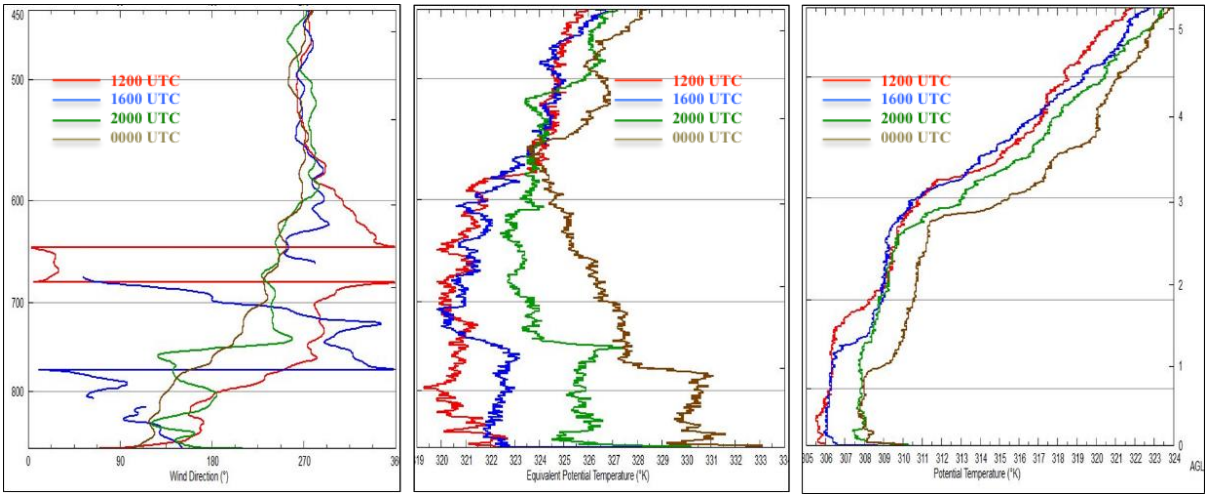

Figure 4.7: *Profiles of wind direction in ° (left), θ_e in K (middle) and θ in K (right) from 4 hourly soundings at MB1 on July 20, 2008. Y-axes are pressure in hPa and height in m AGL. Times are 1200 (red), 1600 (blue), 2000 (green) and 0000 UTC (brown)*

Generally, the depth of the moisture increased throughout the day. Maximum moisture depths were common between sites, however, differed between day types. Moisture depth seemed to depend strongly on the wind direction, as shown above. Heights ranged from 750 hPa or 1.75 km AGL on the 20th while the 21st was shallower with moisture at EA3 only reaching 850 hPa or 750 m AGL. Mixing ratio profiles showed similar trends of increasing moisture depths on all nil thunderstorm days. Low-level dew point depression was about 7 or 8 °C.

For example, on July 20th, WVX surface wind shifted between east and west throughout the day, corresponding with variable r (lower with westerly wind direction and higher with easterly wind direction), shown in Figure 4.8. In contrast, on the 21st the wind was uniformly out of the southwest, shown in Figure 4.9. The moisture as seen in the r plots, displays a deeper moist layer on the 20th, compared to very shallow moisture on the 21st. This would also explain why, on July 20th, WVX surface r was lower (9 g kg^{-1}) than what was observed at EA3 (10 g kg^{-}

[1]). MB2 was similar to EA3. Both also measured east and southeast low-level wind direction accompanied by rather high low-level r, between 7- 8 g kg^{-1}, up to 800 hPa.

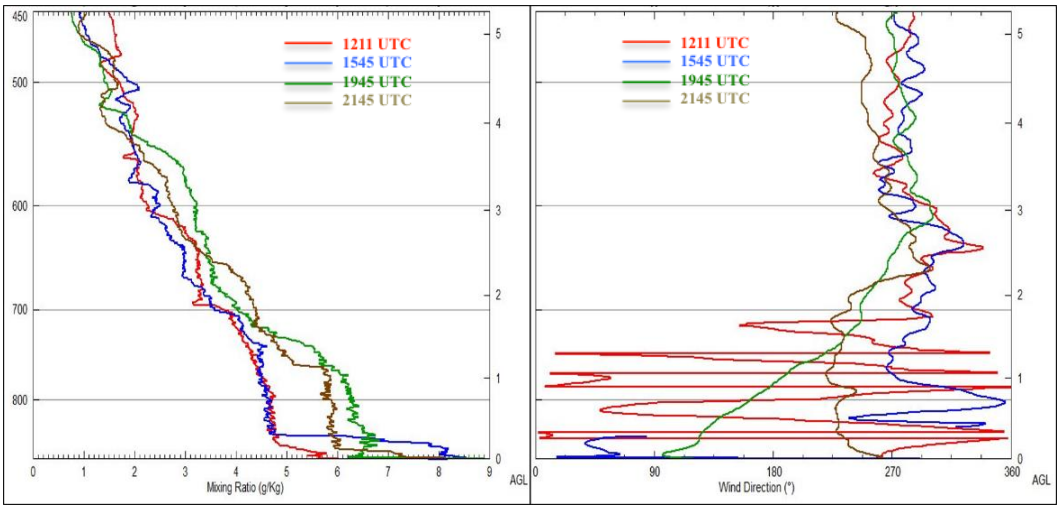

Figure 4.8: *Profiles of mixing ratio (left) and wind direction (right) at WVX on July 20th, 2008 at 1211 (red), 1545 (blue), 1945 (green), and 2145 UTC (brown).*

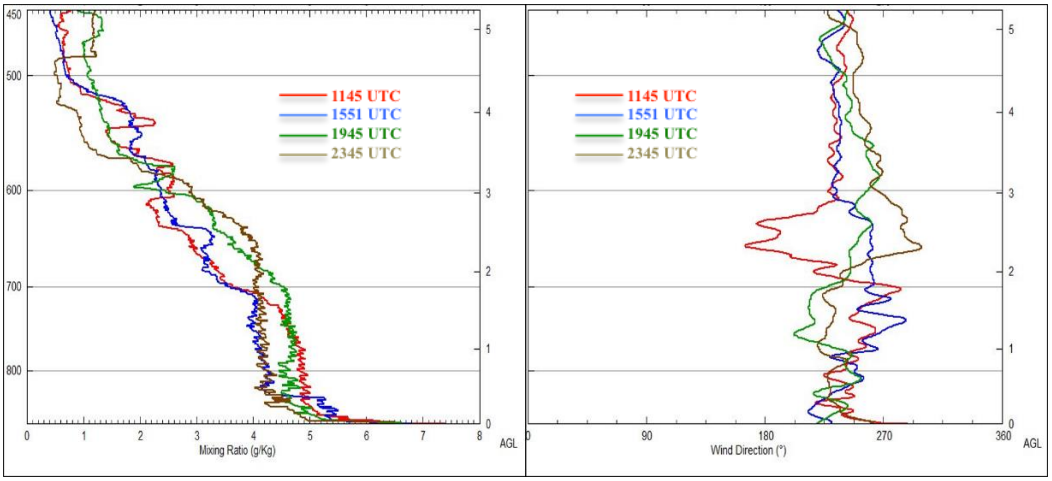

Figure 4.9: *Profiles of mixing ratio (left) in °C and wind direction (right) in ° at WVX on July 21th, 2008 at 1146 (red), 1551 (blue), 1945 (green), and 2345 UTC (brown).*

4.3. Shallow Convective days (SC)

Most shallow convective days in the UNSTABLE region were characterized by either a departing upper level low or an upper level northwesterly flow due to a southwest to northeast pressure gradient associated with an approaching ridge at 250, 500 and 700 hPa, increasing stability. Usually this accompanied differential anticyclonic vorticity advection and either increasing or no change in upper heights. The 850 hPa geopotential heights were characterized by weak features such as a weak low or weak northwest pressure gradient. This was reflected at the surface as either a weak surface low or approaching high pressure. In most cases baroclinicity was located to the south of the UNSTABLE region. Radar observations ranged from no precipitation to weak showers or thunderstorms. Severe thunderstorms were reported outside of the UNSTABLE region as well as sub-severe reports of small hail associated with scattered weak thunderstorms on a few of the SC days within the UNSTABLE region. These days indicated general reflectivities of 30 dBz with maximum values in individual cells up to 45 dBz.

Figure 4.10 illustrates the evolution of the SC day type BL through the field project. The surface nocturnal inversion was evident at EA3 and not at WVX. The surface inversions usually eroded by the second sounding of the day, between 1500-1600 UTC. Diurnal surface temperature variation was usually between 6-10°C and was consistent between sites. A mid-level subsidence inversion at 700 hPa was observed associated with winds from 270° and decreasing Td. This created a shallower mixed layer in the SC day type, up to 800-750 hPa (1 to 1.5 km) depending on the site. What varied between the days and sites was the strength of the inversions. Dew point depression on SC day types is also much less; at 750 hPa by about 2 °C and at the surface dew point depression is closer to 5 °C.

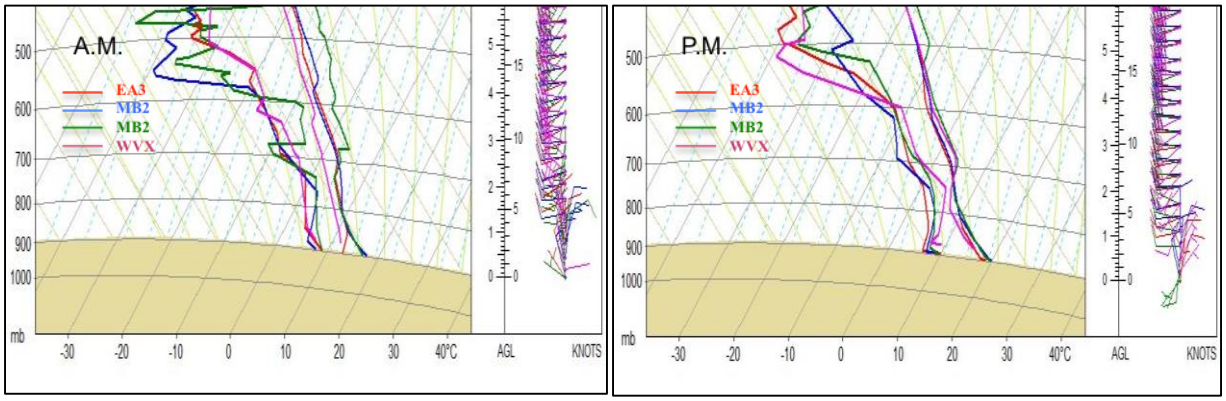

Figure 4.10**:** *Tephigrams of composite soundings by A.M. (left) and P.M. (right) by site EA3 (red), MB1 (blue), MB2 (green) and WVX (pink) for the SC day type.*

θ_e indicated slight decreasing or no change in the 600-500 hPa layer throughout the day. In the layer below 700 hPa, there was a consistent increase, increasing instability through the column. This trend seemed to be consistent between the sites. An interesting feature prominent in the SC day types, most defined on July 22, as shown in Figure 4.11, was a sizable spike in θ_e and associated θ values at about 750 hPa evident at all sites (Figure 4.12). The soundings are displayed in Figure 4.13. This indicated a moist layer, potentially cloud, associated with neutral stability above and stability below as seen in θ. At 700 hPa wind direction backed between 1200 UTC to 0000 UTC from westerly to southerly, indicating a change from dry air advection to slight moist air advection. Surface winds remained primarily from the north throughout day. At EA3 and WVX, the mid-level enhanced θ_e values seemed to be larger in the first sounding of the day at 1145 UTC, whereas at MB2, the mid-level enhanced θ_e values were larger in the last sounding of the day at 2330 UTC. At MB1, the mid-level enhanced θ_e was of similar strength all day. There was about a 5-10 K difference in θ_e between the surface and 700 hPa. A similar layer of higher values was evident in moisture near 700 hPa as observed by mixing ratio and dew

point, although not to the same magnitude. This is important to identify the source of the instability, which in this case may have been an influx of moisture at 700 hPa, since it was more obvious in θ_e as compared to θ.

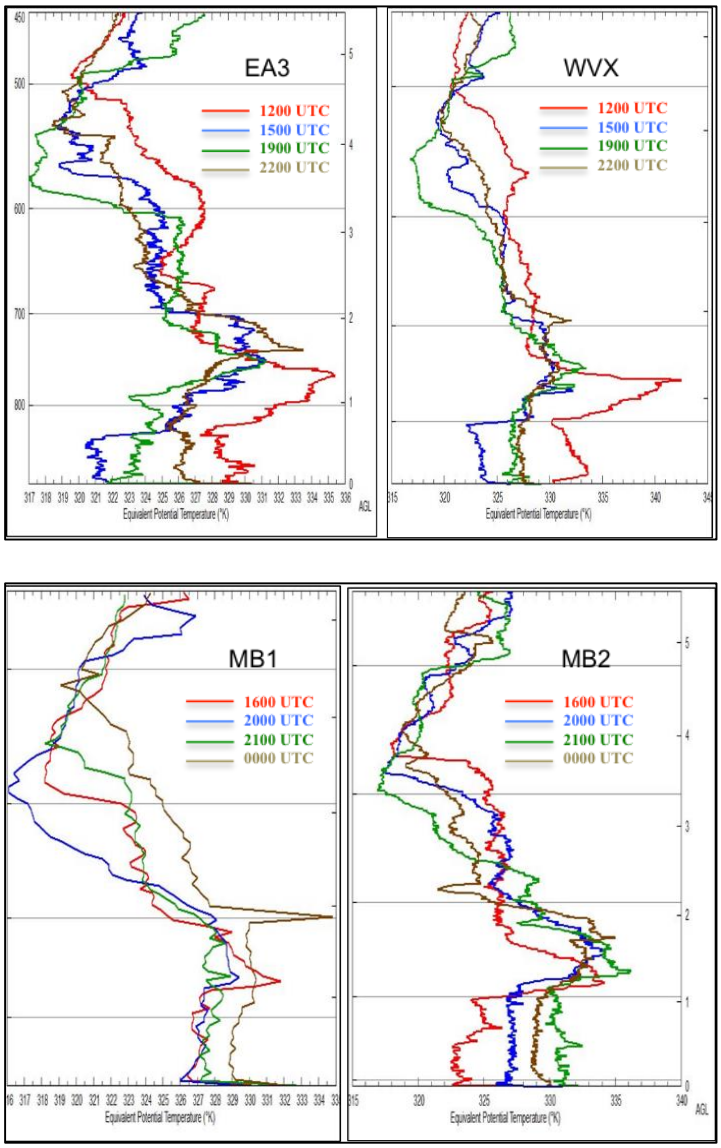

Figure 4.11: *θ_e profiles every four hours on July 22, 2008, a SC day type. EA3 (far left), WVX (middle left), MB1 (middle right) and MB2 (far right) indicating the stable layer in mid-levels. The x-axis is θ_e (K) and the left y-axis is pressure (hPa) and the right y-axis is height (Km AGL). Colors for EA3 and WVX are 1200 (red), 1500 (blue), 1900 (green) and 2200 UTC (brown) and times for MB1 and MB2 are 1600 (red), 2000 (blue), 2100 (green) and 0000 UTC (brown).*

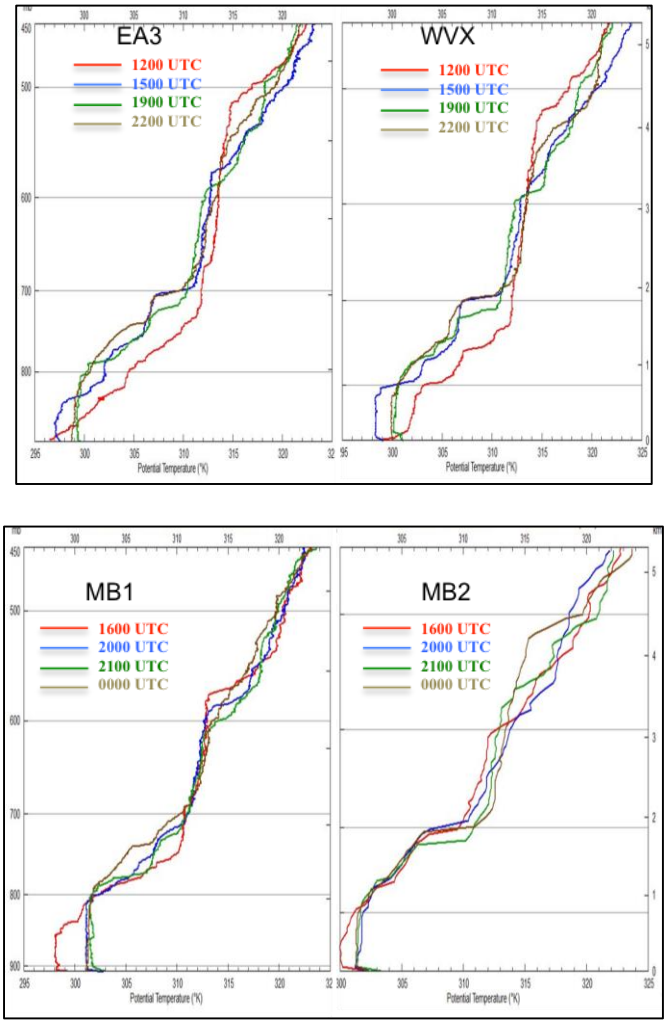

Figure 4.12: *θ profiles every four hours on July 22, 2008, a SC day type. EA3 (far left), WVX (middle left), MB1 (middle right) and MB2 (far right) indicating the stable layer in mid-levels. The x-axis is θ (K) and the left y-axis is pressure (hPa) and the right y-axis is height (Km AGL). Colors for EA3 and WVX are 1200 (red), 1500 (blue), 1900 (green) and 2200 UTC (brown) and times for MB1 and MB2 are 1600 (red), 2000 (blue), 2100 (green) and 0000 UTC (brown).*

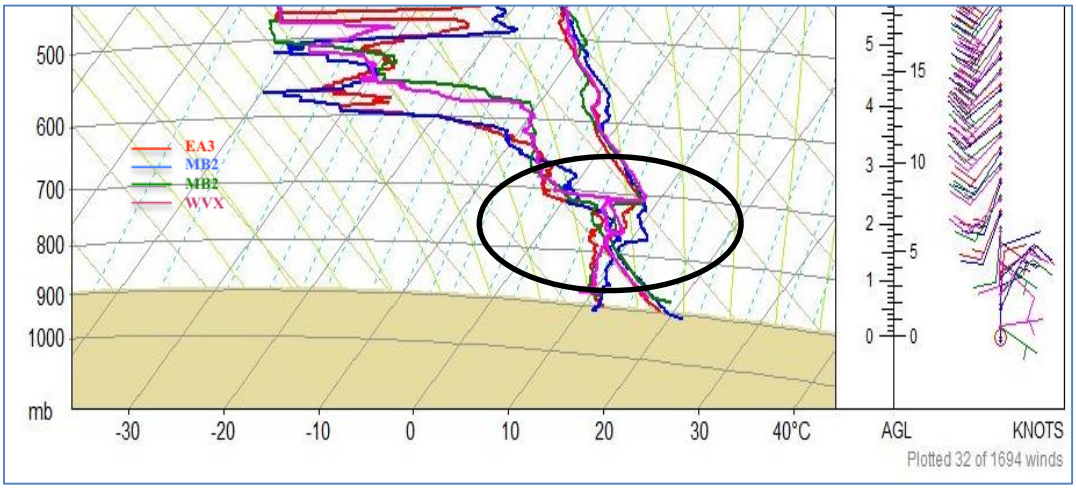

Figure 4.13: *Tephigrams of EA3 (red), MB1 (blue), MB1 (green), and WVX (pink) at 2200 UTC on July 22nd, 2008 illustrating the mid-level enhanced θ and θe values near 700 hPa.*

Surface wind speeds were near or less than 10 kt (5 m s^{-1}) with one outlier near 20 kt (10 m s^{-1}) at the surface. Most days displayed similar speeds and directions between all sites. One case displayed east or northeast winds at EA3 whereas surface winds were westerly at the stations located further west. About 40% of days exhibited a progression of wind direction from southwest to northeast throughout the day with an example shown in Figure 4.14. This may be an example of the mountain-plain circulation.

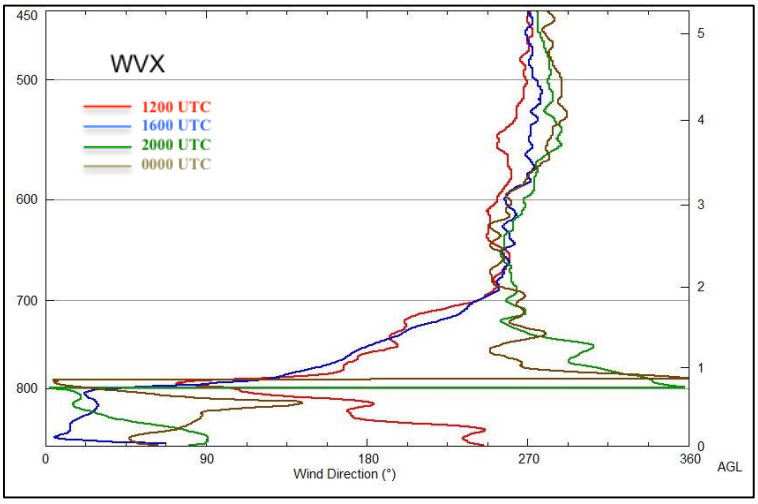

Figure 4.14: *Example diurnal variation of wind direction at WVX on July 14, 2008. Times are 1200 (red), 1600 (blue), 2000 (green) and 0000 (brown).*

4.4. Deep Convective Days (DC)

Most deep convective days in the UNSTABLE region were characterized by a departing upper ridge at 250 and 500 hPa with associated westerly flow. The ridge allows moisture and instability to accumulate, followed by an upper level trough of low pressure, releasing the instability. This is associated with falling 1000-500 hPa thicknesses and differential cyclonic vorticity advection. The 700 hPa geopotential heights were characterized by weak ridging, however, usually confined to southern Alberta with a trough of low pressure following close behind. The 850 hPa geopotential heights exhibited a weak trough of low pressure. Weak surface dynamics facilitated the development of the mountain-plain circulation initiating convection off of the higher terrain.

Composite soundings on the DC day type are shown in Figure 4.15. Morning temperature profiles displayed inversions in all days at EA3 and WVX. Mid-level inversions were either not present or not very strong in DC days. This would indicate cooler mid and upper levels,

increasing overall instability. Diurnal warming took place below 750 hPa or about 1.5 km at MB2 and EA3 whereas at MB1 the warming seemed to take place over a shallower layer, below 725 hPa or about 1.25 km, and over a deeper layer at WVX of about 775 hPa or 1.75 km. MB2 had a slightly drier boundary layer compared to the other sites, whereas EA3 had the most moisture, but was confined to a shallow surface layer. The mixing or boundary layer depths did not vary between sites, which could indicate that surface type contributions were not obvious on DC day types.

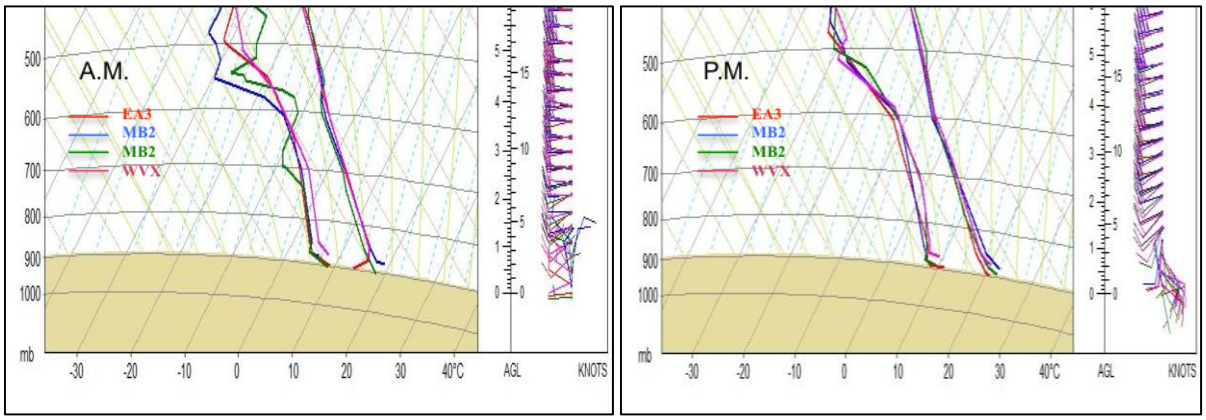

Figure 4.15: *Tephigrams of composite soundings by A.M. (left) and P.M. (right) by site EA3 (red), MB1 (green), MB2 (blue) and WVX (pink) for the DC day type.*

Surface diurnal temperature trends were between 6-12°C. Trends were on the lower end of this scale at MB1 and MB2 and on the larger end at EA3 and WVX. This is due to the lack of early morning soundings at MB1 and MB2. Site location for each IOD is displayed in APPENDIX A. All sites displayed low-level winds up to 1 km from the east of about 10 kt (5 m s^{-1}), possibly exhibiting the mountain-plain circulation and/or synoptic contribution with surface

pressure falls and troughing developing. This affects the amount of moisture advected upslope, underrunning the inversion.

θ_e boundary layer evolution was similar between sites. On most days and at all sites, the highest θ_e values were at the surface, near 335 K, followed by a deep layer above the surface of higher θ_e values of 330 K extending to 800 hPa. Cooling of θ_e values of about 5 K occurred above 500 hPa on some DC days. Neutral stability in θ can be seen throughout the entire column on DC days. This comparison of θ_e BL evolution between examples of a typical DC day type is illustrated in Figure 4.16 and θ evolution in Figure 4.17.

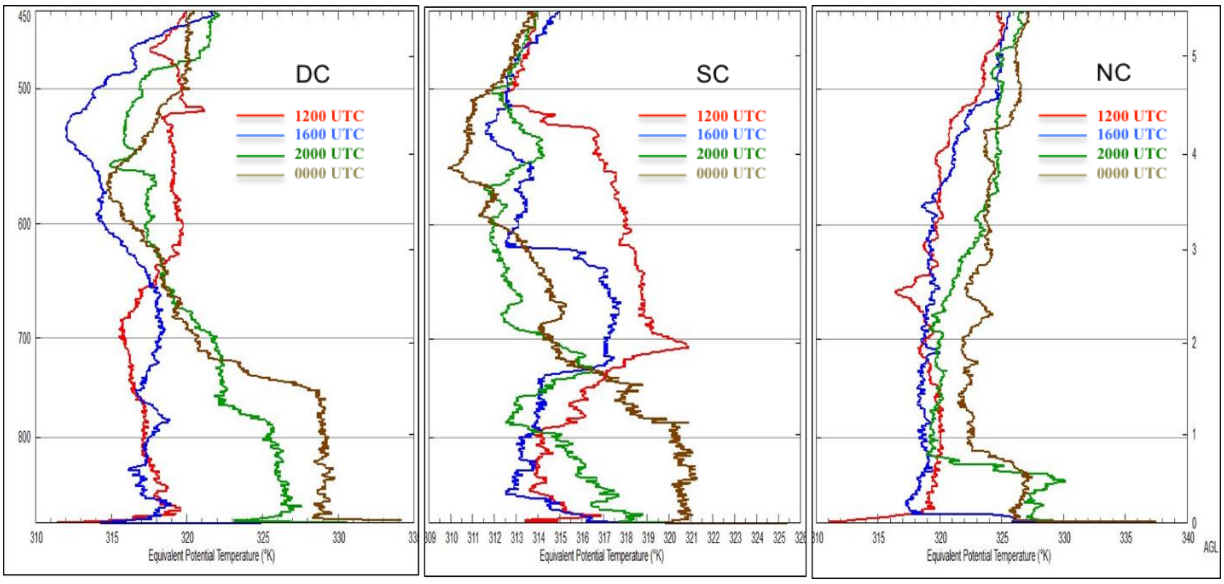

Figure 4.16: *4-houly soundings, 1200 (red), 1600 (blue), 2000 (green) and 0000 UTC (brown), from EA3 on July 13, 2008 DC (left), July 14, 2008 SC (middle) and July 20, 2008 NC (right) day types of θ_e values (K). Y-axis is pressure (hPa) and x-axis is θ_e.*

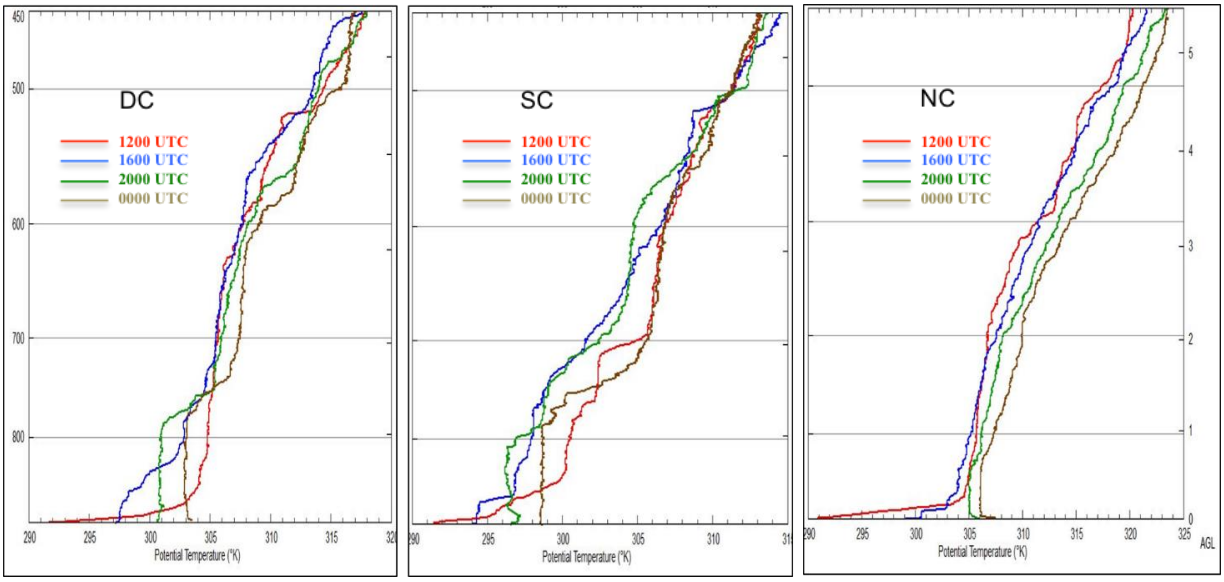

Figure 4.17: *4-houly soundings, 1200 (red), 1600 (blue), 2000 (green) and 0000 UTC (brown), from EA3 on July 13, 2008 DC (left), July 14, 2008 SC (middle) and July 20, 2008 NC (right) day types of θ values (K). Y-axis is pressure (hPa) and x-axis is θ.*

Surface dew points ranged from a mean of 9°C in the morning to a mean of 14°C by afternoon. DC days had moisture extending to 750 to 700 hPa. Near-surface mixing ratio values increased on DC day types from 5 to 11 g kg^{-1}.

Surface wind direction on DC day types was characterized by a shift to an easterly component; whether it was southeast or northeast, in all soundings launched after 1200 UTC. On other day types, this would have been indicative of the mountain-plan circulation developing. However, on DC days, large scale upper-level synoptic ascent may also be inducing easterly flow, causing the upslope moisture advection, so it is not clear what the contributions are from each process (i.e. mountain-plain circulation versus synoptic setting) with regards to the easterly flow and moisture advection. Nonetheless, an easterly flow is still a favorable low-level wind direction for convective initiation and deep convective development. The depth of the easterly wind direction seemed to correspond with the depth of the moisture, as seen in Figure 4.18.

When the wind direction shifted specifically to a northeast direction, as oppose to an easterly or southeasterly direction, a more noticeable increase in moisture was evident. The surface wind speeds were near 10 kt (5 m s^{-1}). Just off of the surface there was frequently a stronger wind maximum observed, usually with speeds near 20-25 kt (10-13 m s^{-1}), which also correlated with an increase in moisture within the respective layer. The average time of the wind shift to an easterly component at WVX was 1440 UTC. EA3 surface wind shifted later, at an average time of 1620 UTC. MB1 and MB2 were mobile and therefore this time would have varied with their location, but their average times were later, 1912 and 1830 UTC respectively. Easterly wind direction was in some cases evident at 1200 UTC, but not all. The maximum time for the switch to a surface easterly direction was at EA3 at 2200 UTC. EA3 was located furthest east from the mountains, and therefore this process occurring at EA3 may or may not be evident of a mountain induced flow.

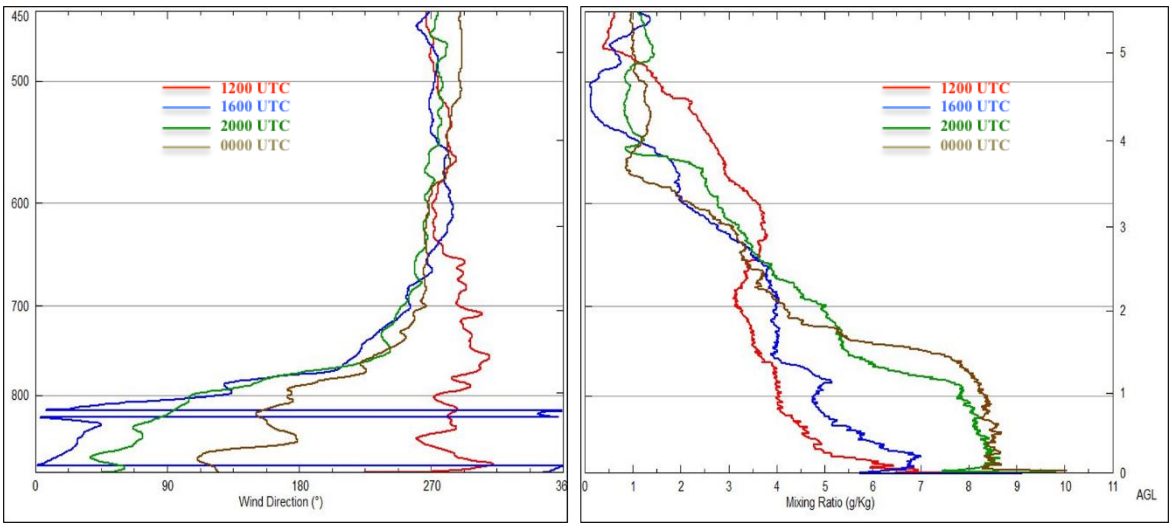

Figure 4.18: *Example of the variation in moisture magnitude and depth every 4 hours corresponding with the wind shift from west in the first sounding of the day, 1200 (red) to east by the last sounding of the day 0000 UTC (brown) at EA3 on July 13, 2008, a DC day type.*

4.5. Statistical Analysis

The objective of this section is to determine whether there is a statistically significant difference between the sounding sites' meteorological parameters to see if surface character at each site (eco-climate zone) may play a role in the meteorological parameters. Sites in different and similar eco-climate zones, or on opposite or similar sides of the forest-crop line are compared. The approximate location of the crop/forest boundary is transitional. It is diffuse in some locations and may not be a perfectly straight line, especially in areas of complex terrain. Two different methods were employed using the standard t-test to evaluate the difference of means between 6 pairs of combinations from four sites. Four BL characteristics were chosen based on their utility; temperature, specific humidity, wind speed and direction. The first method compared the p-value of the entire column between the sites. This is discussed in section 4.5.1. The second method compared the p-value at each pressure level between the sites, discussed in section 4.5.2. An analysis comparing day types between the sites was not possible due to too few soundings in many samples to be able to make statistical conclusions.

4.5.1. Profiles

Statistical differences via daily column p-values are shown in Table 4.1. Tests were calculated at a significance level of 0.05 (red) for all BL characteristics, 0.1 (blue) for temperature, wind direction and speed and 0.2 (green) for specific humidity. P-values within these ranges imply to reject the null hypothesis; that is, there is a statistical difference in the means between two locations at that significance level. It is obvious that MB1 and EA3 are the most similar having only specific humidity and wind speed showing a statistical difference, with specific humidity only different at the highest significance level (0.2). However, they were only

on the same side of the eco-climate transition zone for two of the eight IODs. All of the other site statistical comparisons showed significant differences in every BL characteristic. Wind speed showed the most difference in the site comparisons and temperature the most similar. Thus, the sounding sites were statistically different from each other and suggest that the four different sites are not redundant in any way. These differences are likely at least partially due to the diverse surface characteristics, resulting in different BL characteristics over each location.

Table 4.1: *P-values produced from student's t-test for the atmospheric column between all of the site locations and for each BL characteristic. Red indicates a p-value <=0.05, blue indicates a p-value between 0.05-0.1 and green indicates a p-value between 0.1-0.2.*

	MB1-WVX	MB1-MB2	MB1-EA3	MB2-EA3	MB2-WVX	WVX-EA3
Specific Humidity	0.004	0.019	0.187	0.000	0.000	0.125
Temperature	0.051	0.015	0.543	0.003	0.000	0.191
Wind Speed	0.089	0.000	0.047	0.000	0.000	0.000
Wind Direction	0.001	0.000	0.207	0.000	0.013	0.000

The p-values as analyzed by A.M. and P.M. in Table 4.2, indicates that the MB2-WVX comparison is the most statistically different in both A.M. and P.M. comparisons. In APPENDIX A, these sets of comparisons were most frequently on opposite sides of the crop/forest boundary, four out of the eight IODs. MB1-EA3 is the most similar site comparison in both the A.M. and P.M. with only wind speed indicating a statistical difference in both. MB1 and EA3 were more frequently on opposite sides of the transitional forest to crop boundary, and therefore it was expected that they would be statistically different. A reason for this unexpected result could be either due to the MB1 station changing locations each day, making the results difficult to interpret, or, a synoptic meteorological phenomena driving the similarities between these two sites. Since there were so few soundings, the day type, and therefore synoptic meteorological

patterns, could not be specifically analyzed. This will be further analyzed by pressure level in the forthcoming section. The largest change from A.M. to P.M. occurred between MB2-EA3. This comparison displayed more similarity in the A.M. in contrast to a significant difference in the P.M., evident in all four BL characteristics. This could be due to the convective boundary layer evolution, which is at its mature state in the P.M., allowing larger differences between sites to develop. This is further investigated in the next section by analyzing the p-values at different pressure levels. This analysis will identify where within the column these changes occurred. Wind direction indicated the most differences when separated by A.M. and P.M. in contrast to wind speed, which indicated the most difference when looking at the day as a whole. Temperature remained the most similar BL characteristic in both A.M. and P.M.

Table 4.2**:** *A.M. (top) and P.M. (bottom) p-values produced from student's t-test for the atmospheric column between all of the site locations and for each BL characteristic. Red indicates a p-value <=0.05, blue indicates a p-value between 0.05-0.1 and green indicates a p-value between 0.1-0.2.*

AM	MB1-WVX	MB1-MB2	MB1-EA3	MB2-EA3	MB2-WVX	WVX-EA3
Specific Humidity	0.108	0.014	0.510	0.101	0.000	0.126
Temperature	0.573	0.027	0.317	0.233	0.006	0.179
Wind Speed	0.261	0.241	0.000	0.053	0.034	0.261
Wind Direction	0.002	0.032	0.227	0.002	0.826	0.017

PM	MB1-WVX	MB1-MB2	MB1-EA3	MB2-EA3	MB2-WVX	WVX-EA3
Specific Humidity	0.118	0.170	0.533	0.010	0.000	0.389
Temperature	0.996	0.000	0.998	0.000	0.000	0.801
Wind Speed	0.060	0.000	0.054	0.000	0.000	0.060
Wind Direction	0.000	0.000	0.739	0.000	0.000	0.000

4.5.2. Pressure Levels

By comparing the soundings by pressure level, the differences or similarities can be specified to the level within the atmospheric column. This will facilitate a meteorological explanation for the differences or similarities between the sites. Full tables of p-values of each BL characteristic at each pressure level, by day and separated by A.M. and P.M., are displayed in APPENDIX B. The profile analysis revealed the most difference to be in wind speed and between MB2-EA3 sites, while the most similarity was in temperature between MB1-EA3 sites. These will be analyzed by pressure level in this section for further explanation. Significance levels used were 0.05 and 0.1.

Wind direction displayed the most significant differences in the boundary layer between the surface and 830 hPa and between 750 to 700 hPa. This confirms that the differences are mainly due to BL differences. Comparing the A.M. and P.M. wind direction is more different in the afternoon than in the morning, which is to be expected due to BL maturity in the P.M. The differences extended deeper in the column in the afternoon (up to 690 hPa), while in the morning, the differences were confined to just above the surface (below 840 hPa, with a second near 750 hPa, but only evident in two of the site comparisons). This difference between A.M. and P.M. is due to the diurnal evolution of the boundary layer depth, which is usually at its maximum depth in the afternoon.

Temperature was identified as the most similar weather parameter amongst the site comparisons. The differences were only seen in the P.M. soundings. The boundary layer was similar in all site comparisons except for MB1-EA3, which showed significant differences from the surface up to 780 hPa. It was expected that there would be a greater difference in temperature in the P.M. boundary layer, as discussed earlier, due to the heterogeneous surface types resulting

in maximum potential differences in the P.M. This is in contrast to the profile comparison results which indicated that the MB1-EA3 comparison was statistically similar.

Differences between sites were more evident in specific humidity as compared to temperature when analyzed by pressure level. However, differences in the boundary layer were actually more evident in the A.M. for the MB1-WVX, MB2-WVX and WVX-EA3 site combinations. WVX and EA3 were stationary sounding sites and were always on opposite sides of the transition line from crops to boreal forests, so this comparison may be expected to have significant BL moisture differences. MB2 and WVX were equally on the same side and on opposite sides of the transition zone. MB1 and WVX were more often on the boreal forest side of the transition zone than on opposite sides. Perhaps the specific humidity differences were more evident in the A.M. due to the nocturnal inversion still present and therefore prohibiting mixing of the moisture throughout the deeper layer. The strength and/or height of the low-level nocturnal inversion may also be influenced by surface type, therefore restricting moisture transport throughout the column to different magnitudes at the different sites. In fact, differences in temperature were not at the surface but just above the surface in the layer 870 to 770 hPa, which may reflect the different sensible heating from a surface, in turn controlled by the amount of latent heating from moisture availability. Differences in specific humidity in the P.M. were significant for the WVX-EA3 comparison between 700 to 590 hPa. EA3 being further from the mountains may not experience as strong westerly subsidence as WVX. This would change the moisture in this level. Differences in specific humidity in the P.M. were significant for the MB1-WVX comparison between 430 and 220 hPa. This may suggest that the reason for these differences may be due to other factors aloft, and therefore does not only depend on surface character or BL evolution. These differences may be driven by convective day type

(meteorological factors), however, due to limited soundings, day type was not possible to analyze statistically.

MB2-EA3 and MB2-WVX were identified as the most significantly different site comparisons by profile. MB2-EA3 were on opposite sides of the surface type transition line on three out of six IODs. They showed the most difference in boundary layer wind speed and direction. The differences were contained to below 870 hPa in both and were more different in the P.M. MB2-EA3 showed more difference in temperature in the P.M., than in the A.M., however, these differences were aloft, above 300 hPa. MB2-EA3 showed similar specific humidity in the boundary layer with only some difference at the 0.05 significance level. Most of these BL differences were in the low-levels and can potentially be due to surface inhomogeneity.

MB2-WVX comparisons only began at 870 hPa due to WVX being at a higher elevation. They were on opposite sides of the surface type transition line three out of six IODs. Wind direction was similar between the two sites. Temperature was similar in the A.M. with only some differences in the upper levels (300 to 200 hPa layer) in the P.M. Wind speed was more significantly different in the P.M. and differences were identified just above the surface as well as above 300 hPa.

The MB1-EA3 site comparison was the most similar out of all site combinations. However, they were located on opposite sides of the transition line five of seven of the IODs. A statistical comparison on individual days might further explain the similarities, but there were too few soundings on each day for each site to facilitate such an analysis. When analyzed by pressure level, this comparison actually showed the most difference in boundary layer temperature (below 740 hPa) in the P.M., which makes some sense since MB1 was mostly in the forested area that would have higher sensible heat fluxes. On the other hand, there was no

difference in specific humidity and little difference in wind direction and wind speed, which were mainly between 750 and 630 hPa in the A.M. This is in contrast to other site comparisons, which showed more wind differences in the boundary layer.

4.6. Boundary Layer Evolution Summary

Observations of near surface and boundary layer (BL) thermodynamic parameters are important in the characterization of environmental convective potential. Fully understanding the near-surface and BL evolution aids in identification of thermodynamic and dynamic (wind) processes potentially leading to convective initiation. The evolution of the boundary layer was illustrated by characterizing diurnal changes in temperature, dew point, potential and equivalent potential temperature, mixing ratio, wind speed and direction.

Dew point depression was much less below 750 hPa in SC and DC day types than what was observed in the NC day type. The higher moisture content could be due to the northeast low-level winds, potentially initiated by the mountain-plain circulation. An easterly wind direction occurred simultaneously with a greater magnitude of moisture and greater magnitude of moisture reaching a higher vertical extent within the column. This was more prominent in DC followed by NC days. The potential mountain-plain circulation was present on over half of the deep convective days in contrast to only half of the SC days and one out of three of the NC days. However, this circulation would be more likely to be present on days with weak synoptic forcing. It was found that strong low-level synoptic forcing was present on just over half of the days during the UNSTABLE field campaign. This did not seem to vary according to convective day type. When synoptic strength was compared to the shift to easterly winds, there was also no

correlated shift to easterly wind direction. Therefore, it is not certain whether this shift to easterly wind direction is clearly due to synoptic pattern or the mountain-plain circulation.

Similarly, stronger easterly BL winds on DC day types resulted in greater moisture advection and were reflected in a higher magnitude of moisture. Specifically, MB2 exhibited the most obvious and consistent increase in wind speed throughout the day; this site was usually placed in a cropped or grassland areas. All day types showed increasing dew points from morning to afternoon, however, surface dew points were highest on DC days. The depth of the moisture was much shallower in nature for NC days. SC and DC days were similar in moisture depth, reaching 750 to 700 hPa, whereas NC days extended only to 800 hPa.

The nocturnal surface inversion was present at both WVX and EA3 on NC day type, at EA3 and weakly at WVX on DC days, however, only at EA3 on SC days. The inversions on NC day type were also much stronger and occurred on more days than what was seen in the DC and SC day types. Since EA3 and WVX had early morning soundings and often displayed the surface nocturnal inversion, they also exhibited a larger diurnal temperature variation. Mid-level inversions that were exhibited in SC days were not as strong in NC days and not present in DC days.

BL depth was similar between DC and NC day types, however BL depth was slightly deeper in DC day types, up to 600 hPa (3.5 km) compared to 3 km or 625 hPa on NC day type. BL depth was shallowest and varied between sites on SC day types. It was shallowest at EA3 and deepest at MB1 and MB2. This could be due to higher sensible heat flux over forest surface type compared to crop surface type.

Neutral stability in θ can be seen throughout the entire column on DC days, slight stability on NC days, both days illustrating instability in the low-levels, with the instability extending deeper into the column on DC days. SC day types exhibited a layer of strong stability near 700 hPa that developed in the afternoon.

Comparisons between BL characteristics was also completed using statistical tests comparing entire profiles between sites as well as comparing by pressure level between sites. The comparison between MB1 and EA3 was the most similar and MB2-WVX was the most different. Wind direction was the most different and temperature the most similar when analyzed by profile. A.M. and P.M. comparisons revealed more differences in the afternoon reflecting the differential heating near the surface possibly influenced by eco-climate zone.

When analyzed by pressure level, temperature remained one of the most similar BL characteristics, however, specific humidity was the most different. Comparisons between pressure levels revealed that differences were mainly contained in the near surface layer, below around 790 hPa in the morning and 700 hPa in the afternoon. This emphasizes the influence that surface characteristics may have on the boundary layer. Although, differences were found at other specific levels that could be attributed to where a nocturnal surface inversion may be different strengths at different sites or where mid-level subsident inversions may be different strengths at different sites. Aloft, upper-level meteorological features that could not be identified through this analysis may also contribute to the differences between sites.

These conclusions are similar to the work done by Strong (2000), even though the field of study in UNSTABLE was further south. It is now known that his conclusions apply to a wider area of the Alberta foothills than just the small area that he focused on. These results indicate that this high density network of upper air soundings is pertinent in the observation of boundary layer

evolution. These sounding locations were only on average 90 km apart on any given day, however, they showed significant differences spatially and temporally. Understanding this evolution will aid in anticipation of afternoon conditions to identify where or when convective initiation would occur, and what potential severity exists.

CHAPTER 5: RESULTS

5. DISTINGUISHING BETWEEN CONVECTIVE DAY TYPES

5.1. Overview

This chapter focuses on the second thesis objective of "Distinguishing conditions between days with deep, shallow and no convection". This section will complement chapter 4 by discussing the convective differences and similarities between composite soundings from the different day types and different sites, and fluctuations from A.M. to P.M. Statistical methods are used to compare severe weather parameters to quantify the convective potential and severity of convection. Lastly, comparisons to other research are presented.

5.2. UNSTABLE Convective Comparisons

5.2.1. Daily and P.M. Composites

Comparing the DC day composite and the DC P.M. composite, Figure 5.1, shows the evolution of the near surface layer below 600 hPa or 4.5 km. Warming throughout the day creates a well-mixed surface layer with low-level lapse rates closer to dry adiabatic indicating neutral stability. Surface wind direction and speed are similar between the two profiles. However, just off of the surface in the daily composite, winds veer to northwesterly before backing to westerly at 1 km AGL as oppose to a gradual veering to westerly by 1 km AGL. This is important in controlling the shape of the hodograph, creating potential for mesocyclone and tornadic formation in the P.M. Convective indices such as CAPE, LI and shear increased in the P.M. composite. 500 hPa temperatures decreased, indicating the increase in instability. Similarly, increasing instability is also reflected by the difference between the daily and P.M. 0-3 km

CAPE and increase in SWEAT. Moisture in the low-levels increased from the daily to the P.M. composite. This could influence convective initiation by lowering the height of the LFC and LCL as well as increasing the amount of energy available for thunderstorm development.

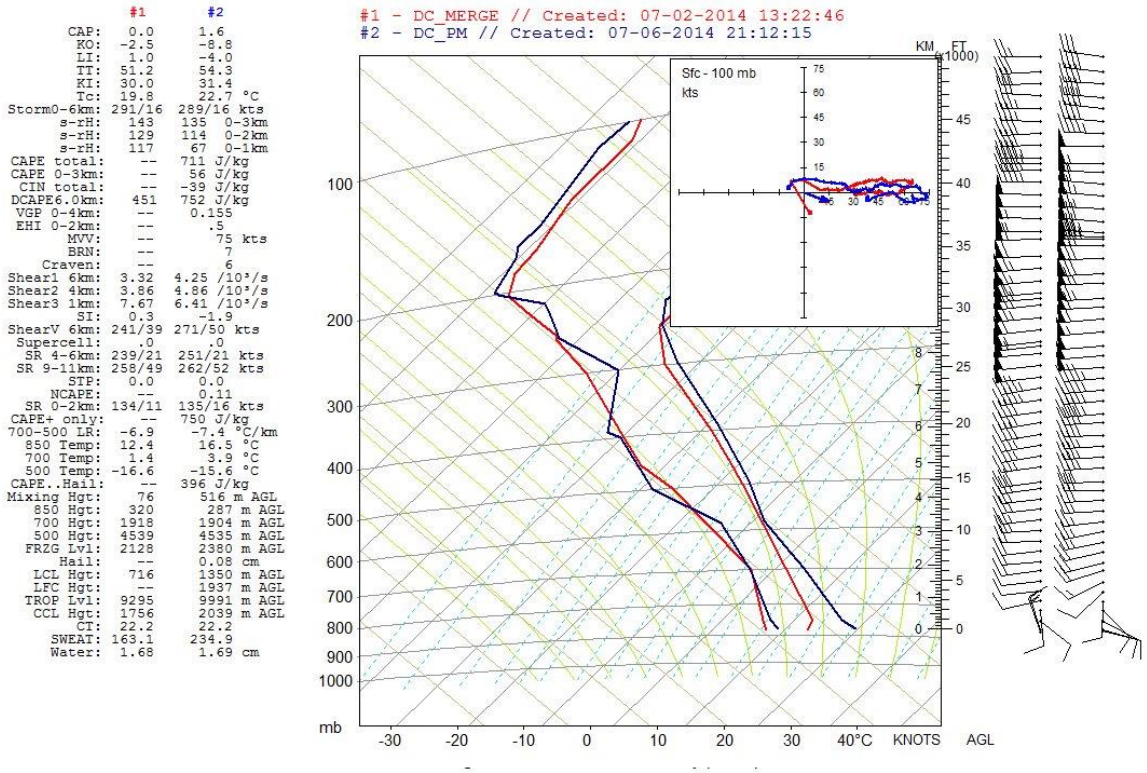

Figure 5.1: *Tephigram of DC day type daily composite (red) and P.M. composite (blue) with analysis parameters (left) and associated wind barbs (right).*

The main difference between SC day composite and SC P.M. composites in Figure 5.2 was in the moisture influx at about 750 hPa or 2 km. A weak cap also developed in the P.M. composite at 700 hPa or 3 km. This may affect thunderstorm initiation as it may act as a stable layer, inhibiting surface initiation as well as creating cloud, reducing daytime heating and the potential of reaching the convective temperature. This may be a feature that is what defines SC day types as it inhibits deep convection from developing. The limiting factor of SC day types therefore may be a mechanism to "break" this cap. The low-level temperature profile did increase by a couple of degrees creating lapse rates closer to dry adiabatic in the P.M. composite

compared to the daily composite. Surface winds shifted from southwest to northwest. Convective parameters such as SWEAT and LI indicated a slight increase in instability in the P.M. composite. Shear parameters such as 0-3 and 0-2 km SRH also increased in the P.M. composite.

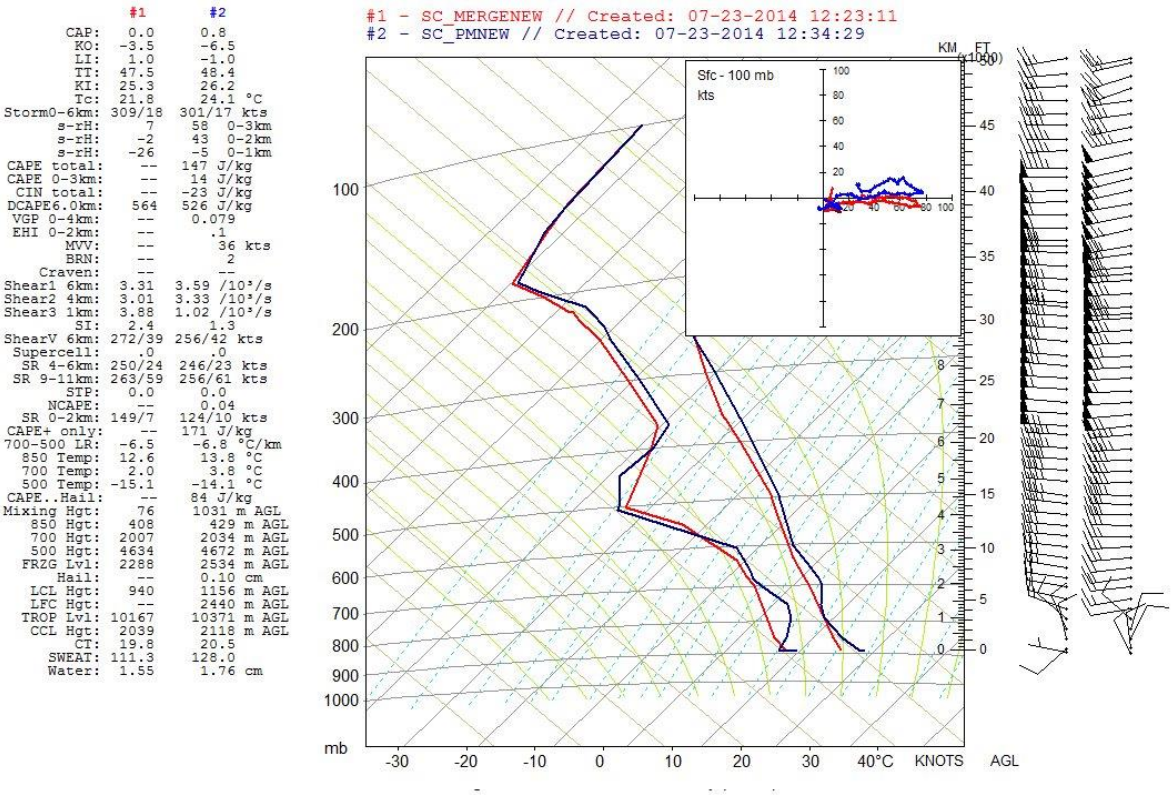

Figure 5.2: *Tephigram of SC day type daily composite (red) and the SC day type P.M. composite (blue) with analysis parameters (left) and associated wind barbs (right).*

Evaluating the NC day composite and the NC P.M. composite, in Figure 5.3 below, reveals a warmer column in the P.M. as well as higher dew point below 700 hPa or 3 km. Surface wind direction remained similar between the daily and P.M. composites, however, the wind speed increased by 5 kts (3 m s^{-1}). NC days were characterized by clear skies, which allowed surface temperatures to reach the maximum potential temperature. This resulted in a

larger diurnal temperature trend than the other day types, about a 6° difference in the surface temperature. In contrast SC day types only had a couple of degrees variation.

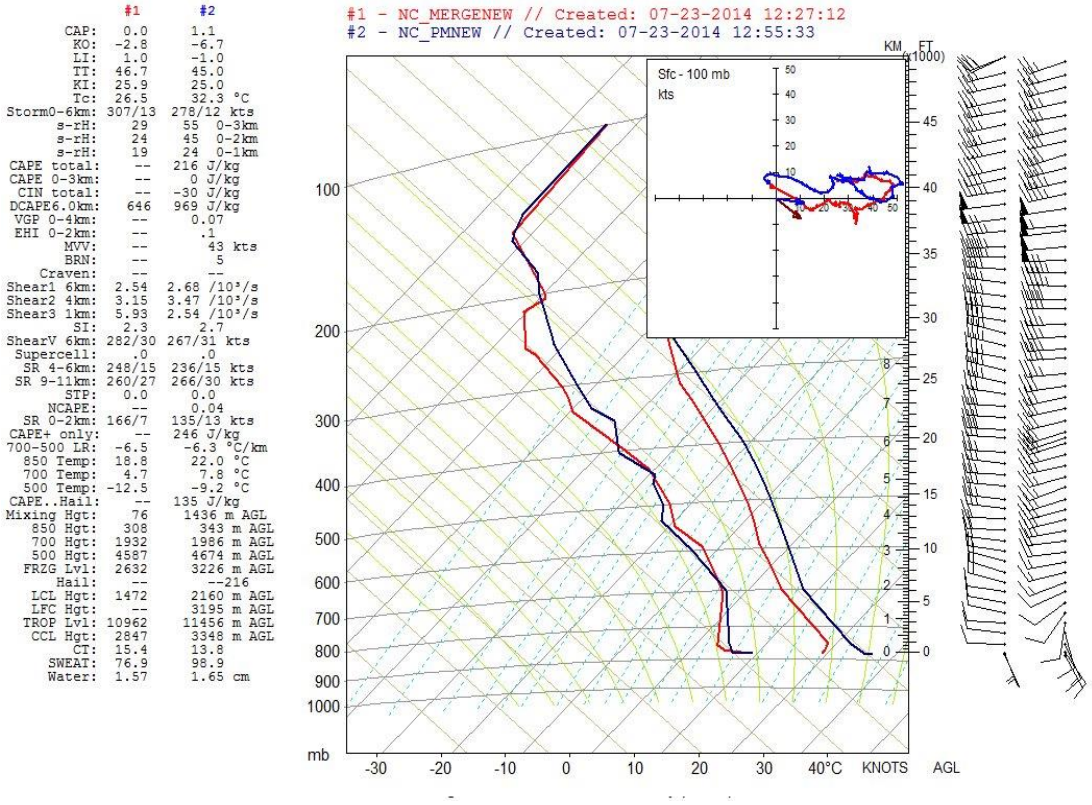

Figure 5.3: *Tephigram of NC day composite (red) and NC P.M. composite (blue) with analysis parameters (left) and associated wind barbs (right).*

All of these changes highlight the diurnal convective variations in the BL. These are important in the initiation and development of convection, and as displayed, will vary according to day type and thus the meteorological dynamics and thermodynamics present. The increased

spatial and temporal resolution with supplemental soundings has shown here to strongly improve observation of these phenomena.

5.2.2. Day Type Composites

The NC P.M. composite is warmer than the other convective day types throughout the entire column shown in Figure 5.4 below. SC temperature profiles have a warm nose near 700 hPa, capping instability. DC days revealed colder upper levels, above 550 hPa or 4 km. Colder air aloft would contribute to stronger instability. Surface dew points were similar between all of the day types. However, the magnitude of moisture from the surface to 700 hPa, is higher in DC days than SC and NC days. Moisture on NC days is limited to just the surface layer. This further indicates the favored environment for inititation and development of thunderstorms on the DC and SC days. Easterly winds advected moisture from the mixed grasslands into the foothills, which were present in DC days. This advection is also occuring in an upslope direction, physically forcing ascent of moist air. The freezing level (height of the 0°C isotherm) was similar between DC and SC days, at about 2.1 km AGL or just over 700 hPa, which is lower than the freezing level in the NC profile, at about 2.8 km or 650 hPa, contributing to larger hail sizes due to less melting and increased hail formation and growth time.

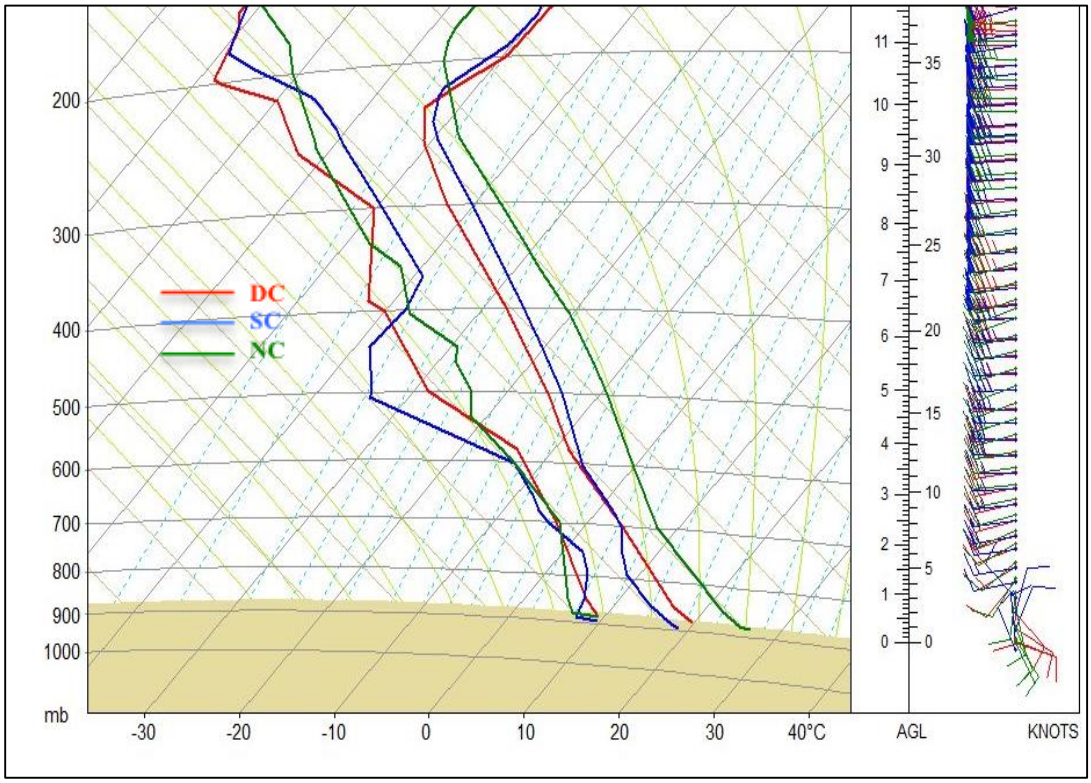

Figure 5.4: *Tephigram of P.M. composites of DC days (red), SC days (blue) and NC days (green) with associated wind barbs (right) in knts.*

On DC days, winds veered through the low-levels to westerly by 1.5 km AGL or 750 hPa, producing low-level environmental directional shear contributing to longer-lived and more developed mesocyclones. In the SC day type, winds backed from northerly to westerly in the low-levels. This contributes to less environmental directional shear, reducing the liklihood of thunderstorm mesocyclone development. This is illustrated in Figure 5.5.

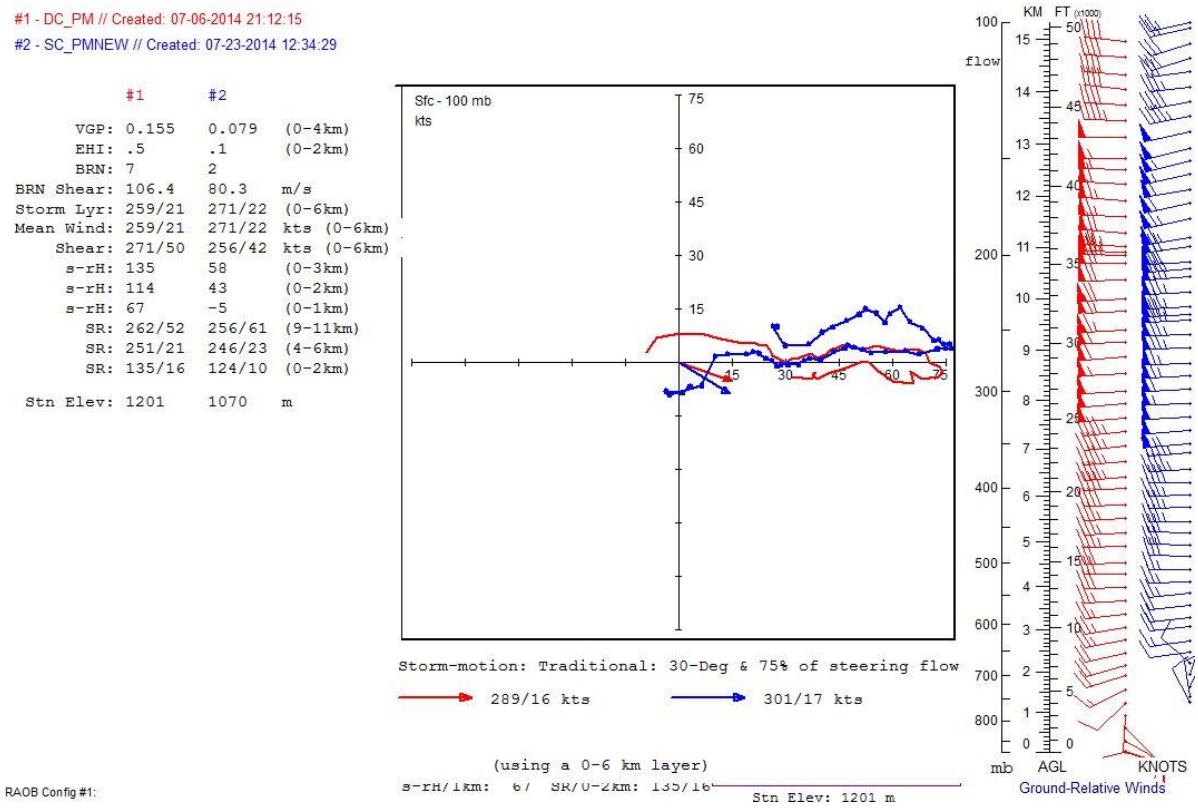

Figure 5.5: *DC P.M. composite hodograph (red) exhibiting a cyclonically looping profile conducive to long-lived mesocyclone development. This is not evident in the SC P.M. wind profiles (blue).*

5.2.3. Site Composites

Further breaking down day types by site, illustrates the NC P.M. profiles in Figure 5.6 are quite similar. All sites displayed weak low-level wind speeds from the southeast to northeast. The moisture at the surface is relatively high but drops off dramatically in the deep well-mixed BL that extends above 700 hPa. The highest surface moisture is evident at EA3 of about 2°C higher than the other sites. This few degrees of additional moisture may be the result of being closer in proximity to the local evapotranspiration source of crops and grasslands. However, dew

points at MB1 and MB2 seem to be a few degrees higher than EA3 and WVX throughout the boundary layer.

Low-level wind direction in P.M. profiles on SC days varied between northeast and south southwesterly, depending on the site. WVX low-level wind direction was from the northeast, and therefore did display higher low-level moisture. However, EA3 also displayed a northeast low-level wind direction, but was only reflected in shallow moisture. MB1 and MB2 displayed northwest and southwest low-level winds respectively with similar low-level moisture in between the EA3 and WVX moisture profiles. The 500 hPa, or 5 km moisture varied between sites, with the driest being EA3 and WVX. All sites indicated a mid-level subsidence inversion at around 700 hPa or 2 km. It was strongest at WVX with steeper lapse rates below the mid-level inversion. All other sites displayed near dry adiabatic lapse rates in the layer below, from the surface to 800 hPa. Surface dew points were similar between the sites, however, WVX displayed deeper moisture compared to the other sites. The dew point depression, being only a couple degrees in the WVX composite between 800-750 hPa, would indicate there was typically low-level cloud present at the top of the BL. This is common in the foothills of Alberta (where WVX is located) (Strong, 2000) with BL cloud developing in the early afternoon, and suggests that the composite SC profiles are representative of the SC environment.

DC days illustrated a fairly large variation in moisture depth and magnitude between the sites (above an 8°C difference at the surface to about a 3°C difference at 750 hPa). MB1 is the driest with EA3 and WVX having the highest moisture content in the low-levels. This could be due to MB1 typically being closer to the mountains and therefore into the higher altitude boreal forest, which produces less evapotranspiration and therefore less low-level moisture. MB2 is

slightly less moist in the lower BL compared to EA3 which may be due to being located further west in somewhat higher terrain some days, but not as far west as MB1 (i.e. MB1 was usually further west than MB2). Boundary layer depths were similar between sites with the most dry adiabatic lapse rates at MB1 and lapse rates near dry adiabatic at the other sites.

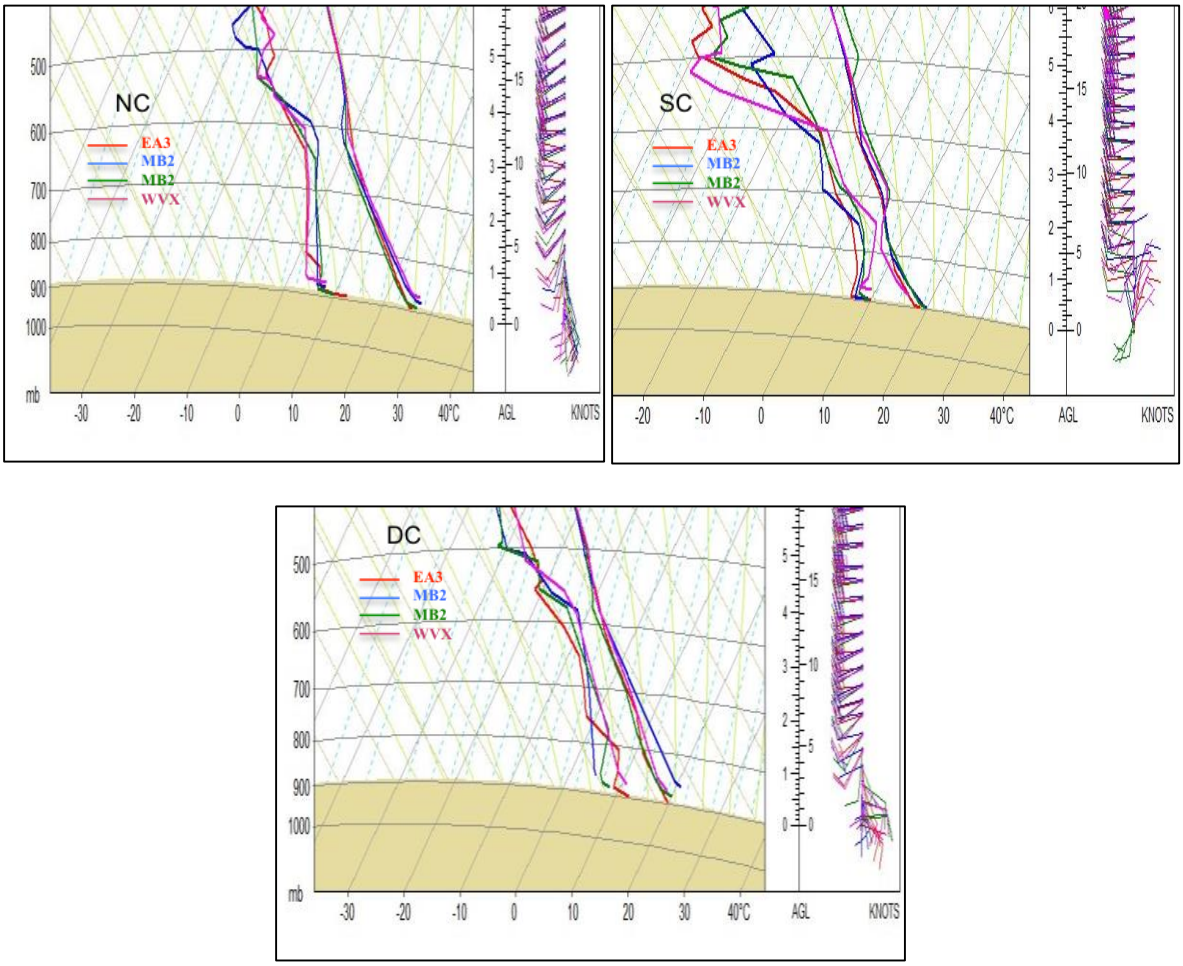

Figure 5.6: *NC (top left) SC (top right) and DC (bottom) P.M. Tephigrams from each site; EA3 (red), MB1 (blue), MB2 (green) and WVX (pink) with associated wind barbs (right) in knots.*

The DC low-level wind direction is more consistently from the east (over a deeper depth) and stronger speeds compared to NC and SC days. This would increase the amount of shear and streamwise SRH available to thunderstorms for prolonged mesocyclone rotation and therefore thunderstorm maintenance and potential for severe weather, enhancing the environment for tornadogenesis. This is illustrated in Figure 5.7. Higher values of SRH are most evident at EA3 and WVX with 61 and 77 $m^2 s^{-2}$ 0-1 km SRH respectively and lower values at MB1 and MB2 with 0-1 km SRH of 39 and 48 $m^2 s^{-2}$ respectively. 0-1 km SRH values on SC and NC day types were all less than 35 $m^2 s^{-2}$.

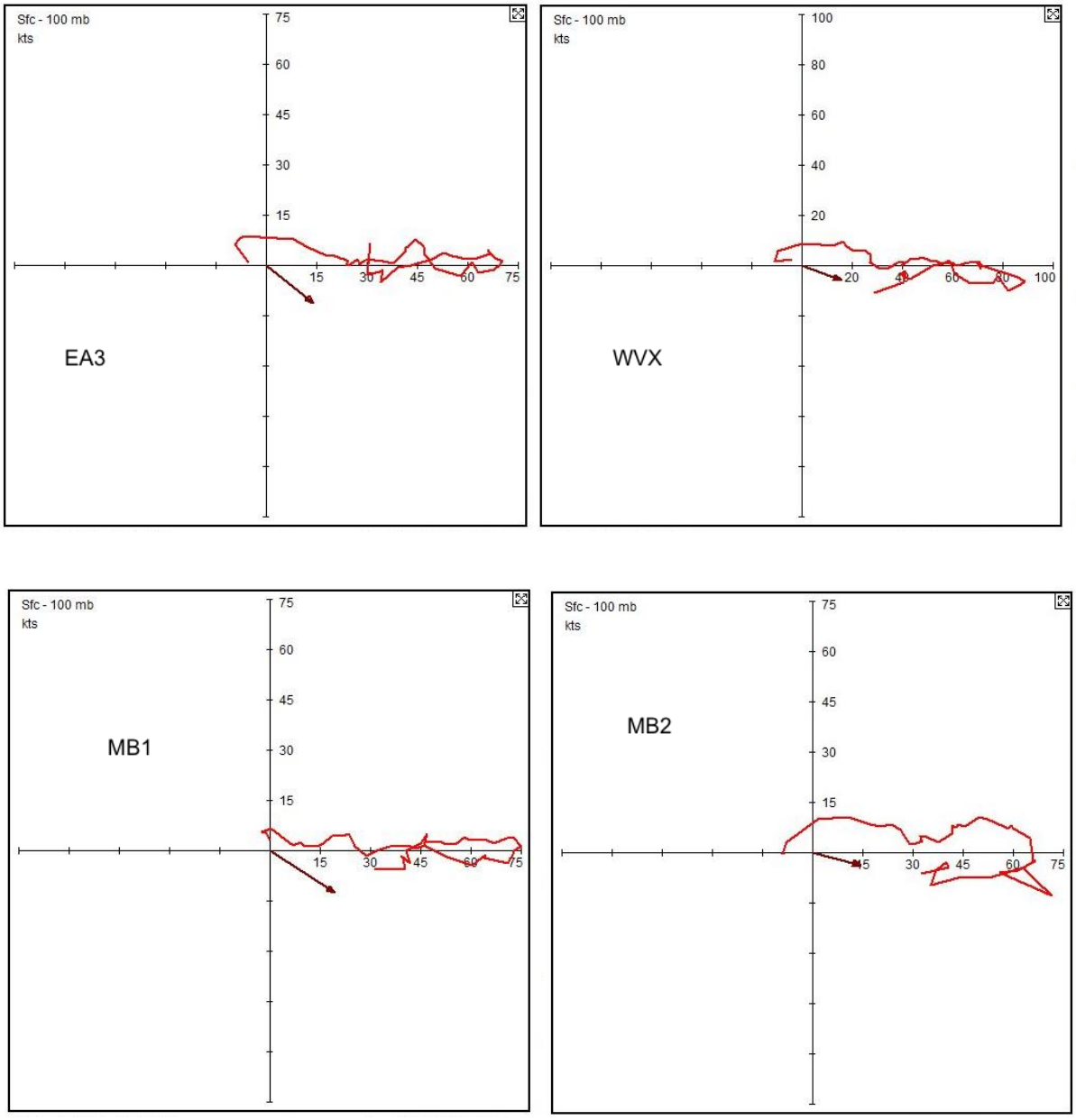

Figure 5.7: *DC P.M. hodographs from EA3 (top left), WVX (top right), MB1 (bottom left) and MB2 (bottom right) illustrating the increased low-level shear and SRH associated with low-level veering with height combined with backing of the surface winds.*

Visualizing the sites by day types (Figure 5.8) continues to reveal similar trends as previously stated. The NC day type has the warmest column at all sites, with a deep well mixed boundary layer and dry adiabatic lapse rates in the low-levels. The mid-level inversion on SC

days appears to be stronger at WVX and MB2. Surface dew point was usually within 2 to 3° between day types at all sites. BL dew points varied the least at MB2, about 2-3° below 700 hPa or 2 km. BL moisture varied the most at EA3 and WVX. Below 700 hPa or 2 km there was up to an 8° difference between day types. Surface wind direction on DC day type was easterly at all sites except MB1, which was from the south. MB2 had the strongest surface wind speed of 10 kt (5 m s^{-1}), whereas the other sites had winds of 5 kt (2.5 m s^{-1}). NC day types had south and southeast low-level winds at all sites. SC day type showed northeast low-level winds at all sites except MB2.

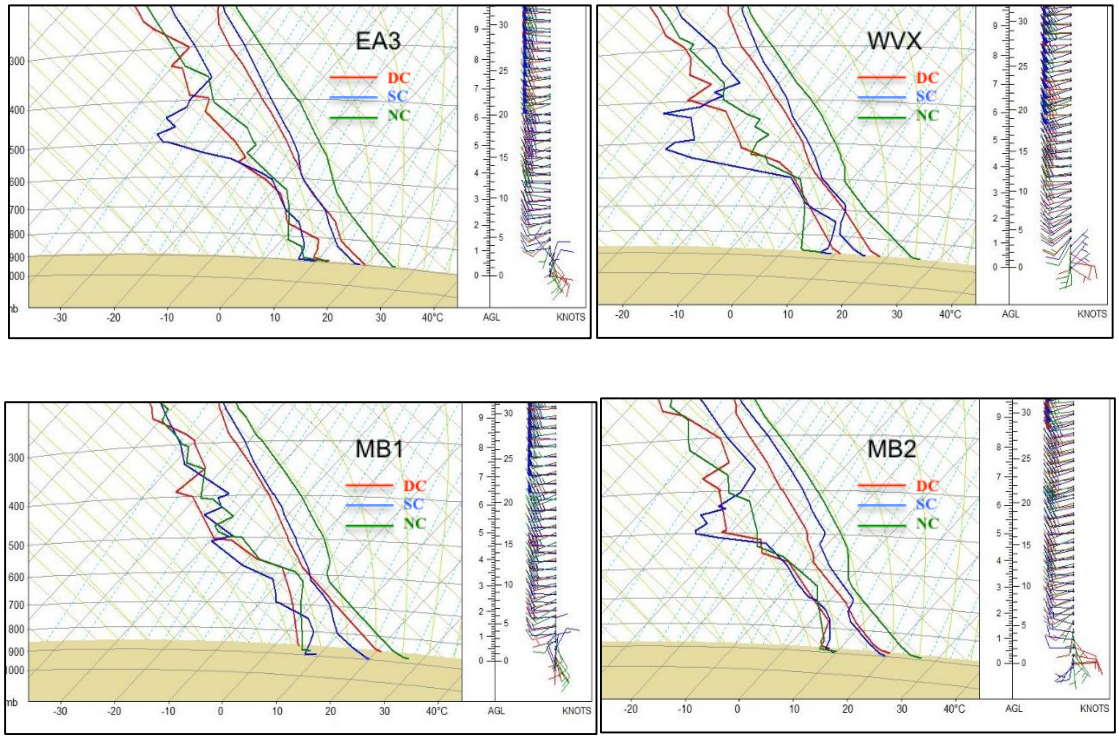

Figure 5.8: *Tephigram of P.M. composites at EA3 (top left), WVX (top right), MB1 (bottom left) and MB2 (bottom right) of DC days (red), SC days (blue) and NC days (green) with associated wind barbs (right) in kts.*

The DC day type had the highest number of soundings and therefore, would be a suitable example to indicate the amount of variation within the composite sounding. As seen in Figure 5.9, there is about a +/-3° variation in temperature and about a +/-2° variation in dew point in the layer below 700 hPa. There is less variation in the upper level, especially in temperature. Dew point has higher variation at 450 hPa. These variations are reflected in the standard deviation (σ) values in Table 5.1. The wind speed σ displayed the highest values and therefore largest variation between the sites in the 250 to 200 hPa level. This is the location of the jet stream and therefore, a much larger range of possible wind speeds.

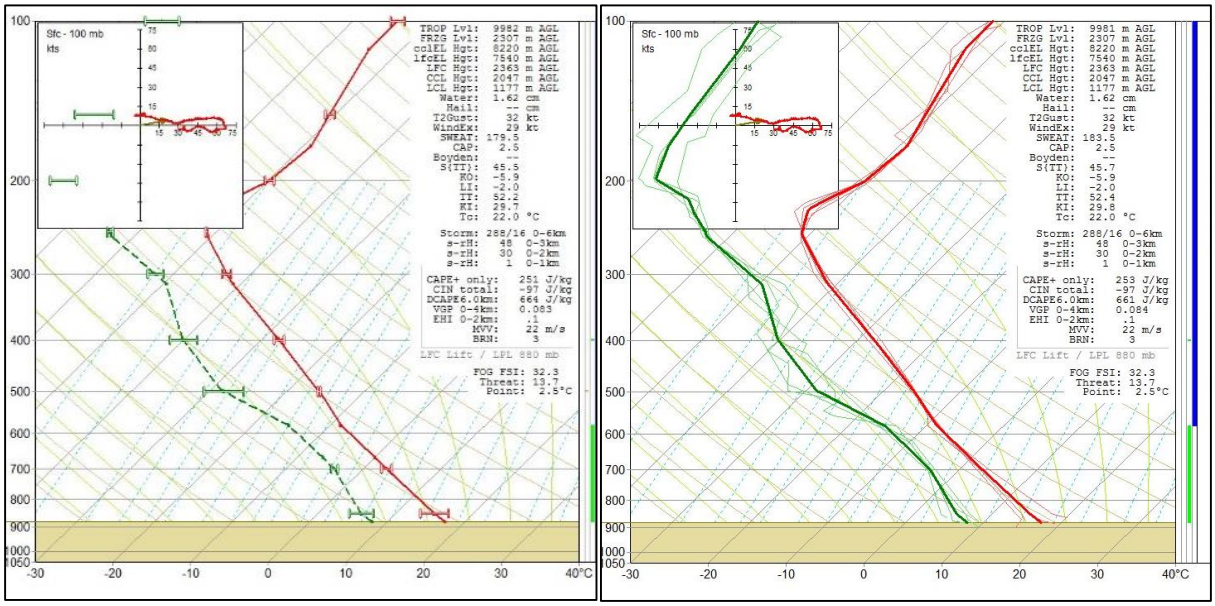

Figure 5.9: *Daily composite skew-T soundings from all sites for DC day type with error bars (left) and spaghetti plot (right) to indicate variation between the composites.*

Table 5.1: *Statistics of the DC day type composite assoicated with the black sounding in Figure 5.10. (°C) is degrees Celcius and S.D. is standard deviation.*

Pressure	Temperature		Dewpoint		Wind	
(hPa)	Mean (°C)	S.D.	Mean (°C)	S.D.	Mean (kts)	S.D.
100	-53.4	1.1	-82.9	1.6	26.9	4.9
150	-49.7	1.9	-80	2.9	44.2	11.5
200	-48.2	2.1	-76.3	2.1	58.3	22.1
250	-50.8	2.1	-63.8	2.4	65.4	20.1
300	-44.5	1.9	-54.2	3	54	18.5
400	-28.7	1.5	-39.8	5.7	39.4	12.7
500	-16.6	1.1	-25.8	5.9	32.1	8.9
700	1.4	1.7	-3.2	0.9	14.5	5.4
850	12.4	3.2	5.6	1.4	9.9	5.7

5.2.4. Severe Weather Parameters

The objective of this section is to identify if there are severe weather indices that can differentiate well between the convective regimes. Statistics were calculated using all P.M. sounding values of each parameter categorized by day type (DC, SC, NC). Parameters that had statistically different means between all day types were 850 and 700 hPa temperatures, SWEAT, LI, SI, 700-500 hPa lapse rate. Their associated box plots are in the figures that follow below. See Table 5.2 at the end of the section for a full list of severe weather parameters and their T-test results. The red lines represent the median of the data, the boxes represent the 75^{th} and 25^{th} quartiles. The whiskers extend to the extreme of the data and outliers are marked as individual points.

Both 850 and 700 hPa temperatures in Figure 5.10 and Figure 5.11 indicate the NC days as having the warmest temperatures, as has been indicated in the tephigram analyses. Both SC

and DC days are cooler than the NC days, however, DC days are warmer than SC days, indicating more low and mid-level instability.

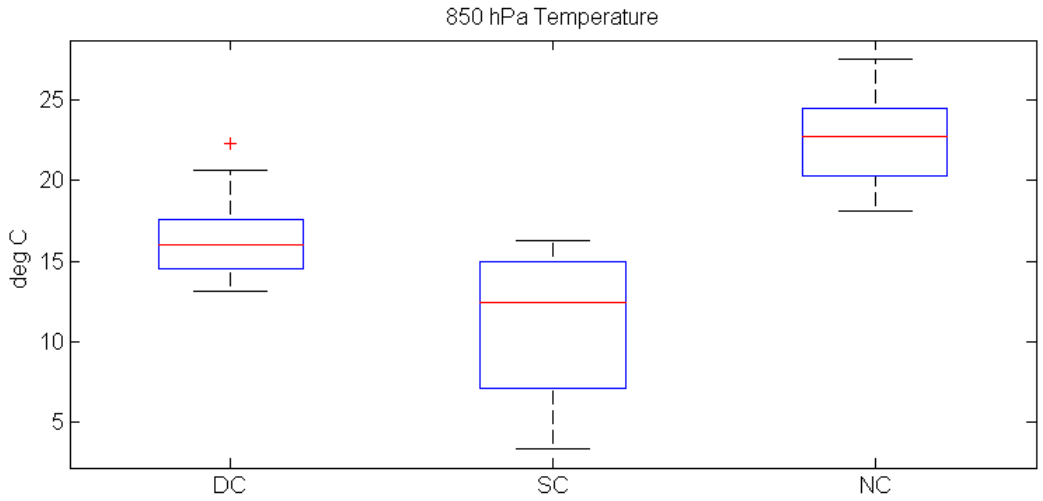

Figure 5.10: *850 hPa temperature with °C on the Y-axis and day type on the X-axis.*

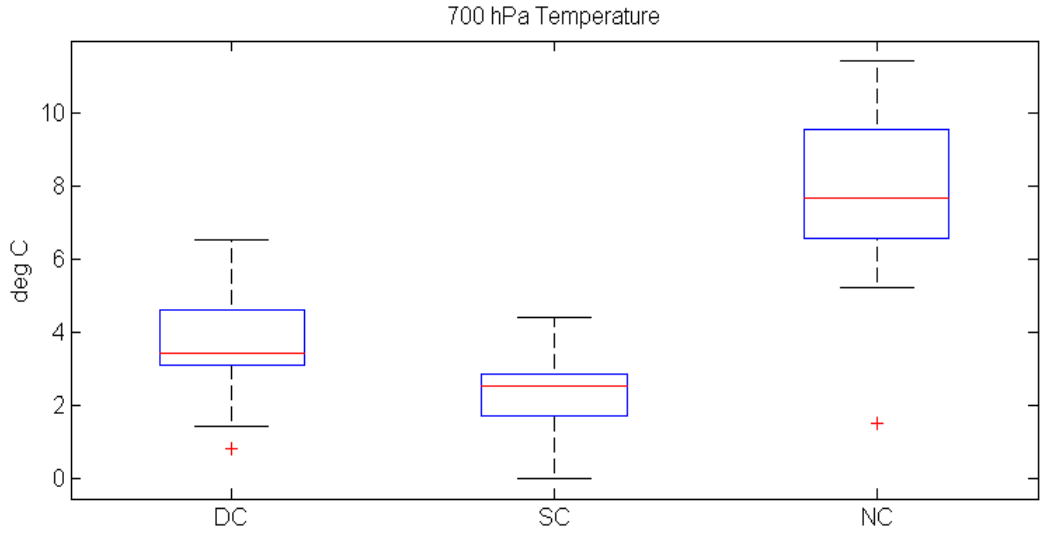

Figure 5.11: *700 hPa temperature with °C on the Y-axis and day type on the X-axis*

The Severe Weather Threat index (SWEAT) is shown in Equation 6. The box plot in Figure 5.12 clearly demonstrates a significantly increasing SWEAT score from NC day type to

DC day type. There is a larger spread in the DC day type compared to the NC day type since there is no upper SWEAT limit on the DC day type.

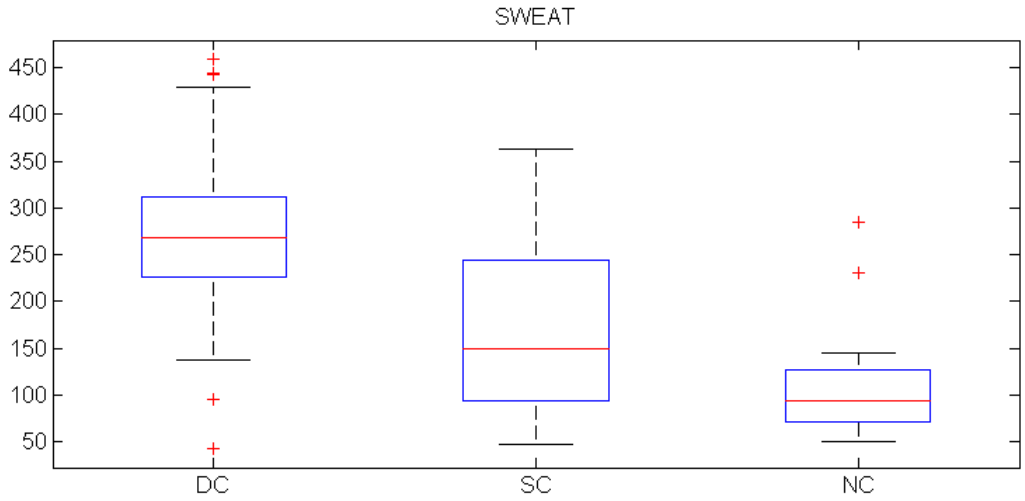

Figure 5.12: *SWEAT index with the dimensionless index on the y-axis and day type on the x-axis.*

The box plot of LI indicates a large difference between DC days and SC and NC days in Figure 5.13. SI shows more of a scale between the three day types in Figure 5.14.

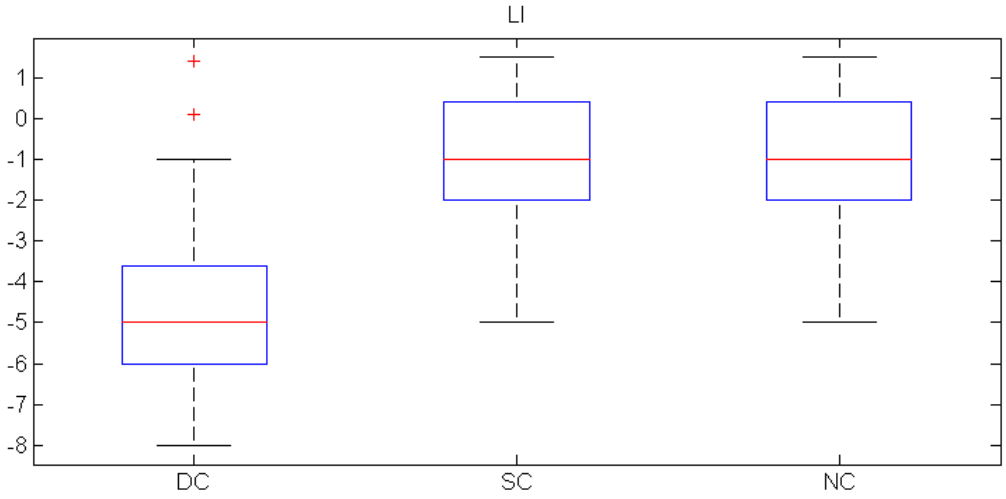

Figure 5.13: *Lifted index with the dimensionless index on the Y-axis and day type on the X-axis.*

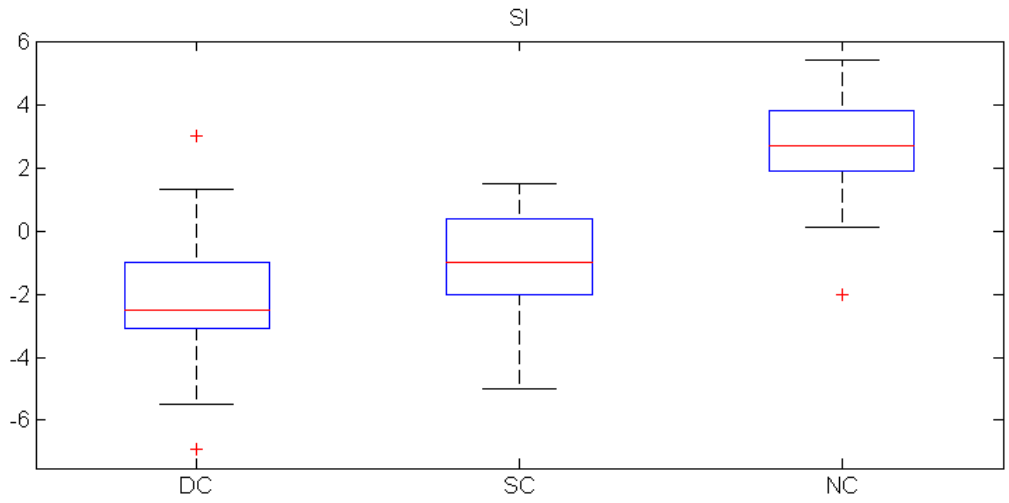

Figure 5.14: *Showalter index with the dimensionless index on the y-axis and day type on the x-axis.*

The 700 – 500 hPa lapse rates in Figure 5.15 are steepest in the DC days, less steep in SC days and even more so in NC day types. This is related to the 850 and 700 hPa temperatures as presented in previous plots.

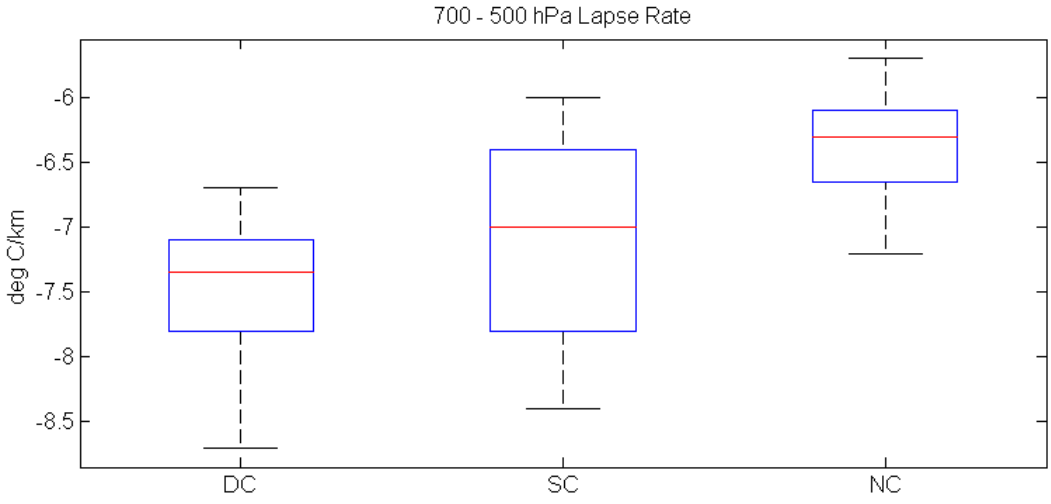

Figure 5.15: *700-500 hPa Lapse Rate with ° C km^{-1} on the y-axis and day type on the x-axis.*

Comparing all of the severe weather parameters between DC and SC P.M. profiles in Figure 5.16 yields higher values of CAPE, 711 J kg^{-1} on DC days and 147 J kg^{-1} on NC days, and wind shear 0-6 km values of 4.25 and 3.59 x$10^{-3}s^{-1}$ for each DC and NC days. All instability indices indicated more instability on DC days compared to the SC days. The CAPE hail parameter was larger in the DC day type (396 compared to 84 J kg^{-1}) indicating stronger ascent in the -10 to -30°C range, leading to a more favorable profile for hail growth. The mean LFC on the DC day types was 1937 m, whereas the SC day type LFC height was much higher, 2440 m, further indicating there would need to be a strong external triggering mechanism for air parcels to ascend.

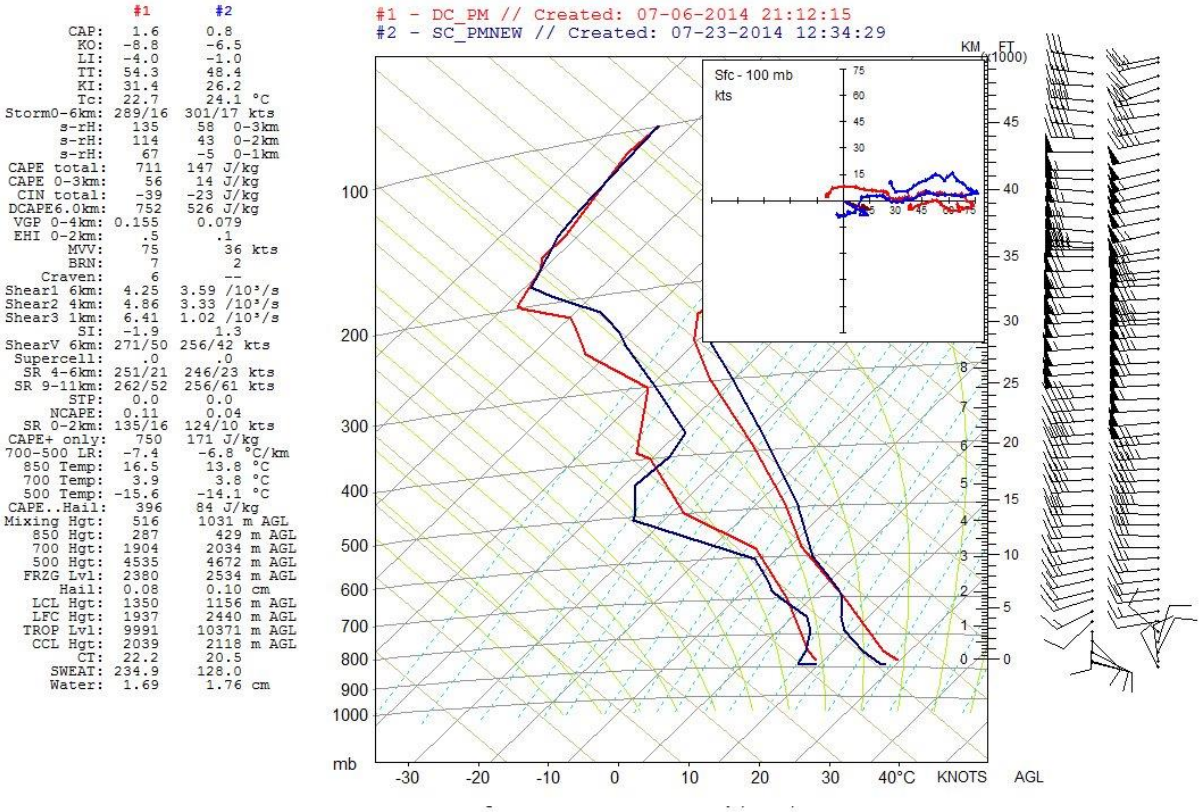

	#1	#2	
CAP:	1.6	0.8	
KO:	-8.8	-6.5	
LI:	-4.0	-1.0	
TT:	54.3	48.4	
KI:	31.4	26.2	
Tc:	22.7	24.1	°C
Storm0-6km:	289/16	301/17	kts
s-rH:	135	58	0-3km
s-rH:	114	43	0-2km
s-rH:	67	-5	0-1km
CAPE total:	711	147	J/kg
CAPE 0-3km:	56	14	J/kg
CIN total:	-39	-23	J/kg
DCAPE6.0km:	752	526	J/kg
VGP 0-4km:	0.155	0.079	
EHI 0-2km:	.5	.1	
MVV:	75	36	kts
BRN:	7	2	
Craven:	6	--	
Shear1 6km:	4.25	3.59	/10³/s
Shear2 4km:	4.86	3.33	/10³/s
Shear3 1km:	6.41	1.02	/10³/s
SI:	-1.9	1.3	
ShearV 6km:	271/50	256/42	kts
Supercell:	.0	.0	
SR 4-6km:	251/21	246/23	kts
SR 9-11km:	262/52	256/61	kts
STP:	0.0	0.0	
NCAPE:	0.11	0.04	
SR 0-2km:	135/16	124/10	kts
CAPE+ only:	750	171	J/kg
700-500 LR:	-7.4	-6.8	°C/km
850 Temp:	16.5	13.8	°C
700 Temp:	3.9	3.8	°C
500 Temp:	-15.6	-14.1	°C
CAPE..Hail:	396	84	J/kg
Mixing Hgt:	516	1031	m AGL
850 Hgt:	287	429	m AGL
700 Hgt:	1904	2034	m AGL
500 Hgt:	4535	4672	m AGL
FRZG Lvl:	2380	2534	m AGL
Hail:	0.08	0.10	cm
LCL Hgt:	1350	1156	m AGL
LFC Hgt:	1937	2440	m AGL
TROP Lvl:	9991	10371	m AGL
CCL Hgt:	2039	2118	m AGL
CT:	22.2	20.5	
SWEAT:	234.9	128.0	
Water:	1.69	1.76	cm

Figure 5.16: *Tephigram of DC P.M. composite in red and SC P.M. composite in blue with severe weather parameters (left) and wind barbs in knots (right).*

Similar results were observed comparing the DC and NC day types, shown in Figure 5.17. Of note, the convective temperature is much higher in the NC day type, 32.3°C compared to 22.7°C on DC day types. On NC days, it was much harder for air parcels to freely rise without a trigger since the convective temperature and LFC (3195 m) are so high. The DC day type hodograph shape is more favorable for severe development. Comparing the storm relative wind and vorticity vectors, low-level SRH, or streamwise vorticity, necessary for tornadic development, is more favorable in the DC day type. 0-1 km SRH values for DC, SC and NC days were 67, -5 and 24 $m^2 s^{-2}$ respectively.

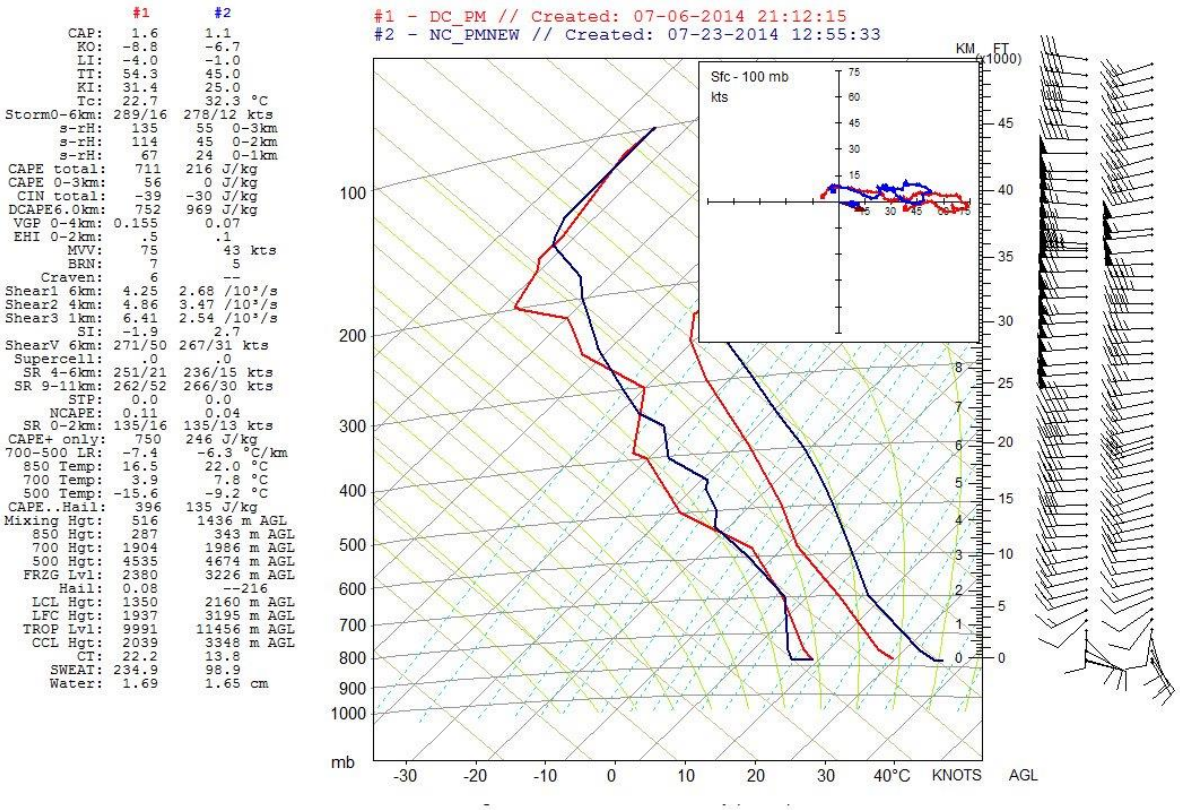

Figure 5.17: *Tephigram of DC P.M. composite in red and NC P.M. composite in blue with severe weather parameters (left) and wind barbs in knots (right).*

Comparable results were observed in the SC and NC assessment as seen in Figure 5.18, although to a lesser degree than the DC and NC day type comparison. Again the convective temperature was much larger on NC day types. The NC profile actually shows more favorable low-level shear as compared to the SC profile. SBCAPE is low in both cases, however, larger on the NC day as oppose to the SC day (171 and 246 J kg^{-1} respectively). If mixed layer CAPE (MLCAPE) is used, 0 J kg^{-1} is calculated for both day types. 700-500 hPa lapse rates were larger in the SC day (-6.8 compared to -6.3 °C km^{-1}).

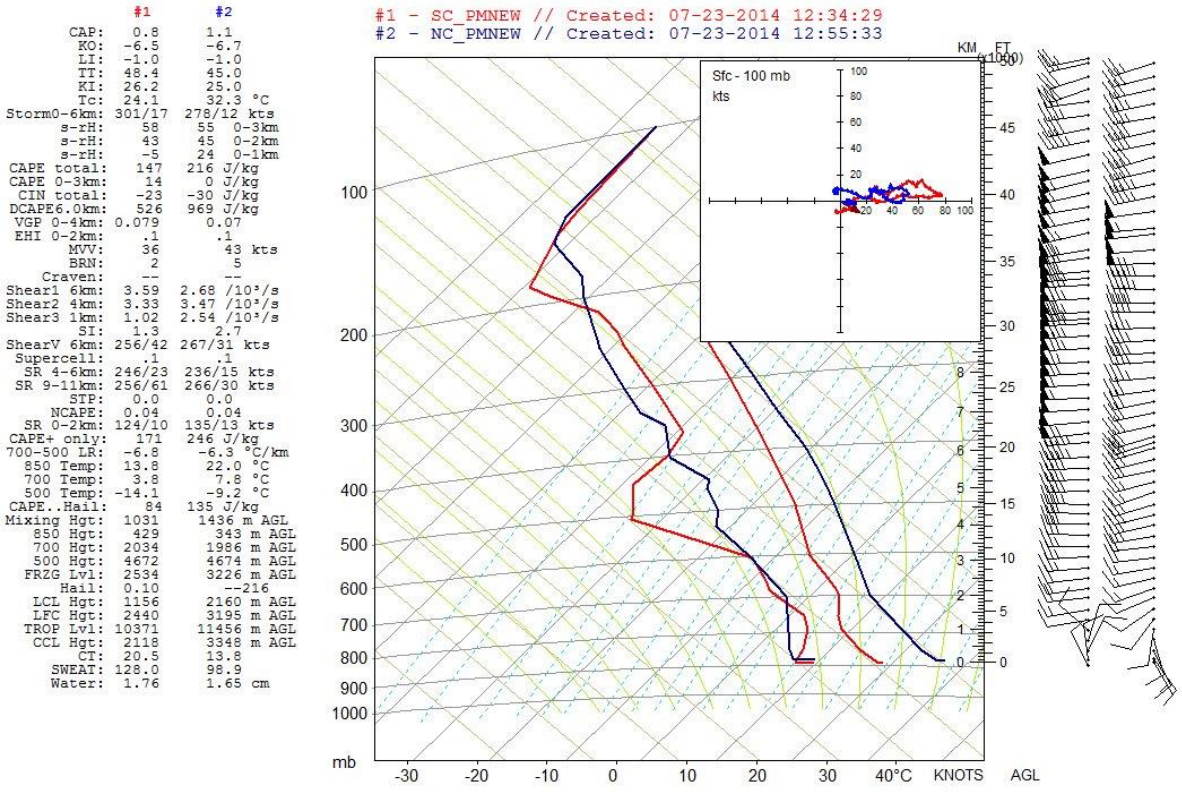

Figure 5.18: *Tephigram of SC P.M. composite in red and NC P.M. composite in blue with severe weather parameters (left) and wind barbs in knots (right).*

Table 5.2: *Severe Weather Parameter Statistical T-Test difference of means results between the different day types at the 0.05 significance level. D represents statistically Different and S represents statistically the Same. Difference between parameters may indicate it is useful for differentiating between day types. Red highlight indicates the parameter was different for all day types and therefore a box plot was analyzed in the previous section.*

	FZG LVL	LFC HGT	CCL HGT	LCL HGT	PW	SWEAT	850-700 LR AGL	T 500
DCvsSC	S	S	S	S	D	D	S	S
DCvsNC	D	D	D	D	S	D	D	D
SCvsNC	D	D	D	D	D	D	S	D

	LI	Tc	0-6 km Storm motion	0-6 km Storm motion	SRH 0-3 km	SRH 0-2 km	Sfc Td	T 700
DCvsSC	D	S	D	S	D	D	S	D
DCvsNC	D	D	S	D	D	D	S	D
SCvsNC	D	D	D	D	S	S	S	D

	SRH 0-1	CAPE total	CAPE 0-3	CIN	BRN	6 km Shear	Sfc T	T 850
DCvsSC	D	D	S	S	D	S	S	D
DCvsNC	S	D	D	D	S	D	D	D
SCvsNC	D	S	D	D	S	D	D	D

	3 km shear	1 km shear	SI	6 km Shear Vector (°)	6 km Shear Vector (kt)	700-500 LR	CAPE hail
DCvsSC	S	D	D	D	S	D	D
DCvsNC	D	D	D	S	D	D	D
SCvsNC	D	S	D	D	D	D	S

5.3. UNSTABLE Result Comparison to Previous Research

To give context to the UNSTABLE results, they will be compared to results from Taylor (1999) (T1999), Dupilka and Reuter (2011) (DR2011) and Rasmussen (2003) (R2003). T1999 used 0000 UTC Stony Plain, AB soundings from 1966 to 1996 to determine a climatology of Severe (Svr) and non-severe (Non Svr) days and their associated severe weather parameters. The Stony Plain sounding site is located 42 km west of Edmonton and is not representative of the UNSTABLE region due to the extreme difference in terrain and far distance away. DR2011 created composite soundings for severe thunderstorms over central Alberta from 1967-2000 also using the 0000 UTC Stony Plain dataset. In an attempt to characterize severe thunderstorms and tornadoes, they created three catagories; Non tornadic (NT), weak tornadic (WT), and strong tornadic (ST) thunderstorms. R2003 used research previously done in 1992 by Rassmunsen and Blanchard in the U.S. which analyzed all 0000 UTC soundings with non-zero CAPE to better differentiate between tornadic thunderstorms (TOR) and supercells (SUP) that produce large hail but no tornado. They created box plots to illustrate the data which are compared to UNSTABLE box plots in the following figures. These studies were chosen for their relevance to the research in this thesis as well as the similarity in study areas.

Table 5.3 displays the UNSTABLE, DR2011 and T1999 results. See Table 5.4 at the end of the chapter for associated mean, minimum, maximum and standard deviation of all of the UNSTABLE severe weather parameters. The surface temperatures during UNSTABLE were notably lower than what was found in DR2011 and T1999. The deep convective days mean temperature was 19.7°C compared to 21.8°C and 20.8°C for DR2011 and T1999 respectively. The surface dew points during UNSTABLE were also lower than both the DR2011 and T1999 studies; 14.4°C, 13.5°C and 9.1°C for Strong tornadic, Severe and DC days respectively. This is

also reflected in less favorable thunderstorm indices such as higher LI and SI. This may be due to the longer data sets that were used in these studies, months and years, in contrast this thesis covers only 2 weeks in July of 2008. The higher dew point on NC days as compared to SC and DC day types would indicate that moisture was not a limiting factor in thunderstorm development or severity, as discussed in section 2.7, 2008 was a relative wet year when compared to normal.

Table 5.3: *Severe weather parameter comparison between three studies: DR2011, T1999 and UNSTABLE 2008. MU represents the most unstable calculation of CAPE and LCL. It is calculated using the most unstable parcel in the lowest 300 hPa of the column.*

Parameter	Unit	DR2011			T1999		UNSTABLE 2008		
		ST	WT	NT	Svr	Non Svr	DC	SC	NC
0–1 km storm relative helicity	$m^2 s^{-2}$	45	20	0			55.9	15.4	27.0
0–3 km storm relative helicity	$m^2 s^{-2}$	169	79	75	58.3	43.8	158.3	96.9	112.7
Surface temperature	°C	21.8	20.4	21.7	20.8	17.5	19.7	18.6	23.1
Surface dewpoint	°C	14.4	11.7	13	13.5	6.4	9.1	8.7	10.1
MUCAPE	$J kg^{-1}$	817	543	1253	1500	258	1096.9	471.1	302.9
MULCL	km AGL	0.9	1.1	1.1			1.3	1.3	1.7
LI		−4	−3	−5			-4.6	-2.4	-0.4
SI		−2	−1	−2			-2.2	0.4	2.2
PW	mm	26	21	21	21.5	15.6	17.8	15.5	19.7
BRN		8	18	24	141	44	15.0	6.9	6.8
0-6 km shear	$x10^{-3} s^{-1}$	4.8	2.5	3.2	5.39	5.31	3.8	4.2	3.1

The figures below further describe the UNSTABLE results compared to the results from R2003 and DR2011. In Figure 5.19, extreme BRN values from UNSTABLE were half the value

from DR2011. Also in DR2011, the lowest BRN was associated with strong tornadoes, whereas the lowest BRN was associated with SC day types during UNSTABLE. The BRN results would indicate that during the UNSTABLE field campaign, most days had a shear to CAPE ratio favorable for supercell development and on some occasions too much shear (i.e. too much shear and not enough CAPE; BRN values less than 10).

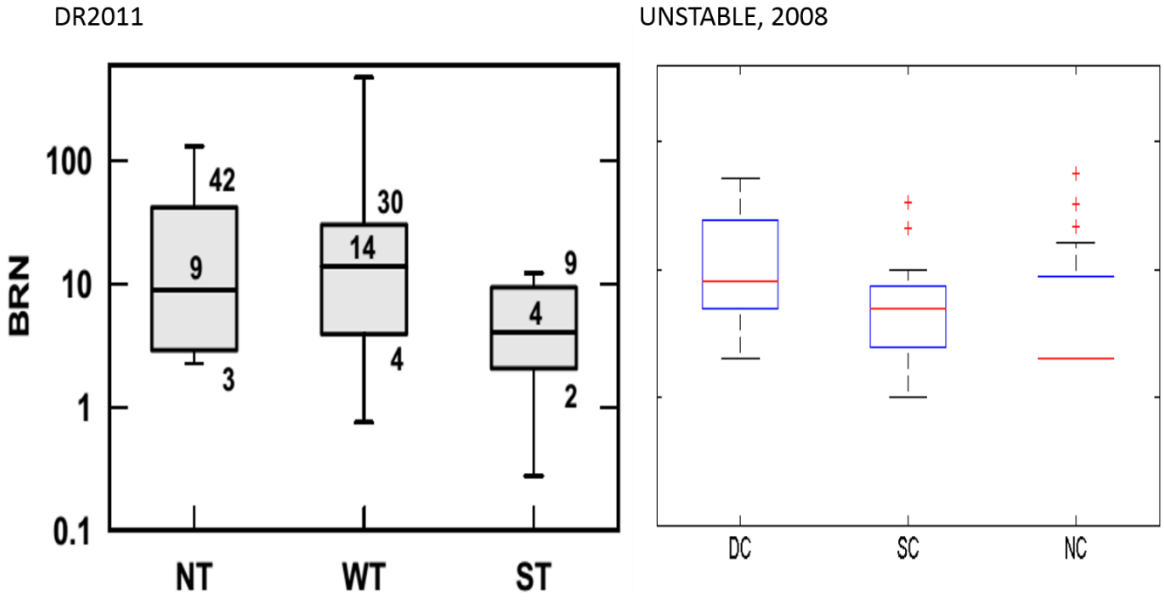

Figure 5.19: *BRN from DR2011 (left) and UNSTABLE, 2008 (right) with the BRN value on the Y-axis and day type on the X-axis.*

Precipitable water values in Figure 5.20 were comparable between DR2011 and UNSTABLE 2008, with mean values near 23 and 18 mm respectively. DR2011 showed the maximum amount associated with strong tornado days, whereas during UNSTABLE the highest PW was associated with SC days, although the means were similar between the three day types.

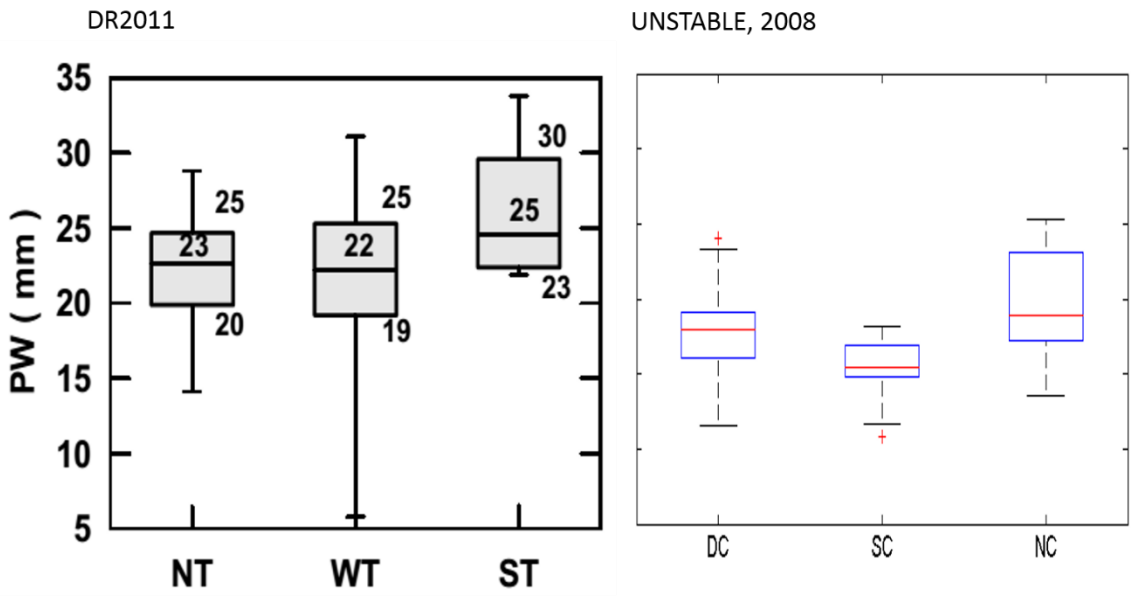

Figure 5.20: *Precipitable Water (PW) from DR2011 (left) and UNSTABLE, 2008 (right) with PW in mm on the y-axis and day type on the x-axis.*

Figure 5.21 indicates the 0-3 km CAPE was higher in the UNSTABLE, 2008 results with the 0-3 CAPE median at about 100 J kg^{-1} on DC days, whereas it was 63 J kg^{-1} for TOR days in the R2003 results. Both indicated larger 0-3 km CAPE with increasing day type severity. This larger value for UNSTABLE DC days than R2003 TOR days may be due to the UNSTABLE results not separating tornadoes from supercells as was done in R2003. However, even comparing the SUP to SC days, the SC days still have a higher 0-3 km CAPE, with median values for 80 J kg^{-1} on SC days and 24 J kg^{-1} on SUP days. This could also be due to the steep mid-level lapse rates that would exist in the UNSTABLE data, however, would not produce a strong signal in the Rasmussen data since soundings from across the entire continental U.S. were used.

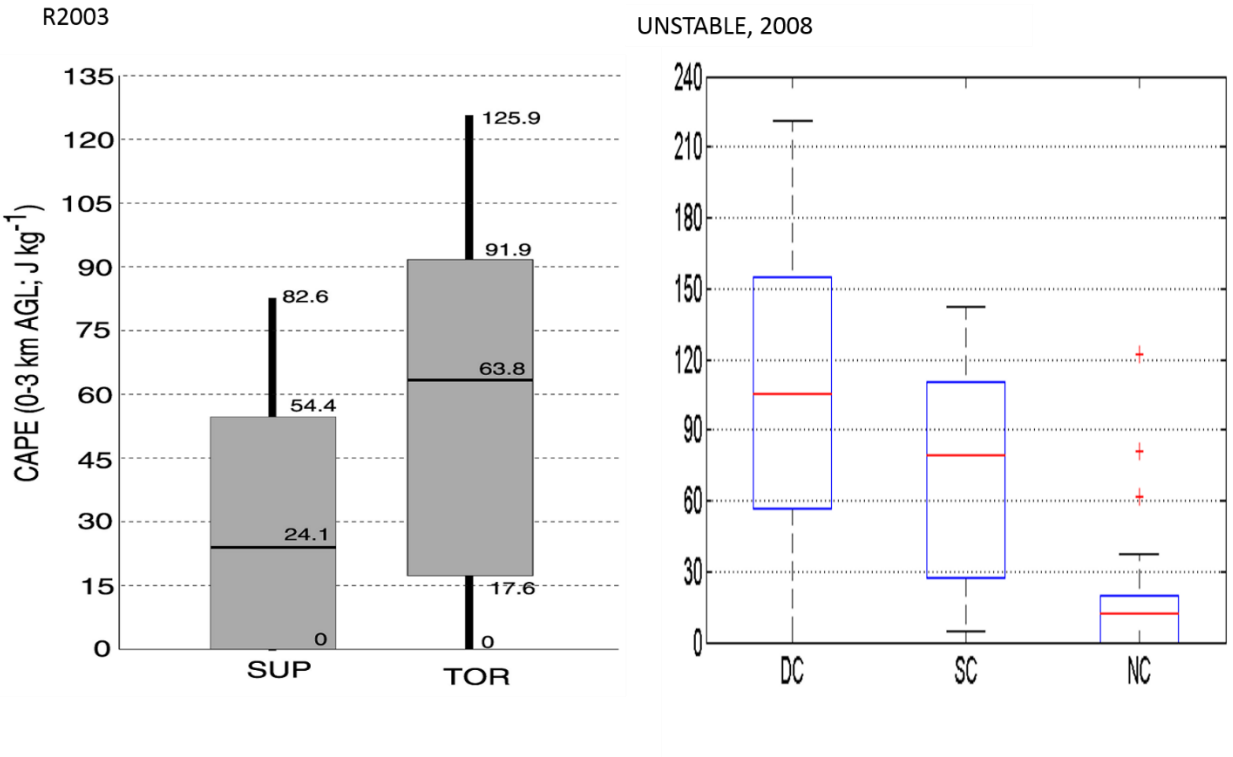

Figure 5.21: *0-3 km CAPE from R2003 (left) and UNSTABLE, 2008 (right) with CAPE in J Kg^{-1} on the y-axis and day type on the x-axis. Note the different y-axis scale on each of the bar graphs.*

0-1 km AGL SRH in Figure 5.22 R2003 and DR2011 illustrate a similar trend of an increase in 0-1 SRH with an increasing severity of day type. However, UNSTABLE, 2008 data illustrated higher SRH on NC days than SC days. This could be due to the unfavorable environmental conditions for convective initiation present on NC day types, therefore the existing SRH was not realized.

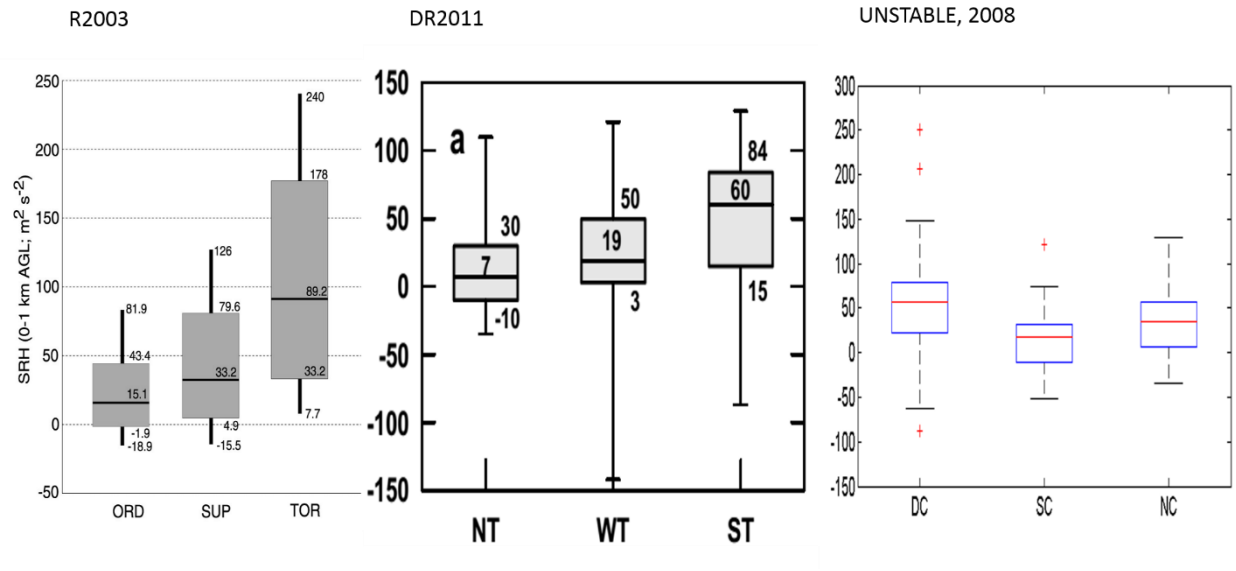

Figure 5.22: *0-1 km AGL SRH from R2003 (left), UNSTABLE, 2008 (middle) and DR2011 (right) with SRH in m^2 s^{-2} on the y-axis and day type on the x-axis. Note the different y-axis scale on each of the bar graphs.*

5.4. Convective Day Type Summary

P.M. composites better represented convective potential when compared to daily composites. Nil convective (NC) day composites were characterized by warm air at all levels associated with an upper ridge which prevented convective initiation. Shallow convective (SC) and deep convective (DC) day composites had similar temperature profiles, except the SC days typically had mid-level warm air to potentially cap deep convection. DC days had weaker mid-level capping and cooler upper levels, generally increasing instability. All day types exhibited the mountain-plain circulation with low-level winds backing throughout the day. Three out of five DC days exhibited backing throughout the day, whereas only one out of three NC days displayed backing. Two out of four SC days exhibited backing. On DC days, this is associated

with moisture advection underneath the capping lid contributing to potentially explosive convection.

Comparisons between day types were also made using sites composite tephigrams. The main difference between sites was the depth and magnitude of moisture. Sites located in areas of local surface evapotranspiration, such as EA3 and WVX, generally exhibited higher surface dew point values as well as deeper BL moisture on DC and SC day types. This could be attributed to the stronger and deeper easterly flow induced by the mountain-plain circulation and/or synoptic forcing. Sites west of the surface moisture gradient, in the Cordillera eco-climate zone (MB1), exhibited lower dew points. This could be due to less evapotranspiration produced by the boreal forest when compared to the crops and grasslands further east. However, this was not consistent as it depended on where the mobile sites (MB1 and MB2) were situated. Deciphering differences among the sites may require a more detailed investigation about land cover and soil moisture character within the UNSTABLE domain and surrounding areas, however, this is beyond the scope of this thesis.

Convective indices comparisons were also compared using statistical methods. Statistical differences at the 0.05 significance level between DC, SC and NC day types were found for LI, SI, 850 and 700 hPa temperatures, 700-500 lapse rates and SWEAT. Overall, warmer low-levels and mild mid-levels led to lower LIs and SIs, higher SWEATs with steeper lapse rates on DC day types. Comparing all parameters between the day types revealed that shear was most favorable on DC days, however, it was also more favorable on NC days rather than SC days. This reveals an important note for individual parameter usage; no one parameter can fully encompass all of the complexities of thunderstorm initiation and severity. Therefore, this

exercise must be used as a method of qualitative description and not explicit as it is important to use other analyses products to deduce the true risk of convection taking place.

Comparing the results from UNSTABLE to other studies, such as R2003 and DR2011, indicated similar results. Of interest was the lower surface dew points observed during the UNSTBALE campaign, which could be a seasonal variation since the other studies were completed in different years. This may also be reflected in the PW values which were much less than what was observed by DR2011. Also of note, 0-3 km CAPE during UNSTABLE was higher in magnitude than the R2003 study, which used over 600 0000 UTC non 0 J kg^{-1} CAPE soundings from the United States in 1992.

Table 5.4: *Mean (μ), minimum (min), maximum (max) and standard deviation (σ) for each severe weather parameter on each convective day type during the UNSTABLE field campaign.*

		μ	Min	Max	σ		μ	Min	Max	σ
	DC	2338.34	2072.00	2561.00	139.75		101.09	-76.00	221.00	71.20
	SC	2305.73	1980.00	2603.00	196.60	**CAPE 0-3**	79.68	5.00	302.00	65.54
FZG LVL (m)	**NC**	3064.00	2512.00	3733.00	314.05	**(J kg^{-1})**	24.80	0.00	122.00	31.16
	DC	1515.09	694.00	3063.00	572.33		-0.16	-102.0	537.00	101.07
LFC HGT	**SC**	1375.63	532.00	2453.00	541.74	**CIN**	-16.89	-62.00	0.00	17.05
(m)	**NC**	2691.35	1771.00	5720.00	938.44	**(J kg^{-1})**	-47.45	-152.0	0.00	41.16
	DC	1854.67	859.00	3084.00	464.25		14.97	2.00	52.00	13.99
CCL HGT	**SC**	1912.27	1023.00	2962.00	634.94		6.89	1.00	34.00	7.41
(m)	**NC**	3232.40	2052.00	4712.00	749.25	**BRN**	11.40	0.00	57.00	13.30
	DC	1272.47	632.00	3063.00	649.92	**6 km Shear**	3.80	1.48	5.52	1.35
LCL HGT	**SC**	1258.52	532.00	1932.00	419.06	**(10^{-3}**	4.24	2.11	6.05	1.35
(m)	**NC**	2218.90	1450.00	3178.00	515.98	**s^{-1})**	2.65	1.57	3.58	0.53
	DC	1.78	1.16	2.40	0.29	**3 km shear**	5.00	1.60	7.97	1.69
PW	**SC**	1.55	1.08	1.82	0.18	**(10^{-3}**	4.78	3.17	6.80	0.96
(cm)	**NC**	1.74	1.36	2.49	0.25	**s^{-1})**	3.27	1.52	5.15	1.11
	DC	271.07	43.00	458.80	97.19	**1 km shear**	5.36	2.07	11.98	2.35
	SC	164.54	46.50	363.70	94.34	**(10^{-3}**	3.84	0.12	7.47	2.04
SWEAT	**NC**	108.07	49.80	284.80	59.29	**s^{-1})**	3.93	1.28	8.42	2.18

Table 5.5: *Mean (μ), minimum (min), maximum (max) and standard deviation (σ) for each severe weather parameter on each convective day type during the UNSTABLE field campaign.*

		μ	Min	Max	σ		μ	Min	Max	σ
	DC	-4.56	-8.00	1.40	2.08		-2.18	-6.90	3.00	2.13
	SC	-2.42	-6.30	1.00	2.01		0.43	-4.70	4.40	2.53
LI	**NC**	-1.02	-5.00	1.50	1.63	**SI**	2.63	-2.00	5.40	1.76
	DC	22.00	19.10	25.70	1.61		267.65	232.00	292.00	15.36
	SC	21.18	14.90	27.40	3.71	**ShearV 6km (°)**	279.79	269.00	297.00	9.41
Tc (°C)	**NC**	31.06	25.00	38.60	4.31		256.40	219.00	311.00	30.93
Storm motion 0-6 km (°)	**DC**	286.65	241.00	324.00	20.63		44.32	17.00	64.00	15.77
	SC	307.54	297.00	317.00	5.97	**ShearV 6km (kt)**	49.46	25.00	71.00	15.79
	NC	278.75	256.00	305.00	15.76		30.90	18.00	42.00	6.20
Storm motion 0-6 km (kt)	**DC**	16.47	8.00	23.00	5.27	**700-500 LR (°C km^{-1})**	-7.42	-8.70	-6.70	0.48
	SC	18.42	14.00	24.00	2.86		-7.07	-8.40	-6.00	0.74
	NC	12.20	7.00	16.00	2.84		-6.37	-7.20	-5.70	0.39
SRH 0-3 (m^2 s^{-2})	**DC**	158.28	-10.00	434.00	114.01		16.36	13.10	22.30	2.40
	SC	96.93	25.00	290.00	58.56	**T 850 (°C)**	13.53	8.10	16.30	2.10
	NC	97.80	4.00	304.00	74.88		22.52	18.10	27.50	2.75
SRH 0-2 (m^2 s^{-2})	**DC**	129.92	-7.00	391.00	99.40		3.79	0.80	6.50	1.45
	SC	79.93	27.00	209.00	48.54	**T 700 (°C)**	2.32	0.00	4.40	0.99
	NC	72.80	-10.00	231.00	66.90		7.65	1.50	11.40	2.25
SRH 0-1 (m^2 s^{-2})	**DC**	55.94	-88.00	250.00	63.79		-15.60	-17.70	-12.70	1.17
	SC	15.41	-52.00	121.00	38.56	**T 500 (°C)**	-16.17	-18.50	-12.80	1.71
	NC	45.50	-22.00	130.00	49.75		-8.98	-11.10	-7.30	1.13
CAPE total (J kg^{-1})	**DC**	1096.88	22.00	2276.00	585.97	**CAPE hail (J kg^{-1})**	441.19	0.00	791.00	222.15
	SC	471.07	4.00	1162.00	344.78		252.52	0.00	633.00	186.64
	NC	506.30	13.00	2271.00	621.30		218.65	0.00	1018.00	265.77
850-700 LR AGL (°C km^{-1})	**DC**	-7.63	-4.13	-9.89	-1.45		19.77	16.00	26.00	2.30
	SC	-8.12	-4.74	-28.45	-5.04	**Sfc T (°C)**	18.64	14.00	23.00	2.90
	NC	-9.03	-7.55	-13.73	-1.30		26.50	16.00	30.00	3.53
Sfc Td (°C)	**DC**	9.00	-1.00	14.00	4.54					
	SC	8.72	5.00	13.00	1.65					
	NC	9.40	5.00	16.00	2.91					

CHAPTER 6: RESULTS

6. TARGETED SOUNDINGS FOR USE IN SEVERE STORM PREDICTION

6.1. Overview

This chapter focuses on the final thesis objective "To illustrate how targeted soundings can be useful for severe storm prediction". Two case studies are presented for this purpose. These two days during the field project were classified as deep convective (DC) days due to tornados that were reported, both on the southern edge of the study area. The following sections will describe the meteorological features present that led to the formation of the tornadoes. Specifically, focusing on the soundings that were launched on these days and their proximity to the events. Potvin et al. (2010) illustrated that proximity sounding are critical in accurately assessing the near and pre-storm environment. They demonstrated an optimal proximity spatiotemporal distance of 40-80 km and 0-1 hour between the event and sounding when attempting to measure the potential for thunderstorm and tornadic development. When compared to the standard synoptic radiosonde launches available, the UNSTABLE mobile soundings launched were more representative of the tornadic environment present by better capturing CAPE, low-level SRH and shears, which will be demonstrated in the subsequent chapter.

6.2. July 7, 2008; An F0 tornado Near Calgary, AB

6.2.1. Overview: Synoptic scale surface and upper air analysis

This day was characterized by an upper trough at 250 and 500 hPa with associated cold air that crossed Alberta from 1200 UTC on the 7th to 0000 UTC on the 8th. A northwest upper 95

kt (49 m s^{-1}) jet at 250 hPa entered the region by 0000 UTC on July 8th. 700 hPa displayed a northwest flow with a moist axis in southeast Alberta by 1200 UTC. At 850 hPa a thermal ridge sat along the Rocky Mountains with a baroclinic zone through central Alberta that exhibited frontolysis by 0000 UTC on the 8th. The tornado on July 7th, 2008 was reported just east of Calgary and it was rated F0. The three UNSTABLE soundings launched on this day were 60-70 km away from the tornado. Two were launched from WVX, one 5 hours before and one 3.5 hours before. One was launched from MB1 which was 38 minutes before the tornado. The closest standard synoptic sounding in proximity to the event was out of Stony Plain (WSE), 324 km away from the event. The standard synoptic soundings are launched every 12 hours; at 1200 (10 hours prior to the event) and 0000 UTC (2 hours after the event). Sounding locations are shown in Figure 6.1.

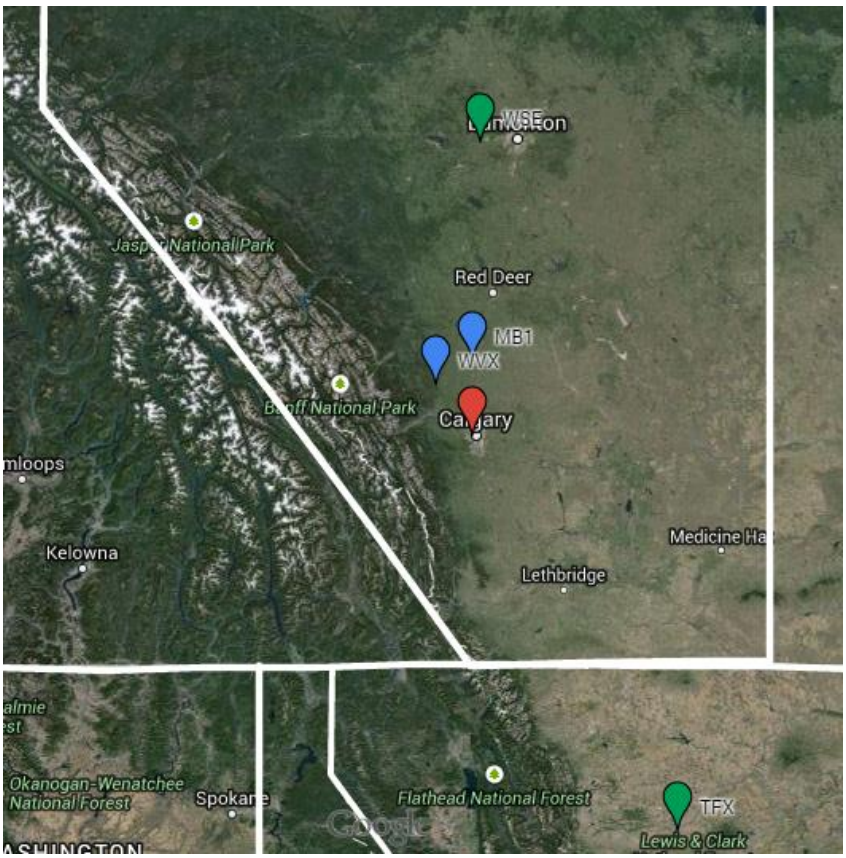

Figure 6.1: *Google Map from July 7th, 2008 of the standard synoptic sounding launch sites in green at Stony Plain, AB (WSE) and Great Falls, MT (TFX), UNSTABLE soundings in blue at MB1 and the location of the Calgary F0 tornado in red for reference.*

6.2.2. BL Evolution

The dew point (Td) and mixing ratio (r) profiles, shown in Figure 6.2, displayed an increasing trend throughout the day below 775 hPa or about 1 km. This was reflected in equivalent potential temperature (θ_e) which displayed a 5 K increase below 800 hPa and about 2 K increase above 800 hPa, overall increasing instability in the column. A deeper moist layer was also exhibited later in the day. Potential temperature (θ) also indicated a destabilization throughout the day. θ_e and θ are shown in Figure 6.3. This is similar to what was found in Chapter 4 in the difference between the DC day types and SC and NC day types. The increase in

moisture depth and magnitude may be due to advection and/or evapotranspiration. T was very similar between the two sites and three soundings, as seen in Figure 6.4. There was not much warming throughout the day. Both sites displayed weak inversions at different altitudes. Surface wind direction was consistently out of the northeast between 90° and 30° for all soundings, indicative of surface moisture advection, and then sharply veered at 800 hPa to west northwest (300°). Winds near the surface in all soundings were weak; near 5 kt (2.5 m s^{-1}). There was no evidence of a low-level wind maximum in the soundings from WVX (1558 and 1729 UTC), shown in Figure 6.5, but by 2238 UTC in the soundings launched from MB1, there seemed to be a mid-level wind maximum developing at 650 hPa of 30 kt (15 m s^{-1}). The winds aloft in all soundings were also stronger than most days during UNSTABLE; 90 kt (46 m s^{-1}) at 250 hPa which weakened through the day to 70 kt (36 m s^{-1}).

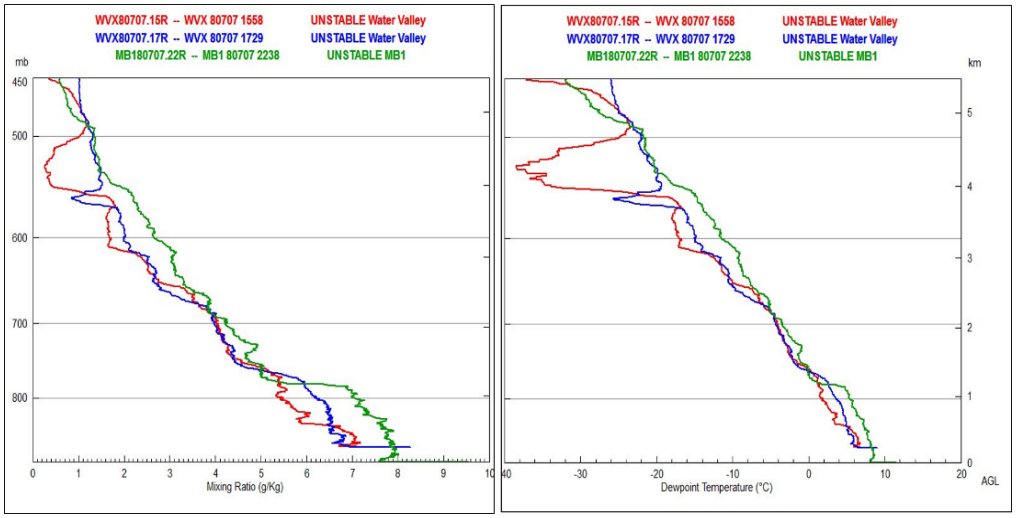

Figure 6.2: *Mixing ratio (right) and dew point temperature (right) profiles on July 7th from WVX at 1558 (red), WVX 1729 (blue) and MB1 at 2238 (green).*

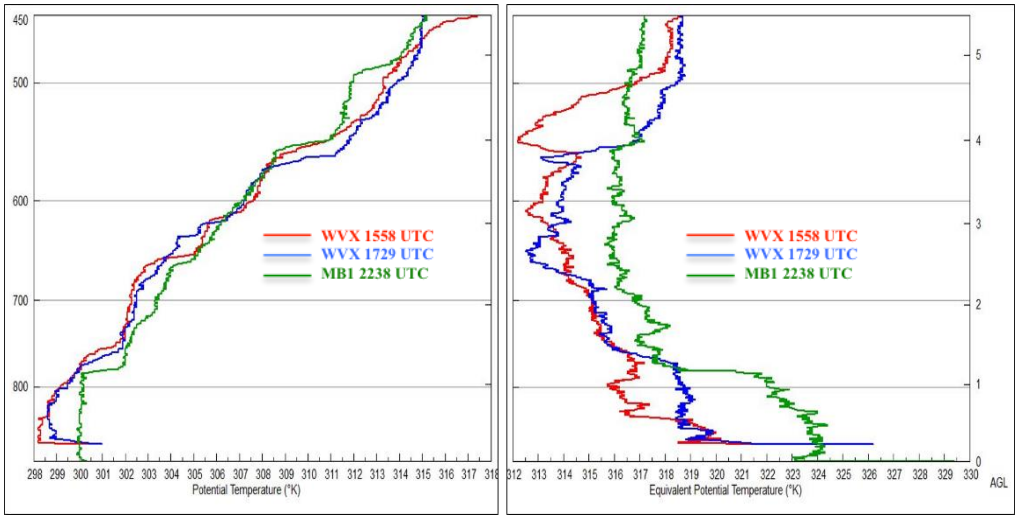

Figure 6.3: *θ (left) and θ_e (right) profiles from July 7th, 2008 from WVX at 1558 (red), WVX 1729 (blue) and MB1 at 2238 (green).*

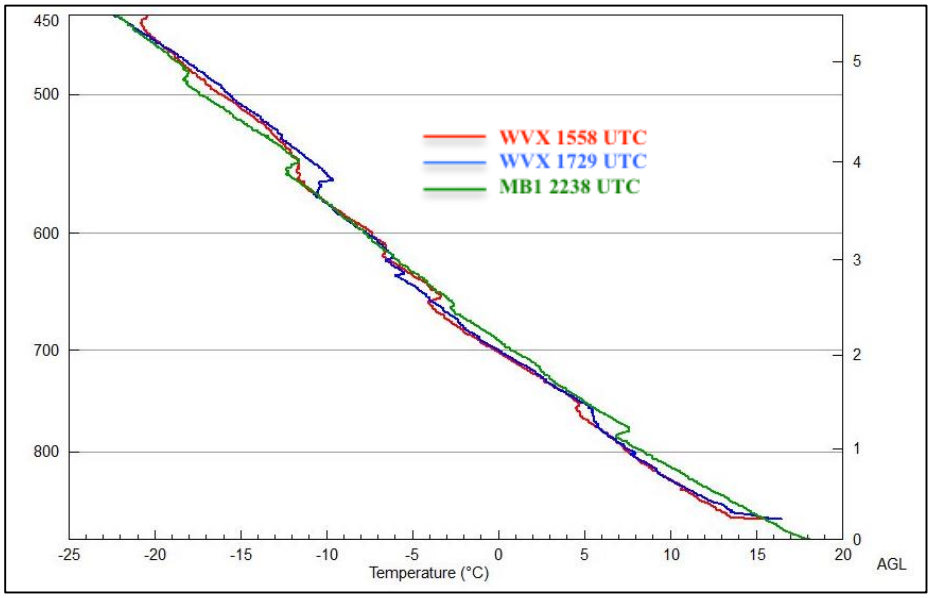

Figure 6.4: *Temperature profiles on July 7, 2008 from WVX at 1558 (red), WVX at 1729 (blue) and MB1 at 2238 (green).*

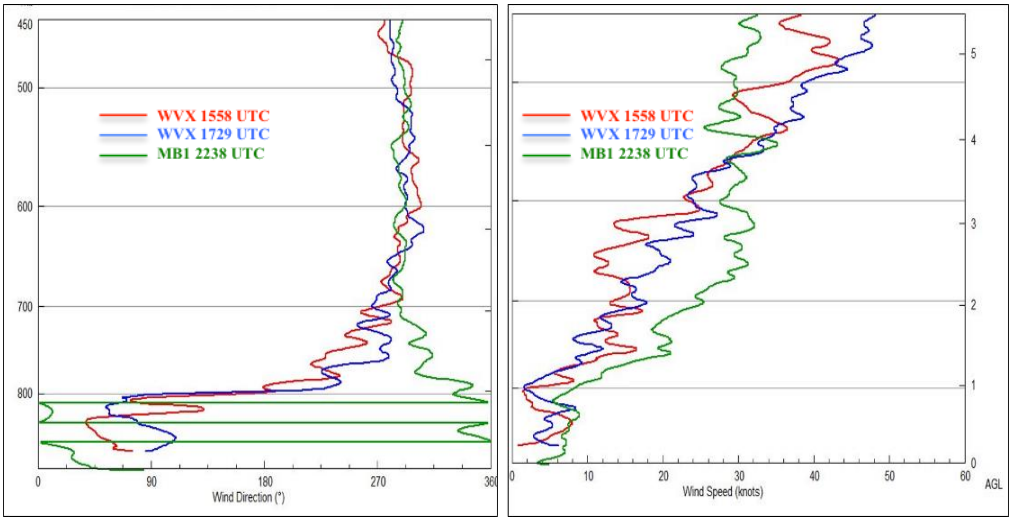

Figure 6.5: *Wind direction (left) and speed (right) profiles on July 7, 2008 from WVX at 1558 (red), WVX at 1729 (blue) and MB1 at 2238 (green).*

6.2.3. Radar chronology

At 1820 UTC the first 1.5 km CAPPI echo was observed on XSM and at a similar time on the WMI radar. The first lightning strike was observed at 1910 UTC and a mesocyclone was identified from XSM Doppler velocity data at 1940 UTC. Radar reflectivities were identified at 7 km by 1950 UTC. The thunderstorm became more organized by 2030 UTC. On the WMI radar at this time it began exhibiting supercellular characteristics such as a hook on the south end of the storm and a v-notch, as seen in Figure 6.6. As it tracked southeast as it passed right over Calgary at 2150 UTC but began to move to the right of the mean wind between 2140 and 2200 UTC. This then placed Calgary, AB (YYC) in the hail and rain swath with the weak tornado just to the south. The hail was 20-30 mm in size with maximum reflectivities reaching 60 dBz at 7 km. Echo tops reached 10 km at 0010 UTC on the 8th before weakening into an area of showers near Strathmore and Brooks, AB.

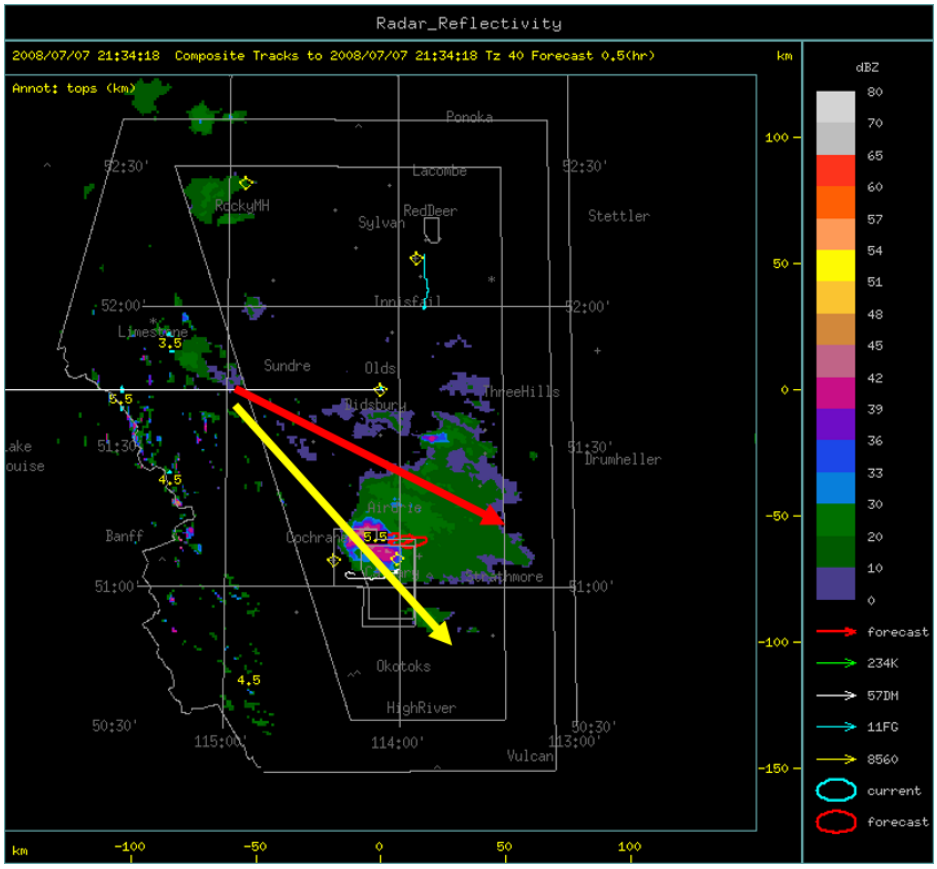

Figure 6.6: *WMI 1.5 km CAPPI radar reflectivities on July 7, 2008 at 2134 UTC. Red vector indicates the mean wind direction, while the yellow vector indicates the right deviant motion of the mature supercell.*

6.2.4. Sounding Representativeness

The MB1 sounding at 2238 UTC in Figure 6.7 and associated hodograph in Figure 6.8 was 71 km away and 38 minutes after the tornado was reported. The MB1 sounding exhibited 1298 J kg^{-1} of surface based CAPE (SBCAPE), which is shaded in red (1386 J kg^{-1} with the virtual correction). It is distributed evenly throughout the column, indicating low-level upward vertical accelerations would not be significant, however, it was enough to sustain an updraft capable of sustaining a long lived mesocyclone which produced hail and a tornado. Low-level shear (0-2 km) was 7.17 10^{-3} s^{-1}. Surface winds were out of the east which is favorable for

upslope advection of moist air, but the winds backed with height, producing associated low negative low-level (0-1 and 0-2 km) SRH values, which are not favorable for tornadogenesis.

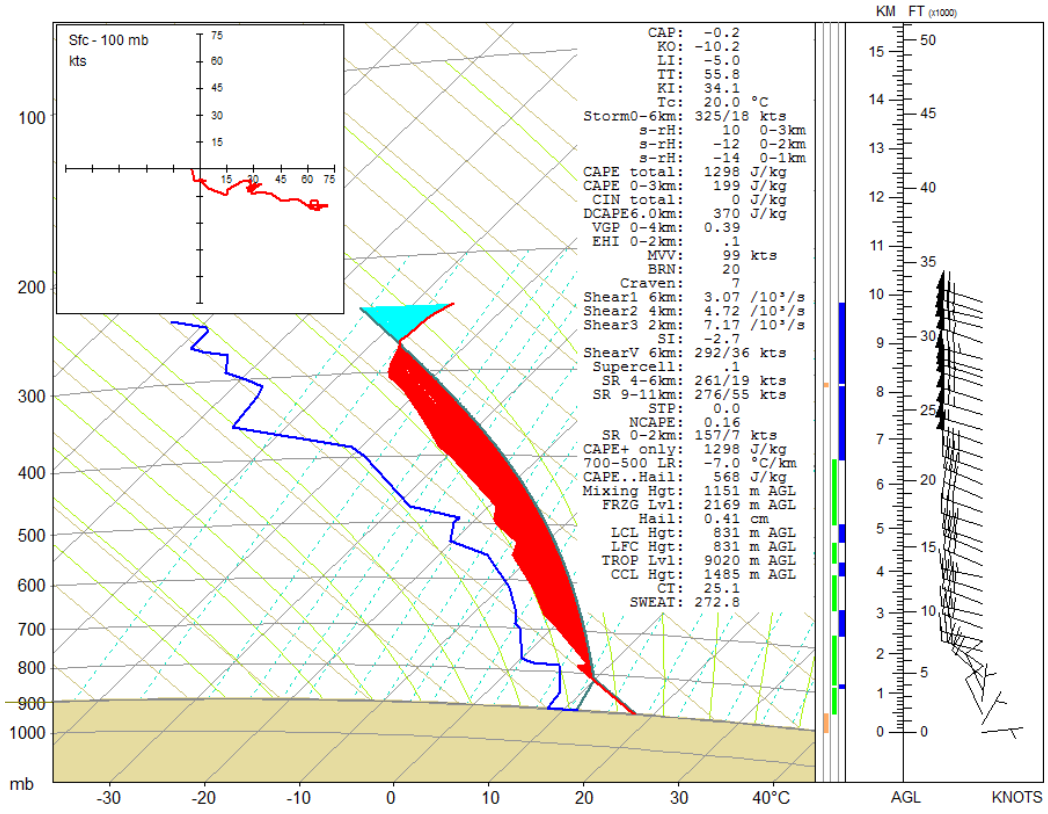

Figure 6.7: *MB1 tephigram on July 7, 2008 at 2238 UTC.*

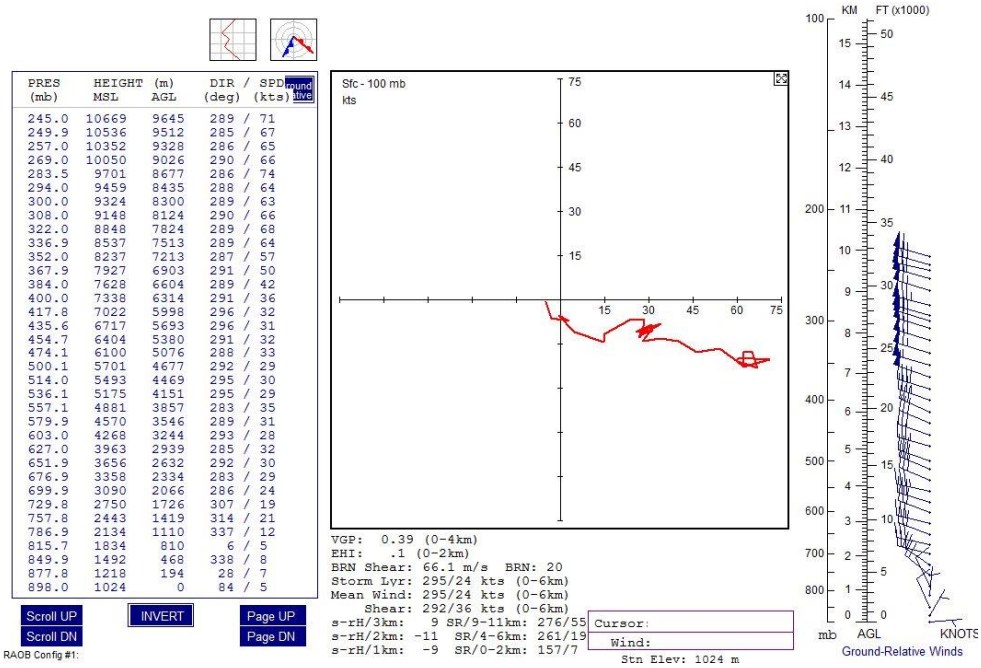

Figure 6.8: *MBI hodograph on July 7, 2008 at 2238 UTC.*

Analyzing the 1729 UTC WVX sounding in Figure 6.9, which was 60 km away and 5.5 hours before the tornado, indicated easterly winds in the lowest 1 km or 800 hPa veering to westerly by 1.5 km or 750 hPa. This is identified in the hodograph in Figure 6.10 and in the SRH values of 62 m^2 s^{-2} and 78 m^2 s^{-2} for 0-1 to 0-3 km respectively. The SBCAPE calculated from this sounding is less, 579 J kg^{-1} but this is due to the time (and possibly the location at which) it was launched since the surface had not yet reached maximum daytime heating to allow maximum potential SBCAPE. Low- level shear was less than what was observed at MB1, however, still significant enough for potential supercell maintenance at 5.95 10^{-3} $s^{-1.}$

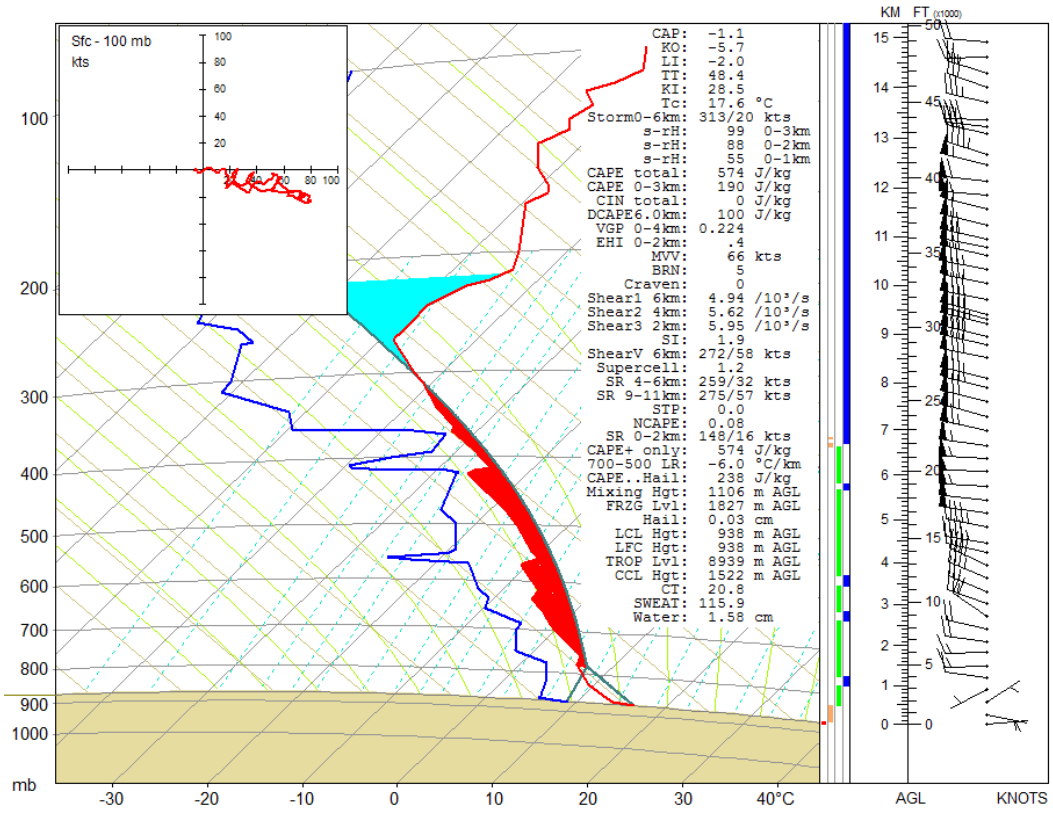

Figure 6.9: *WVX tephigram on July 7, 2008 at 1729 UTC.*

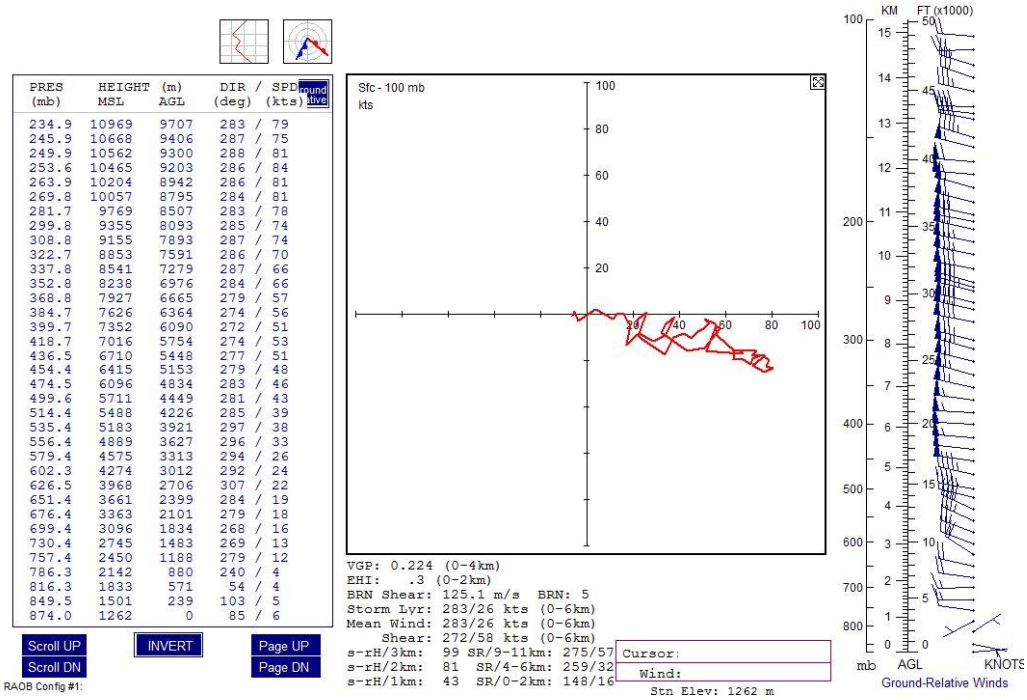

Figure 6.10: *WVX hodograph on July 7, 2008 at 1729 UTC.*

In Figure 6.11, the WSE sounding exhibited northwest winds throughout the column. The air at the surface was also much drier; Td of 6 compared to 11°C in the MB1 sounding. This is because the WSE site is further away from the foothills and into the surface northwest flow, experiencing cold and dry air advection. This produced the low SBCAPE values at WSE of 12 J kg^{-1} (117 J kg^{-1} with the virtual temperature correction) as well as a smaller 0-2 km shear (5.92 10^{-3} s^{-1}). However, it was the 0-6 km shear of 1.56 10^{-3} s^{-1} that was much less than what was seen in the UNSTABLE supplementary soundings (3.07 and 4.94 10^{-3} s^{-1} at MB1 and WVX respectively). LFC heights of about 800 m or just below 800 hPa were lower in the MB1 sounding compared to 1984 m at WSE. The large amount of dry air present and pseudo-adiabatic lapse rate throughout much of the column are also not conducive to deep convection.

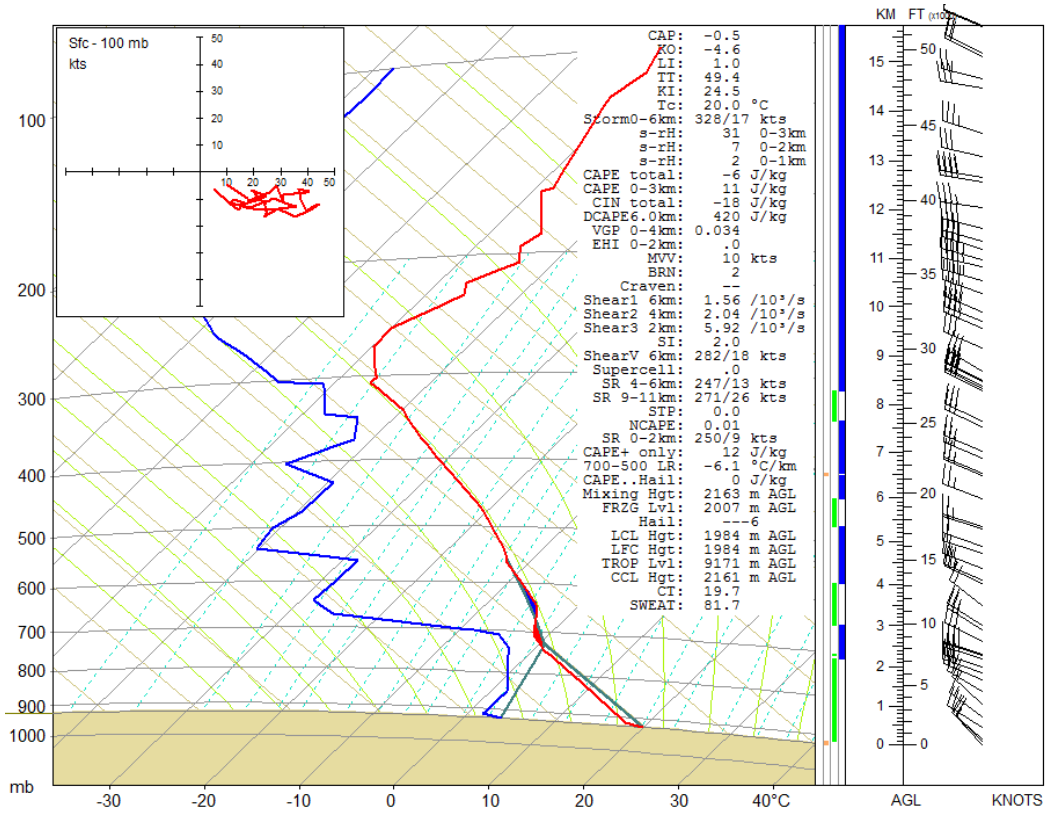

Figure 6.11: *WSE tephigram on July 8, 2008 at 0000 UTC.*

6.3. **July 15, 2008; An F1 Tornado Near Vulcan, AB**

6.3.1. Overview: Synoptic scale surface and upper air analysis

July 15 was initially not identified as a day that fulfilled the UNSTABLE criteria for an Intense Observation Day (IOD). However, it turned out to be the most severe event in Alberta during the field campaign with golf ball size hail and an F1 tornado that followed a 100 m long and 30 m wide path through the southern periphery of the study area. Losses were estimated at $20,000 due to grain silos that were indented, torn from their foundations and thrown approximately 70 m.

At 1200 UTC, the 250 hPa level was characterized by west southwest flow with a jet core of 85 kt (44 m s^{-1}) on the west side of the upper ridge tracking into the southern Alberta region. It remained unchanged at 0000 UTC. At 500 hPa a similar upper ridge was present at 1200 UTC along with associated cyclonic vorticity and falling 1000 to 500 hPa thicknesses which advected into the region by 0000 UTC ahead of an upper trough. At 700 hPa there was a zonal flow as the ridge weakened and the trough tracked eastward. A pocket of higher dew points pooled along a baroclinic zone in southern Alberta. There was a weak flow at 850 hPa at 1200 UTC, however, by 0000 UTC on the 16th a weak low pressure center on the baroclinic zone had developed in the lee of the Rocky Mountains in the very southern section of the province. At the surface a weak ridge was present earlier in the day at 1800 UTC with a low over the foothills and an associated frontal system which tracked east to the Cypress Hills by 0000 UTC on the 16th. The cold front was the mechanism that triggered the line of thunderstorms on this day.

The closest standard synoptic soundings in proximity to this region are launched from Stony Plain (WSE), just outside Edmonton, AB, Great Falls, MT (TFX) and Glasgow, MT (GGW). The distance of these soundings to the Vulcan tornado were 349, 351 and 537 km respectively and the launches occurred at 0000 UTC on the 16th, an hour after the tornado report, or 1200 UTC on the 15th, 11 hours before the event. The soundings that were launched as a part of the UNSTABLE project were out of Water Valley (WVX) at 1145 UTC, Didsbury, AB at 1203 UTC (MB2) and Brant, AB at 2205 UTC (MB2'). The distances from Vulcan, where the tornado was reported were 205, 202 and 31 km respectively. The distance of the Brant sounding to the Vulcan tornado was 31 km and it was released an hour before the event. The locations of these soundings are illustrated in Figure 6.12.

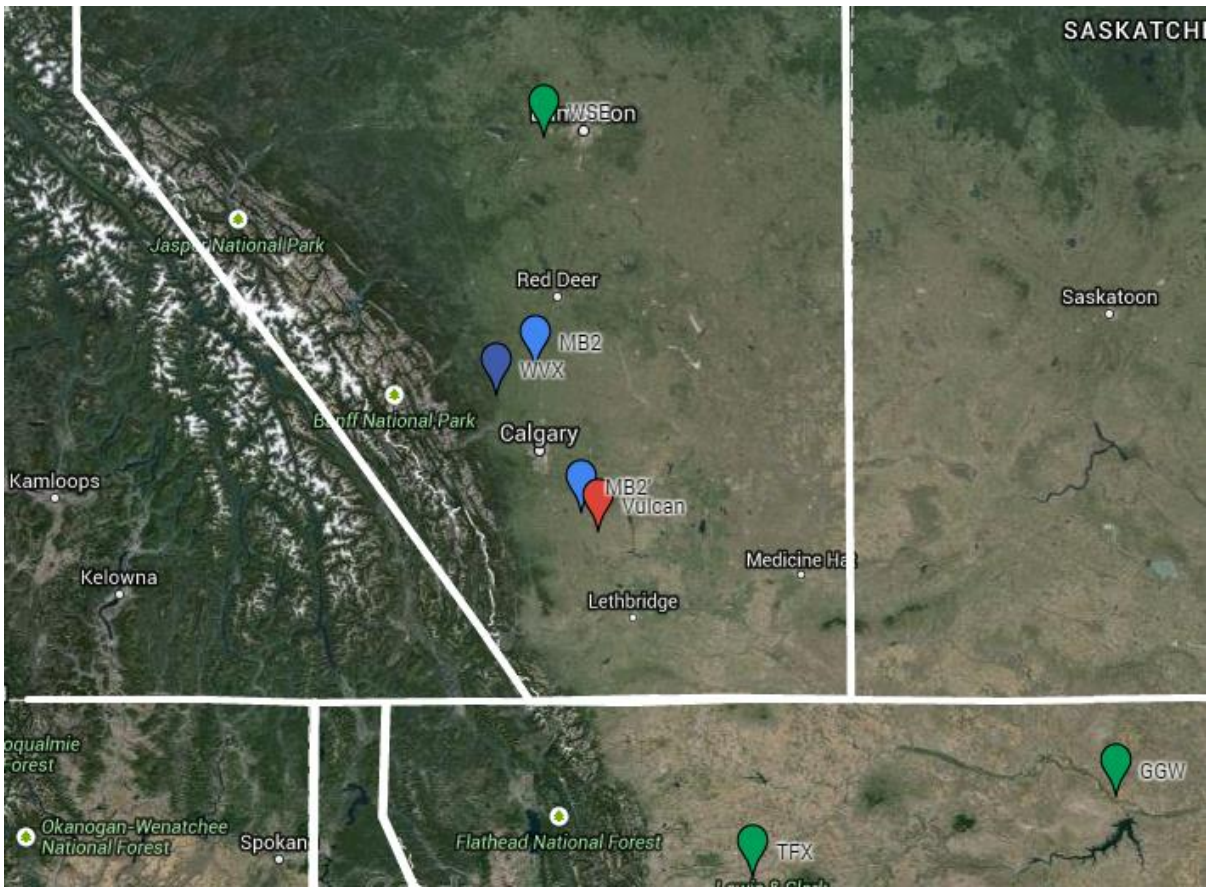

Figure 6.12: *Google Map of the UNSTABLE soundings in blue on July 15, 2008: MB2 at Didsbury, AB at 1203 UTC, WVX at Water Valley, AB at 1145 UTC, MB2' at Brant, AB at 2205 UTC, the standard synoptic soundings in green at Stony Plain, AB (WVX), Great Falls, MT (TFX) and Glasgow, MT (GGW) and the location of the Vulcan tornado in red for reference.*

6.3.2. BL Evolution

The WVX (1145 UTC) sounding indicated the existence of a nocturnal temperature inversion at the surface, as shown in Figure 6.13, which was not evident in the MB2 (1203 UTC) sounding. T profiles warmed by 6°C at the surface throughout the day below 800 hPa from the 1203 to the 2205 UTC MB2 sounding θ_e, in Figure 6.14, indicated a warm nose at WVX at 825 hPa. The MB2 sounding decreased by 3 K above 800 hPa as compared to the WVX sounding.

However, the temperature in the 2205 UTC MB2 sounding increased in the afternoon above 800 hPa by 8 K. A shallow surface layer was about 2 K higher.

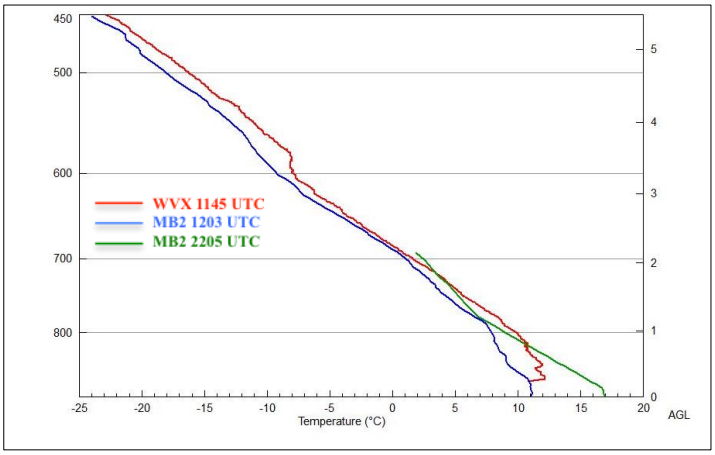

Figure 6.13: *Temperature profiles on July 15 from WVX at 1145 (red), MB2 at 1203 (blue) and MB2 at 2205 UTC (green).*

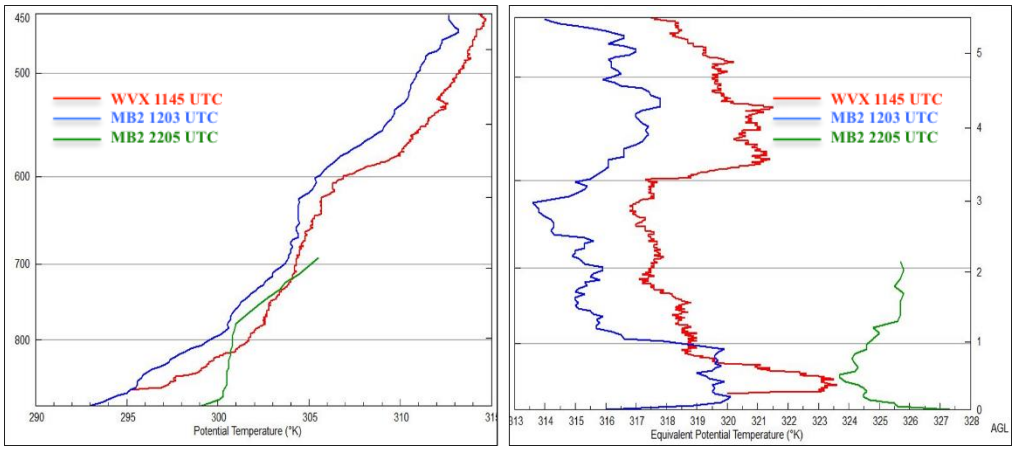

Figure 6.14: *θ (left) and θ_e (right) profiles on July 15 from WVX at 1145 (red), MB2 at 1203 (blue) and MB2 at 2205 UTC (green).*

Td at the surface remained steady throughout the day, however, there was an increase in Td by about 8°C in the 2205 UTC sounding from 825 to 700 hPa. This was reflected in the r

profiles as an increase in magnitude at 700 hPa; in the morning soundings, the r value was near 4 g kg^{-1} but by 2203 UTC it was at about 6.2 g kg^{-1}. Near the surface the r value also increased through the day from 7.5 to 9 g kg^{-1}. This is displayed in Figure 6.15. This retention of moisture as the boundary layer became more mixed was also illustrated in chapter 4 as a separating characteristic between NC, SC and DC day types.

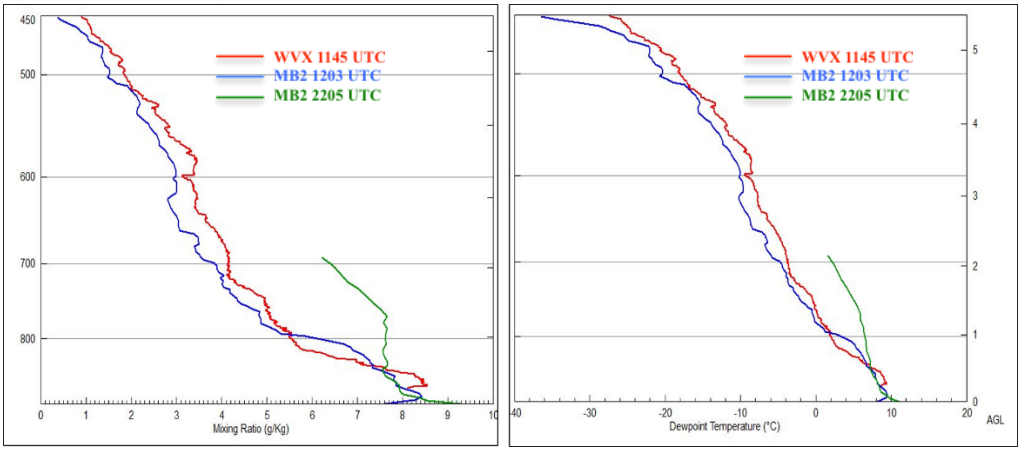

Figure 6.15: *Mixing ratio (left) and dew point (right) profiles on July 15 from WVX at 1145 (red), MB2 at 1203 (blue) and MB2 at 2205 UTC (green).*

Surface winds backed throughout the day from southerly at 160° at 11:45 UTC to 100° at 2205 UTC. In this case, this is indicative of an increase in streamwise vorticity and a higher likelihood for tornado development. This is discussed more in section 6.3.4. There was an obvious low-level wind maximum at 850 hPa which actually decreased in strength from 26 kt (13 m s^{-1}) to 20 kt (10 m s^{-1}) by 2205 UTC, however the vertical shear is more important than the magnitude of the wind speed. This is shown in Figure 6.16.

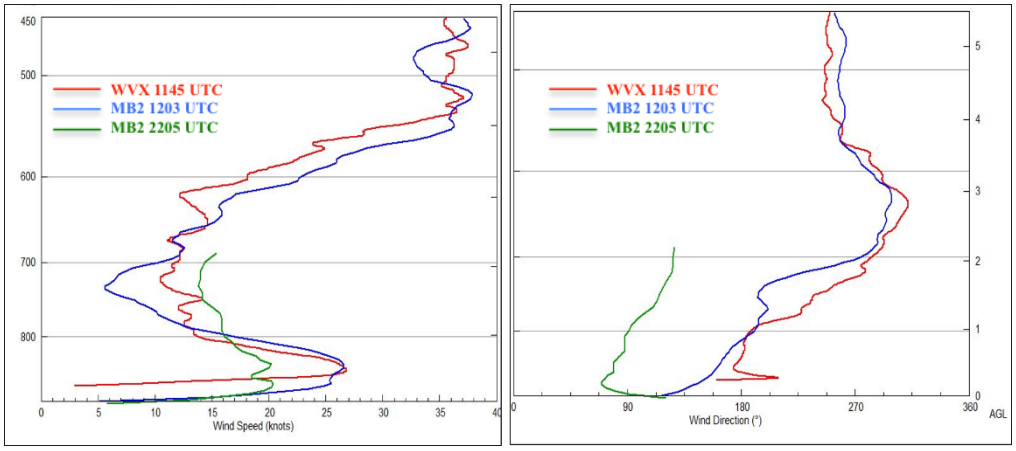

Figure 6.16: *July 15, 2008 wind speed profiles from WVX at 1145 (red), MB2 at 1203 (blue) and MB2 at 2205 UTC (green).*

6.3.3. Radar Chronology

At the WMI radar an area of anomalous propagation (AP) was initially visible in the early morning. This is indicative of an inversion present which acts to confine moisture and instability to the low-levels to be explosively released later in the day. Weak elevated showers and embedded thunderstorms that tracked through the area in the morning added moisture to the low-levels to be used later in the day as fuel for the surface based convection. Surface based convection initiated around 1730 UTC in a northwest to southeast line along the Rocky Mountain foothills as a surface cold front tracked into the region. The surface based convection tracked in a southeast direction. Individual cells had reflectivities approaching 65 dBz at 1.5 km and 55 dBz at 7 km. As they tracked southeast and further developed, echo tops reached 10 km, vertical integrated liquid (VIL) was estimated as 20 kg m^{-2}, max hail (MESH) measuring 5.2 cm with percent of severe hail (POSH) up to 100%, and the height of the 40 dBz reflectivity was 8.5 km. The most severe cell that was identified as producing the tornado that caused F1 damage in

Vulcan exhibited classic supercellular radar signatures, highlighting the possibility of a tornado. First it was a classical “kidney” shape and had a weak hook on the western edge of the cell. On the Doppler velocity scans, a mesoscale velocity couplet was identified. Near the end of the day, after continuously tracking southeast, it took a sudden right turn south. The radar and Doppler images of the storm at its maximum intensity are shown in Figure 6.17 and Figure 6.18 below. This right propagation is indicative of a clockwise turning (veering) hodograph or wind shear profile which indicates the preferred flank for strong continuous updraft development creating the right moving supercell (Monteverdi et al, 2003; Rotunno and Klemp, 1982; Weisman and Klemp, 1982).

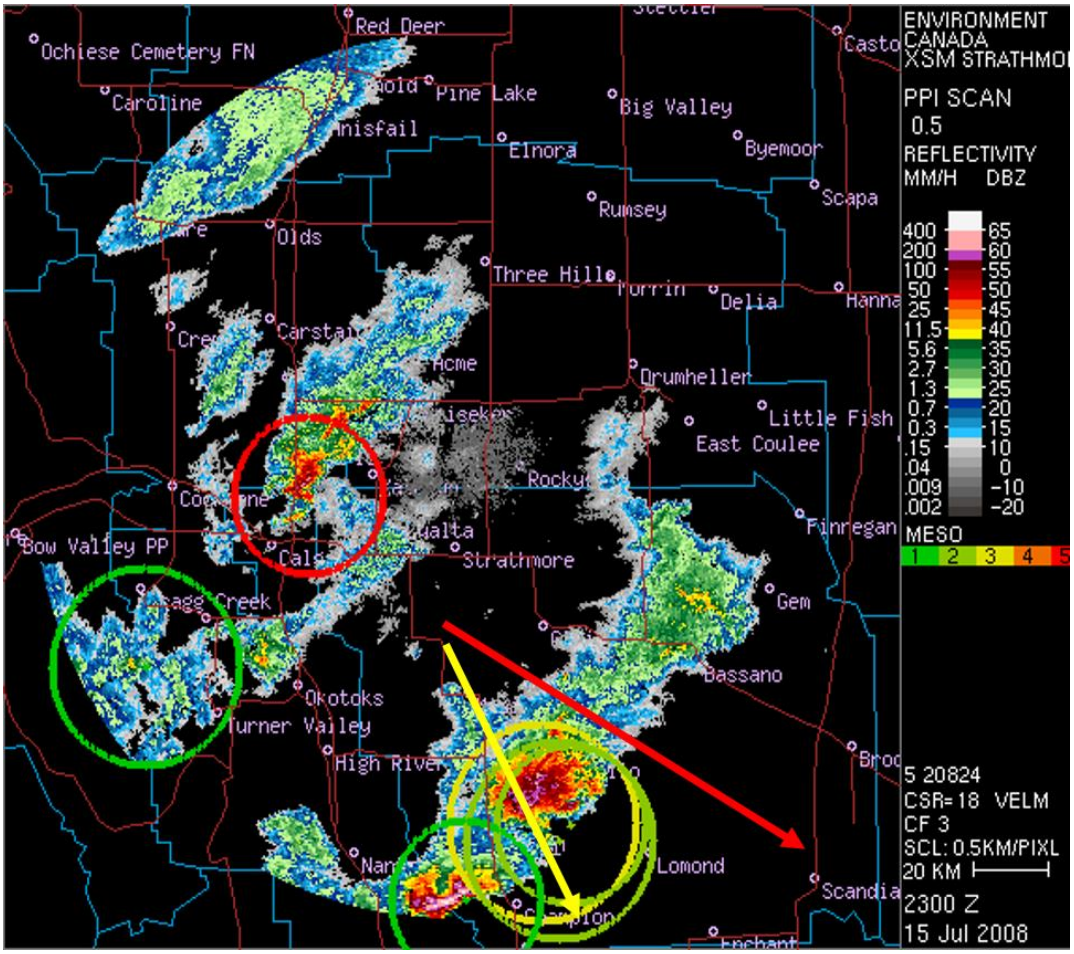

Figure 6.17: *July 15, 2008 2300 UTC 0.5° PPI radar reflectivity of the Vulcan tornado. Colored circles indicate potential mesocyclones with severity indicated by color as defined by the MESO colors 1-5 on the right. Red vector indicates the mean wind direction, while the yellow vector indicates the right deviant motion of the mature supercell.*

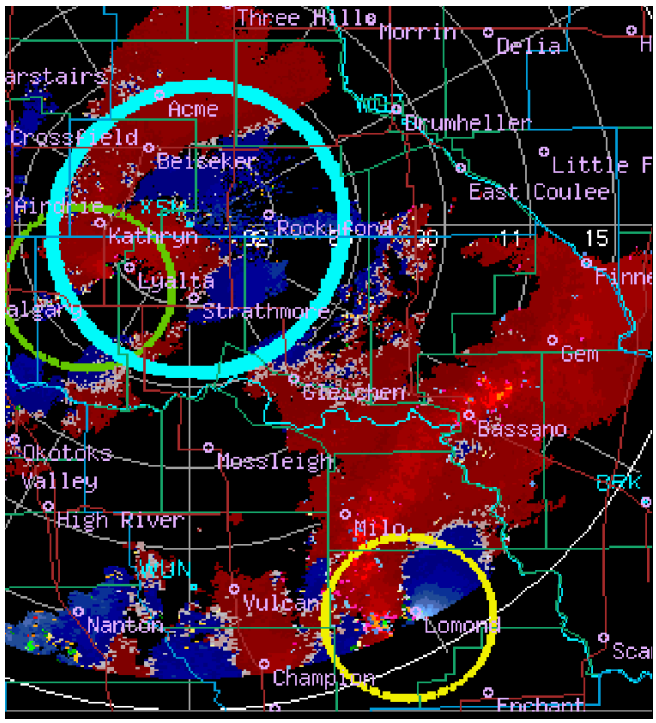

Figure 6.18: *July 15, 2008 2330 UTC doppler radial velocity at 0.5° angle. Red indicates targets are moving away from the radar and blue indicates targets are moving towards the radar. Colored circles indicate potential mesocyclones. The cyclonic rotation couplet, or mesocyclone associated with the Vulcan tornado is indicated by the yellow circle.*

6.3.4. Sounding Representativeness

The synoptic sounding characteristics of note were in the 1200 UTC WSE sounding shown in Figure 6.19, exhibiting a westerly wind in the low-levels, however, by 0000 UTC as seen in Figure 6.20, a southeasterly wind at the surface had developed, which is more favorable for supercell development, given all other ingredients are present. However, backing of the winds with height between 800 and 500 hPa indicated cooling in the mid-levels, characteristic of an approaching surface cold front. Drier air in the mid-levels were displayed as well as a slight decrease in lifted indices which is further descriptive of a convectively unstable column, although an increase in showalter indices and a low SBCAPE value of 655 J kg^{-1} (769 J kg^{-1} with

the virtual temperature correction) are not conducive to strong thunderstorm development in the 0000 UTC sounding.

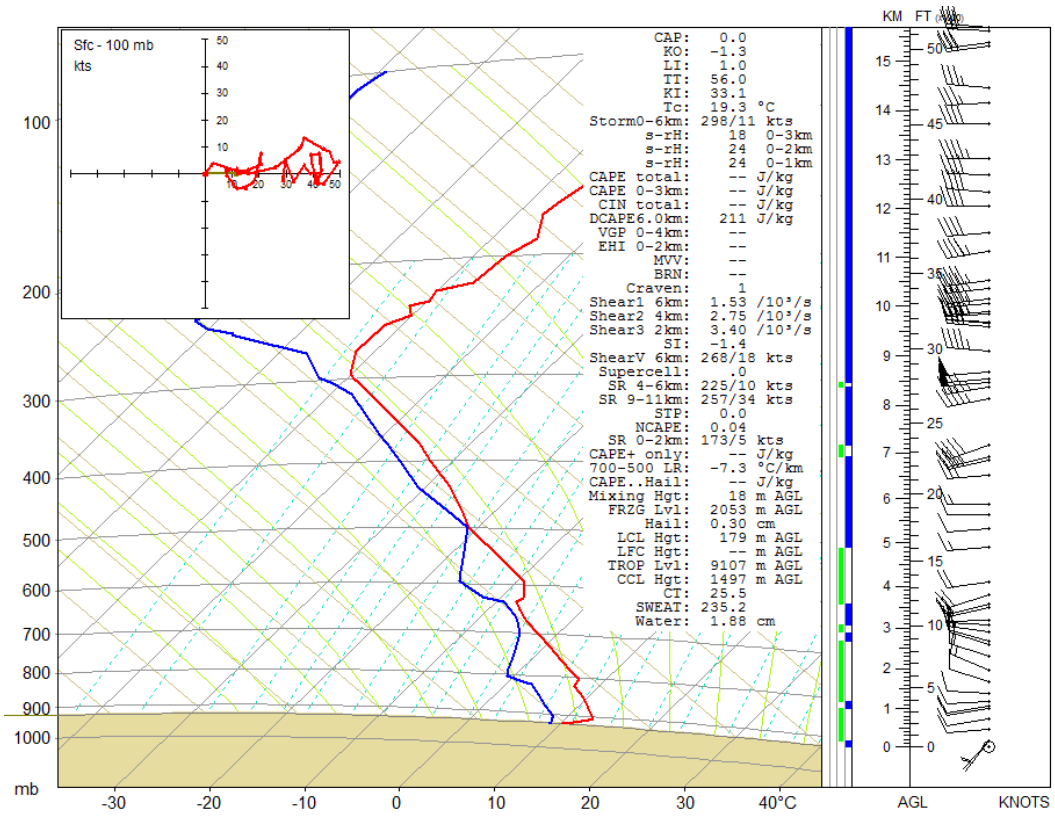

Figure 6.19: *WSE tephigram on July 15, 2008 1200 UTC.*

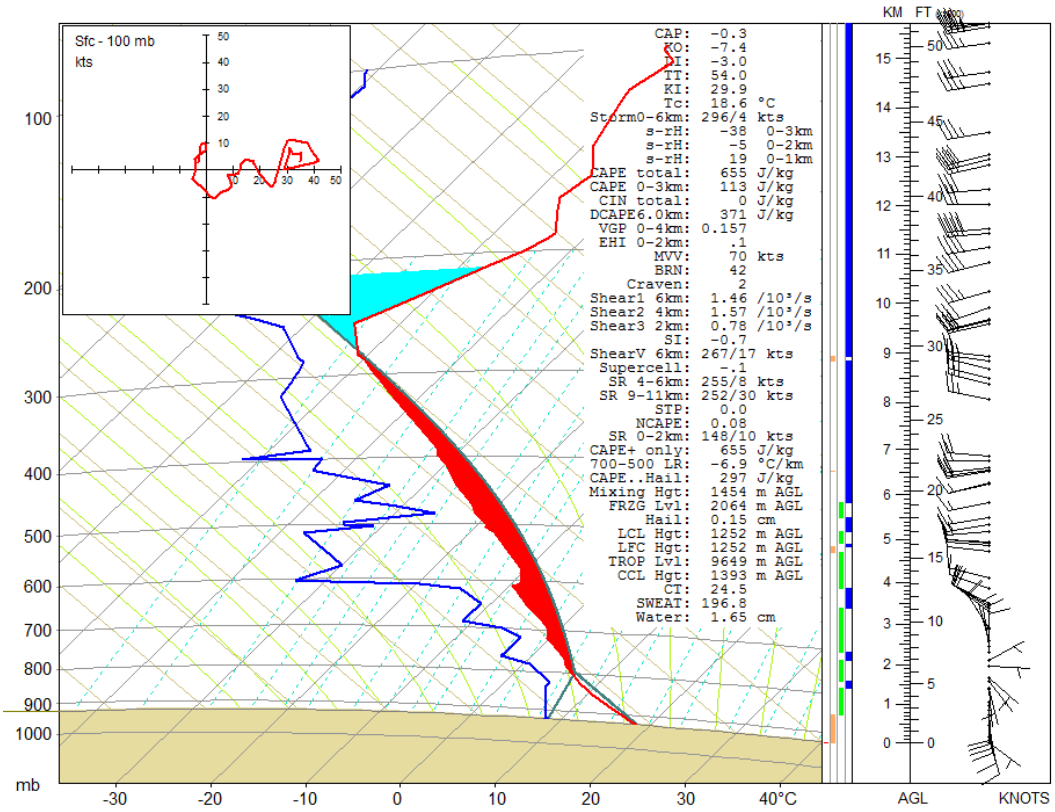

Figure 6.20: *WSE tephigram on July 16, 2008 0000 UTC. Cold air advection associated with the cold front is evident from 800 to 600 hPa by backing winds.*

At TFX in Figure 6.21 and Figure 6.22, the low-levels became dry adiabatic in the afternoon. However, with the increasing depth of the convective boundary layer and the subsident nature of the westerly winds, the low-level moisture also decreased significantly. This resulted in a higher LFC, reduced updraft strength and reduced supercell tornado development potential.

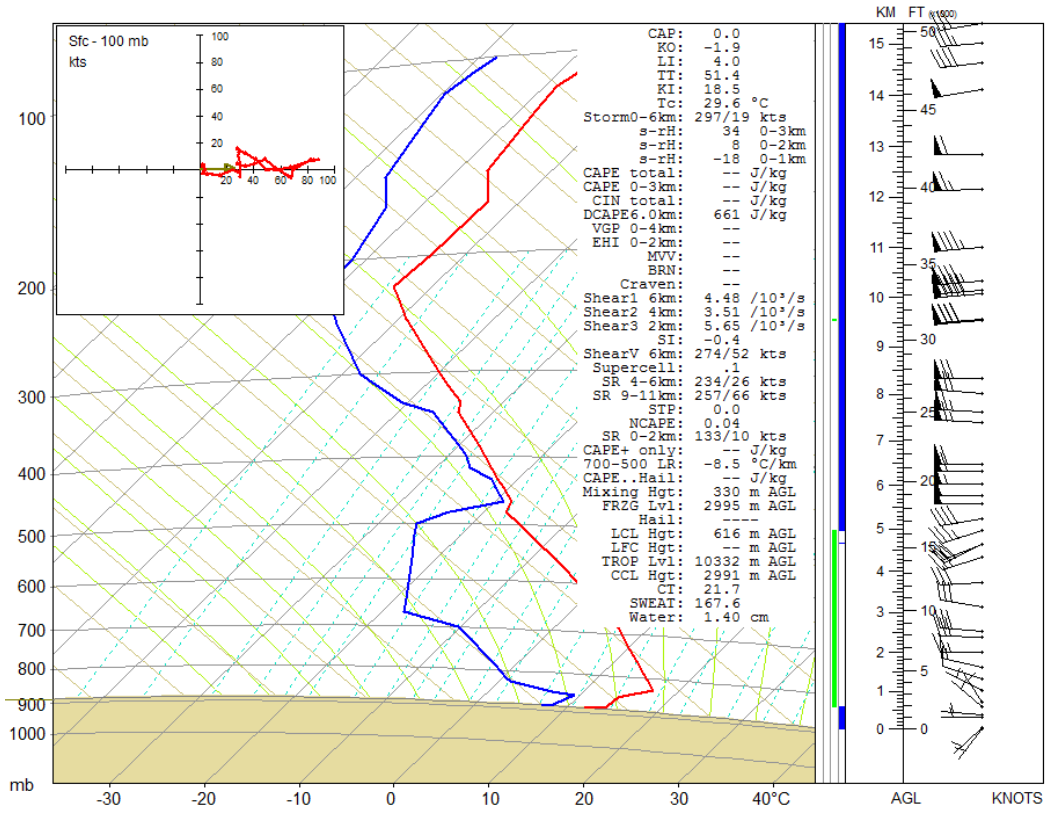

Figure 6.21: *TFX tephigram on July 15, 2008 1200 UTC.*

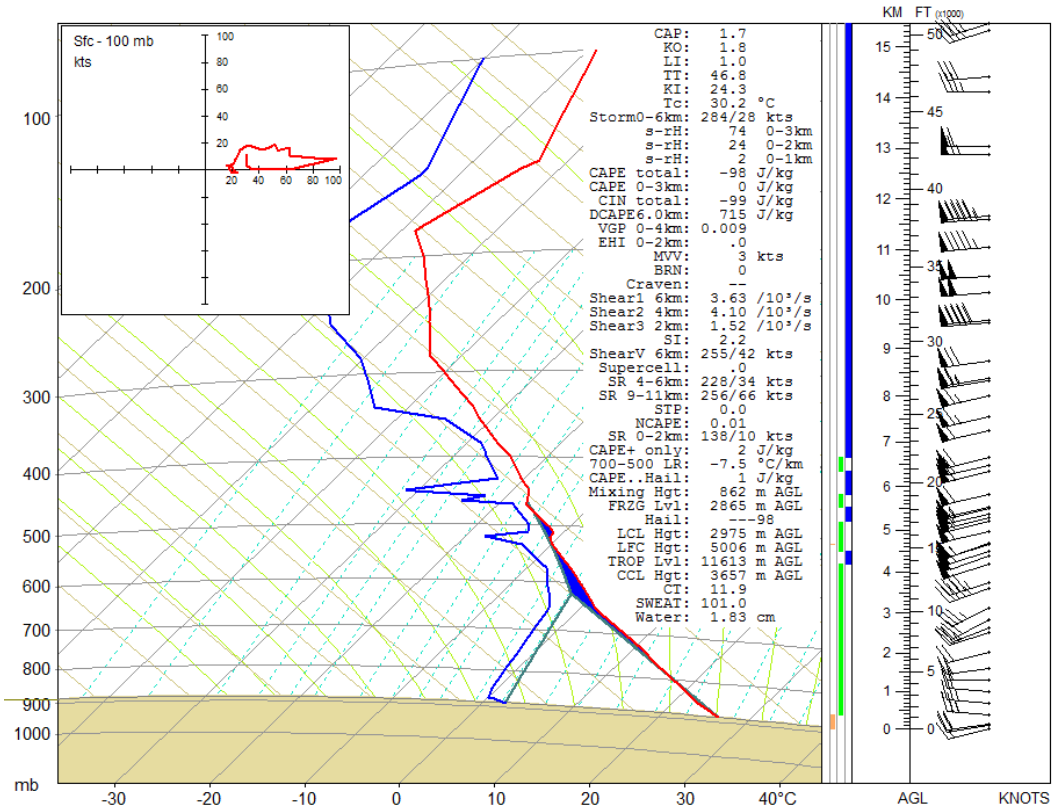

Figure 6.22: *TFX tephigram on July 16, 2008 0000 UTC.*

At GGW in Figure 6.23 and Figure 6.24, the low-levels similarly displayed increasing instability from the morning to the afternoon sounding, increasing the depth of the convective boundary layer while diluting the moisture through a deeper layer. This created a dry layer at the surface more conducive to downburst winds than supercell and tornado development. The low-level winds did exhibit some veering with height from the south at the surface to west at 800 hPa.

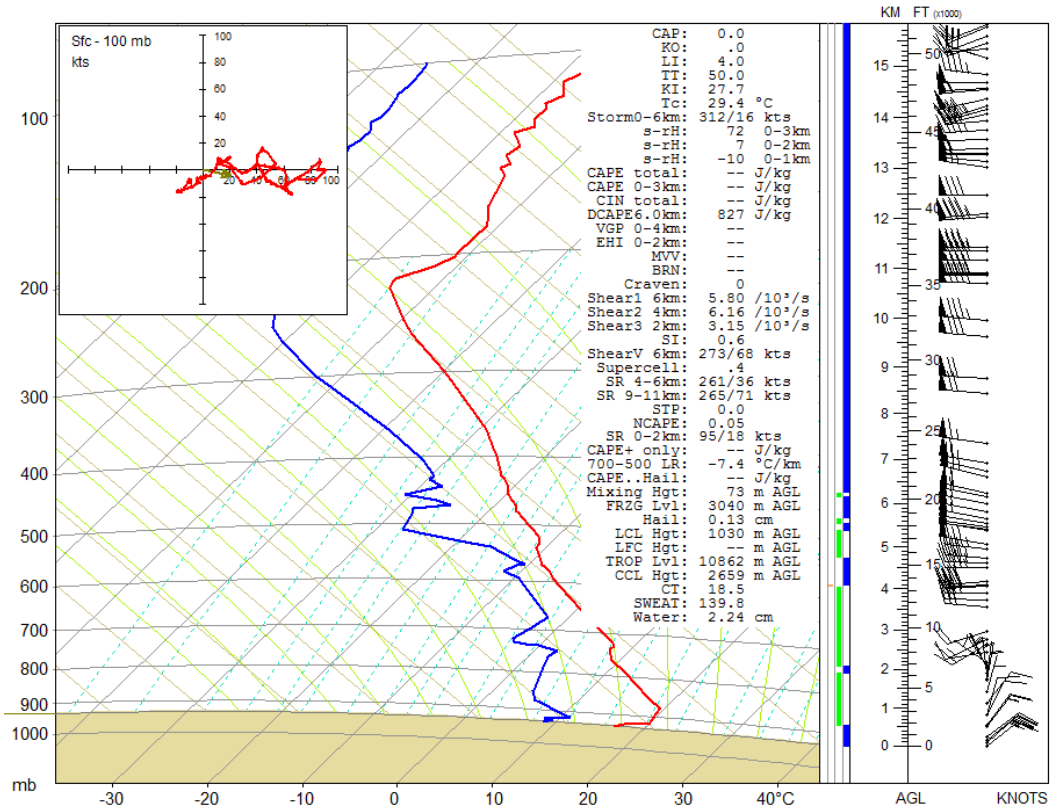

Figure 6.23: *GGW tephigram on July 15, 2008 1200 UTC.*

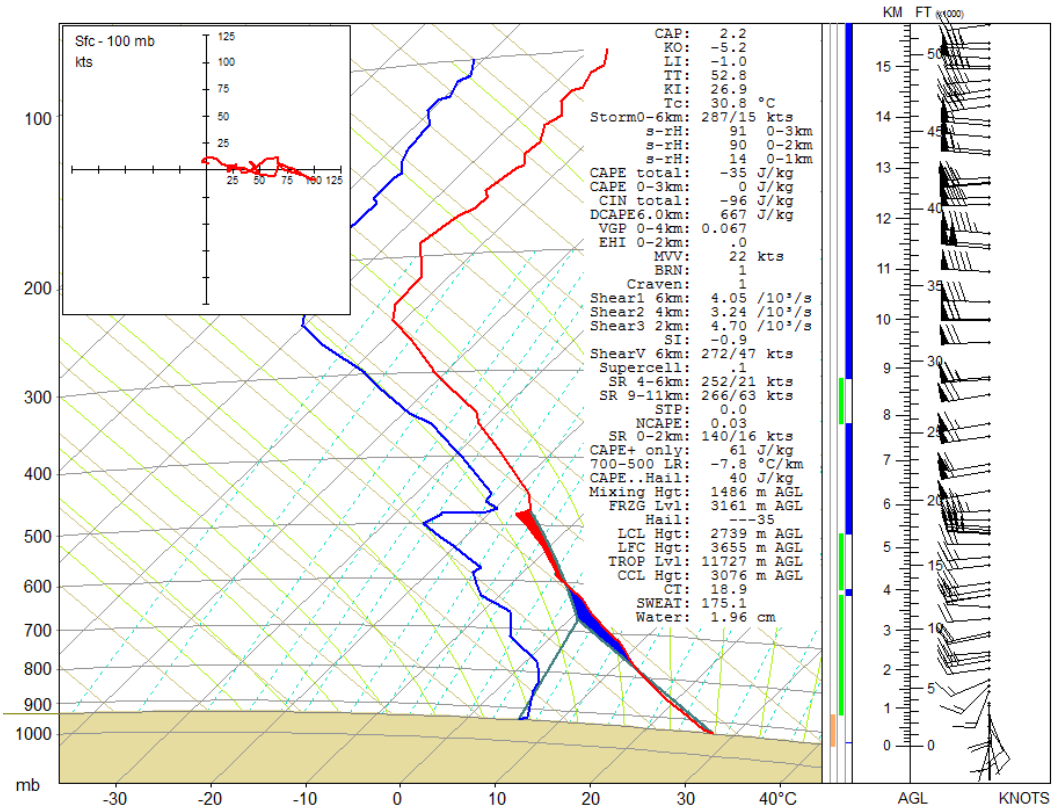

Figure 6.24: *GGW tephigram on July 16, 2008 0000 UTC.*

None of the standard operational synoptic radiosonde sites showed ingredients conducive for supercell storms or tornadoes. Since the only afternoon UNSTABLE sounding only reached 700 hPa, the morning UNSTABLE soundings from WVX and MB2 will be used, while modified at the surface with the temperature and dew point of the MB2' UNSTABLE afternoon sounding. Comparing the July 15, 2008 soundings from the UNSTABLE field data, the WVX sounding, in Figure 6.25, displayed slight low-level veering in the winds. Modifying the surface temperature to the afternoon surface temperature and dew point revealed 1288 J Kg^{-1} of SBCAPE (1354 J Kg^{1} with the virtual temperature correction). Combined with 3.34 10^{-3} s^{-1}(39 kt) of 0-6 km shear (with 3.74 10^{-3} s^{-1} in the 0-2 km layer) indicating that the energy and wind shear conducive for

long lasting, severe thunderstorms and potentially supercells, was present. The 0-6 km shear is actually higher in some of the standard synoptic soundings, however, the low-level 0-2 km shear observed in the UNSTABLE soundings was in most cases higher than the standard soundings.

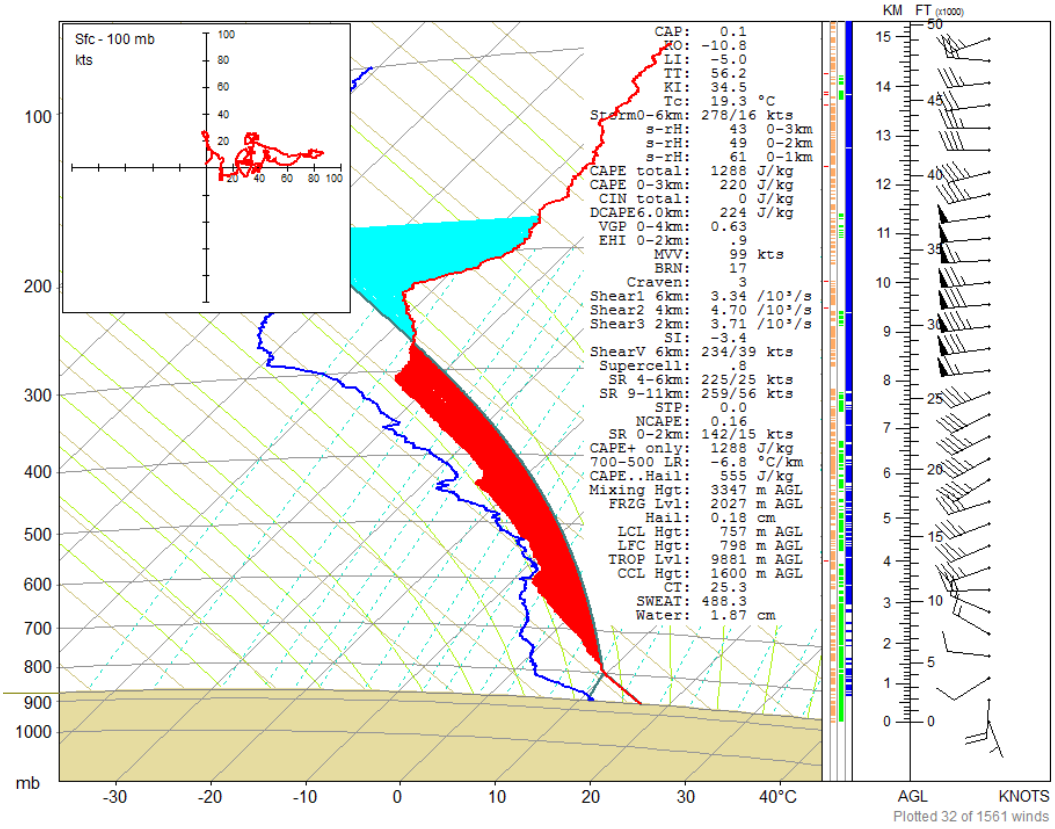

Figure 6.25: *WVX tephigram from July 15, 2008 at 1145 UTC with modified surface temperature modified to the surface temperature and dew point reached in the MB2' afternoon sounding (17/11) mixed dry adiabatically with SBCAPE shaded in red*

The MB2 1203 UTC sounding, in Figure 6.26, showed more favorable low-level winds with southeasterly at the surface veering to westerly by 700 hPa. This low-level southeasterly wind does not only indicate saturated, upslope lift, but since the storm motion, as indicated by the Bunkers method, was 303° (Figure 6.27), it also increases the streamwise nature of the

vorticity, which is what results in a higher likelihood for supercells and tornadogenesis. This was also evident in the July 7th Calgary F0 tornado case.

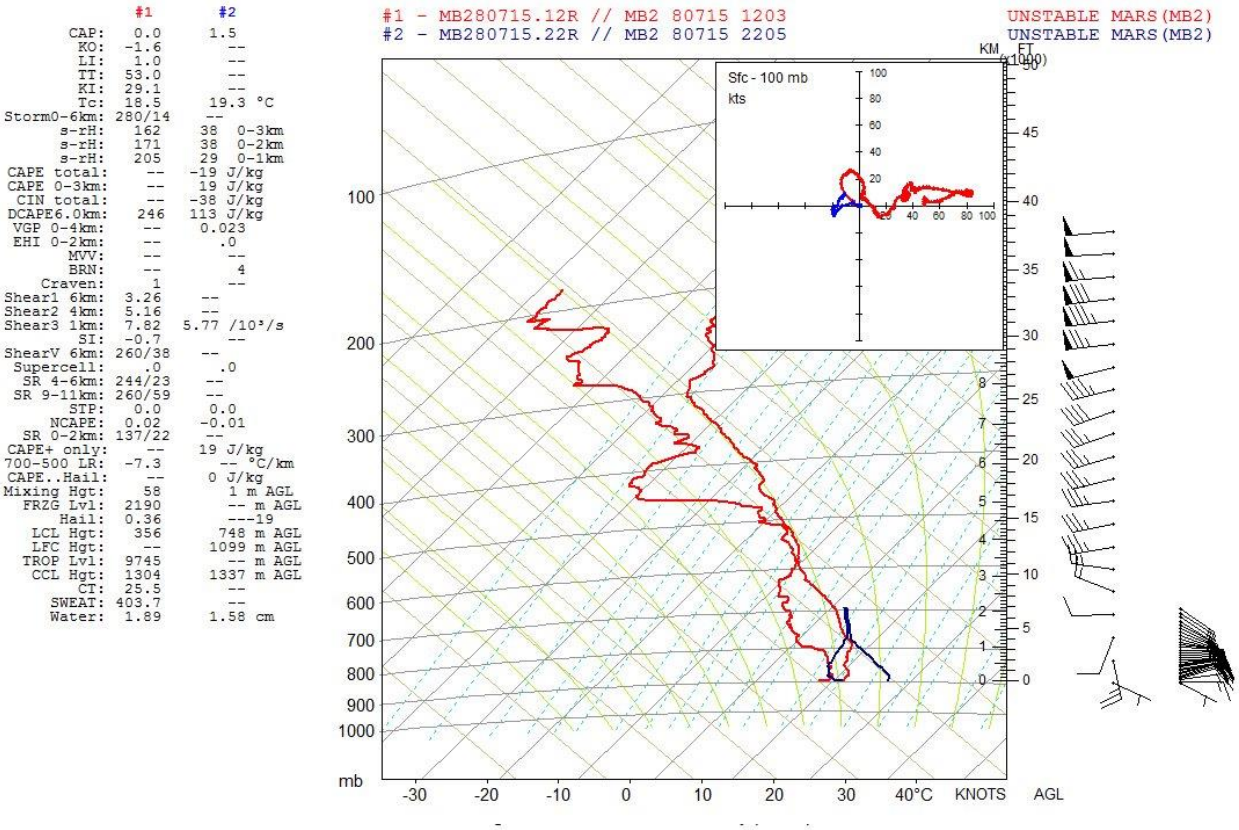

	#1	#2	
CAP:	0.0	1.5	
KO:	-1.6	--	
LI:	1.0	--	
TT:	53.0	--	
KI:	29.1	--	
Tc:	18.5	19.3	°C
Storm0-6km:	280/14	--	
s-rH:	162	38	0-3km
s-rH:	171	38	0-2km
s-rH:	205	29	0-1km
CAPE total:	--	-19	J/kg
CAPE 0-3km:	--	19	J/kg
CIN total:	--	-38	J/kg
DCAPE6.0km:	246	113	J/kg
VGP 0-4km:	--	0.023	
EHI 0-2km:	--	.0	
MVV:	--	--	
BRN:	--	4	
Craven:	1	--	
Shear1 6km:	3.26	--	
Shear2 4km:	5.16	--	
Shear3 1km:	7.82	5.77	/10³/s
SI:	-0.7	--	
ShearV 6km:	260/38	--	
Supercell:	.0	.0	
SR 4-6km:	244/23	--	
SR 9-11km:	260/59	--	
STP:	0.0	0.0	
NCAPE:	0.02	-0.01	
SR 0-2km:	137/22	--	
CAPE+ only:	--	19	J/kg
700-500 LR:	-7.3	--	°C/km
CAPE..Hail:	--	0	J/kg
Mixing Hgt:	58	1	m AGL
FRZG Lvl:	2190	--	m AGL
Hail:	0.36	---19	
LCL Hgt:	356	748	m AGL
LFC Hgt:	--	1099	m AGL
TROP Lvl:	9745	--	m AGL
CCL Hgt:	1304	1337	m AGL
CT:	25.5	--	
SWEAT:	403.7	--	
Water:	1.89	1.58	cm

Figure 6.26: *MB2 Tephigram on July 15, 2008 1203 UTC (red) and 22:05 UTC (blue).*

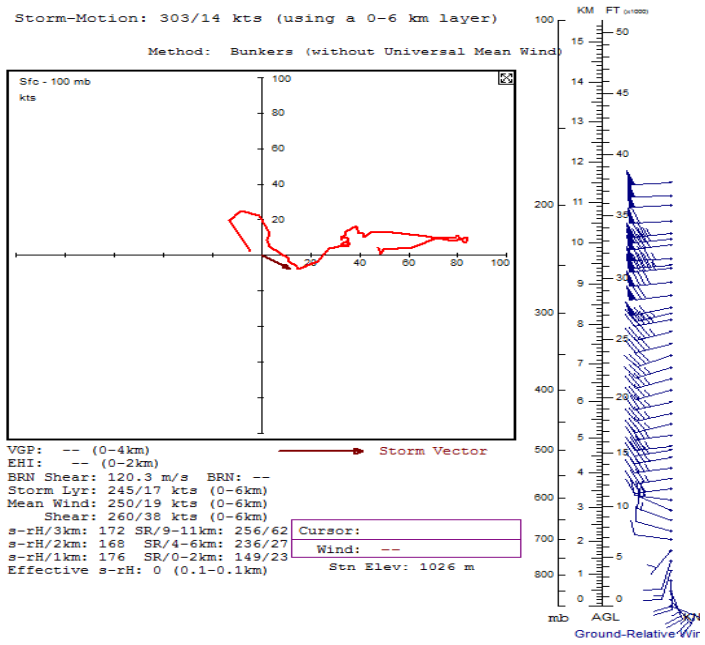

Figure 6.27: *Hodograph from MB2 at 1203 UTC on July 15th, 2008. The storm motion vector as calculated using the Bunkers method is indicated by the south-east arrow from the origin.*

The CAPE was not possible to calculate in the 2205 UTC soundings since it terminated at 700 hPa, but when calculated in the modified 1203 UTC sounding by modifying the surface to the tempeature and dew point reached in the MB2' sounding, in Figure 6.28, it showed higher SBCAPE values than what was calculated at all of the 0000 UTC standard synoptic sites; 1208 J kg^{-1} (1293 J kg^{-1} with the virtual temperature correction) compared to the 0000 UTC standard synoptic sites with maximum SBCAPE between the three sites of 665 J kg^{-1} at WSE. The standard synoptic sites also displayed drying of the low-levels. However, as shown in the 2205 UTC sounding, this moisture in the low-levels was not diluted into a deeper layer due to the moisture advection occuring in this region. This was reflected as an increase in surface Td and the saturation of the mid levels between the 1203 and 2205 UTC soundings. This drying of the

low-levels in the standard synoptic soundings would have had a significant impact on LFC, LCL and therefore CAPE values.

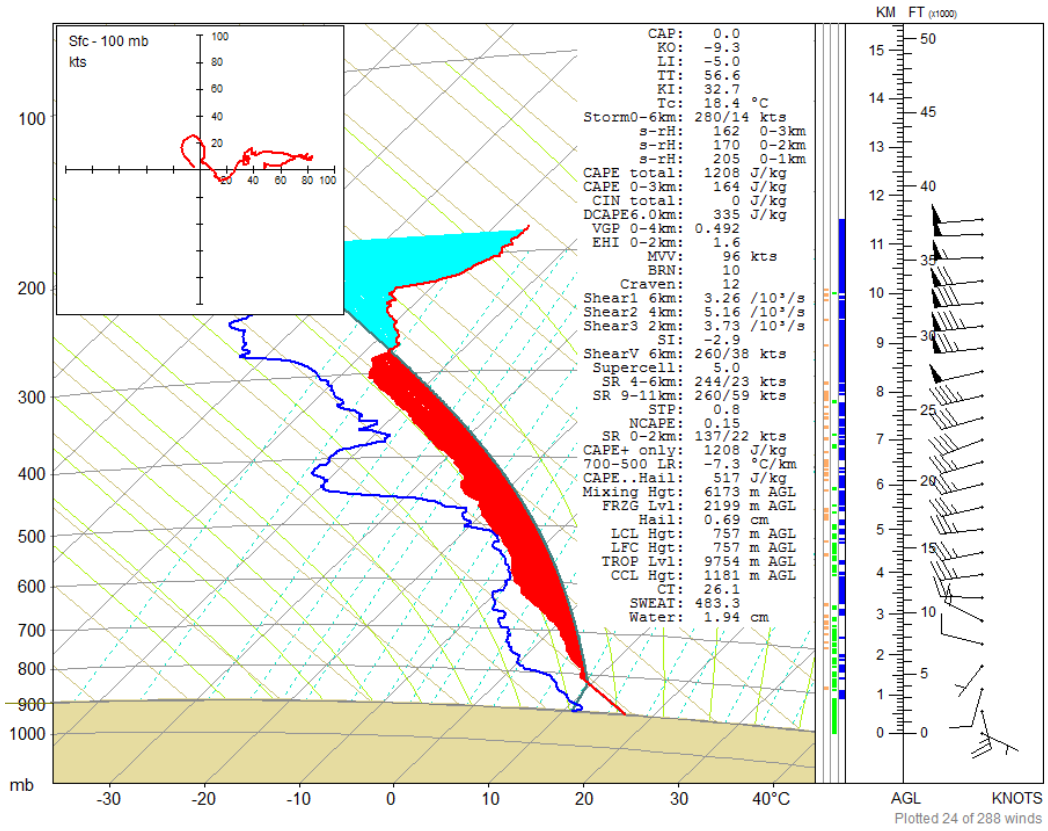

Figure 6.28: *Tephigram MB2 on July 15, 2008 at 1203 UTC with surface temperature modified to the surface temperature and dew point reached in the MB2' afternoon sounding (17/11) mixed dry adiabatically with SBCAPE shaded in red.*

The PW values remained similar between the UNSTABLE and standard sites. LIs were -4 and -5 in the modified morning soundings compared to -2 at the 0000 UTC standard sites. The surface Td was 11°C in the 2205 UTC MB2 sounding which is more than the average surface Td on deep convective days during the UNSTABLE period (9.1°C from Table 5.3), indicating moisture was not a limitation for storm development. TFX and GGW showed lower Td of 3 and 6°C respectively, although WSE showed a Td of 11°C as well, which is why WSE was the

highest SBCAPE value of the standard soundings, with TFX having 2 and GGW 64 J kg^{-1}. The BRN value in the WSE 0000 UTC sounding was 14 compared to 10 in the MB2' 1203 modified with 2205 UTC sounding data. However, WSE didn't have much SBCAPE, so this value would be not be very representative.

6.4. **July 7 to July 15 2008 comparison**

The BL in each case displayed differences and similarities. Surface T on the 15th did increase more through the day than the 7th, generating more SBCAPE for stronger updraft development. Td on the 15th increased significantly in the 700 to 825 hPa or 1.5 to 2 km layer; a difference of 4-7°C. This was reflected in the θ_e difference at 700 hPa of 10 K. The BL on the 15th seemed to be deeper than on the 7th when it was confined to below 850 hPa or about 1 km. The BL can be identified in the r profiles as a sharp gradient beginning at about 750 hPa or 1.75 km. All of these differences on the 15th can act to lower the LFC and LCL which is more favorable for tornadogenesis.

The wind regime on July 15th also indicated it was more favorable for tornadic development than the 7th. The 15th exhibited a low-level wind maximum at 850 hPa of up to 26 kt (13 m s^{-1}) which on the 7th was less than 10 kt (5 m s^{-1}) all day. Higher low-level wind speed increased the low-level SRH, leading to a higher potential of tornadic development. This is evident in the hodographs as a larger low-level cyclonic "looping". A commonality between the days was they both displayed low-level easterly winds creating upslope lift of moist air.

The additional UNSTABLE soundings were closer in proximity and therefore better representing near storm environment. They captured potential instability (SBCAPE) available for

thunderstorm development by more accurately capturing resolving low-level moisture. More accurate low-level wind direction and SRH values were also observed. These features are crucial for the forecasting of tornadogenesis. Since this is an area lacking upper air observations, as well as it being an area where the mesoscale dynamics and surface terrain are complex, more observations leading to better understanding are necessary to improve detection and anticipation of severe weather.

7. CONCLUDING REMARKS

The Rocky Mountain Foothills in Alberta are one of the most active regions for thunderstorms in Canada. Due to the sparse observation network, forecasting thunderstorm initiation in an accurate and timely manner is difficult. This region is also an area of high population emphasizing the importance of forecasting weather and associated hazards.

The UNSTABLE field study was conducted during a two week period, from July 7 to 23, 2008. The thesis objective is to better understand boundary layer characteristics and convective environments in the Alberta foothills. Three sub-objectives are designed to address the overall thesis goal:

1. Characterize the daily evolution of the boundary layer during different convective regimes throughout the intensive observation period (IOP) of the UNSTABLE field campaign,
2. Distinguish conditions between days with deep, shallow and no convection,
3. To illustrate how targeted soundings can be useful for severe storm prediction.

To address the sub-objectives, comparisons were made of average (composite) soundings for the four different sounding locations by time of day and convective regimes. As well, various standard statistical metrics were used to compare soundings and convection-related severe weather parameters. Other meteorological data, such as satellite, radar, upper air and surface maps, was used to augment the analysis as required. By analyzing the tornadic events that occurred during the field study, the benefits of using targeted soundings were illustrated. By comparing these results to other studies, it puts the UNSTABLE data into context in the broader thunderstorm research arena.

For sub-objective 1, by evaluating the evolution of the boundary layer using four sites with 2-hourly profiles of different parameters (wind speed and direction, equivalent potential temperature, potential temperature, mixing ratio and dew point), it was shown that: (1) Nil convective (NC) days were characterized by warmer upper levels, stabilizing the column, (2) Shallow convective (SC) days had a mid-level subsident inversion which was present throughout the day, and (3) Deep convective (DC) days were characterized by a warmer boundary layer combined with cooling upper levels increasing instability. DC days displayed a wind shift to an easterly component by the afternoon via either an enhanced mountain-plain circulation or synoptic pattern. The easterly wind shift contributed to enhanced upslope moisture advection for DC days, more so than SC and NC days. It was not clear which process was responsible for the easterly shift in wind direction, therefore, both synoptic situation and mountain-plain circulation must be considered. Composite soundings of different day types indicated deeper as well as a higher magnitude of moisture available on DC days. SC days had the shallowest as well as lowest magnitude of moisture. This was strongly influenced by the wind direction, which could possibly be controlled by the mountain-plain circulation. The conclusions from this work are similar to the work by Strong (2000), and thus implies that his conclusions are applicable to a larger area of the Alberta foothills than what was initially studied.

EA3 and WVX was the most consistently similar site comparison. This could be due to the close proximity of the station locations to one another; EA3 and WVX being stationary stations were 42 km apart. MB2-EA3 comparisons were the most different, which could be due to these stations having the furthest distance between them (an average of 78 km), however, it is also possible that the stations were in the prime locations to best represent the different eco-climate

zones. Comparisons by A.M. and P.M. exhibited more differences in the P.M., indicating the importance of surface type and albedo influencing diurnal boundary layer characteristics.

Statistical comparisons by pressure level are important to distinguish where differences exist within the profile in an attempt to meteorologically explain these differences. The analysis by pressure level revealed the most differences in all four meteorological parameters were mainly evident in the boundary layer, further emphasizing eco-climate zones and BL evolution having critical roles in driving boundary layer processes. Variability existed between sites, parameters and different days, however, the main signal from the majority of comparisons was higher occurrence of differences in the lower levels of the column, extending deeper in the afternoon.

For sub-objective 2, statistically significant differences between severe weather parameters by day type were found in 850 and 700 hPa temperatures, LI, SI, 700-500 lapse rate and SWEAT. Visually, box plots of the severe weather parameters for each day type were useful in discerning convective day type differences. Severe weather parameters measured during UNSTABLE were compared to other field study results. A few interesting points were that UNSTABLE results had the lowest surface dew point value (8.6°C) than the other two studies, even though the summer of 2008 was a climatologically wet summer. PW values which were much less than what was observed by DR2011. It is not known why dew points and PW were relatively low during UNSTABLE even through 2008 was a wetter year.

For sub-objective 3, detailed analysis of tornadic events and using targeted soundings displayed the importance of sampling the near storm environment. The coarse horizontal spatial resolution of operational upper air launches that are currently available do not fully characterize the thunderstorm initiation and development potential in southern Alberta. Supplementary soundings illustrated higher low-level moisture, resulting in lower LFCs and increased SBCAPE.

Wind profiles were favorable for supercell and tornadic development than standard soundings by better representing the low-level backing winds to generate higher low-level shear and SRH.

It is recognized that this study has limitations. With UNSTABLE having only been completed during a two week period in a single summer, inter and intra seasonal variations or differences are not accounted for. For example, as discussed in Section 2.6, the summer of 2008 was more moist in Southern Alberta compared to 2007 and 2009. Rainfall accumulation leading up the UNSTABLE field project was normal to above normal in southern sections. Therefore, this research may only be representative of a relatively wet year in southern Alberta. It is also assumed that the UNSTABLE large scale circulation patterns were climatologically representative for July, however, it is unknown whether this is indeed the case. It would therefore, be desirable to run similar field projects over multiple summers in future research.

Another limitation includes the use of only four sounding locations, two of which were mobile. Comparison between them may have been more useful had all locations been stationary. It was difficult to make conclusions about MB1 and MB2 since they changed location each day and therefore, were influenced by different surface type. Comparisons by day would have been useful, however, since there were so few soundings, this was not possible. Also having earlier morning soundings from MB1 and MB2 would have been very beneficial. Since A.M. sounding times differed so much between sites, comparisons are hard to make in the morning period. At WXV and EA3, launches began at 1200 UTC, whereas at MB1 and MB2 they were not started until 1500-1600 UTC, a critical time in which the nocturnal inversion erodes.

Soundings can travel great distances horizontally within one vertical profile. This would put the soundings located relatively close to the crop-forest boundary (or within its transition zone) at risk of sampling multiple boundary layer types, depending on the strength and direction of the

low and mid-level winds. Similarly, a sounding site located near the crop-forest transition region, could sample “crop air” or “forest air” depending on the boundary layer winds. For example, WVX was located near the crop-forest transition region, and if boundary layer winds were easterly, crop air would dominate, however, if westerly winds were present, forest air may dominate. Hence, both sonde drift and boundary layer wind direction, could confound site comparisons.

This work contributes to the overall science of thunderstorm initiation and development in the Alberta foothills by building on conceptual models of Strong (2000) and Smith and Yau (1993). Understanding this convective boundary layer evolution, can aid in anticipation of convective initiation and development. This can lead to greater lead time and accuracy of watches and warnings issued in a region that has high population density and growth. By indicating potentially useful severe weather indices, a transfer to operational forecasting is anticipated with this work, i.e. through publication, presentations and distribution, addressing quantitative measures of convective regimes and illustration of tornadic environments. The addition of supplementary soundings could improve the skill of better representing the low-level wind regime and moisture, both necessary for severe storm development.

In summary, Alberta thunderstorms are highly spatially and temporally variable, depending on mesoscale dynamics and thermodynamics, which are currently not resolved by the existing observation network. Differences occurring between sounding locations and specific convective regimes included the depth of the boundary layer, the magnitude and depth of the moisture driven by low-level wind direction or mountain-plains circulation, boundary layer diurnal temperature variation, including the existence of a nocturnal surface inversion and strength of mid-level capping inversion. The analysis suggests that using four different sounding locations

was beneficial for deciphering boundary layer evolution and convective day types. Distinguishing deep convective days from shallow and nil convective days included colder upper levels and a warmer boundary layer with deeper moisture, including higher values at the surface. Upslope wind flow created a natural trigger for thunderstorm initiation as well as veering winds in the low-levels, producing favorable wind profiles in near storm soundings for long lived supercells and possible tornado development.

8. **REFERENCES**

Alberta Agriculture and Rural Development, Economics and Competitiveness Division, Statistics and Data Development Unit. *Crop Conditions as of July 17, 2008*. Rep.: 2008. Print.

Banta, Robert M., 1984: Daytime Boundary-Layer Evolution over Mountainous Terrain. Part 1: Observations of the Dry Circulations. *Mon. Wea. Rev.*, **112**, 340–356.

Brown, Rodger A., 1992: Initiation and Evolution of Updraft Rotation within an Incipient Supercell Thunderstorm. *Journal of the Atmospheric Sciences*. **49**(21): 1997-2031

Browning, K. A., and Coauthors, 2007: The Convective Storm Initiation Project. *Bull. Amer. Meteor. Soc.*, **88,** 1939–1955.

William R. Burrows & Bohdan Kochtubajda (2010) A decade of cloud-to-ground lightning in Canada: 1999–2008. Part 1: Flash density and occurrence, *Atmosphere-Ocean*, **48**:3, 177-194, DOI: 10.3137/AO1118.2010

Byers, Horace, R. and Roscoe R. Braham Jr., 1949: The Thunderstorm: Report of the Thunderstorm project US Govt. Print. Off.

Chisholm, A. J. and J. H. Renick, 1972: The Kinematics of Multi-cell and Supercell Alberta Hailstorms. *Alberta Hail Studies 1972* Alberta Research Council, Edmonton,

Colby, Frank, Convective Inhibition as a Predictor of Convection During AVE-SESAME 2 1984 *Mon. Wea. Rev.* **112** pg 2239-2253

Davies-Jones, R. P., 1984: Streamwise vorticity: The Origin of Updraft Rotation in Supercell Storms. *J. Atmos. Sci.*, 41, 2991–3006. , 1993: Helicity Trends in Tornado Outbreaks. Preprints, *17th Conf. on Severe Local Storms*, St. Louis, MO, Amer. Meteor. Soc., 56–60

Doswell, C.A. (2000). A Primer on Vorticity for Application in Supercells and Tornadoes. *Cooperative Institute for Mesoscale Meteorological Studies*, Norman, Oklahoma, 1-11.

Dupilka, Max L. and Gerhard W. Reuter, 2011: Forecasting Tornadic Thunderstorm Potential in Alberta Using Environmental Sounding Data. Part I: Wind Shear and Buoyancy. *Wea. Forecasting*, **21**, 325–335.

Dupilka, Max L. and Gerhard W. Reuter, 2011: Forecasting Tornadic Thunderstorm Potential in Alberta Using Environmental Sounding Data. Part II: Helicity, Precipitable Water, and Storm Convergence. *Wea. Forecasting*, **21**, 336–346.

Environment Canada: "About Environment Canada." *Http://ec.gc.ca*. N.p., 19 Feb. 2014. Web. 31 Aug. 2014.

Fawbush, Earnets, J., and Robert C. Miller, 1953: A method for forecasting hailstone size at the Earth's surface. *Bull. Amer. Meteor. Soc*. **34** (6):235-245

Galway, Joseph, G., 1965: The Lifted Index as a Predictor of Latent Instability *Bull. Amer. Meteor. Soc*. **37**(10):528-529

Hanesiak, John, M., Richard L. Raddatz and Scott Lobban 2004: Local Initiation of Deep Convection on the Canadian Prairie Provinces *Boundary-Layer Meteorology* **110**: 455-470,

Klemp, Joseph, B. 1987: Dynamics of Thunderstorms. *Ann. Re. Fluid Mech.***19:** 1-33

Klemp, Joseph B. and Robert B. Wilhelmson, 1978: Simulations of Right- and Left-Moving Storms Produced Through Storm Splitting. *J. Atmos. Sci.*, **35**, 1097–1110.

Lawford, R.G., 1970: The behaviour of Thunderstorms over Alberta forests. M.Sc. thesis, University of Alberta, Edmonton, Alberta 176pp.

Little, K., 1990: "A Case of Summer Severe Weather over Alberta Under Weak Supporting Dynamics". Western Region Tech Note 90-N-095, Edmonton: Alta. Wea. Cen, Sept, 1990, 10pp.

Maddox, Robert A. 1976: An Evaluation of Tornado Proximity Wind and Stability Data *Monthly Weather Review*. **104**: 133-143

Markowski, P.M., Rasmussen, E.N., Straka, J.M. 1998: The Occurrence of Tornadoes in Supercells Interacting with Boundaries during VORTEX-95. *Weather and Forecasting*, **13**: 852-859.

Markowski, Paul and Yvette Richardson. Mesoscale Meteorology in Midlatitudes John Wiley & Sons, Ltd (2010) pp 273-293

Marwitz, John, D. 1972: The Structure and Motion of Severe Hailstorms Part 1: Supercell Storms *Journal of Applied Meteorology*. **11**: 166-180

Marwitz, John, D. 1972: The Structure and Motion of Severe Hailstorms Part 2: Multi-Cell Storms. *Journal of Applied Meteorology*. **11**: 180-189

McAulay-Weber, K. 2013: Spatial and Temporal Validation of GEM-LAM Vertical Profiles During Project UNSTABLE. B.Sc. Honours. Thesis, Department of Environment and Geography, University of Manitoba, 133 pp.

McDonald, Michael. 2010: Prairie Summer Severe Weather Event Climatology and Verification Results Report. Rep. 2010. Print.

Miller, R. C., 1972: Notes on Analysis and Severe-storm Forecasting Procedures of the Military Warning Center. Air Weather Service (MAC), Tech. Rep. 200, Scott Air Force Base, IL, 181 pp

Miloshevich, Larry M., Holger Vömel, David N. Whiteman, and Thierry Leblanc. 2009: Accuracy Assessment and Correction of Vaisala RS92 Radiosonde Water Vapor Measurements. *Journal of Geophysical Research* 114.D11

Moller, Alan R., Charles A. Dowsell, Michael P. Foster, Gary R. Woodall. 1994: The Operational and Supercel Thunderstorm Environments and Storm Structures. *Weather and Forecasting*, **9**: 327-347

Monteverdi, J., Doswell, C., & Lipari, G., 2003: Shear Parameter Thresholds for Forecasting Tornadic Thunderstorms in Northern and Central California. *Weather and Forecasting,* **18**: 357-370.

Natural Regions Committee 2006: Natural Regions and Subregions of Alberta. Compiled by D.J. Downing and W.W. Pettapiece. Government of Alberta. Pub. No. T/852.

Newton, C. W., 1963: Dynamics of Severe Convective Storms. *Metor Monogr.*, No. 27, Amer. Meteor. Soc., 33-58

Pielke, Roger A., 2001: Influence of the Spatial Distribution of Vegetation and Soils on the Prediction of Cumulus Convective Rainfall. *Reviews of Geophysics,* **39**(2): 151.

Potvin, Corey K., Kimberly L. Elmore, and Steven J. Weiss, 2010: "Assessing the Impacts of Proximity Sounding Criteria on the Climatology of Significant Tornado Environments." *Weather and Forecasting* **25**(3): 921-30.

Principles of Convection 3: Shear and Convective Storms. *Met Ed*. University Corporation for Atmospheric Research, 2003-2013 Web. 2014.

Rasmussen, Erik N. 2003: Refined Supercell and Tornado Forecast Parameters. *Wea. Forecasting*, **18**: 530–535.

Raddatz, R. L., 1998: Anthropogenic Vegetation Transformation and the Potential for Deep Convection on the Canadian Prairies. *Canadian Journal of Soil Science.* **78**(4): 657-66.

Rotunno, R., & Klemp, J. (1982). The Influence of Shear-Induced Pressure Gradient on Thunderstorm Motion. *Monthly Weather Review,* **110**: 136-151.

Segal, M., W.E. Schreiber, G. Kallos, J. R. Garratt, A. Rodi, J. Weaver and R. A. Pielke, 1989: The impact of Crop Areas in Northeast Colorado on Midsummer Mesoscale Thermal Circulations. *Mon. Wea. Rev.***117**: 809-825

Showalter, AK, 1953: A stability index for thunderstorm forecasting *Bull. Amer. Meteor. Soc.*,**34** (6): 250-252

Smith, S. B., and M. K. Yau, 1993a: The Causes of Severe Convective Outbreaks in Alberta. Part I: A Comparison of a Severe Outbreak with Two Non-Severe Events. *Mon. Wea. Rev.*, **121:** 1099–1125.

—, and —, 1993b: The Causes of Severe Convective Outbreaks in Alberta. Part II: Conceptual model and statistical analysis. *Mon. Wea. Rev.*, **121,** 1126–1133.

Strong, G. S., 1986: Synoptic to Mesoscale Dynamics of Severe Thunderstorm Environments: A Diagnostic Study with Forecasting Implications. Ph.D. Thesis, Department of Geography, University of Alberta, 345 pp.

—, 1989. LIMEX-85: 1. Processing of Datasets from an Alberta Mesoscale Upper-air Experiment. *Clim. Bull.*, **23**: 98–118.

—, 1997: Atmospheric Moisture Budget Estimates of Regional Evapotranspiration from RES-91. *Atmos. Ocean*, **35**: 29–63

—, 2000: A Multi-Scale Conceptual Model of Severe Thunderstorms. *CMOS Bull*., **28**: (2) 45-54

—, and C.D. Smith, 2001: Assessment and prediction of prairie severe thunderstorm weather phenomena. Public Safety and Emergency Preparedness Canada Research Report. Available online at: http://ww3.psepc.gc.ca/research/resactivities/natHaz/Strong_2000D023_ENG_CD_FINAL.pdf

Stull, R., & Ahrens, C. 2000. *Meteorology for scientists and engineers* (2nd ed.). Pacific Grove, CA: Brooks/Cole.

Taylor, Neil M., David M. L. Sills, John M. Hanesiak, Jason A. Milbrandt, Craig D. Smith, Geoff S. Strong, Susan H. Skone, Patrick J. McCarthy, Julian C. Brimelow, 2008: The Understanding Severe Thunderstorms and Alberta Boundary Layers Experiment (UNSTABLE). *Bull. Amer. Meteor. Soc.*, **92**: 739-763

Taylor, Neil M., 1999: Climatology of Sounding Parameters Identifying the Potential for Convective Storm Development over Central Alberta. Thesis. University of Alberta, Print.

Thompson, Richard, L., Corey M. Mead, and Roger Edwards, 2007: Effective Storm-Relative Helicity and Bulk Shear in Supercell Thunderstorm Environments. *Weather and Forecasting*. **22**: 102-116

—, Roger Edwards, John A. Hart, Kimberly L. Elmore, and Paul Markowski, 2003: Close Proximity Soundings within Supercell Environments Obtained from the Rapid Update Cycle. *Wea. Forecasting*, **18**: 1243–1261.

Tsonis, A. (2007). An Introduction to Atmospheric Thermodynamics (2nd ed., p. 198). Cambridge: Cambridge University Press.

Weckwerth, Tammy M., David B. Parsons, Steven E. Koch, James A. Moore, Margaret A. LeMone, Belay B. Demoz, Cyrille Flamant, Bart Geerts, Junhong Wang, and Wayne F. Feltz, 2004: An Overview of the International H2O Project (IHOP_2002) and Some Preliminary Highlights. *Bull. Amer. Meteor. Soc.*, **85**, 253–277.

— and —, 2006: A Review of Convective Initiation and Motivation for IHOP_2002. *Mon. Wea. Rev.* **134:** 5-22

Weisman, M.L. and J. B. Klemp, 1982: The Dependence of Numerically Simulated Convective Storms on Wind Shear and Buoyancy. *Mon. Wea. Rev*. **110**: 504-520

— and —, 1984: The Structure and Classification of Numerically Simulated Convective Storms in Directionally Varying Wind Shears. *Mon. Wea. Rev*. **112**: 2479-2499

— and —, 1986: Characteristics of Isolated Convective Storms. *Mesoscale Meteorology and Forecasting.* Amer. Meteor. Soc., 331-358

Wulfmeyer and Coauthors, 2008: The Convective and Orographically Induced Precipitation Study (COPS) *Bull. Amer. Meteor. Soc.*, 147-157

APPENDIX A

SATELLITE IMAGES OF THE FOUR STUDY SITE LOCATIONS HIGHLIGHTING COVER CLASS DIFFERENCES

Note: Figures 0.1 to 0.8 show the locations of the four radiosonde sites in the UNSTABLE study region of the Alberta foothills. Images where the stations are missing indicate that no radiosonde was launched at the site on that day. MB1 and MB2 are mobile locations and WVX and EA3 are fixed locations. Yellow lines indicate major highways. Purple line represents the approximate location of the crop/forest boundary. This line represents a transitional zone. It is diffuse in some locations and may not be a perfectly straight line, especially in areas of complex terrain). White polygon indicates the approximate UNSTABLE study domain. Images were obtained from Google Earth in September, 2014

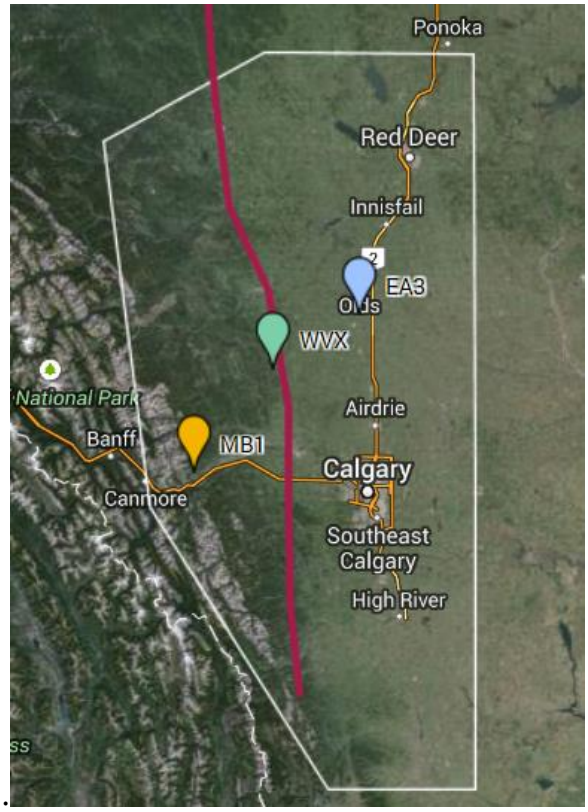

Figure 0.1: *Satellite image of the study region and location of the study sites for IOD1 July 9, 2008.*

Figure 0.2: *Satellite image of the study region and location of the study sites for IOD2 July 12, 2008.*

Figure 0.3: *Satellite image of the study region and location of the study sites for IOD3 July 13, 2008.*

Figure 0.4: *Satellite image of the study region and location of the study sites for IOD4 July 14, 2008.*

Figure 0.5: *Satellite image of the study region and location of the study sites for IOD5 July 17, 2008.*

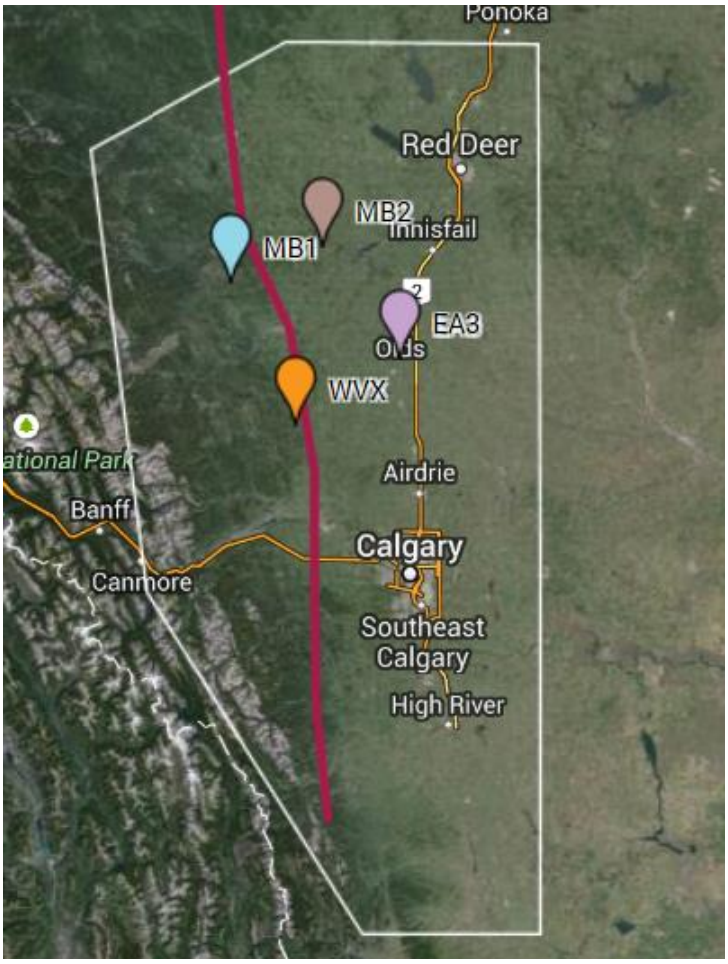

Figure 0.6: *Satellite image of the study region and location of the study sites for IOD6 July 20, 2008.*

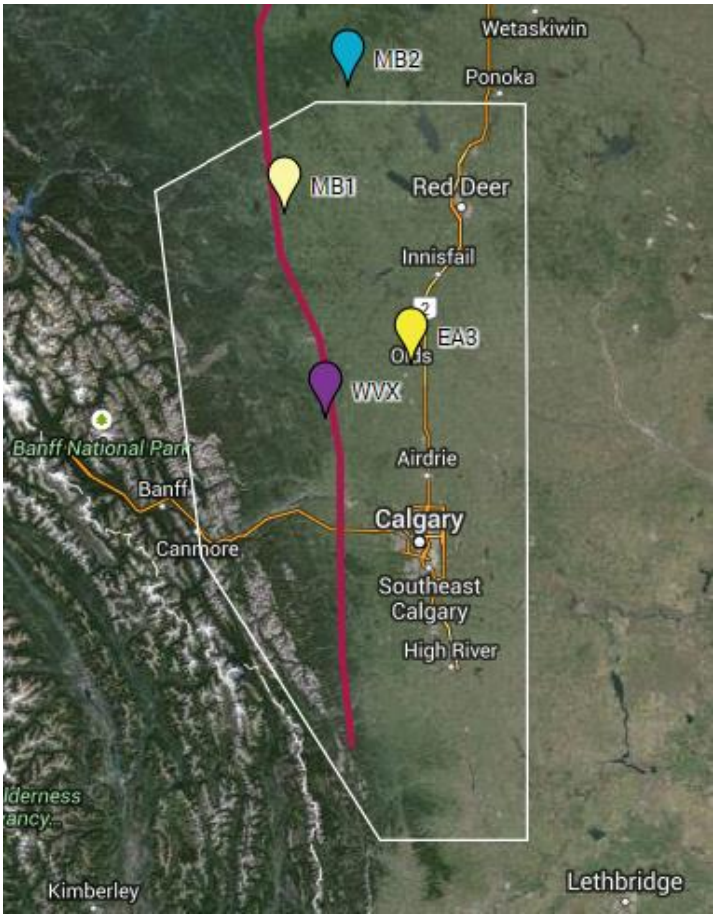

Figure 0.7: *Satellite image of the study region and location of the study sites for IOD7 July 21, 2008.*

Figure 0.8: *Satellite image of the study region and location of the study sites for IOD8 July 22, 2008.*

APPENDIX B

LOCATION COMPARISONS BY PRESSURE LEVEL

Table 0.1**:** *P-values produced from student's t-test for each pressure level between all of the site locations for temperature. Red indicates a p-value <=0.05 and blue indicates a p-value between 0.05-0.1.*

Pressure (mb)	MB1-MB2	MB1-EA3	MB1-WVX	MB2-EA3	MB2-WVX	WVX-EA3
910	0.919					
900	0.519	0.439		0.970		
890	0.916	0.293		0.182		
880	0.846	0.336		0.334		
870	0.353	0.097	0.378	0.307	0.978	0.317
860	0.204	0.053	0.181	0.445	0.903	0.537
850	0.170	0.047	0.163	0.524	0.950	0.577
840	0.189	0.057	0.150	0.522	0.838	0.681
830	0.228	0.079	0.166	0.569	0.828	0.735
820	0.244	0.104	0.197	0.617	0.859	0.759
810	0.302	0.107	0.192	0.561	0.781	0.764
800	0.288	0.132	0.229	0.654	0.878	0.772
790	0.298	0.153	0.348	0.695	0.922	0.626
780	0.284	0.189	0.353	0.813	0.883	0.701
770	0.224	0.171	0.325	0.886	0.799	0.688
760	0.496	0.238	0.473	0.609	0.969	0.638
750	0.578	0.286	0.434	0.576	0.803	0.756
740	0.535	0.274	0.450	0.580	0.864	0.707
730	0.531	0.331	0.506	0.680	0.955	0.724
720	0.502	0.383	0.440	0.783	0.899	0.879
710	0.612	0.420	0.542	0.740	0.905	0.833
700	0.763	0.687	0.619	0.909	0.840	0.935
690	0.817	0.942	0.958	0.883	0.870	0.986
680	0.974	0.905	0.935	0.888	0.916	0.975
670	0.983	0.794	0.922	0.825	0.943	0.890
660	0.964	0.640	0.934	0.704	0.971	0.743
650	0.859	0.631	0.897	0.787	0.972	0.769
640	0.886	0.626	0.965	0.763	0.935	0.711
630	0.711	0.493	0.935	0.797	0.810	0.620
620	0.790	0.407	0.859	0.645	0.939	0.588
610	0.906	0.533	0.987	0.678	0.928	0.599
600	0.961	0.603	0.870	0.638	0.926	0.549
590	0.871	0.601	0.987	0.780	0.894	0.655
580	0.770	0.647	0.996	0.920	0.783	0.676
570	0.796	0.732	0.910	0.965	0.739	0.678

Table 0.2**:** *P-values produced from student's t-test for each pressure level between all of the site locations for temperature. Red indicates a p-value <=0.05 and blue indicates a p-value between 0.05-0.1.*

Pressure (mb)	MB1-MB2	MB1-EA3	MB1-WVX	MB2-EA3	MB2-WVX	WVX-EA3
560	0.811	0.815	0.699	0.981	0.572	0.558
550	0.601	0.877	0.674	0.716	0.377	0.582
540	0.54	0.804	0.758	0.711	0.378	0.589
530	0.514	0.75	0.747	0.734	0.348	0.533
520	0.461	0.761	0.757	0.674	0.316	0.556
510	0.284	0.758	0.92	0.461	0.259	0.695
500	0.78	0.636	0.9	0.936	0.716	0.572
490	0.855	0.627	0.926	0.861	0.808	0.587
480	0.855	0.552	0.942	0.806	0.82	0.534
470	0.815	0.502	0.938	0.799	0.78	0.491
460	0.863	0.545	0.886	0.799	0.791	0.496
450	0.923	0.663	0.748	0.841	0.756	0.496
440	0.846	0.709	0.614	0.946	0.598	0.433
430	0.921	0.71	0.503	0.88	0.584	0.348
420	0.975	0.822	0.414	0.907	0.564	0.351
410	0.999	0.817	0.387	0.88	0.562	0.326
400	0.996	0.859	0.358	0.905	0.536	0.314
390	0.982	0.865	0.356	0.898	0.552	0.306
380	0.99	0.888	0.332	0.921	0.526	0.287
370	0.947	0.898	0.36	0.989	0.505	0.311
360	0.925	0.814	0.418	0.96	0.532	0.315
350	0.972	0.803	0.381	0.907	0.54	0.28
340	0.925	0.763	0.379	0.924	0.502	0.262
330	0.945	0.799	0.524	0.93	0.646	0.396
320	0.202	0.997	0.484	0.222	0.065	0.5
310	0.169	0.842	0.523	0.251	0.06	0.423
300	0.208	0.706	0.516	0.366	0.079	0.325
290	0.202	0.636	0.743	0.394	0.136	0.445
280	0.267	0.483	0.76	0.618	0.184	0.334
270	0.351	0.473	0.84	0.763	0.279	0.374
260	0.437	0.421	0.974	0.927	0.434	0.422
250	0.46	0.398	0.932	0.984	0.524	0.474
240	0.597	0.304	0.626	0.706	0.929	0.603
230	0.926	0.447	0.383	0.547	0.484	0.929
220	0.446	0.55	0.347	0.182	0.091	0.754

Table 0.3**:** *P-values produced from student's t-test for each pressure level between all of the site locations for temperature. Red indicates a p-value <=0.05 and blue indicates a p-value between 0.05-0.1.*

Pressure (mb)	MB1-MB2	MB1-EA3	MB1-WVX	MB2-EA3	MB2-WVX	WVX-EA3
210	0.077	0.847	0.492	0.051	0.014	0.626
200	0.052	0.765	0.969	0.084	0.047	0.733
190	0.217	0.743	0.928	0.316	0.18	0.665
180	0.21	0.64	0.736	0.359	0.322	0.902
170	0.336	0.719	0.388	0.477	0.201	0.312
160	0.237	0.381	0.489	0.739	0.249	0.3
150	0.135	0.332	0.544	0.598	0.242	0.326
140	0.271	0.442	0.432	0.745	0.238	0.291
130	0.217	0.087	0.542	0.725	0.296	0.238
120	0.014	0.037	0.596	0.9	0.228	0.223
110	0.474	0.158	0.383	0.504	0.271	0.165
100	0.473	0.44	0.035	0.785	0.03	0.028

Table 0.4**:** *P-values produced from student's t-test for each pressure level between all of the site locations for specific humidity. Red indicates a p-value <=0.05, and blue indicates a p-value between 0.05-0.1.*

Pressure (mb)	MB1-MB2	MB1-EA3	MB1-WVX	MB2-EA3	MB2-WVX	WVX-EA3
910	0.696					
900	0.706	0.669		0.872		
890	0.428	0.166		0.628		
880	0.928	0.489		0.309		
870	0.706	0.456	0.038	0.698	0.053	0.081
860	0.799	0.340	0.075	0.498	0.131	0.352
850	0.767	0.379	0.226	0.609	0.400	0.696
840	0.816	0.589	0.258	0.773	0.381	0.530
830	0.863	0.701	0.467	0.842	0.583	0.709
820	0.926	0.821	0.703	0.762	0.781	0.568
810	0.880	0.923	0.548	0.817	0.668	0.516
800	0.797	0.769	0.458	0.598	0.626	0.330
790	0.942	0.509	0.754	0.495	0.819	0.377
780	0.717	0.230	0.942	0.445	0.695	0.259
770	0.758	0.225	0.814	0.408	0.623	0.200
760	0.879	0.207	0.646	0.222	0.787	0.131
750	0.889	0.286	0.402	0.301	0.538	0.103
740	0.495	0.474	0.183	0.222	0.532	0.075
730	0.320	0.630	0.201	0.196	0.743	0.125
720	0.262	0.675	0.131	0.192	0.666	0.101
710	0.099	0.942	0.040	0.152	0.487	0.061
700	0.120	0.597	0.055	0.062	0.582	0.029
690	0.215	0.384	0.177	0.050	0.868	0.042
680	0.376	0.269	0.430	0.050	0.886	0.056
670	0.523	0.266	0.476	0.072	0.954	0.057
660	0.911	0.173	0.536	0.121	0.586	0.036
650	0.837	0.191	0.396	0.113	0.495	0.022
640	0.995	0.290	0.339	0.269	0.317	0.036
630	0.754	0.189	0.415	0.312	0.247	0.027
620	0.534	0.131	0.755	0.379	0.342	0.062
610	0.881	0.273	0.470	0.370	0.411	0.085
600	0.636	0.427	0.301	0.214	0.593	0.069
590	0.515	0.398	0.472	0.142	0.989	0.108
580	0.529	0.638	0.858	0.269	0.637	0.504
570	0.528	0.728	0.961	0.302	0.483	0.758
560	0.427	0.914	0.752	0.436	0.611	0.808
550	0.967	0.979	0.899	0.983	0.935	0.908
540	0.746	0.622	0.797	0.912	0.931	0.824
530	0.937	0.389	0.404	0.478	0.486	0.976

Table 0.5*: *P-values produced from student's t-test for each pressure level between all of the site locations for specific humidity. Red indicates a p-value <=0.05, and blue indicates a p-value between 0.05-0.1.

Pressure (mb)	MB1-MB2	MB1-EA3	MB1-WVX	MB2-EA3	MB2-WVX	WVX-EA3
520	0.862	0.711	0.438	0.587	0.353	0.646
510	0.738	0.789	0.284	0.919	0.486	0.376
500	0.936	0.644	0.498	0.622	0.491	0.801
490	0.614	0.886	0.845	0.497	0.487	0.944
480	0.670	0.922	0.990	0.724	0.691	0.937
470	0.581	0.602	0.974	0.321	0.582	0.652
460	0.469	0.735	0.872	0.667	0.595	0.883
450	0.392	0.915	0.955	0.449	0.443	0.965
440	0.389	0.985	0.980	0.385	0.405	0.994
430	0.379	0.638	0.423	0.225	0.149	0.725
420	0.463	0.454	0.439	0.216	0.212	0.917
410	0.437	0.521	0.363	0.238	0.179	0.749
400	0.458	0.569	0.228	0.267	0.136	0.436
390	0.400	0.651	0.261	0.275	0.154	0.444
380	0.327	0.933	0.148	0.304	0.124	0.125
370	0.291	0.852	0.782	0.255	0.241	0.920
360	0.289	0.737	0.946	0.237	0.273	0.752
350	0.399	0.485	0.281	0.294	0.244	0.606
340	0.369	0.281	0.071	0.240	0.172	0.307
330	0.414	0.170	0.134	0.250	0.235	0.808
320	0.723	0.187	0.154	0.157	0.131	0.797
310	0.338	0.180	0.202	0.492	0.552	0.983
300	0.216	0.231	0.253	0.896	0.896	0.984
290	0.219	0.157	0.190	0.602	0.797	0.850
280	0.220	0.189	0.192	0.821	0.824	0.981
270	0.370	0.248	0.308	0.312	0.663	0.594
260	0.347	0.233	0.297	0.332	0.728	0.502
250	0.506	0.324	0.363	0.106	0.263	0.629
240	0.387	0.293	0.335	0.201	0.538	0.421
230	0.330	0.338	0.364	0.854	0.523	0.480
220	0.388	0.328	0.345	0.318	0.497	0.533
210	0.586	0.328	0.351	0.306	0.316	0.329
200				0.160	0.161	0.239
190				0.506	0.330	0.335
180				0.495	0.336	0.333
170				0.491	0.334	0.342
160				0.275	0.363	0.341
150				0.333	0.329	0.084
140				0.347	0.345	0.314

Table 0.6*: *P-values produced from student's t-test for each pressure level between all of the site locations for specific humidity. Red indicates a p-value <=0.05, and blue indicates a p-value between 0.05-0.1.

Pressure (mb)	MB1-MB2	MB1-EA3	MB1-WVX	MB2-EA3	MB2-WVX	WVX-EA3
130				0.254	0.227	0.669
120				0.373	0.261	0.220
110				0.119	0.143	0.497
100				0.144	0.096	0.153

Table 0.7: *P-values produced from student's t-test for each pressure level between all of the site locations for wind direction. Red indicates a p-value <=0.05, and blue indicates a p-value between 0.05-0.1.*

Pressure (mb)	MB1-MB2	MB1-EA3	MB1-WVX	MB2-EA3	MB2-WVX	WVX-EA3
910	0.485					
900	0.282	0.021		0.082		
890	0.476	0.673		0.685		
880	0.282	0.878		0.213		
870	0.417	0.334	0.060	0.031	0.155	0.001
860	0.569	0.392	0.120	0.159	0.322	0.018
850	0.930	0.273	0.460	0.342	0.441	0.091
840	0.461	0.128	0.631	0.464	0.270	0.071
830	0.495	0.091	0.458	0.326	0.192	0.028
820	0.546	0.509	0.542	0.945	0.253	0.237
810	0.502	0.569	0.888	0.912	0.483	0.539
800	0.706	0.173	0.906	0.361	0.658	0.196
790	0.958	0.370	0.766	0.410	0.808	0.591
780	0.719	0.532	0.816	0.320	0.561	0.715
770	0.902	0.697	0.751	0.601	0.846	0.467
760	0.415	0.991	0.412	0.410	0.970	0.406
750	0.158	0.812	0.244	0.236	0.762	0.355
740	0.050	0.345	0.086	0.288	0.723	0.450
730	0.026	0.192	0.019	0.277	0.884	0.295
720	0.081	0.783	0.068	0.053	0.946	0.043
710	0.153	0.960	0.071	0.171	0.868	0.085
700	0.172	0.924	0.245	0.156	0.769	0.227
690	0.254	0.874	0.266	0.283	0.869	0.296
680	0.723	0.296	0.487	0.251	0.369	0.691
670	0.672	0.220	0.719	0.192	0.479	0.292
660	0.611	0.282	0.890	0.177	0.507	0.232
650	0.215	0.687	0.512	0.142	0.386	0.292
640	0.301	0.615	0.721	0.187	0.426	0.407
630	0.639	0.519	0.755	0.934	0.484	0.382
620	0.700	0.579	0.382	0.924	0.257	0.166
610	0.791	0.636	0.422	0.889	0.349	0.225
600	0.893	0.938	0.274	0.842	0.407	0.251
590	0.853	0.661	0.584	0.573	0.751	0.347
580	0.816	0.787	0.700	0.633	0.886	0.533
570	0.439	0.998	0.344	0.464	0.880	0.370
560	0.338	0.866	0.407	0.467	0.891	0.547
550	0.336	0.972	0.439	0.383	0.865	0.481
540	0.417	0.986	0.648	0.466	0.776	0.676
530	0.401	0.968	0.635	0.486	0.754	0.706

Table 0.8: *P-values produced from student's t-test for each pressure level between all of the site locations for wind direction. Red indicates a p-value <=0.05, and blue indicates a p-value between 0.05-0.1.*

Pressure (mb)	MB1-MB2	MB1-EA3	MB1-WVX	MB2-EA3	MB2-WVX	WVX-EA3
520	0.381	0.671	0.773	0.258	0.628	0.545
510	0.316	0.806	0.501	0.258	0.738	0.406
500	0.320	0.837	0.542	0.267	0.729	0.454
490	0.374	0.901	0.332	0.361	0.950	0.324
480	0.468	0.941	0.462	0.552	0.998	0.548
470	0.454	0.912	0.185	0.554	0.643	0.268
460	0.416	0.930	0.122	0.495	0.533	0.175
450	0.366	0.958	0.161	0.384	0.687	0.188
440	0.218	0.974	0.155	0.223	0.698	0.179
430	0.225	0.919	0.184	0.213	0.688	0.177
420	0.207	0.974	0.167	0.226	0.706	0.207
410	0.223	0.849	0.132	0.289	0.842	0.219
400	0.258	0.926	0.110	0.298	0.990	0.151
390	0.268	0.947	0.151	0.297	0.976	0.183
380	0.261	0.837	0.165	0.345	0.965	0.246
370	0.328	0.912	0.234	0.394	0.904	0.296
360	0.290	0.918	0.258	0.340	0.996	0.310
350	0.228	0.868	0.197	0.301	0.970	0.275
340	0.187	0.824	0.233	0.273	0.752	0.357
330	0.234	0.971	0.357	0.236	0.656	0.360
320	0.292	0.970	0.318	0.294	0.794	0.326
310	0.292	0.922	0.304	0.279	0.813	0.293
300	0.342	0.941	0.329	0.336	0.869	0.329
290	0.412	0.957	0.323	0.403	0.998	0.320
280	0.414	0.990	0.343	0.433	0.979	0.368
270	0.441	0.893	0.328	0.388	0.969	0.280
260	0.472	0.879	0.349	0.411	0.956	0.291
250	0.470	0.965	0.270	0.460	0.854	0.269
240	0.465	0.948	0.221	0.510	0.792	0.267
230	0.422	0.991	0.215	0.440	0.830	0.244
220	0.464	0.889	0.201	0.554	0.738	0.283
210	0.485	0.850	0.209	0.609	0.721	0.321
200	0.606	0.985	0.355	0.631	0.753	0.385
190	0.783	0.767	0.238	0.972	0.467	0.367
180	0.746	0.893	0.237	0.826	0.525	0.289
170	0.364	0.672	0.096	0.560	0.639	0.199
160	0.366	0.460	0.045	0.675	0.695	0.218
150	0.390	0.580	0.097	0.620	0.768	0.250
140	0.496	0.867	0.221	0.553	0.979	0.272

Table 0.9: *P-values produced from student's t-test for each pressure level between all of the site locations for wind direction. Red indicates a p-value <=0.05, and blue indicates a p-value between 0.05-0.1.*

Pressure (mb)	MB1-MB2	MB1-EA3	MB1-WVX	MB2-EA3	MB2-WVX	WVX-EA3
130	0.712	0.336	0.084	0.771	0.397	0.406
120	0.935	0.319	0.141	0.537	0.335	0.591
110	0.866	0.999	0.410	0.854	0.399	0.333
100	0.639	0.988	0.296	0.634	0.947	0.232

Table 0.10: *P-values produced from student's t-test for each pressure level between all of the site locations for wind speed. Red indicates a p-value <=0.05 and blue indicates a p-value between 0.05-0.1.*

Pressure (mb)	MB1-MB2	MB1-EA3	MB1-WVX	MB2-EA3	MB2-WVX	WVX-EA3
910	0.368					
900	0.002	0.004		0.105		
890	0.010	0.084		0.000		
880	0.008	0.233		0.007		
870	0.053	0.796	0.003	0.008	0.049	0.000
860	0.342	0.652	0.289	0.095	0.937	0.071
850	0.258	0.900	0.573	0.350	0.492	0.732
840	0.065	0.426	0.670	0.388	0.120	0.560
830	0.079	0.466	0.798	0.253	0.152	0.673
820	0.089	0.554	0.552	0.152	0.332	0.800
810	0.113	0.924	0.475	0.180	0.432	0.706
800	0.158	0.964	0.545	0.342	0.496	0.931
790	0.194	0.545	0.283	0.268	0.964	0.386
780	0.527	0.924	0.627	0.413	0.943	0.517
770	0.570	0.577	0.532	0.765	0.940	0.831
760	0.401	0.387	0.412	0.997	0.936	0.938
750	0.483	0.896	0.846	0.736	0.607	0.379
740	0.601	0.761	0.924	0.915	0.666	0.561
730	0.872	0.802	0.927	0.899	0.930	0.805
720	0.942	0.670	0.832	0.848	0.811	0.633
710	0.963	0.689	0.390	0.680	0.518	0.230
700	0.967	0.891	0.501	0.614	0.563	0.221
690	0.588	0.779	0.402	0.712	0.216	0.087
680	0.820	0.621	0.249	0.715	0.264	0.100
670	0.711	0.722	0.203	0.748	0.190	0.061
660	0.536	0.568	0.195	0.940	0.128	0.095
650	0.452	0.773	0.220	0.836	0.108	0.106
640	0.572	0.882	0.091	0.829	0.075	0.071
630	0.775	0.963	0.094	0.911	0.132	0.106
620	0.949	0.727	0.095	0.926	0.177	0.091
610	0.827	0.963	0.157	0.955	0.176	0.139
600	0.807	0.840	0.158	0.763	0.149	0.181
590	0.626	0.769	0.311	0.545	0.173	0.356
580	0.719	0.508	0.248	0.634	0.168	0.296
570	0.843	0.538	0.231	0.523	0.199	0.423
560	0.901	0.391	0.172	0.522	0.164	0.364
550	0.798	0.490	0.348	0.512	0.259	0.556
540	0.892	0.504	0.495	0.799	0.441	0.542

Table 0.11: *P-values produced from student's t-test for each pressure level between all of the site locations for wind speed. Red indicates a p-value <=0.05 and blue indicates a p-value between 0.05-0.1.*

Pressure (mb)	MB1-MB2	MB1-EA3	MB1-WVX	MB2-EA3	MB2-WVX	WVX-EA3
530	0.961	0.612	0.535	0.828	0.510	0.595
520	0.761	0.598	0.663	0.789	0.891	0.681
510	0.610	0.626	0.700	0.821	0.899	0.926
500	0.457	0.447	0.565	0.615	0.892	0.734
490	0.465	0.614	0.419	0.669	0.891	0.596
480	0.473	0.539	0.314	0.681	0.727	0.466
470	0.384	0.407	0.218	0.703	0.665	0.434
460	0.393	0.399	0.292	0.646	0.779	0.486
450	0.301	0.410	0.252	0.550	0.799	0.443
440	0.108	0.319	0.195	0.235	0.871	0.357
430	0.084	0.349	0.175	0.250	0.828	0.406
420	0.089	0.371	0.225	0.225	0.741	0.438
410	0.117	0.490	0.348	0.222	0.628	0.524
400	0.132	0.538	0.341	0.228	0.657	0.495
390	0.165	0.622	0.310	0.323	0.758	0.525
380	0.248	0.638	0.303	0.327	0.958	0.383
370	0.344	0.823	0.392	0.411	0.982	0.456
360	0.317	0.737	0.441	0.355	0.882	0.477
350	0.254	0.729	0.400	0.319	0.798	0.479
340	0.229	0.624	0.383	0.337	0.787	0.517
330	0.190	0.534	0.368	0.296	0.752	0.503
320	0.248	0.556	0.430	0.365	0.769	0.568
310	0.189	0.561	0.485	0.290	0.623	0.618
300	0.172	0.637	0.477	0.247	0.621	0.571
290	0.183	0.703	0.396	0.213	0.739	0.416
280	0.204	0.836	0.451	0.255	0.727	0.497
270	0.246	0.829	0.455	0.243	0.781	0.432
260	0.174	0.884	0.455	0.188	0.635	0.462
250	0.135	0.769	0.317	0.196	0.698	0.411
240	0.113	0.794	0.238	0.148	0.710	0.298
230	0.082	0.667	0.173	0.132	0.678	0.264
220	0.100	0.675	0.148	0.306	0.775	0.435
210	0.198	0.573	0.227	0.562	0.856	0.666
200	0.196	0.704	0.628	0.592	0.414	0.694
190	0.376	0.761	0.772	0.468	0.531	0.924
180	0.249	0.962	0.959	0.635	0.230	0.363
170	0.113	0.602	0.979	0.759	0.121	0.115
160	0.517	0.529	0.787	0.684	0.411	0.134
150	0.395	0.615	0.946	0.755	0.392	0.133

Table 0.12: *P-values produced from student's t-test for each pressure level between all of the site locations for wind speed. Red indicates a p-value <=0.05 and blue indicates a p-value between 0.05-0.1.*

Pressure (mb)	MB1-MB2	MB1-EA3	MB1-WVX	MB2-EA3	MB2-WVX	WVX-EA3
140	0.206	0.143	0.663	0.603	0.354	0.043
130	0.226	0.597	0.977	0.674	0.250	0.088
120	0.913	0.618	0.343	0.425	0.391	0.033
110	0.402	0.879	0.756	0.066	0.252	0.302
100	0.769	0.915	0.537		0.827	

Table 0.13: *P-values produced from student's t-test for each pressure level between all of the site locations for temperature in A.M. soundings. Red indicates a p-value <=0.05 and blue indicates a p-value between 0.05-0.1.*

Pressure (mb)	MB1-MB2	MB1-EA3	MB1-WVX	MB2-EA3	MB2-WVX	WVX-EA3
910	0.764					
900	0.367	0.936		0.382		
890	0.819	0.875		0.649		
880	0.919	0.948		0.832		
870	0.713	0.623	0.963	0.851	0.701	0.605
860	0.494	0.587	0.584	0.951	0.890	0.952
850	0.460	0.648	0.567	0.845	0.869	0.962
840	0.425	0.707	0.478	0.756	0.959	0.799
830	0.431	0.827	0.550	0.645	0.858	0.766
820	0.476	0.997	0.664	0.553	0.811	0.714
810	0.611	0.963	0.639	0.638	0.952	0.667
800	0.588	0.924	0.709	0.590	0.861	0.693
790	0.642	0.908	0.925	0.626	0.723	0.854
780	0.578	0.946	0.884	0.603	0.693	0.857
770	0.463	0.894	0.731	0.635	0.699	0.885
760	0.920	0.958	0.786	0.976	0.869	0.865
750	0.913	0.890	0.662	0.955	0.728	0.827
740	0.993	0.837	0.716	0.837	0.708	0.929
730	0.865	0.906	0.854	0.802	0.721	0.978
720	0.998	0.956	0.717	0.955	0.716	0.814
710	0.996	0.975	0.683	0.978	0.681	0.708
700	0.802	0.728	0.747	0.898	0.590	0.550
690	0.880	0.514	0.875	0.644	0.996	0.647
680	0.740	0.460	0.852	0.690	0.914	0.635
670	0.751	0.409	0.816	0.634	0.964	0.629
660	0.748	0.339	0.822	0.569	0.949	0.549
650	0.687	0.333	0.825	0.623	0.892	0.546
640	0.846	0.356	0.950	0.554	0.915	0.489
630	0.871	0.327	0.993	0.523	0.900	0.438
620	0.976	0.326	0.954	0.455	0.983	0.457
610	0.798	0.424	0.913	0.395	0.896	0.452
600	0.728	0.465	0.814	0.379	0.907	0.411
590	0.858	0.449	0.855	0.466	0.987	0.430
580	0.960	0.503	0.784	0.574	0.866	0.411
570	0.881	0.660	0.680	0.638	0.850	0.467
560	0.780	0.889	0.554	0.715	0.815	0.520
550	0.992	0.888	0.570	0.893	0.627	0.537
540	0.997	0.817	0.573	0.830	0.616	0.490

Table 0.14: *P-values produced from student's t-test for each pressure level between all of the site locations for temperature in A.M. soundings. Red indicates a p-value <=0.05 and blue indicates a p-value between 0.05-0.1.*

Pressure (mb)	MB1-MB2	MB1-EA3	MB1-WVX	MB2-EA3	MB2-WVX	WVX-EA3
530	0.970	0.808	0.577	0.846	0.589	0.494
520	0.926	0.792	0.631	0.866	0.604	0.526
510	0.952	0.658	0.769	0.716	0.748	0.524
500	0.915	0.491	0.878	0.589	0.821	0.472
490	0.988	0.490	0.970	0.533	0.985	0.531
480	0.885	0.461	0.959	0.580	0.942	0.552
470	0.798	0.407	0.940	0.581	0.886	0.512
460	0.641	0.373	0.937	0.668	0.754	0.485
450	0.492	0.327	0.935	0.739	0.633	0.453
440	0.438	0.339	0.992	0.842	0.536	0.434
430	0.416	0.322	0.975	0.831	0.496	0.399
420	0.428	0.336	0.888	0.873	0.453	0.374
410	0.467	0.360	0.829	0.866	0.446	0.362
400	0.457	0.379	0.757	0.900	0.395	0.339
390	0.548	0.458	0.694	0.903	0.408	0.349
380	0.500	0.435	0.760	0.957	0.414	0.370
370	0.501	0.413	0.824	0.936	0.451	0.389
360	0.436	0.409	0.860	0.969	0.419	0.406
350	0.405	0.367	0.883	0.977	0.404	0.383
340	0.404	0.354	0.904	0.980	0.409	0.378
330	0.449	0.442	0.646	0.943	0.720	0.749
320	0.436	0.583	0.618	0.777	0.718	0.940
310	0.407	0.517	0.574	0.818	0.730	0.909
300	0.377	0.406	0.594	0.869	0.675	0.767
290	0.340	0.304	0.453	0.934	0.769	0.801
280	0.302	0.286	0.490	0.911	0.684	0.728
270	0.239	0.227	0.431	0.934	0.639	0.667
260	0.216	0.244	0.387	0.827	0.630	0.763
250	0.149	0.229	0.371	0.715	0.509	0.745
240	0.203	0.313	0.384	0.737	0.595	0.847
230	0.362	0.661	0.567	0.615	0.689	0.901
220	0.727	0.876	0.628	0.836	0.905	0.732
210	0.838	0.259	0.812	0.417	0.654	0.103
200	0.568	0.236	0.805	0.668	0.720	0.352
190	0.525	0.247	0.903	0.747	0.576	0.267
180	0.512	0.303	0.815	0.879	0.643	0.434
170	0.594	0.260	0.842	0.647	0.473	0.176
160	0.884	0.207	0.975	0.222	0.860	0.205

Table 0.15: *P-values produced from student's t-test for each pressure level between all of the site locations for temperature in A.M. soundings. Red indicates a p-value <=0.05 and blue indicates a p-value between 0.05-0.1.*

Pressure (mb)	MB1-MB2	MB1-EA3	MB1-WVX	MB2-EA3	MB2-WVX	WVX-EA3
150	0.387	0.254	0.987	0.750	0.363	0.234
140	0.871	0.256	0.899	0.399	0.944	0.281
130	0.820	0.166	0.433	0.400	0.736	0.453
120	0.123	0.109	0.105	0.359	0.512	0.634
110	0.721	0.281	0.733	0.327	0.602	0.403
100		0.781	0.307			0.322

Table 0.16: *P-values produced from student's t-test for each pressure level between all of the site locations for temperature in P.M. soundings. Red indicates a p-value <=0.05 and blue indicates a p-value between 0.05-0.1.*

Pressure (mb)	MB1-MB2	MB1-EA3	MB1-WVX	MB2-EA3	MB2-WVX	WVX-EA3
910	0.835					
900	0.898	0.181		0.397		
890	0.975	0.208		0.133		
880	0.799	0.227		0.224		
870	0.357	0.074	0.287	0.188	0.797	0.331
860	0.289	0.037	0.239	0.254	0.833	0.394
850	0.256	0.029	0.226	0.283	0.872	0.397
840	0.311	0.035	0.228	0.246	0.773	0.428
830	0.378	0.043	0.237	0.236	0.704	0.466
820	0.374	0.044	0.236	0.248	0.708	0.478
810	0.355	0.046	0.239	0.269	0.753	0.461
800	0.350	0.056	0.262	0.317	0.801	0.488
790	0.338	0.066	0.323	0.382	0.936	0.451
780	0.354	0.094	0.346	0.475	0.964	0.518
770	0.328	0.110	0.385	0.575	0.910	0.496
760	0.445	0.148	0.558	0.518	0.865	0.414
750	0.539	0.204	0.587	0.512	0.956	0.485
740	0.445	0.199	0.572	0.582	0.859	0.479
730	0.363	0.213	0.558	0.725	0.751	0.509
720	0.391	0.252	0.566	0.734	0.781	0.550
710	0.503	0.258	0.762	0.638	0.719	0.411
700	0.546	0.379	0.824	0.782	0.711	0.521
690	0.590	0.463	0.944	0.851	0.652	0.524
680	0.732	0.605	0.940	0.865	0.695	0.578
670	0.797	0.700	0.974	0.901	0.788	0.697
660	0.811	0.809	0.993	0.996	0.819	0.816
650	0.888	0.819	0.941	0.935	0.844	0.782
640	0.987	0.863	0.913	0.886	0.910	0.800
630	0.745	0.954	0.837	0.817	0.910	0.901
620	0.760	0.796	0.787	0.967	0.963	0.997
610	0.718	0.861	0.848	0.867	0.861	0.998
600	0.830	0.909	0.967	0.923	0.869	0.945
590	0.736	0.901	0.823	0.837	0.896	0.932
580	0.698	0.914	0.788	0.782	0.883	0.882
570	0.682	0.886	0.833	0.786	0.831	0.949
560	0.641	0.839	0.991	0.781	0.636	0.832
550	0.545	0.913	0.937	0.612	0.494	0.849

Table 0.17: *P-values produced from student's t-test for each pressure level between all of the site locations for temperature in P.M. soundings. Red indicates a p-value <=0.05 and blue indicates a p-value between 0.05-0.1.*

Pressure (mb)	MB1-MB2	MB1-EA3	MB1-WVX	MB2-EA3	MB2-WVX	WVX-EA3
540	0.483	0.878	0.945	0.564	0.512	0.930
530	0.474	0.823	0.963	0.595	0.484	0.853
520	0.435	0.854	0.993	0.535	0.428	0.857
510	0.230	0.942	0.894	0.253	0.265	0.953
500	0.807	0.930	0.991	0.852	0.798	0.919
490	0.847	0.932	0.948	0.890	0.811	0.878
480	0.902	0.869	0.909	0.985	0.841	0.774
470	0.898	0.858	0.888	0.990	0.825	0.746
460	0.970	0.970	0.820	0.951	0.915	0.790
450	0.834	0.821	0.637	0.943	0.937	0.810
440	0.869	0.775	0.515	0.988	0.810	0.729
430	0.788	0.747	0.407	0.943	0.813	0.628
420	0.733	0.644	0.361	0.954	0.827	0.668
410	0.730	0.678	0.361	0.928	0.831	0.638
400	0.730	0.659	0.363	0.937	0.835	0.648
390	0.772	0.729	0.399	0.927	0.835	0.618
380	0.748	0.674	0.316	0.929	0.789	0.542
370	0.812	0.648	0.310	0.990	0.730	0.558
360	0.793	0.734	0.362	0.940	0.793	0.556
350	0.720	0.691	0.301	0.887	0.814	0.514
340	0.746	0.717	0.287	0.905	0.768	0.484
330	0.767	0.762	0.246	0.899	0.716	0.406
320	0.343	0.646	0.198	0.190	0.042	0.419
310	0.286	0.768	0.213	0.208	0.041	0.361
300	0.389	0.844	0.216	0.325	0.067	0.314
290	0.411	0.813	0.300	0.328	0.106	0.435
280	0.592	0.990	0.320	0.598	0.183	0.344
270	0.840	0.896	0.365	0.759	0.334	0.440
260	0.994	0.980	0.471	0.978	0.554	0.464
250	0.821	0.970	0.524	0.850	0.768	0.567
240	0.695	0.738	0.914	0.520	0.783	0.688
230	0.412	0.588	0.495	0.242	0.197	0.916
220	0.073	0.562	0.382	0.037	0.015	0.819
210	0.013	0.449	0.460	0.003	0.002	0.941
200	0.041	0.821	0.776	0.018	0.020	0.941
190	0.296	0.878	0.849	0.211	0.227	0.955
180	0.304	0.960	0.803	0.277	0.400	0.817
170	0.442	0.895	0.410	0.346	0.269	0.427

Table 0.18: *P-values produced from student's t-test for each pressure level between all of the site locations for temperature in P.M. soundings. Red indicates a p-value <=0.05 and blue indicates a p-value between 0.05-0.1.*

Pressure (mb)	MB1-MB2	MB1-EA3	MB1-WVX	MB2-EA3	MB2-WVX	WVX-EA3
160	0.222	0.754	0.490	0.260	0.275	0.424
150	0.254	0.631	0.543	0.430	0.336	0.447
140	0.254	0.857	0.421	0.331	0.264	0.393
130	0.157	0.256	0.438	0.770	0.263	0.295
120	0.045	0.163	0.405	0.836	0.230	0.254
110	0.235	0.338	0.342	0.946	0.235	0.235
100	0.755	0.410	0.075	0.548	0.073	0.064

Table 0.19: *P-values produced from student's t-test for each pressure level between all of the site locations for wind direction in A.M. soundings. Red indicates a p-value <=0.05 and blue indicates a p-value between 0.05-0.1.*

Pressure (mb)	MB1-MB2	MB1-EA3	MB1-WVX	MB2-EA3	MB2-WVX	WVX-EA3
910	0.388					
900	0.194	0.449		0.848		
890	0.723	0.555		0.808		
880	0.047	0.138		0.390		
870	0.396	0.665	0.078	0.146	0.286	0.007
860	0.360	0.509	0.068	0.145	0.491	0.018
850	0.713	0.542	0.257	0.399	0.567	0.123
840	0.809	0.386	0.394	0.621	0.355	0.118
830	0.814	0.346	0.326	0.536	0.285	0.080
820	0.726	0.826	0.352	0.899	0.233	0.279
810	0.356	0.748	0.575	0.519	0.719	0.788
800	0.443	0.220	0.645	0.797	0.719	0.463
790	0.728	0.905	0.977	0.788	0.684	0.864
780	0.682	0.899	0.773	0.753	0.851	0.869
770	0.578	0.873	0.754	0.693	0.384	0.638
760	0.992	0.597	0.331	0.676	0.452	0.709
750	0.304	0.214	0.067	0.780	0.757	0.974
740	0.216	0.168	0.043	0.762	0.892	0.815
730	0.437	0.602	0.104	0.776	0.723	0.454
720	0.598	0.680	0.338	0.454	0.894	0.321
710	0.963	0.736	0.711	0.785	0.709	0.505
700	0.740	0.856	0.953	0.873	0.595	0.755
690	0.700	0.431	0.607	0.752	0.998	0.690
680	0.899	0.437	0.247	0.535	0.405	0.576
670	0.912	0.290	0.272	0.455	0.453	0.981
660	0.772	0.378	0.500	0.375	0.455	0.667
650	0.281	0.841	0.503	0.311	0.391	0.612
640	0.330	0.775	0.669	0.383	0.413	0.879
630	0.581	0.943	0.682	0.598	0.377	0.600
620	0.785	0.982	0.266	0.792	0.244	0.229
610	0.894	0.959	0.346	0.923	0.392	0.302
600	0.982	0.973	0.414	0.960	0.500	0.400
590	0.986	0.951	0.666	0.944	0.703	0.703
580	0.978	0.936	0.977	0.963	0.998	0.955
570	0.856	0.957	0.845	0.820	0.990	0.804
560	0.873	0.758	0.874	0.678	0.773	0.885
550	0.777	0.743	0.925	0.586	0.843	0.685
540	0.806	0.729	0.814	0.616	0.974	0.609
530	0.837	0.697	0.958	0.611	0.884	0.686

Table 0.20: *P-values produced from student's t-test for each pressure level between all of the site locations for wind direction in A.M. soundings. Red indicates a p-value <=0.05 and blue indicates a p-value between 0.05-0.1.*

Pressure (mb)	MB1-MB2	MB1-EA3	MB1-WVX	MB2-EA3	MB2-WVX	WVX-EA3
520	0.795	0.538	0.857	0.441	0.689	0.669
510	0.800	0.505	0.891	0.410	0.706	0.573
500	0.934	0.418	0.851	0.423	0.805	0.545
490	0.797	0.658	0.738	0.520	0.957	0.470
480	0.990	0.810	0.816	0.805	0.810	0.961
470	0.986	0.744	0.921	0.764	0.940	0.798
460	0.912	0.778	0.748	0.716	0.854	0.576
450	0.759	0.847	0.670	0.664	0.936	0.595
440	0.923	0.769	0.730	0.721	0.831	0.555
430	0.948	0.662	0.693	0.647	0.778	0.434
420	0.891	0.567	0.754	0.524	0.893	0.397
410	0.874	0.605	0.724	0.542	0.881	0.409
400	0.747	0.768	0.546	0.567	0.818	0.402
390	0.747	0.711	0.497	0.502	0.749	0.304
380	0.747	0.778	0.504	0.560	0.765	0.354
370	0.846	0.785	0.689	0.660	0.861	0.518
360	0.823	0.819	0.637	0.672	0.842	0.505
350	0.765	0.939	0.553	0.732	0.812	0.547
340	0.787	0.861	0.572	0.692	0.823	0.519
330	0.874	0.766	0.616	0.679	0.784	0.460
320	0.824	0.864	0.481	0.724	0.701	0.439
310	0.842	0.865	0.527	0.744	0.734	0.485
300	0.847	0.898	0.543	0.775	0.755	0.523
290	0.907	0.835	0.541	0.771	0.689	0.461
280	0.951	0.756	0.544	0.738	0.650	0.390
270	0.903	0.770	0.503	0.707	0.654	0.360
260	0.930	0.799	0.508	0.763	0.644	0.396
250	0.955	0.721	0.471	0.802	0.516	0.314
240	0.861	0.683	0.550	0.856	0.511	0.349
230	0.996	0.730	0.502	0.781	0.596	0.367
220	0.977	0.928	0.494	0.922	0.621	0.521
210	0.982	0.778	0.559	0.829	0.636	0.477
200	0.976	0.674	0.612	0.742	0.657	0.405
190	0.967	0.801	0.588	0.849	0.609	0.471
180	0.957	0.579	0.665	0.652	0.668	0.341
170	0.807	0.594	0.588	0.478	0.815	0.312
160	0.865	0.945	0.425	0.831	0.732	0.429
150	0.621	0.919	0.397	0.577	0.894	0.372

Table 0.21: *P-values produced from student's t-test for each pressure level between all of the site locations for wind direction in A.M. soundings. Red indicates a p-value <=0.05 and blue indicates a p-value between 0.05-0.1.*

Pressure (mb)	MB1-MB2	MB1-EA3	MB1-WVX	MB2-EA3	MB2-WVX	WVX-EA3
140	0.647	0.781	0.279	0.796	0.887	0.531
130	0.676	0.460	0.163	0.985	0.765	0.614
120	0.674	0.825	0.233	0.545	0.227	0.326
110	0.670	0.343	0.553	0.499	0.221	0.039
100		0.167	0.991			0.072

Table 0.22: *P-values produced from student's t-test for each pressure level between all of the site locations for wind direction in P.M. soundings. Red indicates a p-value <=0.05 and blue indicates a p-value between 0.05-0.1.*

Pressure (mb)	MB1-MB2	MB1-EA3	MB1-WVX	MB2-EA3	MB2-WVX	WVX-EA3
910	0.048					
900	0.612	0.062		0.020		
890	0.421	0.953		0.272		
880	0.920	0.443		0.338		
870	0.807	0.304	0.323	0.091	0.263	0.013
860	0.872	0.458	0.637	0.508	0.481	0.216
850	0.597	0.331	0.901	0.587	0.510	0.280
840	0.421	0.184	0.416	0.509	0.098	0.041
830	0.473	0.141	0.413	0.382	0.117	0.029
820	0.641	0.477	0.557	0.763	0.282	0.211
810	0.973	0.626	0.279	0.608	0.301	0.151
800	0.763	0.428	0.665	0.280	0.871	0.255
790	0.783	0.284	0.787	0.161	0.588	0.456
780	0.917	0.355	0.303	0.256	0.215	0.891
770	0.541	0.665	0.646	0.249	0.226	0.989
760	0.313	0.713	0.905	0.139	0.181	0.760
750	0.305	0.519	0.987	0.058	0.213	0.409
740	0.116	0.975	0.307	0.075	0.460	0.227
730	0.028	0.274	0.035	0.201	0.582	0.351
720	0.078	0.872	0.072	0.039	0.824	0.026
710	0.080	0.817	0.061	0.103	0.832	0.080
700	0.141	0.936	0.078	0.101	0.967	0.039
690	0.304	0.651	0.322	0.125	0.801	0.089
680	0.601	0.497	0.718	0.236	0.816	0.251
670	0.437	0.540	0.381	0.183	0.966	0.123
660	0.564	0.534	0.662	0.262	0.823	0.283
650	0.671	0.443	0.998	0.262	0.647	0.416
640	0.867	0.308	0.890	0.255	0.760	0.354
630	0.917	0.386	0.779	0.468	0.872	0.549
620	0.766	0.424	0.711	0.657	0.974	0.647
610	0.784	0.509	0.681	0.736	0.941	0.757
600	0.834	0.837	0.913	0.714	0.911	0.769
590	0.773	0.487	0.861	0.392	0.668	0.607
580	0.705	0.764	0.970	0.550	0.689	0.796
570	0.366	0.945	0.767	0.454	0.529	0.849
560	0.258	0.634	0.653	0.551	0.441	0.919

Table 0.23: *P-values produced from student's t-test for each pressure level between all of the site locations for wind direction in P.M. soundings. Red indicates a p-value <=0.05 and blue indicates a p-value between 0.05-0.1.*

Pressure (mb)	MB1-MB2	MB1-EA3	MB1-WVX	MB2-EA3	MB2-WVX	WVX-EA3
550	0.306	0.841	0.916	0.497	0.399	0.921
540	0.413	0.815	0.630	0.590	0.271	0.543
530	0.378	0.726	0.599	0.617	0.232	0.453
520	0.377	0.936	0.639	0.399	0.248	0.738
510	0.302	0.881	0.979	0.400	0.347	0.911
500	0.267	0.797	0.896	0.393	0.339	0.905
490	0.394	0.931	0.965	0.472	0.439	0.967
480	0.417	0.844	0.824	0.557	0.568	0.983
470	0.393	0.755	0.380	0.575	0.920	0.598
460	0.392	0.811	0.372	0.532	0.957	0.529
450	0.404	0.995	0.503	0.432	0.801	0.538
440	0.212	0.921	0.485	0.237	0.365	0.574
430	0.213	0.904	0.588	0.239	0.330	0.683
420	0.202	0.719	0.454	0.284	0.376	0.718
410	0.221	0.614	0.384	0.357	0.464	0.737
400	0.291	0.816	0.462	0.364	0.550	0.622
390	0.301	0.796	0.566	0.385	0.513	0.750
380	0.287	0.694	0.548	0.433	0.553	0.820
370	0.326	0.780	0.596	0.453	0.606	0.796
360	0.287	0.808	0.626	0.381	0.529	0.794
350	0.235	0.835	0.525	0.309	0.492	0.675
340	0.181	0.707	0.571	0.285	0.346	0.854
330	0.212	0.905	0.773	0.244	0.293	0.866
320	0.289	0.996	0.780	0.294	0.387	0.782
310	0.275	0.938	0.685	0.262	0.412	0.644
300	0.326	0.939	0.723	0.313	0.459	0.683
290	0.371	0.996	0.745	0.377	0.507	0.753
280	0.348	0.867	0.748	0.416	0.479	0.881
270	0.400	0.971	0.806	0.386	0.507	0.778
260	0.409	0.927	0.830	0.372	0.503	0.759
250	0.345	0.889	0.654	0.399	0.537	0.758
240	0.287	0.731	0.480	0.414	0.575	0.724
230	0.279	0.836	0.507	0.359	0.543	0.665
220	0.332	0.873	0.445	0.403	0.694	0.563
210	0.357	0.761	0.357	0.493	0.812	0.554
200	0.516	0.896	0.597	0.581	0.837	0.683
190	0.668	0.731	0.527	0.851	0.953	0.744
180	0.675	0.677	0.546	0.886	0.994	0.824
170	0.370	0.428	0.361	0.700	0.799	0.855

Table 0.24: *P-values produced from student's t-test for each pressure level between all of the site locations for wind direction in P.M. soundings. Red indicates a p-value <=0.05 and blue indicates a p-value between 0.05-0.1.*

Pressure (mb)	MB1-MB2	MB1-EA3	MB1-WVX	MB2-EA3	MB2-WVX	WVX-EA3
160	0.346	0.390	0.318	0.652	0.738	0.856
150	0.520	0.500	0.407	0.786	0.868	0.854
140	0.675	0.855	0.947	0.603	0.691	0.777
130	0.943	0.588	0.558	0.753	0.721	0.942
120	0.868	0.360	0.992	0.662	0.871	0.346
110	0.939	0.750	0.866	0.735	0.960	0.540
100	0.702	0.484	0.886	0.986	0.778	0.634

Table 0.25: *P-values produced from student's t-test for each pressure level between all of the site locations for wind speed in A.M. soundings. Red indicates a p-value <=0.05 and blue indicates a p-value between 0.05-0.1.*

Pressure (mb)	MB1-MB2	MB1-EA3	MB1-WVX	MB2-EA3	MB2-WVX	WVX-EA3
910	#DIV/0!					
900	0.205	0.180		0.977		
890	0.171	0.272		0.152		
880	0.109	0.237		0.073		
870	0.275	0.828	0.228	0.090	0.661	0.052
860	0.063	0.379	0.127	0.234	0.441	0.476
850	0.038	0.620	0.204	0.211	0.154	0.614
840	0.029	0.401	0.285	0.403	0.074	0.886
830	0.054	0.216	0.389	0.678	0.159	0.554
820	0.093	0.303	0.241	0.508	0.568	0.902
810	0.126	0.726	0.138	0.238	0.952	0.256
800	0.060	0.347	0.030	0.377	0.640	0.224
790	0.048	0.232	0.018	0.509	0.677	0.310
780	0.410	0.423	0.262	0.911	0.709	0.867
770	0.822	0.265	0.910	0.245	0.872	0.200
760	0.853	0.636	0.971	0.392	0.755	0.550
750	0.822	0.126	0.411	0.175	0.540	0.399
740	0.737	0.254	0.395	0.479	0.653	0.781
730	0.579	0.158	0.570	0.502	0.872	0.277
720	0.465	0.090	0.337	0.503	0.956	0.338
710	0.473	0.132	0.231	0.509	0.868	0.520
700	0.506	0.232	0.605	0.737	0.784	0.459
690	0.846	0.195	0.460	0.334	0.662	0.491
680	0.503	0.182	0.587	0.684	0.769	0.345
670	0.586	0.152	0.530	0.616	0.924	0.405
660	0.796	0.354	0.684	0.689	0.978	0.599
650	0.909	0.230	0.916	0.469	0.965	0.235
640	0.772	0.183	0.565	0.513	0.922	0.394
630	0.651	0.197	0.490	0.602	0.965	0.514
620	0.559	0.226	0.367	0.679	0.939	0.650
610	0.722	0.387	0.543	0.721	0.902	0.765
600	0.771	0.443	0.671	0.714	0.940	0.736
590	0.751	0.389	0.633	0.646	0.901	0.719
580	0.785	0.493	0.593	0.707	0.810	0.894
570	0.792	0.415	0.525	0.632	0.757	0.841
560	0.796	0.379	0.487	0.591	0.712	0.846
550	0.865	0.451	0.681	0.596	0.834	0.716
540	0.916	0.401	0.788	0.491	0.884	0.529

Table 0.26: *P-values produced from student's t-test for each pressure level between all of the site locations for wind speed in A.M. soundings. Red indicates a p-value <=0.05 and blue indicates a p-value between 0.05-0.1.*

Pressure (mb)	MB1-MB2	MB1-EA3	MB1-WVX	MB2-EA3	MB2-WVX	WVX-EA3
530	0.964	0.491	0.939	0.529	0.980	0.473
520	0.922	0.548	0.865	0.638	0.784	0.374
510	0.754	0.492	0.975	0.769	0.716	0.425
500	0.676	0.331	0.870	0.645	0.759	0.342
490	0.743	0.395	0.920	0.628	0.793	0.385
480	0.818	0.320	0.976	0.411	0.816	0.251
470	0.842	0.222	0.900	0.282	0.932	0.225
460	0.861	0.225	0.872	0.295	0.979	0.249
450	0.924	0.238	0.896	0.289	0.975	0.282
440	0.856	0.206	0.760	0.324	0.931	0.297
430	0.870	0.216	0.940	0.344	0.925	0.250
420	0.855	0.255	0.961	0.414	0.887	0.270
410	0.936	0.425	0.987	0.526	0.925	0.416
400	0.910	0.461	0.935	0.565	0.847	0.394
390	0.903	0.469	0.954	0.574	0.855	0.402
380	0.982	0.499	0.989	0.535	0.971	0.468
370	0.906	0.650	0.851	0.584	0.956	0.507
360	0.985	0.709	0.852	0.725	0.882	0.569
350	0.997	0.652	0.754	0.698	0.795	0.453
340	0.921	0.713	0.758	0.685	0.871	0.512
330	0.893	0.625	0.808	0.582	0.936	0.483
320	0.820	0.580	0.797	0.481	0.997	0.427
310	0.789	0.628	0.740	0.501	0.980	0.426
300	0.799	0.708	0.727	0.570	0.953	0.492
290	0.796	0.728	0.827	0.584	0.956	0.595
280	0.810	0.802	0.813	0.652	0.985	0.646
270	0.733	0.828	0.758	0.600	0.962	0.616
260	0.786	0.857	0.739	0.668	0.972	0.616
250	0.908	0.497	0.737	0.631	0.855	0.746
240	0.921	0.518	0.618	0.627	0.726	0.876
230	0.830	0.515	0.561	0.690	0.738	0.944
220	0.841	0.530	0.582	0.701	0.763	0.917
210	0.791	0.295	0.553	0.473	0.791	0.574
200	0.932	0.459	0.842	0.522	0.919	0.530
190	0.936	0.624	0.951	0.561	0.875	0.588
180	0.845	0.935	0.760	0.887	0.579	0.621
170	0.835	0.841	0.713	0.987	0.487	0.476
160	0.981	0.635	0.602	0.717	0.651	0.232

Table 0.27: *P-values produced from student's t-test for each pressure level between all of the site locations for wind speed in A.M. soundings. Red indicates a p-value <=0.05 and blue indicates a p-value between 0.05-0.1.*

Pressure (mb)	MB1-MB2	MB1-EA3	MB1-WVX	MB2-EA3	MB2-WVX	WVX-EA3
150	1.000	0.659	0.961	0.645	0.959	0.436
140	0.920	0.380	0.911	0.336	0.817	0.215
130	0.939	0.697	0.871	0.427	0.891	0.231
120	0.144	0.603	0.277	0.212	0.382	0.200
110	0.393	0.731	0.826	0.290	0.256	0.598
100		0.542	0.766			0.457

Table 0.28: *P-values produced from student's t-test for each pressure level between all of the site locations for wind speed in P.M. soundings. Red indicates a p-value <=0.05 and blue indicates a p-value between 0.05-0.1.*

Pressure (mb)	MB1-MB2	MB1-EA3	MB1-WVX	MB2-EA3	MB2-WVX	WVX-EA3
910	0.608					
900	0.052	0.050		0.508		
890	0.118	0.306		0.227		
880	0.217	0.740		0.168		
870	0.278	0.490	0.009	0.020	0.010	0.000
860	0.456	0.157	0.941	0.433	0.400	0.104
850	0.803	0.559	0.899	0.705	0.866	0.552
840	0.593	0.836	0.761	0.703	0.777	0.913
830	0.602	0.889	0.965	0.466	0.537	0.917
820	0.585	0.835	0.928	0.373	0.631	0.744
810	0.565	0.762	0.809	0.297	0.748	0.554
800	0.859	0.428	0.742	0.255	0.581	0.668
790	0.836	0.892	0.784	0.694	0.922	0.659
780	0.861	0.599	0.965	0.498	0.844	0.687
770	0.434	0.107	0.183	0.532	0.635	0.914
760	0.413	0.172	0.029	0.749	0.270	0.339
750	0.380	0.332	0.040	0.981	0.394	0.376
740	0.488	0.390	0.049	0.939	0.331	0.325
730	0.656	0.659	0.173	0.949	0.478	0.365
720	0.633	0.682	0.142	0.913	0.484	0.354
710	0.791	0.754	0.354	0.984	0.598	0.579
700	0.682	0.459	0.495	0.816	0.873	0.927
690	0.543	0.332	0.657	0.809	0.791	0.550
680	0.463	0.188	0.840	0.694	0.385	0.150
670	0.401	0.256	0.883	0.862	0.472	0.317
660	0.327	0.247	0.959	0.959	0.349	0.269
650	0.291	0.326	0.910	0.894	0.258	0.286
640	0.359	0.365	0.924	0.925	0.345	0.353
630	0.455	0.428	0.862	0.959	0.393	0.364
620	0.569	0.663	0.912	0.861	0.541	0.625
610	0.581	0.518	0.944	0.986	0.568	0.516
600	0.604	0.817	0.993	0.763	0.605	0.813
590	0.399	0.829	0.592	0.506	0.690	0.748
580	0.523	0.724	0.593	0.332	0.874	0.365
570	0.722	0.742	0.873	0.501	0.834	0.618
560	0.750	0.628	0.937	0.420	0.687	0.678
550	0.671	0.731	0.891	0.433	0.746	0.597

Table 0.29: *P-values produced from student's t-test for each pressure level between all of the site locations for wind speed in P.M. soundings. Red indicates a p-value <=0.05 and blue indicates a p-value between 0.05-0.1.*

Pressure (mb)	MB1-MB2	MB1-EA3	MB1-WVX	MB2-EA3	MB2-WVX	WVX-EA3
540	0.857	0.760	0.675	0.641	0.853	0.429
530	0.990	0.814	0.812	0.807	0.826	0.603
520	0.666	0.708	0.750	0.928	0.425	0.442
510	0.654	0.852	0.621	0.771	0.339	0.468
500	0.516	0.763	0.751	0.718	0.334	0.532
490	0.454	0.913	0.979	0.521	0.471	0.898
480	0.410	0.880	0.768	0.496	0.627	0.877
470	0.298	0.805	0.655	0.422	0.579	0.831
460	0.303	0.818	0.883	0.419	0.423	0.950
450	0.175	0.842	0.836	0.219	0.304	0.973
440	0.048	0.729	0.774	0.081	0.136	0.990
430	0.036	0.727	0.576	0.061	0.141	0.804
420	0.041	0.702	0.572	0.077	0.169	0.820
410	0.050	0.720	0.722	0.095	0.121	0.984
400	0.071	0.809	0.669	0.113	0.186	0.842
390	0.102	0.913	0.599	0.126	0.277	0.675
380	0.145	0.887	0.632	0.191	0.352	0.734
370	0.172	0.970	0.720	0.199	0.354	0.755
360	0.166	0.804	0.772	0.269	0.320	0.956
350	0.119	0.833	0.637	0.183	0.294	0.795
340	0.083	0.633	0.562	0.196	0.251	0.906
330	0.063	0.617	0.622	0.169	0.190	0.988
320	0.081	0.748	0.665	0.165	0.199	0.915
310	0.032	0.704	0.659	0.098	0.101	0.961
300	0.030	0.757	0.693	0.082	0.094	0.938
290	0.038	0.823	0.734	0.084	0.112	0.911
280	0.056	0.933	0.867	0.093	0.117	0.937
270	0.067	0.891	0.845	0.116	0.143	0.953
260	0.034	0.933	0.931	0.059	0.071	0.995
250	0.048	0.905	0.912	0.051	0.065	0.998
240	0.033	0.877	0.876	0.029	0.039	0.991
230	0.021	0.988	0.965	0.023	0.026	0.954
220	0.027	0.964	0.860	0.037	0.052	0.900
210	0.118	0.980	0.892	0.115	0.108	0.911
200	0.082	0.966	0.299	0.076	0.013	0.317
190	0.218	0.984	0.191	0.213	0.033	0.198
180	0.250	0.931	0.256	0.226	0.053	0.294
170	0.114	0.715	0.303	0.201	0.028	0.194

Table 0.30: *P-values produced from student's t-test for each pressure level between all of the site locations for wind speed in P.M. soundings. Red indicates a p-value <=0.05 and blue indicates a p-value between 0.05-0.1.*

Pressure (mb)	MB1-MB2	MB1-EA3	MB1-WVX	MB2-EA3	MB2-WVX	WVX-EA3
160	0.597	0.910	0.265	0.668	0.166	0.234
150	0.371	0.968	0.382	0.405	0.159	0.404
140	0.151	0.430	0.526	0.331	0.083	0.180
130	0.283	0.967	0.239	0.320	0.081	0.269
120	0.381	0.571	0.236	0.220	0.093	0.554
110	0.791	0.932	0.196	0.829	0.429	0.199
100	0.330	0.879	0.799	0.323	0.380	0.884

Table 0.31: *P-values produced from student's t-test for each pressure level between all of the site locations for specific humidity in A.M. soundings. Red indicates a p-value <=0.05 and blue indicates a p-value between 0.05-0.1.*

Pressure (mb)	MB1-MB2	MB1-EA3	MB1-WVX	MB2-EA3	MB2-WVX	WVX-EA3
910	0.910					
900	0.652	0.877		0.657		
890	0.436	0.287		0.907		
880	0.774	0.662		0.798		
870	0.849	0.868	0.047	0.974	0.008	0.008
860	0.977	0.995	0.012	0.884	0.021	0.008
850	0.869	0.910	0.007	0.729	0.043	0.005
840	0.859	0.534	0.012	0.438	0.066	0.004
830	0.960	0.631	0.067	0.594	0.159	0.039
820	0.853	0.206	0.261	0.316	0.291	0.025
810	0.662	0.193	0.446	0.469	0.340	0.049
800	0.687	0.250	0.591	0.531	0.439	0.108
790	0.560	0.277	0.984	0.677	0.578	0.254
780	0.465	0.271	0.778	0.719	0.635	0.366
770	0.602	0.260	0.968	0.585	0.638	0.262
760	0.856	0.232	0.949	0.450	0.836	0.218
750	0.870	0.380	0.654	0.635	0.620	0.259
740	0.873	0.468	0.429	0.547	0.628	0.210
730	0.858	0.551	0.520	0.583	0.701	0.306
720	0.753	0.761	0.302	0.680	0.538	0.311
710	0.546	0.902	0.144	0.657	0.438	0.261
700	0.672	0.584	0.181	0.450	0.259	0.142
690	0.687	0.454	0.318	0.351	0.462	0.164
680	0.747	0.434	0.372	0.341	0.401	0.141
670	0.755	0.445	0.384	0.345	0.412	0.135
660	0.979	0.362	0.602	0.375	0.401	0.147
650	0.888	0.424	0.432	0.383	0.309	0.113
640	0.831	0.522	0.371	0.463	0.334	0.140
630	0.997	0.391	0.615	0.386	0.504	0.152
620	0.792	0.328	0.865	0.406	0.571	0.207
610	0.672	0.498	0.509	0.277	0.810	0.187
600	0.482	0.780	0.378	0.286	0.923	0.257
590	0.593	0.829	0.449	0.422	0.854	0.315
580	0.733	0.896	0.803	0.682	0.953	0.687
570	0.514	0.721	0.481	0.846	0.932	0.747
560	0.509	0.341	0.264	0.718	0.664	0.962
550	0.757	0.348	0.287	0.504	0.451	0.942
540	0.978	0.635	0.696	0.509	0.554	0.903

Table 0.32: *P-values produced from student's t-test for each pressure level between all of the site locations for specific humidity in A.M. soundings. Red indicates a p-value <=0.05 and blue indicates a p-value between 0.05-0.1.*

Pressure (mb)	MB1-MB2	MB1-EA3	MB1-WVX	MB2-EA3	MB2-WVX	WVX-EA3
530	0.976	0.842	0.970	0.993	0.843	0.790
520	0.833	0.824	0.841	0.869	0.889	0.967
510	0.860	0.845	0.978	0.865	0.975	0.816
500	0.647	0.947	0.516	0.815	0.804	0.591
490	0.436	0.730	0.288	0.726	0.765	0.435
480	0.807	0.886	0.680	0.991	0.797	0.763
470	0.955	0.882	0.770	0.921	0.799	0.636
460	0.736	0.804	0.642	0.973	0.868	0.817
450	0.745	0.975	0.777	0.806	0.998	0.793
440	0.707	0.915	0.775	0.835	0.989	0.845
430	0.808	0.665	0.936	0.534	0.893	0.604
420	0.738	0.464	0.944	0.696	0.708	0.380
410	0.703	0.369	0.990	0.471	0.839	0.293
400	0.768	0.570	0.964	0.652	0.870	0.508
390	0.928	0.774	0.959	0.590	0.796	0.782
380	0.913	0.606	0.417	0.411	0.228	0.673
370	0.845	0.588	0.537	0.414	0.312	0.928
360	0.733	0.802	0.468	0.989	0.436	0.344
350	0.573	0.669	0.278	0.908	0.208	0.131
340	0.495	0.451	0.194	0.850	0.156	0.223
330	0.534	0.423	0.210	0.734	0.158	0.326
320	0.445	0.455	0.213	0.940	0.216	0.213
310	0.359	0.348	0.210	0.939	0.392	0.399
300	0.211	0.331	0.263	0.352	0.639	0.633
290	0.304	0.279	0.272	0.785	0.737	0.917
280	0.271	0.373	0.333	0.208	0.430	0.658
270	0.373	0.358	0.352	0.834	0.773	0.926
260	0.284	0.357	0.366	0.198	0.160	0.878
250	0.326	0.332	0.347	0.878	0.691	0.722
240	0.356	0.328	0.344	0.562	0.840	0.585
230	0.336	0.340	0.352	0.783	0.492	0.477
220	0.358	0.342	0.346	0.734	0.823	0.800
210	0.379	0.339	0.340	0.136	0.133	0.942
200	0.390	0.339	0.349	0.008	0.025	0.188
190	0.333	0.337	0.337	0.660	0.653	0.988
180	0.330	0.345	0.340	0.321	0.454	0.392
170	0.329	0.331	0.342	0.561	0.149	0.040
160	0.342	0.336	0.340	0.888	0.960	0.295

Table 0.33: *P-values produced from student's t-test for each pressure level between all of the site locations for specific humidity in A.M. soundings. Red indicates a p-value <=0.05 and blue indicates a p-value between 0.05-0.1.*

Pressure (mb)	MB1-MB2	MB1-EA3	MB1-WVX	MB2-EA3	MB2-WVX	WVX-EA3
150	0.871	0.356	0.454	0.669	0.715	0.748
140	0.594	0.785	0.838	0.602	0.556	0.615
130	0.796	0.882	0.547	0.781	0.855	0.423
120	0.000	0.554	0.963	0.000	0.000	0.526
110	0.389	0.383	0.417	0.275	0.316	0.797
100		0.041	0.068			0.912

Table 0.34: *P-values produced from student's t-test for each pressure level between all of the site locations for specific humidity in P.M. soundings. Red indicates a p-value <=0.05 and blue indicates a p-value between 0.05-0.1.*

Pressure (mb)	MB1-MB2	MB1-EA3	MB1-WVX	MB2-EA3	MB2-WVX	WVX-EA3
910	0.756					
900	0.201	0.700		0.692		
890	0.717	0.398		0.637		
880	0.777	0.660		0.384		
870	0.745	0.563	0.015	0.818	0.095	0.082
860	0.786	0.331	0.114	0.504	0.177	0.383
850	0.778	0.345	0.258	0.566	0.390	0.674
840	0.840	0.415	0.225	0.550	0.320	0.595
830	0.825	0.569	0.266	0.728	0.372	0.527
820	0.774	0.811	0.193	0.955	0.428	0.388
810	0.635	0.684	0.116	0.956	0.307	0.297
800	0.552	0.901	0.127	0.629	0.333	0.176
790	0.608	0.788	0.242	0.431	0.448	0.141
780	0.958	0.401	0.248	0.392	0.349	0.075
770	0.986	0.387	0.222	0.427	0.336	0.075
760	0.767	0.376	0.260	0.283	0.624	0.088
750	0.780	0.374	0.122	0.288	0.715	0.133
740	0.455	0.576	0.095	0.231	0.739	0.114
730	0.260	0.750	0.068	0.190	0.978	0.181
720	0.220	0.698	0.042	0.161	0.923	0.178
710	0.087	0.931	0.028	0.118	0.824	0.098
700	0.107	0.761	0.058	0.064	0.989	0.038
690	0.230	0.554	0.178	0.073	0.859	0.037
680	0.342	0.379	0.333	0.061	0.765	0.056
670	0.512	0.367	0.277	0.097	0.841	0.043
660	0.819	0.279	0.240	0.180	0.424	0.019
650	0.800	0.255	0.228	0.156	0.498	0.020
640	0.953	0.343	0.223	0.371	0.291	0.034
630	0.718	0.272	0.239	0.503	0.156	0.017
620	0.569	0.207	0.164	0.568	0.213	0.032
610	0.594	0.308	0.119	0.703	0.173	0.047
600	0.957	0.321	0.091	0.431	0.377	0.034
590	0.728	0.296	0.157	0.211	0.694	0.039
580	0.589	0.555	0.435	0.276	0.860	0.262
570	0.740	0.415	0.773	0.245	0.637	0.445
560	0.562	0.519	0.979	0.179	0.535	0.476
550	0.904	0.487	0.631	0.548	0.731	0.786
540	0.772	0.298	0.690	0.479	0.757	0.693
530	0.997	0.324	0.383	0.337	0.350	0.974

Table 0.35: *P-values produced from student's t-test for each pressure level between all of the site locations for specific humidity in P.M. soundings. Red indicates a p-value <=0.05 and blue indicates a p-value between 0.05-0.1.*

Pressure (mb)	MB1-MB2	MB1-EA3	MB1-WVX	MB2-EA3	MB2-WVX	WVX-EA3
520	0.861	0.514	0.352	0.384	0.386	0.954
510	0.659	0.609	0.350	0.988	0.885	0.883
500	0.859	0.496	0.481	0.673	0.999	0.665
490	0.930	0.621	0.907	0.576	0.936	0.496
480	0.653	0.978	0.993	0.666	0.718	0.398
470	0.489	0.620	0.956	0.269	0.964	0.206
460	0.491	0.813	0.921	0.631	0.951	0.549
450	0.400	0.869	0.750	0.489	0.877	0.520
440	0.410	0.963	0.347	0.402	0.669	0.611
430	0.369	0.812	0.075	0.309	0.336	0.915
420	0.319	0.745	0.023	0.246	0.248	0.977
410	0.335	0.957	0.003	0.330	0.192	0.511
400	0.404	0.779	0.000	0.315	0.138	0.262
390	0.416	0.730	0.000	0.328	0.203	0.430
380	0.332	0.799	0.000	0.373	0.251	0.397
370	0.278	0.850	0.000	0.300	0.293	0.957
360	0.256	0.784	0.000	0.231	0.270	0.676
350	0.340	0.524	0.000	0.287	0.269	0.829
340	0.298	0.411	0.000	0.247	0.221	0.670
330	0.342	0.203	0.000	0.266	0.266	0.997
320	0.568	0.182	0.000	0.086	0.111	0.949
310	0.766	0.311	0.000	0.410	0.453	0.976
300	0.859	0.489	0.000	0.557	0.359	0.697
290	0.517	0.310	0.000	0.600	0.366	0.662
280	0.668	0.218	0.000	0.235	0.108	0.563
270	0.904	0.450	0.000	0.306	0.302	0.968
260	0.735	0.379	0.000	0.034	0.053	0.957
250	0.032	0.954	0.000	0.039	0.047	0.984
240	0.488	0.435	0.000	0.265	0.370	0.752
230	0.810	0.649	0.000	0.996	0.987	0.972
220	0.333	0.953	0.000	0.331	0.441	0.673
210	0.335	0.802		0.336	0.341	0.450
200				0.169	0.169	0.585
190				0.468	0.336	0.333
180				0.466	0.343	0.336
170				0.466	0.340	0.338
160				0.204	0.342	0.041
150				0.349	0.347	0.278

Table 0.36: *P-values produced from student's t-test for each pressure level between all of the site locations for specific humidity in P.M. soundings. Red indicates a p-value <=0.05 and blue indicates a p-value between 0.05-0.1.*

Pressure (mb)	MB1-MB2	MB1-EA3	MB1-WVX	MB2-EA3	MB2-WVX	WVX-EA3
140				0.365	0.364	0.528
130				0.060	0.055	0.751
120				0.763	0.574	0.190
110				0.042	0.049	0.489
100				0.357	0.295	0.490